Master's thesis

NTNU
Norwegian University of Science and Technology
Faculty of Natural Sciences
Department of Physics

Kjell Søren Heinrich

# Curvature-Induced Phenomena in Superconductors and Josephson Junctions

## In the Clean and Dirty Limits

Master's thesis in Physics (MScPhys)
Supervisor: Sol H. Jacobsen
May 2024

NTNU
Norwegian University of Science and Technology

Kjell Søren Heinrich

# Curvature-Induced Phenomena in Superconductors and Josephson Junctions

## In the Clean and Dirty Limits

Master's thesis in Physics (MScPhys)
Supervisor: Sol H. Jacobsen
May 2024

Norwegian University of Science and Technology
Faculty of Natural Sciences
Department of Physics

NTNU
Norwegian University of
Science and Technology

# Abstract

We investigate curvature-induced effects in superconductors and Josephson junctions. We give the derivation for the strain-induced spin-orbit coupling and express the curvilinear coordinate systems for multiple geometries. A derivation of the Usadel equation, an equation of motion in the quasiclassical approximation, is given. It assumes a high density of impurities and describes the dirty limit. We present the Usadel equation in curvilinear coordinates to describe geometrically curved superconductor-ferromagnet-superconductor (S-F-S) proximity systems. We derive the Eilenberger equation in curvilinear coordinates in the low impurity limit to investigate increases in the p-wave contribution due to curvature. We compare the quasiclassical results to ones obtained with the Bogoliubov-de Gennes method, a lattice model we use to describe systems in the clean limit. We find that $0 - \pi$ transitions in Josephson junctions can be induced in both limits. In the dirty limit, a ferromagnet and curvature are needed. A normal metal with considerable strain-induced spin-orbit is sufficient in the clean limit. We use geometries with non-constant curvature in one-dimensional superconductors to show that p-wave pairings can be induced and localized to points of high curvature and strain-induced spin-orbit coupling. In two-dimensional S-N-S junctions in the clean limit, we find that the strain induces a spin magnetization in the binormal direction.

# Sammendrag

Vi undersøker krumning i superledere og Josephson-koblinger. Vi gir utledningen for stressindusert spinn-bane kobling og uttrykker det krumlinjede koordinatsystemet for flere ulike geometrier. En utlending for Usadel-likningen, en bevegelsesligning i den kvasiklassiske tilnærmingen, blir gitt. Den antar en høy tetthet av urenheter i materialet og beskriver den urene grensen. Vi presenterer Usadel-likningen i krummlinjede koordinater for å beskrive geometrisk krumme superleder-ferromagnet-superleder (S-F-S) proksimitetssystemer. Vi utleder Eilenberger-likningen i krummlinjede koordinater i den lave urenhet grensen for å undersøke økninger i p-bølge bidraget grunnet krumning. Vi sammenligner de kvasiklassiske resultatene med de som er oppnådd med Bogoljubov-de Gennes-metoden, en gittermodell vi bruker for å beskrive systemer i den rene grensen. Vi finner at $0-\pi$ overganger i Josephson-koblinger kan induseres i begge grensene. I den urene grensen trengs det en ferromagnet og krumning. Et normalt metall med betydelig stressindusert spinn-bane-kobling er tilstrekkelig i den rene grensen. Vi bruker geometrier med ikke konstant krumning i en-dimensjonale superledere for å vise at p-bølge korrelasjoner induseres og lokaliseres til punkter med høy krumning og stressindusert spinn-bane kobling. I to-dimensjonale S-N-S koblinger i den rene grensen finner vi at krumningen induserer en spinnmagnetisering i den binormale retningen.

# Preface

This thesis was written as a requirement for the two-year Master's in Physics (MSPHYS) program at the Norwegian University of Science and Technology (NTNU). The project amounts to 60 ECTS points, and Dr. Sol H. Jacobsen supervised it at the center of QuSpin. The project is purely theoretical and required me to get familiar with an entirely new area of physics. I have learned about the two main methods of simulating superconducting systems. Therefore, most of the project was spent familiarizing myself with the methods and writing code for numerical analysis.

I want to thank Sol for introducing me to such an exciting research area and providing guidance throughout my project this past year. I also want to thank Morten Amundsen and Henning G. Hugdal for your input on my research during our group meetings, which has been something I looked forward to each week. Next, I want to thank Melissa Silva for being a great friend, Håvard Fyhn for being an excellent training partner, and Maxim Tjøtta for being a wonderful study partner the last year. You made my Master's studies enjoyable with engaging discussions, particularly on physics, but also on every other imaginable topic. I want to express my gratitude to my partner, Iselin Eriksen. You have been a great source of encouragement throughout the writing of this thesis. You have been especially supportive when I encountered difficulties and have gotten stuck. Most importantly, you have helped me take my mind off school when I needed it. Our kanelbolleonsdag-dates have truly been the highlight of my week.

# Notation and units

This thesis will contain a variety of matrices and dimensions. We will use the following notation: an underlined quantity $\underline{M}$ denotes a $2 \times 2$ matrix in spin space, $\hat{M}$ a $4 \times 4$ matrix Nambu⊗spin space, and $\check{M}$ a $8 \times 8$ matrix in Keldysh space. Adding or multiplying matrices of different dimensions should be understood as taking the Kronecker product between the matrix of the lowest dimension and the appropriate identity matrix. For example the matrix $\hat{A}\check{B} + \underline{C}$ should be read as $(\underline{I} \otimes \hat{A})\check{B} + (\hat{I} \otimes \underline{C})$, where $\underline{I}$ is the $2 \times 2$ identity matrix, and $\hat{I}$ is the $4 \times 4$ identity matrix. The $8 \times 8$ identity matrix is denoted $\check{I}$. This applies mainly to the quasiclassical theory since we juggle multiple matrices of multiple dimensions. In the lattice models, we stray away from the notation above and specify when the dimensionality of matrices is unclear.

Scalar quantities are written in italic fonts, such as $a, b, c$. Vectors will be written with a bold, italic font $\boldsymbol{v}$ and may be expressed as a column vector $\boldsymbol{v} = (v_x, v_y, v_z)$ of scalars in Cartesian coordinates. In terms of unit vectors, the vector can be written as $\boldsymbol{v} = v_x\hat{\boldsymbol{e}}_x + v_y\hat{\boldsymbol{e}}_y + v_z\hat{\boldsymbol{e}}_z$. The unit vectors $\hat{\boldsymbol{e}}_j$ are normalized vectors with a single component in Cartesian coordinates, not $4 \times 4$ matrices as defined above, and that is why they have a bold font.

Partial derivatives with respect to an arbitrary variable $x$ will be written as $\partial_x \equiv \frac{\partial}{\partial x}$. Therefore the gradient operator may be written as $\nabla = (\partial_x, \partial_y, \partial_z)$ in Cartesian coordinates. The Laplace operator in the same coordinate system is written as $\nabla^2 \equiv \nabla \cdot \nabla = \partial_x^2 + \partial_y^2 + \partial_z^2$.

Our choice of basis for the Hilbert space of $2 \times 2$ Hermitian matrices is the Pauli matrices. These will be used throughout the thesis for the spin space and are defined as

$$\underline{\sigma}_0 = \begin{pmatrix} 1 & 0 \\ 0 & 1 \end{pmatrix}, \quad \underline{\sigma}_1 = \begin{pmatrix} 0 & 1 \\ 1 & 0 \end{pmatrix}, \quad \underline{\sigma}_2 = \begin{pmatrix} 0 & -i \\ i & 0 \end{pmatrix}, \quad \underline{\sigma}_3 = \begin{pmatrix} 1 & 0 \\ 0 & -1 \end{pmatrix}.$$

The same matrices in Nambu space are denoted by $\tau_i$ to separate them. Hence, they act upon a different Hilbert space but are defined equally,

$$\underline{\tau}_0 = \begin{pmatrix} 1 & 0 \\ 0 & 1 \end{pmatrix}, \quad \underline{\tau}_1 = \begin{pmatrix} 0 & 1 \\ 1 & 0 \end{pmatrix}, \quad \underline{\tau}_2 = \begin{pmatrix} 0 & -i \\ i & 0 \end{pmatrix}, \quad \underline{\tau}_3 = \begin{pmatrix} 1 & 0 \\ 0 & -1 \end{pmatrix}.$$

The Pauli matrices in spin space are often collected into a Cartesian vector called the Pauli vector, written as $\boldsymbol{\sigma} = (\underline{\sigma}_1, \underline{\sigma}_2, \underline{\sigma}_3)$, using the same notation as before. We can use the two sets of bases to write a generalization in Nambu⊗spin space as

$$\begin{aligned} \hat{\tau}_0 &= \underline{\tau}_0 \otimes \underline{\sigma}_0, \\ \hat{\tau}_1 &= \underline{\tau}_1 \otimes \underline{\sigma}_0, \\ \hat{\tau}_2 &= \underline{\tau}_2 \otimes \underline{\sigma}_0, \\ \hat{\tau}_3 &= \underline{\tau}_3 \otimes \underline{\sigma}_0, \end{aligned}$$

Complex conjugation will be written with an asterisk $*$ as $(a+ib)^* = a-ib$, and Hermitian conjugation, which is the combination of transposing and complex conjugating, will be written with a dagger $\dagger$. Commutation relations will be written using the commutator $[\cdot,\cdot]$ and anticommutator $\{\cdot,\cdot\}$. For two matrices $A$ and $B$, they are defined as

$$[A,B] = AB - BA, \qquad \{A,B\} = AB + BA.$$

If either is equal to zero, $A$ and $B$ are said to commute and anti-commute, respectively.

Throughout the thesis, the convention of natural units will be used. This convention assigns unity to multiple natural constants,

$$c = \epsilon_0 = \mu_0 = \hbar = k_B = 1.$$

Here, $c$ is the speed of light, $\epsilon_0$ the vacuum permittivity, $\mu_0$ is the permeability and $k_B$ is the Boltzmann constant.

# Contents

# Chapter 1

# Introduction

In this thesis, we will explore different methods to manipulate the spins and superconducting correlations in superconducting systems. We will mainly analyze the use of ferromagnets and geometrical curvature since these are promising ways to achieve this goal. In this chapter, we will provide an overview of superconducting spintronics and proximity systems and present recent research results on the use of curvature in such systems.

## 1.1 Superconducting spintronics

Spintronics has a broad definition, with various subjects that fall under it. It is the study of electron spin in condensed matter physics and how to utilize this intrinsic property for data processing and storage. In comparison, the electron's charge and transport are the basis of modern electronics. The spintronics research field aims to provide high-density logic and memory electronic devices with high-speed performance and low power consumption [1]. Therefore, making devices spin-dependent could change the trajectory of numerous global issues associated with the electrification of society [2]. One area of research concentrates on manipulating and controlling single localized spins at a single atomic site within a metal [3]. This can be realized in quantum dots, which are a viable option for creating spin qubits, ideal for quantum computing. These could potentially replace storage devices utilized in electronics currently [4–6]. Another research area focuses on the transport of spins. The energy efficiency of transport can be enhanced by utilizing magnetic materials or superconductors with long spin lifetimes. The currents flowing in a superconductor have zero electric resistance and are dissipationless. Therefore, implementing superconductors is one of the main propositions for creating low-dissipation spintronics that could change the outlook on the energy requirement of electronics [7–9].

Superconductivity was discovered in 1911 by Heike Kamerlingh Onnes when he cooled down mercury below its critical temperature $T_c$ [10]. He discovered that the electric resistance dropped abruptly to zero below this critical temperature. This phenomenon is not a unique property of mercury but of most metals with conducting electrons. H. K. Onnes's find was the first encounter with superconductivity the world ever had, leading to his Nobel Prize in 1913. Since quantum mechanics was yet to be invented, a theoretical description of this phenomenon took a long time to develop. One of the theories is known as the BSC-theory or Bardeen–Cooper–Schrieffer theory, named after its inventors [11], which won them the Nobel Prize in 1972. BCS theory is one of the most successful theories for describing conventional superconductors [12]. Other classes of superconductivity are not well described by the BCS theory.

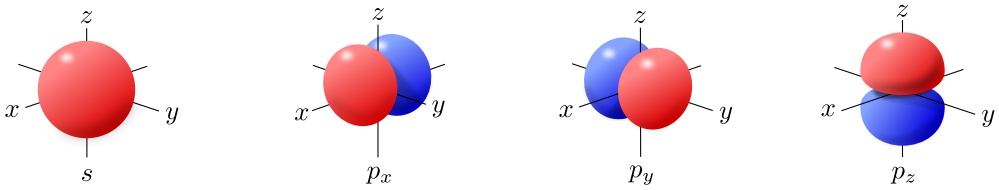


Figure 1.1: Qualitative drawing of the orbital part of the superconducting order parameter with s- and p-wave orbital symmetry. The two lobes (red/blue) in the p-wave orbitals have opposite signs (±).

Before a microscopic theory was developed, there were several phenomenological theories, for instance, London theory [13] and Ginzburg–Landau theory [14]. The BCS theory describes what is known as conventional superconductivity, where the pairing between electrons is isotropic. However, other anisotropic attractive interactions between electrons exist that might create superconducting correlations [15]. To capture these unconventional pairings, one has to use phenomenological theories or extensions of BCS theory [16]. Of high interest are superconductors with a p-wave orbital symmetry [17], illustrated in fig. 1.1. These are spin triplets and are of high interest because of their edge states [18]. The edge states are created at interfaces of unconventional superconductors where reflections cause a sign change of the order parameter [19, 20]. It makes them a key ingredient in the search for Majorana fermions in condensed matter systems [21–24]. In this thesis, we will model the superconductors we are analyzing as conventional, with an s-wave orbital symmetry. However, we will show that p-wave pairings can arise. We will also show that we can control where these correlations appear within a wire.

Superconductivity has two main features that define it, the first being the aforementioned resistanceless flow of electrons. The abrupt change in resistivity is illustrated in fig. 1.2a, where the sudden drop defines the critical temperature of the superconductor. Here, the material transitions into the superconducting state, and superconducting correlations appear. However, this is not an intrinsic property of the material but can depend on many factors, such as the external magnetic field or the amount of impurities.

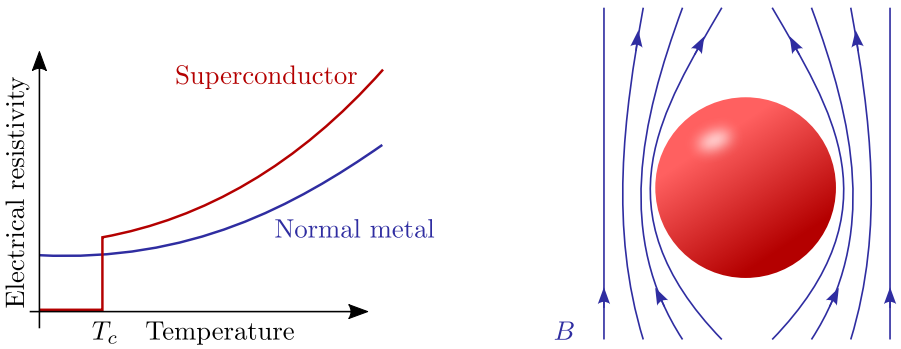


Figure 1.2: (a) Graph illustrating how the resistivity in normal and superconducting metals change as a function of the temperature and (b) the Meissner effect. These two attributes define a superconductor.

The second feature defining a superconductor is the Meissner effect. It was first discovered in 1933 by Walther Meissner and Robert Ochsenfeld [25]. They found that a superconductor acts as a perfect paramagnet when applying an external magnetic field below its critical temperature. If a type-I superconductor is brought into an external magnetic field, it creates a spontaneous dissipationless electric current that prevents the magnetic field from entering. It can be thought of as analogous to Lenz's law, but where the induced currents do not disappear because of their resistanceless flow. A qualitative illustration is given in fig. 1.2b. In type-I superconductors, the superconductivity vanishes for external magnetic fields stronger than a critical strength $B_c$. However, there exist superconductors that can let magnetic field lines pass through them without superconductivity breaking down. These are known as type-II superconductors [26].

When a conventional superconductor enters the superconducting phase, Cooper pairs are formed. These are electrons on opposite sides of the Fermi sphere with opposite spin. Thus, they are in a singlet state where the electrons move in opposite directions. These pairs form through an attractive interaction between the electrons, often mediated by phonons. A qualitative picture has been given in fig. 1.3. The illustration shows a blue electron moving through a lattice of red positively charged ions. When in proximity to the ions, the electron attracts them slightly, creating a positively charged tail trailing behind it. Another electron, with opposite momentum, will be attracted to the net positively charged trail and thus form a Cooper pair with the first electron.

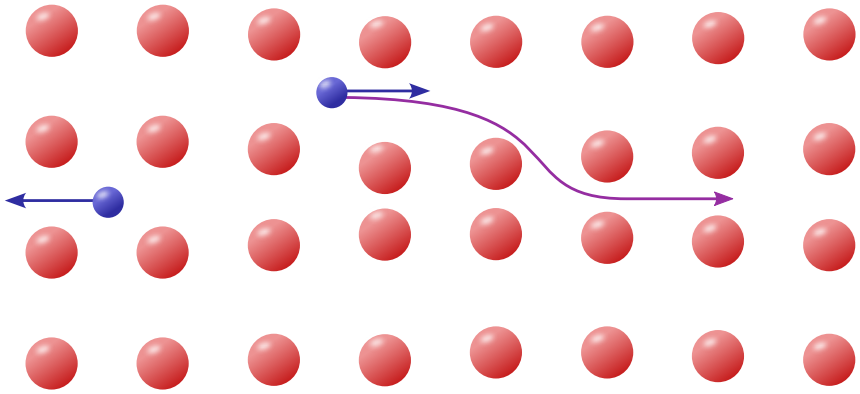

Figure 1.3: Illustration of how Cooper pairs might form in a positively charged ion lattice (red). The negatively charged electron (blue) traveling to the left leaves a positively charged trail, which attracts the electron traveling to the right.

The BCS theory builds upon the idea that the Cooper pairs form due to an attractive potential $V_{\boldsymbol{k}\boldsymbol{k}'}$. The BCS Hamiltonian can be written as

$$\mathcal{H} = \sum_{\boldsymbol{k},\sigma} (\epsilon_{\boldsymbol{k}} - \mu)\, c^\dagger_{\boldsymbol{k},\sigma} c_{\boldsymbol{k},\sigma} + \sum_{\boldsymbol{k}\boldsymbol{k}'} V_{\boldsymbol{k}\boldsymbol{k}'}\; c^\dagger_{\boldsymbol{k}\uparrow} c^\dagger_{-\boldsymbol{k}\downarrow} c_{-\boldsymbol{k}'\downarrow} c_{\boldsymbol{k}'\uparrow}, \tag{1.1}$$

which does not yet assume anything about the potential except that it is attractive in a thin shell around the Fermi surface. The operators $c_{\boldsymbol{k},\sigma}$ and $c^\dagger_{\boldsymbol{k},\sigma}$ are annihilation and creation operators, respectively. They annihilate or create an electron with momentum $\boldsymbol{k}$ and spin $\sigma$. The operators $c_{-\boldsymbol{k}'\downarrow} c_{\boldsymbol{k}'\uparrow}$ may have nonzero expectation values $b_{\boldsymbol{k}'}$ in the superconducting state [27]. Therefore, we express the product as

$$c_{-\boldsymbol{k}'\downarrow} c_{\boldsymbol{k}'\uparrow} = b_{\boldsymbol{k}'} + \left( c_{-\boldsymbol{k}'\downarrow} c_{\boldsymbol{k}'\uparrow} - b_{\boldsymbol{k}'} \right) , \tag{1.2}$$

where the parathesis describes small fluctuations around the average. Inserting eq. (1.2) and its Hermitian conjugate in eq. (1.1), lets us introduce the superconducting order parameter, denoted $\Delta_{\boldsymbol{k}}$, which is only nonzero when below the critical temperature $T_c$. It is defined as

$$\Delta_k \equiv -\sum_{\boldsymbol{k}'} V_{\boldsymbol{k}\boldsymbol{k}'}\, b_{\boldsymbol{k}'} = -\sum_{\boldsymbol{k}'} V_{\boldsymbol{k}\boldsymbol{k}'} \langle c_{-\boldsymbol{k}'\downarrow} c_{\boldsymbol{k}'\uparrow} \rangle. \tag{1.3}$$

The brackets $\langle \cdots \rangle$ denote a statistical average, in this expression, applied to the annihilation operators. This order parameter also manifests itself in the excitation spectrum of the system, creating an energy gap $|\Delta_{\boldsymbol{k}}|$. This contrasts normal metals, which can excite new states with an arbitrarily small amount of energy. For an electrical conductor, this can be a bad thing. Even at low temperatures, the thermal fluctuations might be able to excite and thus scatter the current-carrying electrons. Conversely, a superconductor has a minimum energy $|\Delta_{\boldsymbol{k}}|$ required to create excitations. Thus, the supercurrents are protected from experiencing resistive scattering in the superconducting state.

## 1.2 Ferromagnetism

A ferromagnet is a material that exhibits spontaneous alignment of internal magnetic moments without applying an external field. Metals with this property were found long before the invention of quantum mechanics, and the first phenomenological theory was published in 1907 by Pierre Weiss [28]. In 1928, Werner Heisenberg, a prominent figure in quantum mechanics, published the first comprehensive quantum mechanical approach to ferromagnetism [29]. His model is still widely used and can be summarized by the following Hamiltonian

$$\mathcal{H} = -\sum_{\langle ij \rangle} J_{ij} \boldsymbol{S}_i \cdot \boldsymbol{S}_j. \tag{1.4}$$

The bracket below the summation denotes the sum over all lattice sites $i$ and its nearest neighbors $j$. The vectors $\boldsymbol{S}_i$ are the spin operators defined as $\boldsymbol{S}_i \equiv \frac{1}{2}\boldsymbol{\sigma}_i$. The factor $\boldsymbol{S}_i \cdot \boldsymbol{S}_j$ is called the exchange interaction, and $J_{ij}$ is the exchange constant. If we assume $J_{ij} = J$, ferromagnetism is described by $J > 0$. From the Hamiltonian in eq. (1.4), it is clear that the system can minimize its energy by orienting all spins in the same direction since the exchange interaction is positive for parallel spins. Cooper pairs have a spin structure, so exciting phenomena can occur when a superconductor is placed in electrical contact with a ferromagnet. As electrons from the superconductor leak into the ferromagnet, the spin structure of the pair can change, which can be utilized in spintronic devices.

## 1.3 Proximity effect and Andreev reflections

This section will explore the effects of placing a superconductor in electrical contact with a non-superconducting metal. De Gennes investigated the effects in superconductor-normal metal (S-N) structures as early as the beginning of the 1960s [30]. It was found that the superconducting Cooper pairs would leak into the metal, changing the properties of it. This is known as the proximity effect. Conversely, the superconductor's properties also change, which is called the inverse proximity effect. Researchers discovered that the superconductor's critical temperature in an S-N system decreases as the N-layer's thickness

increases. This effect suggests that some Cooper pairs break down because one of the electrons enters the normal metal, where the other electron in the pair no longer attracts it. The study of superconductor-ferromagnet (S-F) structures displays some of the same effects. Whereas the singlet states ($\uparrow\downarrow - \uparrow\downarrow$) decay exponentially in a normal metal, they will oscillate into the ferromagnet, in addition to getting a triplet state ($\uparrow\downarrow + \uparrow\downarrow$) [9]. This decay and oscillation are illustrated in fig. 1.4. This is known as spin-mixing, where the spin axis changes, and triplet correlations are generated. The exchange field lifts the spin degeneracy, and the Cooper pairs gain a center of mass momentum [31]. The momentum is present as a position-dependent phase, and that is why the singlet and triplets oscillate out of phase compared to each other. The oscillation is enveloped by an exponential decay, and the penetration length of the Cooper pair amplitude depends on how strongly the ferromagnet is spin-polarized. For strong exchange fields, the superconducting correlations decay rapidly.

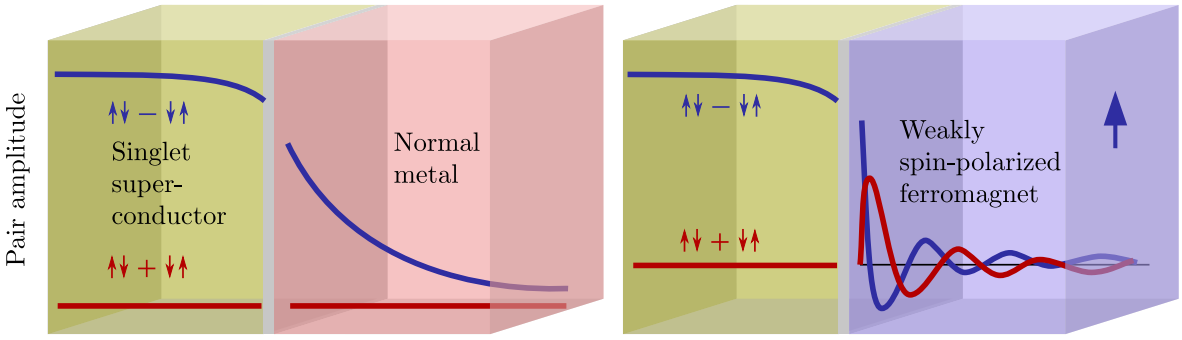


Figure 1.4: Diffusion of superconducting pair amplitude into a normal metal and a weakly spin-polarized ferromagnet. Redrawn from M. Eschrig, Physics Today (2011) [9].

Electrons may travel from the normal metal into the superconductor. What happens at the interface between the materials is described by Andreev reflections. These provide the conversion of electrical currents in normal metals into dissipationless supercurrents [32]. The process can be viewed as an electron traveling toward the S-N interface. If a hole is reflected in the metal, the electron might travel into the superconductor, forming a Cooper pair with another electron. Thus, Andreev reflections are a two electron process. It makes them a central part of discussing interface effects in superconducting heterostructures.

The next natural step in this discussion is to ask what happens when we sandwich a normal metal between two superconductors in an S-N-S junction. In 1962, Brian Josephson predicted that supercurrents could pass through a non-superconducting material, causing a potential phase difference between the superconducting wavefunctions on either side of the junction [33]. The process can be understood as the pair amplitude moving from one side and diffusing into the metal. The electron energy levels in the N-layer have phase-dependent Andreev-bound states that can carry a supercurrent. They are confined to the normal metal since they have energies below the superconducting gap. To determine the overall supercurrent, the contributions of the current-carrying states must be added up. These states are dependent on the phase difference $\phi$ between the superconductors. Therefore, if we consider a S-F-S junction, it is possible to introduce an overall phase shift $\pi$ to the superconducting wavefunction. The amplitude oscillates in magnitude, and if the thickness of the F-layer is adjusted to match the peak of this oscillation, it can display a $0 - \pi$ transition. The superconducting wavefunction for such a system is illustrated in fig. 1.5.

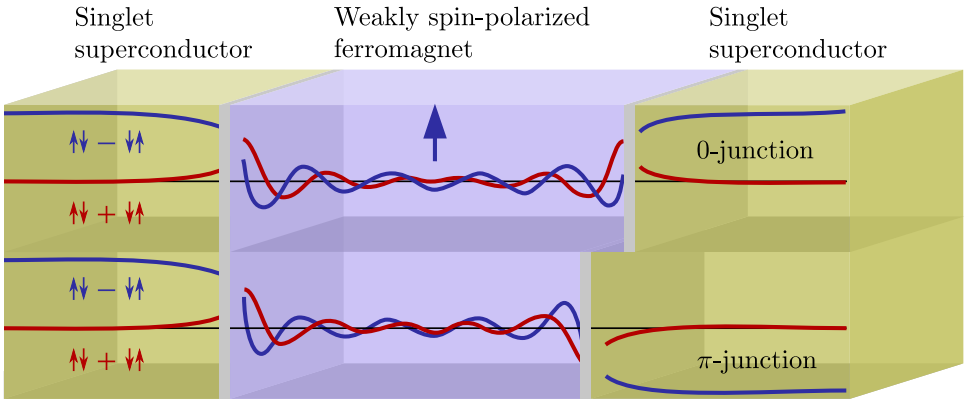


Figure 1.5: Qualitative illustration of superconducting pair amplitude in a 0 and $\pi$ Josephson junction in a weakly polarized S-F-S structure. Redrawn from M. Eschrig, Physics Today (2011) [9].

The proximity effect, Andreev's reflections, and Josephson's junctions have been examined above, but these consider only singlet superconductors. It is possible to make long-ranged spin-polarized triplets that propagate further in a magnet than the aforementioned spin singlets and carry a net spin. Excitations can be created through a process called spin singlet-triplet mixing. It builds upon the rotational asymmetry of triplet pairs. Whereas the singlet state $(\uparrow\downarrow - \uparrow\downarrow)$ is invariant regardless of the quantization direction, the triplet state $(\uparrow\downarrow + \uparrow\downarrow)$ in the $y$-basis transforms into $i(\uparrow\uparrow + \downarrow\downarrow)$ in the $z$-basis [9]. Changing basis could, in practice, be done in an S-F junction if the interface magnetization is in another direction than the bulk of the ferromagnet. It is also possible to achieve this in materials with an intrinsic inhomogeneous magnetization. Namely, a class of materials with conical-shaped spin polarization exists, such as the ferromagnet holmium [34].

## 1.4 Curved systems

Superconductors and superconducting junctions are very active research fields that hold promise for spintronic device implementation. In the last decade, the study of geometrically curved systems has gained more interest [35–41]. This includes the study of curved superconducting wires with an intrinsic p-wave gap and superconducting sheets in external magnetic fields [42–47]. Z.-J. Ying et al. have analyzed how the squeezing of an s-wave superconducting ring with intrinsic Rashba spin-orbit coupling affected the s-wave order parameter magnitude but not the p-wave. Because of the possibilities of p-wave superconductivity mentioned above, we will investigate if it is possible to induce p-wave correlations by curving a superconductor with an intrinsic s-wave order parameter. Investigating how superconductors respond to curvature can also be useful in the nano-SQUID design discussion [48]. There have been made nano-SQUIDs which were able to measure the magnetic moment of single electron spins [49]. These were made with curved superconductors, namely superconductors with a circular geometry. Curved S-N-S and S-F-S junctions have also been studied [50–56]. However, what these studies have in common, is that the curvature is introduced in the weak link only. Thus, the second topic in this thesis is S-N-S junctions with curvature in all three parts of the junction: curvature in the superconductors and the normal metal.

This thesis consists of two main parts: the derivation of the relevant theories and the results. To analyze the systems we are interested in, we will use two different approaches: the quasiclassical theory and the Bogoliubov-de Gennes method. Both methods have been used to study curvature effects in superconducting systems. In the quasiclassical framework, we derive the equations for studying curvature effects in the low impurity limit; in section 6.4 we express the Eilenberger in curvilinear coordinates, which is novel work. Using the Bogoliubov-de Gennes method, we analyze strain effects caused by geometric curvature. This is new in that only intrinsic spin-orbit coupling in curved superconductors and junctions has been studied previously, and not the effects of the strain-induced spin-orbit interaction.

# Chapter 2

# Fundamental concepts

Before presenting the derivation of the relevant equations, we review some important concepts. The relations and intuition built in this chapter will be essential for the rest of the thesis.

## 2.1 Second quantization

In the first quantization, operators represent physical properties. Take momentum, for instance, $\boldsymbol{p} = -i\nabla$, such that its eigenvalue is the physical momentum. In second quantization, operators are used to express both physical properties and particles themselves. In the occupation number representation, a particle with quantum numbers $\boldsymbol{\lambda} = (\lambda_1, \lambda_2, \ldots)$ is expressed as the creation operator $\hat{c}_\lambda^\dagger$ acting upon the vacuum state. Thus, the state with a particle with quantum numbers $\lambda$ is written as $|1_\lambda\rangle = \hat{c}_\lambda^\dagger |0_\lambda\rangle$. Similarly, it is possible to remove a particle from this state with the annihilation operator, $\hat{c}_\lambda |1_\lambda\rangle = |0_\lambda\rangle$. A many-particle state may be written as $|n_0, n_1, \ldots\rangle = |n_0\rangle |n_1\rangle \cdots$, where $n_i$ denotes the occupation number of a particle with quantum numbers $\boldsymbol{\lambda}_i$. If the creation and annihilation operators $\hat{c}_\lambda^\dagger$ and $\hat{c}_\lambda$ are fermions, they should obey $\hat{c}_\lambda^\dagger |1_\lambda\rangle = 0$ and $\hat{c}_\lambda |0_\lambda\rangle = 0$. The fermionic anti-commutation relations can encapsulate these properties,

$$\{\hat{c}_{\lambda_i}, \hat{c}_{\lambda_j}\} = 0, \qquad \{\hat{c}_{\lambda_i}^\dagger, \hat{c}_{\lambda_j}^\dagger\} = 0, \qquad \{\hat{c}_{\lambda_i}^\dagger, \hat{c}_{\lambda_j}\} = \delta_{\lambda_i,\lambda_j}, \tag{2.1}$$

where $\delta_{i,j}$ is the Kronecker delta. Next, only considering electrons, the operators can be expressed as field operators using the position-spin basis $|\boldsymbol{r}, \sigma\rangle$. The creation and annihilation operators take the form

$$\hat{\psi}_\sigma(\boldsymbol{r}) = \sum_{\lambda_i} \langle \boldsymbol{r}|\lambda_i\rangle \, \hat{c}_{\lambda_i} = \sum_i \phi_i(\boldsymbol{r}) \hat{c}_i, \tag{2.2}$$

$$\hat{\psi}_\sigma^\dagger(\boldsymbol{r}) = \sum_{\lambda_i} \langle \lambda_i|\boldsymbol{r}\rangle \, \hat{c}_{\lambda_i}^\dagger = \sum_i \phi_i^*(\boldsymbol{r}) \hat{c}_i^\dagger \tag{2.3}$$

in this basis, respectively. Physically, these can be understood as destroying an electron $\hat{\psi}_\sigma(\boldsymbol{r})$ with spin $\sigma$ at position $\boldsymbol{r}$, or creating one $\hat{\psi}_\sigma^\dagger(\boldsymbol{r})$ at these coordinates. Also, these obey the anti-commutation relations from before, namely

$$\{\hat{\psi}_\sigma(\boldsymbol{r}), \hat{\psi}_{\sigma'}(\boldsymbol{r}')\} = 0, \tag{2.4}$$

$$\{\hat{\psi}_\sigma^\dagger(\boldsymbol{r}), \hat{\psi}_{\sigma'}^\dagger(\boldsymbol{r}')\} = 0, \tag{2.5}$$

$$\{\hat{\psi}_\sigma^\dagger(\boldsymbol{r}), \hat{\psi}_{\sigma'}(\boldsymbol{r}')\} = \delta_{\sigma,\sigma'} \delta(\boldsymbol{r} - \boldsymbol{r}'). \tag{2.6}$$

Thus the many-particle state in Fock space can be written as

$$|\boldsymbol{r}_1, \sigma_1;\ \boldsymbol{r}_2, \sigma_2;\ \ldots; \boldsymbol{r}_n, \sigma_n\rangle = \hat{\psi}_{\sigma_1}^\dagger(\boldsymbol{r}_1) \hat{\psi}_{\sigma_n}^\dagger(\boldsymbol{r}_n) \cdots \hat{\psi}_{\sigma_n}^\dagger(\boldsymbol{r}_n) \, |0\rangle \, . \tag{2.7}$$

## 2.2 Averages

In this thesis, the average $\langle \cdots \rangle$ will represent a thermal and quantum average in the system at hand. This will depend on the number of particles in the system, which in turn depends on the temperature in the system. We denote the inverse temperature as $\beta = 1/k_B T$. In the grand canonical ensemble, the number of particles may vary. Therefore, the chemical potential $\mu$, which in some sense determines the particle number, is introduced. The density matrix of the system is

$$\rho = \frac{1}{Z} \exp\left[-\beta(\mathcal{H} - \mu N)\right], \tag{2.8}$$

where $Z$ is the partition function. It is defined as

$$Z = \mathrm{Tr} \exp\left[-\beta(\mathcal{H} - \mu N)\right]. \tag{2.9}$$

The average of an arbitrary operator in the system $\mathcal{O}$ may be written in terms of the two above definitions, which gives

$$\langle \mathcal{O} \rangle = \mathrm{Tr}(\rho \mathcal{O}). \tag{2.10}$$

The trace can be expanded with a basis set spanned by $|\phi_n\rangle$, which are normalized eigenstates of the system Hamiltonian $\mathcal{H}$ with eigenvalues $E_n$. The average above is therefore written as

$$\langle \mathcal{O} \rangle = \frac{1}{Z} \sum_n \langle \phi_n | \mathcal{O} | \phi_n \rangle \exp\left[-\beta(E_n - \mu N_n)\right], \tag{2.11}$$

where $N_n$ is the number of particles in state $|\phi_n\rangle$.

## 2.3 Tensor notation

We define a coordinate system in two dimensions with basis vectors $\boldsymbol{e}_1$ and $\boldsymbol{e}_2$ to keep it intuitive. If we want to do a basis transformation, there exists a matrix $\Lambda$ with elements $\lambda_{\mu\nu}$ which allows us to write

$$\boldsymbol{e}'_1 = \lambda_{11}\boldsymbol{e}_1 + \lambda_{12}\boldsymbol{e}_2 , \tag{2.12}$$
$$\boldsymbol{e}'_2 = \lambda_{21}\boldsymbol{e}_1 + \lambda_{22}\boldsymbol{e}_2 . \tag{2.13}$$

The elements $\lambda_{\mu\nu}$ can be interpreted as the projection of $\boldsymbol{e}'_\mu$ onto $\boldsymbol{e}_\nu$. For a vector denoted $\boldsymbol{v} = v_1\boldsymbol{e}_1 + v_2\boldsymbol{e}_2$, we can write down a similar transformation using $\Lambda$,

$$v'_\mu = \left(\Lambda^{-1}\right)^T_{\mu\nu} v_\nu . \tag{2.14}$$

Why $\Lambda$ is inversed and transposed has a simple intuitive explanation. Consider that we only scale one of the basis vectors, $\boldsymbol{e}'_\mu = \boldsymbol{e}_\mu / a$. Therefore, the vector component $\mu$ must scale as $\boldsymbol{v}'_\mu = a\boldsymbol{v}_\mu$ in the new coordinate system. The element $\left(\Lambda^{-1}\right)^T_{\mu\nu}$ is therefore the projection of $\boldsymbol{e}_\mu$ onto $\boldsymbol{e}'_\nu$. In transformations between Cartesian coordinate systems described by orthonormal basis vectors $\left(\Lambda^{-1}\right)^T = \Lambda$. Therefore, ordinary vectors and basis vectors are transformed in the same way. This means that gradients of scalar fields also transform as ordinary vectors since these transform as the basis vectors [57]. However, this thesis focuses on transformations in which this is not true. Therefore, we will refer to such gradients as covariant vectors for the remainder of this thesis.

To explore how these covariant vectors behave in greater detail, we consider an $n$-dimensional manifold with coordinates $x_1, x_2, \ldots, x_n$. We define a homogeneous linear coordinate transformation

$$x'_\mu = A^\mu{}_\nu \, x_\nu \, . \tag{2.15}$$

We also define the gradient of the scalar function $f(x_1, x_2, \ldots, x_n)$ as

$$(\nabla f)_\mu = \frac{\partial f}{\partial x_\mu} = w_\mu \, . \tag{2.16}$$

If we use the chain rule for the covariant vector in the primed coordinate system, we find that

$$\begin{aligned} w'_\nu &= \frac{\partial f}{\partial x'_\nu} \\ &= \frac{\partial x_1}{\partial x'_\nu}\frac{\partial f}{\partial x_1} + \frac{\partial x_2}{\partial x'_\nu}\frac{\partial f}{\partial x_2} + \cdots + \frac{\partial x_n}{\partial x'_\nu}\frac{\partial f}{\partial x_n} \\ &= \frac{\partial x_\mu}{\partial x'_\nu}\frac{\partial f}{\partial x_\mu} \\ &= \frac{\partial x_\mu}{\partial x'_\nu} w_\nu \\ &= \left(A^{-1}\right)^\nu{}_\mu \, w_\nu \, . \end{aligned} \tag{2.17}$$

This is the transformation rule of a covariant vector. Note that we have used the relation $(B^T)^\mu{}_\nu = B_\nu{}^\mu$. In addition to the covariant vector, it is useful to introduce the contravariant vector. We denote this with a superscript, and it obeys the following transformation rule,

$$v'^\mu = A^\mu{}_\nu \, v^\nu = \frac{\partial x'_\mu}{\partial x_\nu} v^\nu \, . \tag{2.18}$$

With these, we wish to define an invariant inner product. Obtaining an expression for the magnitude of inner products independent of the coordinate system is very useful. Using both the contravariant vector $x^\mu$ and the covariant vector $y_\mu$, we write the inner product in the primed frame as

$$s' = x'^\mu \, y'_\mu = A^\mu{}_\alpha \, x^\alpha (A^{-1})^\beta{}_\mu \, y_\beta = \delta^\beta{}_\alpha \, x^\alpha \, y_\beta = s \, , \tag{2.19}$$

where we used the relation $\partial x'_\mu / \partial x'_\nu = \delta^\mu{}_\nu$. Clearly, this inner product is invariant of the coordinate system. However, the same will not be true for the product between two contravariant vectors. For that reason, we define a new inner product, namely

$$\begin{aligned} s' &= e'_\mu \, e'_\nu \, x'^\mu \, y'^\nu \\ &= (A^{-1})^\mu{}_\alpha \, e_\mu \, (A^{-1})^\nu{}_\beta \, e_\nu \, A^\alpha{}_\rho \, x^\rho \, A^\beta{}_\sigma \, y^\sigma \\ &= \delta^\mu{}_\rho \, \delta^\nu{}_\sigma e_\mu \, e_\nu \, x^\rho \, y^\sigma \\ &= e_\mu \, e_\nu \, x^\mu \, y^\nu \\ &= s \, . \end{aligned} \tag{2.20}$$

We define a new quantity $\mathcal{G}_{\mu\nu} = e_\mu \, e_\nu$, which has the property of raising and lowering indices. Therefore, we can write the invariant inner product in multiple ways

$$s = x^\mu \, y_\mu = \mathcal{G}_{\mu\nu} x^\mu \, y^\nu = \mathcal{G}^{\mu\nu} x_\nu \, y_\mu \, . \tag{2.21}$$

The quantity $\mathcal{G}_{\mu\nu}$ is called the metric tensor. Tensors are mathematical objects that obey specific transformation criteria. To begin with, we introduce the rank of a tensor. It is the number of indices needed to describe the object fully. A rank-0 tensor would be represented by a scalar, a rank-1 tensor by a vector, and a rank-2 tensor by a matrix. Note, however, that matrices can represent all rank-2 tensors, but not all matrices are rank-2 tensors. Assume we have a rank-$(n+m)$ tensor $t$, with $n$ contravariant indices and $m$ covariant ones. It will transform as

$$t'^{\alpha_1\ldots\alpha_n}{}_{\beta_1\ldots\beta_m} = A^{\alpha_1}{}_{\mu_1}\cdots A^{\alpha_n}{}_{\mu_n}(A^{-1})^{\nu_1}{}_{\beta_1}\cdots(A^{-1})^{\nu_m}{}_{\beta_m}\, t^{\mu_1\ldots\mu_n}{}_{\nu_1\ldots\nu_m}\,. \tag{2.22}$$

Now, we have a framework to deal with contravariant and covariant vectors and coordinate transformations. However, we still need an important ingredient for analyzing dynamic systems. The derivatives of contravariant and covariant vectors do not transform as we wish [58]. When we consider a curved surface or manifold, the concept of a straight line becomes less straightforward. In such cases, we need a way to generalize the notion of differentiation to account for this curvature. Therefore, we have to introduce a new derivative that transforms correctly. Writing the ordinary coordinate derivative as $\partial_\mu = \partial/\partial x^\mu$, we define the covariant derivative of a contravariant vector field $v^\mu$ as

$$\mathcal{D}_\mu v^\nu = \partial_\mu v^\nu + \Gamma^\nu_{\mu\lambda} v^\lambda\,, \tag{2.23}$$

where we have introduced a new quantity $\Gamma^\nu_{\mu\lambda}$ called a Chrsitoffel symbol. Note that this symbol does not transform like a tensor [57]. It contains all the information about the curvature of the coordinate system and goes to zero in a coordinate system with straight coordinates. In curved coordinate systems, the Christoffel symbols capture how vectors change as we move along curves on the manifold. They represent the connection between different tangent spaces at nearby points on the manifold. The Christoffel symbols are also present in the definition of the covariant derivative of a covariant vector as

$$\mathcal{D}_\mu w_\nu = \partial_\mu v_\nu - \Gamma^\lambda_{\mu\nu} v_\nu\,. \tag{2.24}$$

Since the Christoffel symbols contain information about the curvature, it is closely related to the metric tensor $\mathcal{G}_{\mu\nu}$ and $\mathcal{G}^{\mu\nu}$. We can write it as

$$\Gamma^\lambda_{\mu\nu} = \frac{1}{2}\mathcal{G}^{\lambda\sigma}\left(\frac{\partial \mathcal{G}_{\sigma\nu}}{\partial x^\mu} + \frac{\partial \mathcal{G}_{\sigma\mu}}{\partial x^\nu} - \frac{\partial \mathcal{G}_{\mu\nu}}{\partial x^\sigma}\right)\,. \tag{2.25}$$

The same Christoffel symbols are also present when considering derivatives of tensors. Therefore, for completeness sake, we write the covariant derivative of a tensor $t^{\mu\nu}$ and $t^\mu{}_\nu$,

$$\mathcal{D}_\mu t^{\nu\lambda} = \partial_\mu t^{\nu\lambda} + \Gamma^\nu_{\mu\sigma} t^{\sigma\lambda} + \Gamma^\lambda_{\mu\sigma} t^{\nu\sigma}\,, \tag{2.26}$$

$$\mathcal{D}_\mu t^\nu{}_\lambda = \partial_\mu t^\nu{}_\lambda + \Gamma^\nu_{\mu\sigma} t^\sigma{}_\lambda - \Gamma^\sigma_{\mu\lambda} t^\nu{}_\sigma\,. \tag{2.27}$$

We have now completed the review of tensor notation. The concepts and relationships we have covered will be of great use later in the thesis. The metric tensor will capture all the curvature, while the covariant and contravariant vectors and derivatives will be indispensable when we introduce the curvilinear coordinate system. Since we will be analyzing geometrically curved systems, the Christoffel symbols will play a crucial role in maintaining the invariance of the derivatives.

## 2.4 Green's functions

The treatment of quantum many-body systems using Green's functions was primarily developed during the 1950s and early 1960s [59]. The method was, however, first introduced by the mathematician George Green in the 1820s [60, 61]. A general overview is given before exploring the intricacies of this formulation in condensed matter physics. In mathematics, Green's functions can be viewed as the inverse of a differential operator. It is a tool to find the solution of a differential equation even if the source term changes. To illustrate this, consider the differential equation with the linear operator $\mathrm{L}(\boldsymbol{r})$, source term $f(\boldsymbol{r})$, and desired solution $u(\boldsymbol{r})$ written as

$$\mathrm{L}\, u(\boldsymbol{r}) = f(\boldsymbol{r}). \tag{2.28}$$

The Green's function is defined as the impulse response to the operator $\mathrm{L}(\boldsymbol{r})$. In mathematical terms, this can be expressed as

$$\mathrm{L}\, G(\boldsymbol{r}, \boldsymbol{s}) = \delta(\boldsymbol{r} - \boldsymbol{s}). \tag{2.29}$$

From this form of the Green's function, the solution to eq. (2.28) can be written as

$$u(\boldsymbol{r}) = \int d\boldsymbol{s}\; G(\boldsymbol{r}, \boldsymbol{s}) f(\boldsymbol{s}). \tag{2.30}$$

From the above equations, it is evident that if eq. (2.29) is solved, eq. (2.28) does not need to be resolved for every $f(\boldsymbol{r})$. Thus, the Green's function provides a method for solving the problem for any source term. The Green's function has a different meaning in physics than in mathematics. The function $G(\boldsymbol{r}, t|\boldsymbol{r}', t')$ can be interpreted as the probability amplitude for a particle located at a point $\boldsymbol{r}'$ at time $t'$ to be found at $\boldsymbol{r}$ at another time $t$. Because of this, it is often referred to as a propagator. The propagation can also be seen from a short analysis of the general Schrödinger equation,

$$i\partial_t \psi(\boldsymbol{r}, t) = \mathcal{H}(\boldsymbol{r})\psi(\boldsymbol{r}, t). \tag{2.31}$$

The Hamiltonian $\mathcal{H}$ has been assumed time-independent for simplicity. Now, for each set of initital system states $\psi(\boldsymbol{r}, t = 0) \equiv \psi_0(\boldsymbol{r})$, the Schrödinger equation must be resolved to find $\psi(\boldsymbol{r})$. Next, introducing the time evolution operator $U(t - t')$, any state can be written as

$$|\psi(t)\rangle = \exp\left[-i\mathcal{H}(t - t')\right] \left|\psi(t')\right\rangle. \tag{2.32}$$

Using the completeness relation of the position basis $\int d\boldsymbol{r}\, |\boldsymbol{r}\rangle \langle \boldsymbol{r}| = 1$ and the projection $\psi(\boldsymbol{r}, t) \equiv \langle \boldsymbol{r}|\psi(t)\rangle$, the wavefunction may be written as

$$\begin{aligned} \psi(\boldsymbol{r}, t) &= \langle \boldsymbol{r}| \exp\left[-i\mathcal{H}(\boldsymbol{r})\,(t - t')\right] \int d\boldsymbol{r'} \left|\boldsymbol{r'}\right\rangle \left\langle \boldsymbol{r'}\right|\psi(t')\rangle \\ &= \int d\boldsymbol{r'} G(\boldsymbol{r}, t|\boldsymbol{r'}, t')\psi_0(\boldsymbol{r'}, t'), \end{aligned} \tag{2.33}$$

where the Green's function has been defined as

$$G(\boldsymbol{r}, t|\boldsymbol{r'}, t') \equiv \langle \boldsymbol{r}|\, U(t - t') \left|\boldsymbol{r'}\right\rangle. \tag{2.34}$$

As defined above, it is clear that $G$ propagates the particle through space and time. There are numerous Green's functions in condensed matter physics. Although not all are operator inverses, they describe states' propagation and evolution. Because of this, they are invaluable to the study of systems central to the development of spintronics.

# Chapter 3

# Curvature

To discuss curvature effects in condensed matter systems, we introduce the appropriate framework. We will develop a formulation where coordinates follow the space curve to which the superconducting quasiparticles are constricted. To ensure that all quantities transform correctly, we develop the general formulation, such as the metric tensor and the Christoffel symbols. The theories regarding coordinate transformations and curvature are well studied [35, 36, 57, 62, 63], so this chapter collects and presents the relevant ones to this thesis. To conclude this chapter, we present the space curve parameterizations that will be used to analyze different systems.

## 3.1 Curviliear coordinates

This section will build upon the tensor notation introduced in section 2.3 for curved coordinate systems. This guarantees that physical quantities and their derivatives remain unaffected by the choice of coordinate system used to represent them. Our choice is curvilinear coordinates in the Frenet-Serret frame.

### 3.1.1 Curved two-dimensional system

We will use a new set of orthogonal unit vectors which follow the curved surface to describe our geometries. We denote them $\hat{\boldsymbol{\mathcal{T}}}(s)$ for the tangential direction, $\hat{\boldsymbol{\mathcal{N}}}(s)$ for the normal, and $\hat{\boldsymbol{\mathcal{B}}}(s)$ for the binormal direction. These have been illustrated in fig. 3.1. We assume that the curvature is along the tangential axis in a 2D plane and that the system has no torsion. Therefore, we can define a vector $\boldsymbol{r}(s)$ parametrized by the arclength $s$ along the tangential direction. The 3D space in the vicinity of the stress-free surface $\boldsymbol{R}$ is parametrized as

$$\boldsymbol{R}(s,n,b) = \boldsymbol{r}(s) + b\hat{\mathcal{B}}(s) + n\hat{\boldsymbol{\mathcal{N}}}(s). \tag{3.1}$$

In the Frenet-Serret frame, the three unit vectors are connected and can be summarized by the following equation

$$\frac{\partial}{\partial s}\begin{pmatrix}\hat{\mathcal{N}}(s)\\ \hat{\mathcal{T}}(s)\\ \hat{\mathcal{B}}(s)\end{pmatrix} = \begin{pmatrix}0 & -\kappa(s) & 0\\ \kappa(s) & 0 & 0\\ 0 & 0 & 0\end{pmatrix}\begin{pmatrix}\hat{\mathcal{N}}(s)\\ \hat{\mathcal{T}}(s)\\ \hat{\mathcal{B}}(s)\end{pmatrix}, \tag{3.2}$$

where $\kappa(s)$ is the local curvature. We can also rewrite the above equation as $\partial_s u_\mu = F_{\mu\nu}u_\nu$, where $F_{\mu\nu}$ is the Frenet tensor [63]. To express the metric tensor, we need to find the basis vectors $\boldsymbol{e}_{s,n,b}$, where $s, n, b$ are for the tangential, normal, and binormal components,

respectively. We define the basis vectors as the derivatives of $\boldsymbol{R}(s,n,b)$. Using the Frenet-Serret frame equations, we can express them as

$$\boldsymbol{e}_s = \partial_s \boldsymbol{R}(s,n,b) = [1 - n\,\kappa(s)]\,\hat{\mathcal{T}}(s)\,, \tag{3.3}$$

$$\boldsymbol{e}_n = \partial_n \boldsymbol{R}(s,n,b) = \hat{\mathcal{N}}(s)\,, \tag{3.4}$$

$$\boldsymbol{e}_b = \partial_b \boldsymbol{R}(s,n,b) = \hat{\mathcal{B}}(s), \tag{3.5}$$

where we have used the relation $\partial_s \boldsymbol{r}(s) = \hat{\mathcal{T}}(s)$. We can use the basis vectors to define the metric tensor and its inverse. It is defined as $\mathcal{G}_{\mu\nu} = \boldsymbol{e}_\mu \cdot \boldsymbol{e}_\nu$, where $\mu, \nu$ run over the indices $s, n, b$. We find that

$$\mathcal{G}_{\mu\nu} = \begin{pmatrix} \eta(s,n)^2 & 0 & 0 \\ 0 & 1 & 0 \\ 0 & 0 & 1 \end{pmatrix}, \qquad \mathcal{G}^{\mu\nu} = \begin{pmatrix} 1 & 0 & 0 \\ 0 & 1/\eta(s,n)^2 & 0 \\ 0 & 0 & 1/\eta(s,n)^2 \end{pmatrix}, \tag{3.6}$$

where $\eta(s,n) = 1 - n\kappa(s)$. We can find Christoffel symbols for the covariant derivative operator with the metric tensor in place. Since the metric tensor is diagonal, we can set $\lambda = \sigma$ in the definition found in eq. (2.25). We find that

$$\Gamma^\lambda_{\mu\nu} = \frac{1}{2}\mathcal{G}^{\lambda\lambda}\left(\frac{\partial \mathcal{G}_{\lambda\nu}}{\partial x^\mu} + \frac{\partial \mathcal{G}_{\lambda\mu}}{\partial x^\nu} - \frac{\partial \mathcal{G}_{\mu\nu}}{\partial x^\lambda}\right). \tag{3.7}$$

It can be shown [64] that there are only four non-zero Christoffel symbols for this system. They are as follows

$$\Gamma^s_{ss} = \frac{1}{\eta(s,n)}\partial_s \eta(s,n), \tag{3.8}$$

$$\Gamma^n_{ss} = -\frac{1}{\eta(s,n)}\partial_n \eta(s,n), \tag{3.9}$$

$$\Gamma^s_{ns} = \Gamma^s_{sn} = \frac{1}{\eta(s,n)}\partial_n \eta(s,n). \tag{3.10}$$

### 3.1.2 Including torsion

In the last subsection, we derived the Christoffel symbols for a coordinate system with curvilinear coordinates for a curved two-dimensional plane. In this subsection, we will also include torsion, in mathematical terms $\partial_s \hat{\mathcal{B}}(s) \neq 0$. The approach is the same as previously, starting from the space parametrization in eq. (3.1). Here, $\boldsymbol{r}(s)$ has a shape which induces torsion. Respectively, the tangential, normal, and binormal vectors can be written as

$$\hat{\mathcal{T}}(s) = \frac{\partial_s \boldsymbol{r}(s)}{|\partial_s \boldsymbol{r}(s)|}, \tag{3.11}$$

$$\hat{\mathcal{N}}(s) = \frac{\partial_s \hat{\mathcal{T}}(s)}{|\partial_s \hat{\mathcal{T}}(s)|}, \tag{3.12}$$

$$\hat{\mathcal{B}}(s) = \hat{\mathcal{T}}(s) \times \hat{\mathcal{N}}(s). \tag{3.13}$$

In the Frenet-Serret frame, their relation can again be summarized in a matrix equation $\partial_s u_\mu = F_{\mu\nu} u_\nu$. However, the Frenet tensor has a somewhat different structure. Including torsion, it can be written as

$$F_{\mu\nu} = \begin{pmatrix} 0 & \kappa(s) & 0 \\ -\kappa(s) & 0 & \tau(s) \\ 0 & -\tau(s) & 0 \end{pmatrix}, \tag{3.14}$$

where $\kappa(s) = |\partial_s \hat{\mathcal{T}}(s)|$ and $\tau(s) = |\partial_s \hat{\mathcal{B}}(s)|$. These describe the curvature and torsion, respectively. Next, we introduce covariant basis vectors, which are defined as

$$\boldsymbol{e}_s \equiv \partial_s \boldsymbol{R}(s,n,b) = \eta(s,n)\,\hat{\mathcal{T}}(s) - b\tau(s)\,\hat{\mathcal{N}}(s) + n\tau(s)\,\hat{\mathcal{B}}(s), \tag{3.15}$$

$$\boldsymbol{e}_n \equiv \partial_n \boldsymbol{R}(s,n,b) = \hat{\mathcal{N}}(s), \tag{3.16}$$

$$\boldsymbol{e}_b \equiv \partial_b \boldsymbol{R}(s,n,b) = \hat{\mathcal{B}}(s). \tag{3.17}$$

Note that the above basis vectors are not necessarily normalized to one, and the normalized unit basis vectors can be obtained by $\hat{e}_\mu = \boldsymbol{e}_\mu/\sqrt{\mathcal{G}_{\mu\mu}}$, where the metric tensor has the same definition as before $\mathcal{G}_{\mu\nu} = \boldsymbol{e}_\mu \cdot \boldsymbol{e}_\nu$. We can expect that the metric tensor is not diagonal since the covariant basis vectors are not orthogonal. Writing out the metric tensor and its inverse, we get

$$\mathcal{G}_{\mu\nu} = \begin{pmatrix} \eta(s,n)^2 + \zeta(s,n,b)^2 & -b\tau(s) & n\tau(s) \\ -b\tau(s) & 1 & 0 \\ n\tau(s) & 0 & 1 \end{pmatrix}, \tag{3.18}$$

$$\mathcal{G}^{\mu\nu} = \frac{1}{\eta(s,n)^2} \begin{pmatrix} 1 & b\tau(s) & -n\tau(s) \\ b\tau(s) & \eta(s,n)^2 + b^2\tau(s)^2 & -nb\tau(s)^2 \\ -n\tau(s) & -nb\tau(s)^2 & \eta(s,n)^2 + n^2\tau(s)^2 \end{pmatrix}, \tag{3.19}$$

where $\zeta(s,n,b) = \tau(s)\sqrt{n^2+b^2}$. There is an interesting point to be made here [63]: Since $\mathcal{G}_{\mu\nu}$ is symmetric and invariant under the interchange $\mu \leftrightarrow \nu$, the Christoffel symbols $\Gamma^\lambda_{\mu\nu}$ will be as well. We have

$$\Gamma^s_{\mu\nu} = \frac{1}{\eta(s,n)} \begin{pmatrix} \partial_s\eta(s,n) + b\tau(s)\kappa(s) & -\kappa(s) & 0 \\ -\kappa(s) & 0 & 0 \\ 0 & 0 & 0 \end{pmatrix}, \tag{3.20}$$

$$\Gamma^n_{\mu\nu} = \frac{1}{\eta(s,n)} \begin{pmatrix} \big[-\eta(s,n)^2\partial_n\eta(s,n) + b\partial_s\left(\eta(s,n)\tau(s)\right) & -b\tau(s)\kappa(s) & -\tau(s) \\ +\kappa(s)\zeta(s,n,b)^2 - n\tau(s)^2\big] & & \\ -b\tau(s)\kappa(s) & 0 & 0 \\ -\tau(s) & 0 & 0 \end{pmatrix}, \tag{3.21}$$

$$\Gamma^b_{\mu\nu} = \frac{1}{\eta(s,n)} \begin{pmatrix} n\tau(s)\partial_s\eta(s,n) - n\eta(s,n)\partial_s\tau(s) - b\tau(s)^2 & \tau(s) & 0 \\ \tau(s) & 0 & 0 \\ 0 & 0 & 0 \end{pmatrix}. \tag{3.22}$$

The derivation of the first Christoffel symbol in eq. (3.20) is derived in appendix A. The derivations of the remaining two are identical. It is clear from eqs. (3.20) to (3.22) that all three symbols are symmetric under $\mu \leftrightarrow \nu$ as stated above. This concludes the section describing the coordinate transformations that will become useful in describing curved systems. Next, we will consider the strain effects and consequences of curving a material.

## 3.2 Curvature and spin-orbit interactions

This section will focus on spin-orbit coupling in condensed matter systems. We will consider intrinsic spin-orbit coupling from symmetry breaking in the material. We will also see how curvature and strain alter the crystal structure and induce an effective spin-orbit coupling. Lastly, based on the system's dimensionality, we derive specific expressions for the interaction. However, these will also depend on the geometry or parametrization. The next section will present a few geometries used in the results.

Before seeing how curvature can induce an effective spin-orbit coupling, we give a general description of how a moving particle in an electric field can experience this interaction. We denote the velocity of this particle as $\boldsymbol{v}$ and the electric field as $\boldsymbol{E}$. The coupling becomes clear when we go to the electron's rest frame. Here, it experiences a magnetic field $\boldsymbol{B} = -\boldsymbol{v} \times \boldsymbol{E}$. For an electron, the magnetic moment $\boldsymbol{\mu}_e$ couples to the magnetic field $\boldsymbol{B}$ through the Zeeman interaction. The Hamiltonian of the interaction can be written as

$$\mathcal{H}_{\text{soc}} = -\boldsymbol{\mu}_e \cdot \boldsymbol{B} = \frac{eg}{2m} \boldsymbol{S} \cdot (\boldsymbol{v} \times \boldsymbol{E}), \tag{3.23}$$

where $\boldsymbol{S}$ is the spin vector, $g$ is the g-factor, $e$ is the electron charge, and $m$ the electron mass. Rewriting using the Pauli vector $\boldsymbol{\sigma} = 2\boldsymbol{S}$, we get

$$\mathcal{H}_{\text{soc}} = \frac{eg}{4m^2} \boldsymbol{\sigma} \cdot (\boldsymbol{p} \times \boldsymbol{E}). \tag{3.24}$$

The above is a quite general expression, so next, we consider an example. If we take the electric field to be in the $z$-direction $\boldsymbol{E} = E\hat{\boldsymbol{e}}_z$, it creates an asymmetry at the surface [65]. The coupling arising due to the lack of surface inversion symmetry is called Rashba spin-orbit coupling. It can be summarized in

$$\mathcal{H}_{\text{Rsoc}} = \frac{\alpha}{m}(\sigma_x p_y - \sigma_y p_x), \tag{3.25}$$

where $\alpha = \frac{egE}{4m}$ is called the Rashba coefficient. Structures that break bulk inversion symmetry exhibit Dresselhaus spin-orbit coupling [66], and materials might display an intrinsic combination of the two types [67].

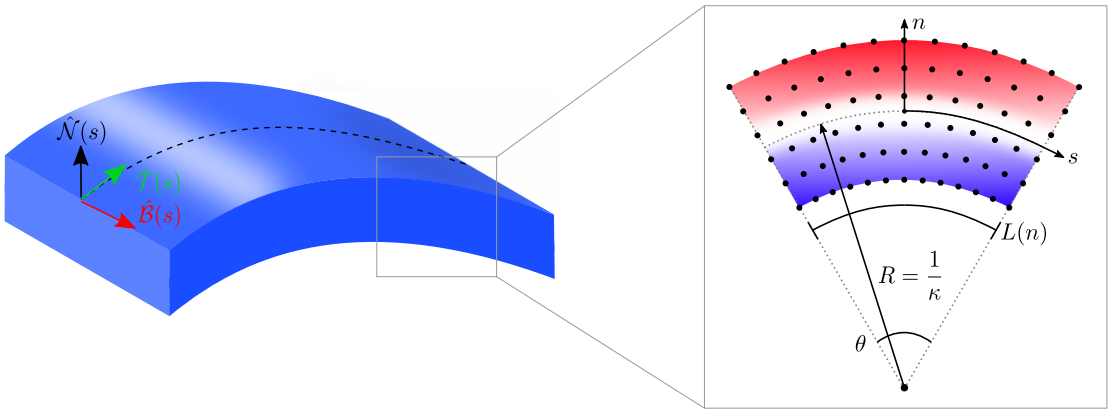


Figure 3.1: Cross section of a portion of the bent nanostructure with $n$ as the coordinate in the normal direction and $s$ as the arc length parameter. The curvature effect leads to regions under tensile strain for $n > 0$ and compressive for $n < 0$. The radius of curvature is $R = 1/\kappa$, the length of the portion at $n$ is $L(n)$, and $\theta$ is the curvature angle. Inspired by figure 2 in ref. [36], figure 6 in ref. [62] and figure 4.1 in ref. [63].

### 3.2.1 Strain-induced spin-orbit coupling

A curved wire may experience no strain and still exhibit curvature effects. However, curvature will cause strain in systems when the curvature is high enough to alter the atomic structure. This section will present how strain can be a source of spin-orbit coupling, while other curvature effects will be revisited. To see where the strain-induced spin-orbit

coupling comes from, we consider the cross-section of a curved nanostructure as shown in fig. 3.1. The deformation due to curvature results in a variable strain of the material. It should induce a shift in the conduction band energies, predicted by linear deformation potential theory [68–70]. We will now see exactly how this prediction comes about by considering the strain distribution in the material. To begin with, we say that there is no in-plane strain, so $\epsilon_{bb} = 0$. We assume the nanostructure has a larger characteristic dimension along the binormal direction than the remaining coordinates, justifying the previous condition. The strain is tensile for $n > 0$ and compressive for $n < 0$. The strain along the bent direction is defined as

$$\epsilon_{ss} = \frac{L(n) - L(0)}{L(0)}, \tag{3.26}$$

where $L(n)$ is the length of the bent material at a distance $n$ from the center of curvature, and $L(0)$ is the length of the unstrained material. Using the radius $R = 1/\kappa(s)$, we can write

$$\epsilon_{ss} = \frac{(R+n)\theta - R\theta}{R\theta} = \kappa(s)n. \tag{3.27}$$

The deformation of the material can be assumed to create a potential that is linear in strain. It stems from the shift in band energies, attracting the conducting electrons toward the tensile regions of the material [36]. This approximation is valid when the thickness of the curved material is much smaller than the radius of curvature. We write the potential as

$$V(s,n) = \Lambda\kappa(s)n, \tag{3.28}$$

where $\Lambda$ is the deformation potential constant. We can write the electric field due to the curvature potential as

$$\boldsymbol{E} = -\nabla V = -\frac{\hat{\boldsymbol{e}}^{\lambda}}{\sqrt{\mathcal{G}_{\lambda\lambda}}}\partial_{\lambda}(\Lambda\kappa(s)n) = -\frac{\Lambda n(\partial_s\kappa(s))}{\sqrt{\eta(s,n)^2 + \zeta(s,n,b)^2}}\hat{\mathcal{T}} - \Lambda\kappa(s)\hat{\mathcal{N}}\,. \tag{3.29}$$

The field produced by the strain creates an asymmetric confinement in the normal direction of the bent surface. Integrating over $n$, and using the Jacobian $|J| = \sqrt{G} = \eta(s,n)$, we get an average electric field $E(s)\hat{\mathcal{N}}(s)$ whose strength is proportional to the curvature of the nanostructure. We find that

$$E(s) = \Lambda\kappa(s)\,. \tag{3.30}$$

If we substitute the electric field in eq. (3.24) with the above, we get an effective strain-induced Rashba spin-orbit interaction. The Hamiltonian now reads

$$\mathcal{H}_{\mathrm{SO}} = -\frac{\alpha_N}{m}\,\boldsymbol{\sigma}\cdot(\boldsymbol{p}\times\hat{\mathcal{N}}(s)), \tag{3.31}$$

where the coefficient $\alpha_N = \frac{g\Lambda\kappa(s)}{4m}$. Please note that the strength of the spin-orbit interaction, denoted by $\alpha_N$, is directly proportional to the curvature, represented by $\kappa(s)$. This means that the curvature of the material can control the spin-orbit interaction strength. Hence, we associate the prefactor $\alpha_N$ with the strain-induced interaction. However, there may be intrinsic origins of spin-orbit coupling, where the values of $\alpha_T$ and $\alpha_B$ are not equal to zero. In the following subsections, we will consider this possibility.

### 3.2.2 The spin-orbit field

In addition to the strain-induced spin-orbit coupling, the material may have an additional intrinsic coupling. In general, we may introduce a spin-orbit vector whose components represent the spin-orbit strength due to the asymmetric confinement in different curvilinear directions,

$$\boldsymbol{\alpha} = \alpha_T \hat{\mathcal{T}}(s) + \alpha_N \hat{\mathcal{N}}(s) + \alpha_B \hat{\mathcal{B}}(s). \tag{3.32}$$

If we neglect potentials, the Hamiltonian describing the dynamics of particles in the presence of spin-orbit coupling can be written as

$$\mathcal{H} = \frac{\boldsymbol{p}^2}{2m} - \boldsymbol{\alpha} \cdot \frac{\boldsymbol{\sigma} \times \boldsymbol{p}}{m}, \tag{3.33}$$

where as usual $\boldsymbol{p} = -i\hbar\nabla$. Assuming we have a curved system, we replace the derivative operator with the covariant derivative, which is defined by eqs. (2.23) and (2.24). The Hamiltonian takes the form

$$\mathcal{H} = -\frac{\hbar^2 \mathcal{G}^{\lambda\mu}}{2m} \mathcal{D}_\lambda \mathcal{D}_\mu + \frac{i\hbar}{m} \frac{\epsilon^{\lambda\mu\nu}}{\sqrt{G}} \alpha_\lambda \sigma_\mu \mathcal{D}_\nu, \tag{3.34}$$

where $\epsilon^{\lambda\mu\nu}$ is the Levi-Civita symbol, $G$ is the determinant of the metric tensor $\mathcal{G}_{\lambda\mu}$, and $\lambda, \mu, \nu$ are indices running over $s, n, b$. To simplify the expression, we define a contravariant spin-orbit field as

$$A^\nu = \epsilon^{\lambda\mu\nu} \frac{\alpha_\lambda \sigma_\mu}{\sqrt{G}} = \mathcal{G}^{\nu\mu} A_\mu. \tag{3.35}$$

The field $A_\mu$ is a complex 2x2 matrix-valued SU(2) vector potential [71]. Rewriting the Hamiltonian by including the covariant spin-orbit field, we get

$$\mathcal{H} = -\frac{\hbar^2 \mathcal{G}^{\lambda\mu}}{2m} \mathcal{D}_\lambda \mathcal{D}_\mu + \frac{i\hbar}{m} \mathcal{G}^{\nu\mu} A_\mu \mathcal{D}_\nu. \tag{3.36}$$

In the next step, we assume that the spin-orbit coupling is weak, so we only let terms linear in $A_\mu$ contribute. Therefore, we add an artificial $\mathcal{G}^{\lambda\mu} A_\lambda A_\mu$ term which is quadratic $\mathcal{O}(A_\mu^2)$. It lets us write the Hamiltonian as

$$\mathcal{H} = -\frac{\hbar^2 \mathcal{G}^{\lambda\mu}}{2m} \left(\mathcal{D}_\lambda - iA_\lambda\right)\left(\mathcal{D}_\mu - iA_\mu\right). \tag{3.37}$$

With this assumption, the Hamiltonian describes a particle minimally coupled to a vector potential $A_\lambda$. Hence, the spin-orbit coupling becomes an effective background SU(2) field. Expressing it as such, the Hamiltonian is gauge invariant under any local SU(2) rotation with $\hat{\mathcal{U}}$ if the vector potential transforms as $A_\lambda \to \hat{\mathcal{U}} A_\lambda \hat{\mathcal{U}}^{-1} - i(\partial_\lambda \hat{\mathcal{U}})\hat{\mathcal{U}}^{-1}$ [72]. Similar to the covariant derivatives, we can include spin-orbit coupling in the problem by transforming the derivatives. We, therefore, introduce the space-gauge covariant derivative

$$\tilde{\mathcal{D}}_\lambda v_\mu = \partial_\lambda v_\mu - \Gamma^\nu_{\lambda\mu} v_\nu - i\left[A_\lambda, v_\mu\right]. \tag{3.38}$$

With the equation above, we conclude the discussion concerning derivatives. We can use the space-gauge covariant derivative to account for changes in curved systems in the presence of a spin-orbit field.

### 3.2.3 Hamiltonian Rashba nanowire

In this subsection, we will derive the vector field expression for a nanowire with both strain-induced and intrinsic spin-orbit coupling. We start from the Hamiltonian with covariant derivatives given in eq. (3.34) since we are still very much interested in the curvature effects. Writing out the derivatives with the Christoffel symbols, we have

$$\mathcal{H} = -\frac{\hbar^2 \mathcal{G}^{\lambda\mu}}{2m}\left(\partial_\lambda\partial_\mu - \Gamma^\nu_{\lambda\mu}\partial_\nu\right) + \frac{i\hbar}{m}\frac{\epsilon^{\lambda\mu\nu}}{\sqrt{G}}\alpha_\lambda\sigma_\mu\partial_\nu, \tag{3.39}$$

where $\sqrt{G} = 1-n\kappa(s)$ is the determinant of the metric tensor, and where we have neglected constant shifts to the energy. Here, $\sigma_\mu$ are the curvilinear Pauli matrices since the Greek letters run over the indexes $s, n, b$. The curvilinear Pauli matrices are

$$\sigma_s = \sigma_T\eta(s,n) + \sigma_B\tau(s)n - \sigma_N\tau(s)b, \tag{3.40}$$
$$\sigma_n = \sigma_N, \tag{3.41}$$
$$\sigma_b = \sigma_B, \tag{3.42}$$

where $\sigma_{T,N,B} = \boldsymbol{\sigma}\cdot\{\hat{\mathcal{T}},\hat{\mathcal{N}},\hat{\mathcal{B}}\}$. To obtain an effective Hamiltonian for the system, we can do a thin-wall quantization procedure [73, 74]. Since the only coordinate we wish to keep is $s$, we can expand in powers of $n$ and $b$, employing an adiabatic approximation to the zeroth power terms to separate them from $s$. The exact derivation can be found in ref. [35]. This means that the derivatives $\partial_{n,b} \to 0$, and also effectively means setting $n, b = 0$, such that $\eta(s,n) = 1$ and $\zeta(s,n,b) = 0$. If we collect all terms for the tangential part only, i.e., dependent on the variable $s$, we are left with the Hamiltonian

$$\begin{aligned}\mathcal{H}_s = &-\frac{\hbar^2}{2m}\left(\partial_s^2 + \frac{\kappa(s)^2}{4} + \frac{\tau(s)^2}{2}\right) - \frac{i\hbar}{m}\alpha_N\left(\sigma_B\partial_s - \frac{\tau(s)}{2}\sigma_N\right)\\ &+ \frac{i\hbar}{m}\alpha_B\left(\sigma_N\partial_s - \frac{\kappa(s)}{2}\sigma_T + \frac{\tau(s)}{2}\sigma_B\right),\end{aligned} \tag{3.43}$$

where we have assumed non-zero curvature and torsion. We ignore all shifts in energy, which means all terms that do not contain a derivative of $s$. If we compare the above expression with eq. (3.36), we can recognize the tangential component of the SU(2) gauge field. The entire field vector is

$$A_\lambda = (\alpha_N\sigma_B - \alpha_B\sigma_N, 0, 0), \tag{3.44}$$

where $\alpha_N$ is due to the strain-induced spin-orbit coupling, and $\alpha_B$ is an intrinsic Rashba spin-orbit coupling given in eq. (3.25).

### 3.2.4 Hamiltonian tunnel

In this subsection, we find the Hamiltonian for a curved thin film so that it forms a tunnel. We will assume no torsion, $\tau(s) = 0$. We assume there is an intrinsic Rashba spin-orbit coupling in the binormal direction, such that the spin-orbit vector can be written as $\boldsymbol{\alpha} = \alpha_N\hat{\mathcal{N}} + \alpha_B\hat{\mathcal{B}}$. The Hamiltonian is written as

$$\mathcal{H} = -\frac{\hbar^2}{2m}\mathcal{G}^{\lambda\mu}\left(\partial_\lambda\partial_\mu - \Gamma^\nu_{\lambda\mu}\partial_\nu\right) + \frac{\alpha_N}{\hbar}\boldsymbol{\sigma}\cdot\boldsymbol{p}\times\hat{\mathcal{N}}(s) + \frac{\alpha_B}{\hbar}\boldsymbol{\sigma}\cdot\boldsymbol{p}\times\hat{\mathcal{B}}(s). \tag{3.45}$$

If we assume a geometric confinement in the binormal direction, as in fig. 3.2a, we can write an effective Hamiltonian for the tangential and normal degrees of freedom. Because

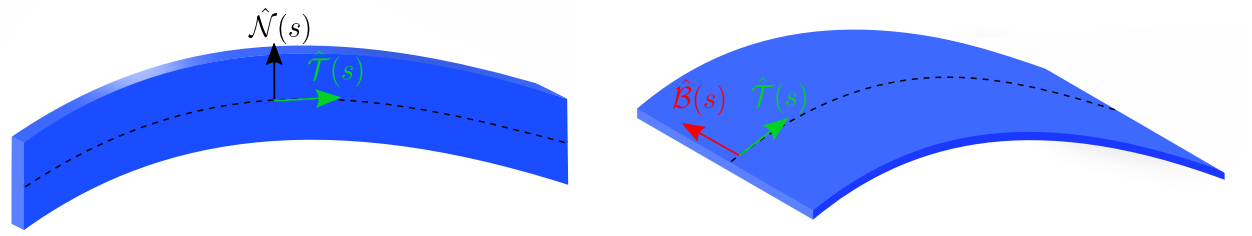


(a) (b)

Figure 3.2: Illustrations of curved two-dimensional surfaces. In (a), the surface is described by the normal $n$ and tangential $s$ coordinates. In (b), we parametrize the tunnel using binormal $b$ and tangential $s$ coordinates.

the metric tensor and Christoffel symbols contribute, we get

$$\begin{aligned}\mathcal{H}_{s,n} =& \frac{-\hbar^2}{2m}\left(\partial_s^2 + \frac{1}{\eta(s,n)^2}\partial_n^2\right) - \frac{\hbar^2}{2m}\frac{\kappa(s)}{\eta(s,n)}\partial_n \\ &- \frac{i\hbar}{m}\frac{1}{\eta(s,n)}\left(\alpha_N\sigma_B\partial_s - \alpha_B\sigma_N\partial_s + \eta(s,n)\alpha_B\sigma_T\partial_n\right) . \end{aligned} \tag{3.46}$$

We get another two-dimensional system with different dynamics if we assume confinement in the normal direction, as in fig. 3.2b. Assuming that the confinement potential is centered at $n = 0$, the metric tensor reduces to the identity matrix, and the relevant Christoffel symbols vanish. The Hamiltonian we are left with is

$$\mathcal{H}_{s,b} = -\frac{\hbar^2}{2m}(\partial_s^2 + \partial_b^2) + \frac{i\hbar}{m}\alpha_N\left(\sigma_B\,\partial_s - \sigma_T\,\partial_b\right) , \tag{3.47}$$

where we have neglected geometric potentials, as they only contribute to an overall energy shift. We also discarded the Rashba spin-orbit coupling since it will be in the normal direction and only act as a shift in the strain-induced factor $\alpha_N$. For this example, we can write the spin-orbit vector field as

$$A_\mu = (\alpha_N\sigma_B, 0, \alpha_N\sigma_T). \tag{3.48}$$

The spin-orbit fields derived in this section will be used to analyze systems with strain-induced and intrinsic spin-orbit coupling in different dimensions and geometries. This will alter the curvilinear Pauli matrices, which we will consider in the next section.

## 3.3 Parametrizations

This section will derive the curvilinear unit vectors $\hat{\mathcal{T}}(s)$, $\hat{\mathcal{N}}(s)$ and $\hat{\mathcal{B}}(s)$ for different geometries. These depend on the curvature $\kappa(s)$ and the torsion $\tau(s)$. However, not all the geometries we consider in this thesis will have torsion. We will also write down the curvilinear Pauli matrices $\sigma_{T,N,B}$ for the different parameterizations. These will be used when analyzing specific systems.

### 3.3.1 Circular curvature

To begin with, we consider a circular curvature. We choose the curve to lie in the $xy$-plane, such that the binormal is in the $z$-direction. We parameterize it in terms of the arc length $s$ and have $\kappa(s)$ as a variable we can tune. We choose the curve to be a line segment of

a circle, thus assuming constant curvature, so $\kappa(s) = \kappa$ becomes a real constant. We can write the parametrization vector as

$$\boldsymbol{r}(s) = \frac{1}{\kappa}\cos(\kappa s)\hat{\boldsymbol{e}}_x + \frac{1}{\kappa}\sin(\kappa s)\hat{\boldsymbol{e}}_y. \tag{3.49}$$

From the relations presented in eqs. (3.11) to (3.13) we can calculate the curvilinear unit vectors, which become

$$\hat{\mathcal{T}}(s) = -\sin(\kappa s)\hat{\boldsymbol{e}}_x + \cos(\kappa s)\hat{\boldsymbol{e}}_y, \tag{3.50}$$

$$\hat{\mathcal{N}}(s) = -\cos(\kappa s)\hat{\boldsymbol{e}}_x - \sin(\kappa s)\hat{\boldsymbol{e}}_y, \tag{3.51}$$

$$\hat{\mathcal{B}}(s) = \hat{\boldsymbol{e}}_z. \tag{3.52}$$

Now, we calculate the curvilinear Pauli vector $\boldsymbol{\sigma}$, which the vectors above transform. We can write the vector components as

$$\sigma_T = \begin{pmatrix} 0 & -ie^{-i\kappa s} \\ ie^{i\kappa s} & 0 \end{pmatrix}, \quad \sigma_N = \begin{pmatrix} 0 & -e^{-i\kappa s} \\ -e^{i\kappa s} & 0 \end{pmatrix}, \quad \sigma_B = \begin{pmatrix} 1 & 0 \\ 0 & -1 \end{pmatrix}. \tag{3.53}$$

We can clearly see how they are dependent on the coordinate $s$. Note that $\sigma_T$ and $\sigma_N$ rotate with the material. They are both a mix of $\sigma_x$ and $\sigma_y$, and will follow the curvature of the parametrization vector in the lab frame.

### 3.3.2 Helical nanowire

The parametrization of a helix is a circular curve with an out-of-plane contribution. This corresponds to the torsion of the wire. Imagine a spring that we stretch: it increases the length out of the plane but, in return, reduces the in-plane curvature. Thus, there must be a constriction for the relation between the curvature and torsion. First, we begin by writing down the vector in terms of the azimuthal angle $\phi$, not the arclength. We write it as

$$\boldsymbol{r}(\phi) = R\cos(\phi)\,\hat{\boldsymbol{e}}_x \;\pm\; R\sin(\phi)\,\hat{\boldsymbol{e}}_y \;+\; c\,\phi\,\hat{\boldsymbol{e}}_z, \tag{3.54}$$

where the upper sign in the second term is for a righthanded helix, and the lower sign is for a lefthanded one. The variable $c$ is the pitch, which controls the out-of-plane component and the torsion. We will continue the parametrization for a righthanded helix. We find that the arc length is

$$s(\phi) = \int_0^{\phi} |\boldsymbol{r}'(\sigma)|\, d\sigma = \phi\sqrt{R^2 + c^2}\,. \tag{3.55}$$

Thus, we can write the curve parametrization in terms of the arc length,

$$\boldsymbol{r}(s) = R\cos\left(\frac{s}{\sqrt{R^2+c^2}}\right)\hat{\boldsymbol{e}}_x + R\sin\left(\frac{s}{\sqrt{R^2+c^2}}\right)\hat{\boldsymbol{e}}_y + c\frac{s}{\sqrt{R^2+c^2}}\hat{\boldsymbol{e}}_z\,. \tag{3.56}$$

From the relations presented in eqs. (3.11) to (3.13) we can calculate the curvilinear unit vectors, which become

$$\hat{\mathcal{T}}(s) = -\frac{R}{\sqrt{R^2+c^2}}\sin\phi\,\hat{\boldsymbol{e}}_x + \frac{R}{\sqrt{R^2+c^2}}\cos\phi\,\hat{\boldsymbol{e}}_y + \frac{c}{\sqrt{R^2+c^2}}\hat{\boldsymbol{e}}_z\,, \tag{3.57}$$

$$\hat{\mathcal{N}}(s) = -\cos\phi\,\hat{\boldsymbol{e}}_x - \sin\phi\,\hat{\boldsymbol{e}}_y\,, \tag{3.58}$$

$$\hat{\mathcal{B}}(s) = \frac{c}{\sqrt{R^2+c^2}}\sin\phi\,\hat{\boldsymbol{e}}_x - \frac{c}{\sqrt{R^2+c^2}}\cos\phi\,\hat{\boldsymbol{e}}_y + \frac{R}{\sqrt{R^2+c^2}}\hat{\boldsymbol{e}}_z\,. \tag{3.59}$$

Using eq. (3.69), we can identify the curvature and torsion of the helix. We write them as

$$\kappa = \frac{R}{R^2 + c^2}, \qquad \tau = \frac{c}{R^2 + c^2}. \tag{3.60}$$

This establishes a relation between the radius and pitch to the curvature and torsion. We can write that

$$R^2 + c^2 = \frac{1}{\kappa^2 + \tau^2}\,. \tag{3.61}$$

Using the notation in ref. [63], we introduce a quantity $\alpha = \text{atan}(\tau/\kappa)$. This allows us to write the vectors in a much more compact form, namely

$$\hat{\mathcal{T}}(\phi) = -\cos\alpha\,\sin\phi\,\hat{\boldsymbol{e}}_x + \cos\alpha\,\cos\phi\,\hat{\boldsymbol{e}}_y + \sin\alpha\,\hat{\boldsymbol{e}}_z\,, \tag{3.62}$$

$$\hat{\mathcal{N}}(\phi) = -\cos\phi\,\hat{\boldsymbol{e}}_x - \sin\phi\,\hat{\boldsymbol{e}}_y\,, \tag{3.63}$$

$$\hat{\mathcal{B}}(\phi) = \sin\alpha\,\sin\phi\,\hat{\boldsymbol{e}}_x - \sin\alpha\,\cos\phi\,\hat{\boldsymbol{e}}_y + \cos\alpha\,\hat{\boldsymbol{e}}_z\,. \tag{3.64}$$

An important point concerning curvature and torsion is that they have a specific relation if we consider a fixed-length helix. The length of a nanowire is given by $L = 2\pi n\sqrt{R^2 + c^2}$, where $n$ is the number of turns. This means that varying the torsion of a curved wire gives

$$\kappa = \sqrt{(2\pi n/L)^2 - \tau^2}\,, \tag{3.65}$$

where $\tau \leq 2\pi n/L$. This correspondence can be thought of as stretching a spring, which results in a higher torsion and lower curvature since it cannot change its overall length. Finally, the curvilinear Pauli matrices with this parametrization are

$$\underline{\sigma}_T = \begin{pmatrix} \sin\alpha & -i\cos\alpha\, e^{-i\phi} \\ i\cos\alpha\, e^{i\phi} & -\sin\alpha \end{pmatrix}, \tag{3.66}$$

$$\underline{\sigma}_N = \begin{pmatrix} 0 & -e^{-i\phi} \\ -e^{i\phi} & 0 \end{pmatrix}, \tag{3.67}$$

$$\underline{\sigma}_B = \begin{pmatrix} \cos\alpha & i\sin\alpha\, e^{-i\phi} \\ -i\sin\alpha\, e^{i\phi} & -\cos\alpha \end{pmatrix}. \tag{3.68}$$

In the limit where $\tau = 0$, the quantity $\alpha = 0$, and we obtain the same result as for a circular curved wire.

### 3.3.3 Elliptical ring

The two previous subsections have only considered constant curvature $\kappa(s) = \kappa$, so we present a parametrization with nonconstant curvature in this section. To take the constant curvature a step further, we squeeze it, making an ellipse. In this section, we parametrize an ellipse in terms of a variable $\varphi$, where this is not the arclength again. Thus, the Frenet-Serret formulas look somewhat different

$$\frac{\partial}{\partial\varphi}\begin{pmatrix} \hat{\mathcal{T}}(\varphi) \\ \hat{\mathcal{N}}(\varphi) \\ \hat{\mathcal{B}}(\varphi) \end{pmatrix} = |\partial_\varphi \boldsymbol{r}(\varphi)| \begin{pmatrix} 0 & \kappa(\varphi) & 0 \\ -\kappa(\varphi) & 0 & \tau(\varphi) \\ 0 & -\tau(\varphi) & 0 \end{pmatrix} \begin{pmatrix} \hat{\mathcal{T}}(\varphi) \\ \hat{\mathcal{N}}(\varphi) \\ \hat{\mathcal{B}}(\varphi) \end{pmatrix}, \tag{3.69}$$

where the norm of the derivative of $\boldsymbol{r}(\varphi)$ is picked up due to the chain rule. We do the normalization manually to show another approach than the arclength parametrization.

The curvilinear unit vectors are related to the parametrization through

$$\hat{\mathcal{T}}(\varphi) = \frac{\boldsymbol{r}'(\varphi)}{|\boldsymbol{r}'(\varphi)|}\,, \tag{3.70}$$

$$\hat{\mathcal{N}}(\varphi) = \frac{\hat{\mathcal{T}}'(\varphi)}{|\hat{\mathcal{T}}'(\varphi)|}\,, \tag{3.71}$$

$$\hat{\mathcal{B}}(\varphi) = \hat{\mathcal{T}}(\varphi) \times \hat{\mathcal{N}}(\varphi)\,. \tag{3.72}$$

To express an ellipse in this frame, we begin with the standard equation in Euclidean space

$$\left(\frac{x}{a}\right)^2 + \left(\frac{y}{a\sqrt{1-\mathscr{E}^2}}\right)^2 = 1, \tag{3.73}$$

where $a$ is the semi-major-axis, and $\mathscr{E}$ is the eccentricity relating the semi-major- and minor-axis by $b^2 = a^2(1-\mathscr{E}^2)$. If we use polar coordinates $x = \rho\cos\varphi$ and $y = \rho\sin\varphi$, we find that the radius varies as

$$\rho(\varphi) = \sqrt{\frac{b^2}{1-\mathscr{E}^2\cos^2\varphi}}. \tag{3.74}$$

In a later chapter, we consider a closed ellipse, and therefore, the variable $\varphi$ ranges from zero to $2\pi/L$. Using the above expression for the radius, we parametrize our curve $\boldsymbol{r}$ as

$$\boldsymbol{r}(\varphi) = \rho(\varphi)\,\cos\varphi\,\hat{\boldsymbol{e}}_x + \rho(\varphi)\,\sin\varphi\,\hat{\boldsymbol{e}}_y\,, \tag{3.75}$$

which in turn lets us write the unit vectors as

$$\hat{\mathcal{T}}(\varphi) = \frac{\sin\varphi}{\sqrt{\sin^2\varphi + (1-\mathscr{E}^2)^2\cos^2\varphi}}\hat{\boldsymbol{e}}_x + \frac{(1-\mathscr{E}^2)\cos\varphi}{\sqrt{\sin^2\varphi + (1-\mathscr{E}^2)^2\cos^2\varphi}}\hat{\boldsymbol{e}}_y\,, \tag{3.76}$$

$$\hat{\mathcal{N}}(\varphi) = \frac{\sqrt{2}\,(\mathscr{E}^2-1)\cos\varphi}{\sqrt{(\mathscr{E}^4-2\mathscr{E}^2)(\cos 2\varphi+1)+2}}\hat{\boldsymbol{e}}_x + \frac{\sqrt{2}\,\sin\varphi}{\sqrt{(\mathscr{E}^4-2\mathscr{E}^2)(\cos 2\varphi+1)+2}}\hat{\boldsymbol{e}}_y\,, \tag{3.77}$$

$$\hat{\mathcal{B}}(\varphi) = \hat{\boldsymbol{e}}_z\,. \tag{3.78}$$

We can also express the local curvature as

$$\kappa(\varphi) = \frac{1}{2b}\left(\mathscr{E}^2\cos 2\varphi + \mathscr{E}^2 - 2\right)\frac{\left(\mathscr{E}^2-1\right)\sqrt{1-\mathscr{E}^2\cos^2\varphi}}{\left(\sin^2\varphi + (1-\mathscr{E}^2)^2\cos^2\varphi\right)^{3/2}}\,, \tag{3.79}$$

where $b$ is the semi-minor axis. Clearly, the curvature is not constant and is at its highest at the vertex. We write a strain-induced spin-orbit factor that looks similar but has a different physical interpretation,

$$\alpha_N(\varphi) = \frac{a_N\,\mathscr{E}^2}{2}\,(\cos 2\varphi + 1)\,\frac{\left(1-\mathscr{E}^2\right)\sqrt{1-\mathscr{E}^2\cos^2\varphi}}{\left(\sin^2\varphi + (1-\mathscr{E}^2)^2\cos^2\varphi\right)^{3/2}}\,. \tag{3.80}$$

Since it is proportional to the curvature, we have written it as $\alpha_N = a_N\kappa$ in the above. In section 6.5 we will assume that we have a ring we can squeeze in situ to get an ellipse. Assuming the the wire was manufactured as a circle it should not have strain-induced spin-orbit coupling. In the expression above, $\alpha_N \to 0$ as $\mathscr{E} \to 0$. Therefore, it only gives finite strain effect for non-constant curvature and is highest at the ellipse vertex.

# Chapter 4

# Green's functions and quasiclassical theory

In condensed matter physics, Green's functions describe the behavior of particles in or out of equilibrium. Using non-equilibrium Green's functions, we will derive the equations of motion. The approach is similar to the one in ref. [75], but with more weight on the diagram technique. The parametrization and boundary conditions are taken from ref. [67]. Lastly, we present the relations between the Green's function and physical observables.

## 4.1 Non-equilibrium Keldysh Green's functions

Intuitively, the single-particle Green's function, or propagator, discussed in the previous section, should be an expectation value of a creation and an annihilation operator. Annihilating a particle at $(\boldsymbol{r}_1, t_1)$ and creating it at $(\boldsymbol{r}_2, t_2)$ means it must have propagated between the positions in a time $t_1 - t_2$. This assumption is almost correct. We define the non-equilibrium Green's function as the time-ordered field operators [76], namely

$$iG_{\sigma_1\sigma_2}(\boldsymbol{r}_1, t_1;\ \boldsymbol{r}_2, t_2) = \langle T\hat{\psi}_{\sigma_1}(\boldsymbol{r}_1, t_1)\hat{\psi}^\dagger_{\sigma_2}(\boldsymbol{r}_2, t_2)\rangle. \tag{4.1}$$

In contrast to the equilibrium case where the averaging is taken over the stationary state $|0\rangle$, the Green's function as defined in eq. (4.1) is averaged over any quantum state $|n\rangle$ in the system. The $T$ appearing in the average is the time ordering operator, which commutes operators such that they are sorted chronologically by the times $t_1$ and $t_2$. The Green's function can thus be written explicitly as

$$iG_{\sigma_1\sigma_2}(\boldsymbol{r}_1, t_1;\ \boldsymbol{r}_2, t_2) = \begin{cases} \langle\hat{\psi}_{\sigma_1}(\boldsymbol{r}_1, t_1)\hat{\psi}^\dagger_{\sigma_2}(\boldsymbol{r}_2, t_2)\rangle, & t_1 > t_2 \\ -\langle\hat{\psi}^\dagger_{\sigma_2}(\boldsymbol{r}_2, t_2)\hat{\psi}_{\sigma_1}(\boldsymbol{r}_1, t_1)\rangle, & t_1 < t_2. \end{cases} \tag{4.2}$$

Note that $\sigma_1$ and $\sigma_2$ appearing in the propagators are spin indices, either $\uparrow$ or $\downarrow$, and should not be confused with the Pauli matrices $\underline{\sigma}_i$. Next, partially following the notation of Chandrasekhar [75], defining the following Green's functions will be of use later,

$$G^{\alpha\alpha}_{\sigma_1\sigma_2}(\boldsymbol{r}_1, t_1;\ \boldsymbol{r}_2, t_2) = -i\langle T\hat{\psi}_{\sigma_1}(\boldsymbol{r}_1, t_1)\hat{\psi}^\dagger_{\sigma_2}(\boldsymbol{r}_2, t_2)\rangle, \tag{4.3}$$

$$G^{\beta\beta}_{\sigma_1\sigma_2}(\boldsymbol{r}_1, t_1;\ \boldsymbol{r}_2, t_2) = i\langle \tilde{T}\hat{\psi}_{\sigma_1}(\boldsymbol{r}_1, t_1)\hat{\psi}^\dagger_{\sigma_2}(\boldsymbol{r}_2, t_2)\rangle, \tag{4.4}$$

$$G^{\alpha\beta}_{\sigma_1\sigma_2}(\boldsymbol{r}_1, t_1;\ \boldsymbol{r}_2, t_2) = -i\langle \hat{\psi}_{\sigma_1}(\boldsymbol{r}_1, t_1)\hat{\psi}^\dagger_{\sigma_2}(\boldsymbol{r}_2, t_2)\rangle, \tag{4.5}$$

$$G^{\beta\alpha}_{\sigma_1\sigma_2}(\boldsymbol{r}_1, t_1;\ \boldsymbol{r}_2, t_2) = i\langle \hat{\psi}^\dagger_{\sigma_2}(\boldsymbol{r}_2, t_2)\hat{\psi}_{\sigma_1}(\boldsymbol{r}_1, t_1)\rangle. \tag{4.6}$$

In eq. (4.3), we have the standard non-equilibrium Green's function from before. For $t_1 > t_2$ it describes the probability amplitude of a hole at $\boldsymbol{r}_2$ with spin $\sigma_2$ moving to $\boldsymbol{r}_1$,

arriving with spin $\sigma_1$ after a time $t_1 - t_2$. This propagation happens in the non-equilibrium state $|n\rangle$. If, however, $t_1 < t_2$, the fields are commuted, and a hole is created rather than an electron. The elecrtron propagates from $\boldsymbol{r}_1$ with $\sigma_1$ at $t_1$, and ends up in $\boldsymbol{r}_2$ with $\sigma_2$ at $t_2$. Whereas in eq. (4.4), the operator $\tilde{T}$ employs a reverse chronological order to arrange the fields based on their respective times. Thus, for $t_1 > t_2$, the first field removes an electron at $\boldsymbol{r}_1$ with spin $\sigma_1$, which propagates to at $\boldsymbol{r}_2$ with spin $\sigma_2$. Exactly the same is true if $t_1 < t_2$, for which a hole propagates from $\boldsymbol{r}_1$ to $\boldsymbol{r}_2$. The propagator in eq. (4.5) has a somewhat different physical meaning since it contains no time ordering operator. It always describes the propagation of a hole from $\boldsymbol{r}_2$ with $\sigma_2$ to $\boldsymbol{r}_1$ with $\sigma_1$. In the case that $t_1 > t_2$, the hole moves forward in time. If $t_1 < t_2$, the Green's function describes propagation backward in time. Another way to interpret this expression is that it counts the density of holes. There is no time ordering in eq. (4.6), which means that the fields remove an electron at $\boldsymbol{r}_1$ with $\sigma_1$ which moves to $\boldsymbol{r}_2$ with $\sigma_2$, either backwards or forward in time depending on $\mathrm{sgn}(t_1 - t_2)$. It can also be understood as the electron density in the system. The Green's function in eq. (4.5) and eq. (4.6) are often referred to as the greater $G^{>}$ and lesser $G^{<}$ Green's functions, respectively. Generally, the single particle propagator $G^{\alpha\alpha}$ can incorporate the interaction with an external potential $U$, so we denote the non-interacting free electron propagator as $G^{(0)}$. The inverse operator we denote

$$G^{-1}_{(0)}(\boldsymbol{r}_i, t_i) = i\frac{\partial}{\partial t_i} + \frac{\nabla^2_{\boldsymbol{r}_i}}{2m} + \mu\,. \tag{4.7}$$

Acting with this operator on the ideal gas propogator $G^{(0)\alpha\alpha}$, we get a discontinuity at $t_1 = t_2$. The same applies to $G^{(0)\beta\beta}$. Therefore, we can write the following relations

$$G^{-1}_{(0)}(\boldsymbol{r}_1, t_1) G^{(0)\alpha\alpha}_{\sigma_1\sigma_2}(\boldsymbol{r}_1, t_1; \boldsymbol{r}_2, t_2) = \delta(t_1 - t_2)\delta(\boldsymbol{r}_1 - \boldsymbol{r}_2)\,, \tag{4.8}$$

$$G^{-1}_{(0)}(\boldsymbol{r}_1, t_1) G^{(0)\beta\beta}_{\sigma_1\sigma_2}(\boldsymbol{r}_1, t_1; \boldsymbol{r}_2, t_2) = -\delta(t_1 - t_2)\delta(\boldsymbol{r}_1 - \boldsymbol{r}_2)\,, \tag{4.9}$$

$$G^{-1}_{(0)}(\boldsymbol{r}_1, t_1) G^{(0)\alpha\beta}_{\sigma_1\sigma_2}(\boldsymbol{r}_1, t_1; \boldsymbol{r}_2, t_2) = 0\,, \tag{4.10}$$

$$G^{-1}_{(0)}(\boldsymbol{r}_1, t_1) G^{(0)\beta\alpha}_{\sigma_1\sigma_2}(\boldsymbol{r}_1, t_1; \boldsymbol{r}_2, t_2) = 0\,. \tag{4.11}$$

Similar to the Feynman technique in field theory, we can use a diagrammatic approach to Keldysh Green's functions [77]. The dressed and non-interacting Green's functions will be drawn as


Each line and vertex has a mathematical equivalent: We represent each vertex as a convolution of the diagram elements it connects. Without specifying its form, we introduce an external potential $U$. Intuitively, we can argue that the total propagator $G^{\alpha\alpha}$ can be written as a sum of ideal gas solutions $G^{(0)}$ interacting an arbitrary amount with $U$ during the propagation as long as the particle has the correct state at the beginning and end. Thus, the following two first-order interactions should contribute to the total propagation

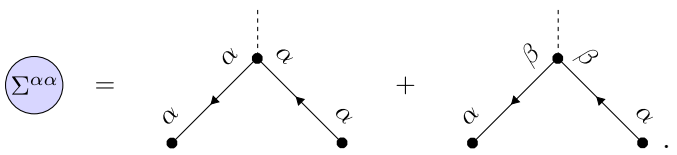


The convolutions $\left(G^{(0)\alpha\alpha} \bullet G^{(0)\alpha\alpha}\right)$ and $\left(G^{(0)\alpha\beta} \bullet G^{(0)\beta\alpha}\right)$ are sums over all possible times and positions the ideal gas in state $\alpha$ can interact once with $U$ in an arbitrary state, and end in state $\alpha$ again. We have also introduced the self-energy $\Sigma^{\alpha\beta}$, which is related to

the interaction with $U$. We now employ a trick that lets us draw the Green's function as a sum of all orders of interactions the electron may experience during the propagation. Factorizing the higher-order interactions, we obtain a recursive equation for $G^{\alpha\alpha}$. Diagrammatically, we can draw it as

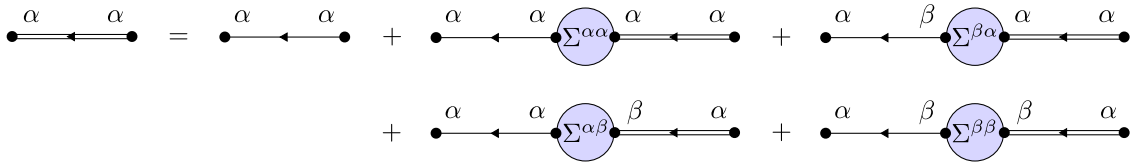


We can write similar equations for the other propagators as well. Therefore, it is useful to collect all of them into a matrix, where the superscripts denote the index, such that the matrix reads

$$\underline{G}_{\sigma_1\sigma_2}(\boldsymbol{r}_1,t_1;\boldsymbol{r}_2,t_2)=\begin{pmatrix} G^{\alpha\alpha}_{\sigma_1\sigma_2}(\boldsymbol{r}_1,t_1;\boldsymbol{r}_2,t_2) & G^{\alpha\beta}_{\sigma_1\sigma_2}(\boldsymbol{r}_1,t_1;\boldsymbol{r}_2,t_2) \\ G^{\beta\alpha}_{\sigma_1\sigma_2}(\boldsymbol{r}_1,t_1;\boldsymbol{r}_2,t_2) & G^{\beta\beta}_{\sigma_1\sigma_2}(\boldsymbol{r}_1,t_1;\boldsymbol{r}_2,t_2)\end{pmatrix}. \tag{4.12}$$

We have only found the equation for the upper left element. However, finding the rest is trivial. Writing the equation in the diagram for all of the propagators simultaneously, we express it as

$$\underline{G}(x_1,x_2)=\underline{G}^{(0)}(x_1,x_2)+\underline{G}^{(0)}(x_1,x_4)\bullet\underline{\Sigma}(x_4,x_3)\bullet\underline{G}(x_3,x_2), \tag{4.13}$$

where we introduced the self-energy matrix

$$\underline{\Sigma}_{\sigma_1\sigma_2}(\boldsymbol{r}_1,t_1;\boldsymbol{r}_2,t_2)=\begin{pmatrix} \Sigma^{\alpha\alpha}_{\sigma_1\sigma_2}(\boldsymbol{r}_1,t_1;\boldsymbol{r}_2,t_2) & \Sigma^{\alpha\beta}_{\sigma_1\sigma_2}(\boldsymbol{r}_1,t_1;\boldsymbol{r}_2,t_2) \\ \Sigma^{\beta\alpha}_{\sigma_1\sigma_2}(\boldsymbol{r}_1,t_1;\boldsymbol{r}_2,t_2) & \Sigma^{\beta\beta}_{\sigma_1\sigma_2}(\boldsymbol{r}_1,t_1;\boldsymbol{r}_2,t_2)\end{pmatrix}. \tag{4.14}$$

The bullet product is a convolution over internal variables and a matrix product in Keldysh space. The formal definition is given in eq. (B.1). Equation (4.13) is called the Dyson equation and relates the non-interacting propagator with the interacting one. The interaction is encoded in the self-energy. Note that the four Green's functions in eq. (4.12) are not linearly independent. Therefore, they are related by linear equations of the form

$$G^{\alpha\alpha}+G^{\beta\beta}=G^{\alpha\beta}+G^{\beta\alpha}. \tag{4.15}$$

Using the definitions of the Green's functions in eq. (4.3)-(4.6) the non-equilibrium retarded and advanced Green's functions are defined as

$$G^A=G^{\alpha\alpha}-G^{\alpha\beta}=G^{\beta\alpha}-G^{\beta\beta}, \tag{4.16}$$
$$G^R=G^{\alpha\alpha}-G^{\beta\alpha}=G^{\alpha\beta}-G^{\beta\beta}. \tag{4.17}$$

Exactly how they act and what they describe in terms of electron or hole propagation becomes evident when writing them as averages. They can be expressed as

$$G^A_{\sigma_1\sigma_2}(\boldsymbol{r}_1,t_1;\ \boldsymbol{r}_2,t_2)=\begin{cases} 0, & t_1>t_2 \\ i\langle\{\hat{\psi}_{\sigma_1}(\boldsymbol{r}_1,t_1),\hat{\psi}^\dagger_{\sigma_2}(\boldsymbol{r}_2,t_2)\}\rangle, & t_1<t_2\end{cases} \tag{4.18}$$

$$G^R_{\sigma_1\sigma_2}(\boldsymbol{r}_1,t_1;\ \boldsymbol{r}_2,t_2)=\begin{cases} -i\langle\{\hat{\psi}_{\sigma_1}(\boldsymbol{r}_1,t_1),\hat{\psi}^\dagger_{\sigma_2}(\boldsymbol{r}_2,t_2)\}\rangle, & t_1>t_2 \\ 0, & t_1<t_2,\end{cases} \tag{4.19}$$

where the anti-commutator has been inserted. These relate to the electron and hole densities for particles propagating forwards in time for $G^R$ and backward for $G^A$. Since the elements in eq. (4.12) are not linearly independent, expressing it such that one of

the entries is zero can be advantageous. We perform the rotation $\underline{G} \to \underline{\sigma}_3\,\underline{G}$, and then $\underline{G} \to \underline{Q}\,\underline{G}\,\underline{Q}^\dagger$ where

$$\underline{Q} = \frac{1}{\sqrt{2}}\left(\underline{\sigma}_0 - i\underline{\sigma}_2\right). \tag{4.20}$$

The resulting matrix has the form

$$\underline{G} = \begin{pmatrix} G^A & G^K \\ 0 & G^R \end{pmatrix}, \tag{4.21}$$

where the retarded and advanced Green's functions have been defined in eq. (4.18) and (4.19), and where $G^K$ is the Keldysh Green's function, which is defined as

$$G^K_{\sigma_1\sigma_2}(\boldsymbol{r}_1, t_1; \boldsymbol{r}_2, t_2) = -i\left\langle\left[\hat{\psi}_{\sigma_1}(\boldsymbol{r}_1, t_1), \hat{\psi}^\dagger_{\sigma_2}(\boldsymbol{r}_2, t_2)\right]\right\rangle. \tag{4.22}$$

Whereas the advanced and retarded Green's functions are related to the electron densities, the Keldysh component describes properties of the system out of equilibrium. We note that all the above propagators describe single-particle behavior. Superconductivity is mediated by an interaction between pairs of particles. Thus, we introduce Nambu⊗spin space. We will use it throughout this thesis to organize interactions and dynamics for electrons and holes. In Nambu⊗spin space, the hole-spin field operators are defined as

$$\hat{\boldsymbol{\Psi}}_1 = \begin{pmatrix} \hat{\psi}_\uparrow(\boldsymbol{r}_1, t_1) \\ \hat{\psi}_\downarrow(\boldsymbol{r}_1, t_1) \\ \hat{\psi}^\dagger_\uparrow(\boldsymbol{r}_1, t_1) \\ \hat{\psi}^\dagger_\downarrow(\boldsymbol{r}_1, t_1) \end{pmatrix}, \qquad \hat{\boldsymbol{\Psi}}_2^\dagger = \begin{pmatrix} \hat{\psi}^\dagger_\uparrow(\boldsymbol{r}_2, t_2) & \hat{\psi}^\dagger_\downarrow(\boldsymbol{r}_2, t_2) & \hat{\psi}_\uparrow(\boldsymbol{r}_2, t_2) & \hat{\psi}_\downarrow(\boldsymbol{r}_2, t_2) \end{pmatrix}. \tag{4.23}$$

The Green's functions used in eq. (4.21) are defined very similarly in this formalism. We must transpose the product twice to ensure the commutation is correct. The propagators can be written as

$$\hat{G}^A(\boldsymbol{r}_1, t_1; \boldsymbol{r}_2, t_2) = \begin{cases} 0, & t_1 > t_2 \\ +i\hat{\tau}_3\langle \hat{\boldsymbol{\Psi}}_1\hat{\boldsymbol{\Psi}}_2^\dagger + \left(\hat{\boldsymbol{\Psi}}_2^{\dagger T}\hat{\boldsymbol{\Psi}}_1^T\right)^T\rangle, & t_1 < t_2 \end{cases} \tag{4.24}$$

$$\hat{G}^R(\boldsymbol{r}_1, t_1; \boldsymbol{r}_2, t_2) = \begin{cases} -i\hat{\tau}_3\langle \hat{\boldsymbol{\Psi}}_1\hat{\boldsymbol{\Psi}}_2^\dagger + \left(\hat{\boldsymbol{\Psi}}_2^{\dagger T}\hat{\boldsymbol{\Psi}}_1^T\right)^T\rangle, & t_1 > t_2 \\ 0, & t_1 < t_2 \end{cases} \tag{4.25}$$

$$\hat{G}^K(\boldsymbol{r}_1, t_1; \boldsymbol{r}_2, t_2) = -i\langle \hat{\boldsymbol{\Psi}}_1\hat{\boldsymbol{\Psi}}_2^\dagger - \left(\hat{\boldsymbol{\Psi}}_2^{\dagger T}\hat{\boldsymbol{\Psi}}_1^T\right)^T\rangle. \tag{4.26}$$

We can write out the advanced Green's function. Doing so should also help make the next steps in the derivation clearer. In matrix form, with the Heaviside step function $\theta$, it is written as

$$\hat{G}^A(x_1, x_2) = i\theta(t_2 - t_1)\begin{pmatrix} \langle\{\hat{\psi}_{1\uparrow}, \hat{\psi}^\dagger_{2\uparrow}\}\rangle & \langle\{\hat{\psi}_{1\uparrow}, \hat{\psi}^\dagger_{2\downarrow}\}\rangle & \langle\{\hat{\psi}_{1\uparrow}, \hat{\psi}_{2\uparrow}\}\rangle & \langle\{\hat{\psi}_{1\uparrow}, \hat{\psi}_{2\downarrow}\}\rangle \\ \langle\{\hat{\psi}_{1\downarrow}, \hat{\psi}^\dagger_{2\uparrow}\}\rangle & \langle\{\hat{\psi}_{1\downarrow}, \hat{\psi}^\dagger_{2\downarrow}\}\rangle & \langle\{\hat{\psi}_{1\downarrow}, \hat{\psi}_{2\uparrow}\}\rangle & \langle\{\hat{\psi}_{1\downarrow}, \hat{\psi}_{2\downarrow}\}\rangle \\ -\langle\{\hat{\psi}^\dagger_{1\uparrow}, \hat{\psi}^\dagger_{2\uparrow}\}\rangle & -\langle\{\hat{\psi}^\dagger_{1\uparrow}, \hat{\psi}^\dagger_{2\downarrow}\}\rangle & -\langle\{\hat{\psi}^\dagger_{1\uparrow}, \hat{\psi}_{2\uparrow}\}\rangle & -\langle\{\hat{\psi}^\dagger_{1\uparrow}, \hat{\psi}_{2\downarrow}\}\rangle \\ -\langle\{\hat{\psi}^\dagger_{1\downarrow}, \hat{\psi}^\dagger_{2\uparrow}\}\rangle & -\langle\{\hat{\psi}^\dagger_{1\downarrow}, \hat{\psi}^\dagger_{2\downarrow}\}\rangle & -\langle\{\hat{\psi}^\dagger_{1\downarrow}, \hat{\psi}_{2\uparrow}\}\rangle & -\langle\{\hat{\psi}^\dagger_{1\downarrow}, \hat{\psi}_{2\downarrow}\}\rangle \end{pmatrix}. \tag{4.27}$$

Note that the above matrix's bottom half essentially is the upper half's complex conjugate. This is because there is a symmetry between the electron and hole part of the propagator. In this thesis, we will concern ourselves with equilibrium systems. In that case, the

advanced, retarded, and Keldysh Green's functions are closely related. We can write the following relations [78]

$$\hat{G}^A = -\hat{\tau}_3\big(\hat{G}^R\big)^\dagger\hat{\tau}_3\,, \qquad \hat{G}^K = \big(\hat{G}^A - \hat{G}^R\big)\tanh\!\left(\frac{\beta\mathcal{E}}{2}\right). \tag{4.28}$$

Next, we introduce the anomalous Green's functions, which are quite similar to eqs. (4.18) and (4.19), but differ in the operators, only containing $\hat{\psi}_\sigma(\boldsymbol{r},t)$ and none of the Hermitian conjugate counterparts $\hat{\psi}^\dagger_\sigma(\boldsymbol{r},t)$. They are written as

$$F^A_{\sigma_1\sigma_2}(\boldsymbol{r}_1,t_1;\boldsymbol{r}_2,t_2) = \begin{cases} 0, & t_1 > t_2 \\ +i\left\langle\{\hat{\psi}_{\sigma_1}(\boldsymbol{r}_1,t_1),\hat{\psi}_{\sigma_2}(\boldsymbol{r}_2,t_2)\}\right\rangle, & t_1 < t_2 \end{cases} \tag{4.29}$$

$$F^R_{\sigma_1\sigma_2}(\boldsymbol{r}_1,t_1;\boldsymbol{r}_2,t_2) = \begin{cases} -i\left\langle\{\hat{\psi}_{\sigma_1}(\boldsymbol{r}_1,t_1),\hat{\psi}_{\sigma_2}(\boldsymbol{r}_2,t_2)\}\right\rangle, & t_1 > t_2 \\ 0, & t_1 < t_2 \end{cases} \tag{4.30}$$

$$F^K_{\sigma_1\sigma_2}(\boldsymbol{r}_1,t_1;\boldsymbol{r}_2,t_2) = -i\left\langle\{\hat{\psi}_{\sigma_1}(\boldsymbol{r}_1,t_1),\hat{\psi}_{\sigma_2}(\boldsymbol{r}_2,t_2)\}\right\rangle. \tag{4.31}$$

We can write the Green's functions in Nambu⊗spin space by applying the above definitions and the observations about the matrix structure. They are

$$\hat{G}^{A,R}(x_1,x_2) = \begin{pmatrix} \underline{G}^{A,R}(x_1,x_2) & \underline{F}^{A,R}(x_1,x_2) \\ \underline{F}^{A,R}(x_1,x_2)^* & \underline{G}^{A,R}(x_1,x_2)^* \end{pmatrix}, \tag{4.32}$$

$$\hat{G}^{K}(x_1,x_2) = \begin{pmatrix} \underline{G}^{K}(x_1,x_2) & \underline{F}^{K}(x_1,x_2) \\ -\underline{F}^{K}(x_1,x_2)^* & -\underline{G}^{K}(x_1,x_2)^* \end{pmatrix}, \tag{4.33}$$

where the components are 2x2 matrices in spin space that can be summarized as

$$\underline{G}^{A,R,K}(x_1,x_2) = \begin{pmatrix} G^{A,R,K}_{\uparrow\uparrow}(x_1,x_2) & G^{A,R,K}_{\uparrow\downarrow}(x_1,x_2) \\ G^{A,R,K}_{\downarrow\uparrow}(x_1,x_2) & G^{A,R,K}_{\downarrow\downarrow}(x_1,x_2) \end{pmatrix}, \tag{4.34}$$

$$\underline{F}^{A,R,K}(x_1,x_2) = \begin{pmatrix} F^{A,R,K}_{\uparrow\uparrow}(x_1,x_2) & F^{A,R,K}_{\uparrow\downarrow}(x_1,x_2) \\ F^{A,R,K}_{\downarrow\uparrow}(x_1,x_2) & F^{A,R,K}_{\downarrow\downarrow}(x_1,x_2) \end{pmatrix}. \tag{4.35}$$

These components are the Green's functions defined in eqs. (4.18), (4.19), (4.22) and (4.29) to (4.31). Similarily to eq. (4.21), we can define a Green's function to collect all these parts, as well as the self-energy

$$\check{G}(x_1,x_2) = \begin{pmatrix} \hat{G}^A(x_1,x_2) & \hat{G}^K(x_1,x_2) \\ 0 & \hat{G}^R(x_1,x_2) \end{pmatrix}, \tag{4.36}$$

$$\check{\Sigma}(x_1,x_2) = \begin{pmatrix} \hat{\Sigma}^A(x_1,x_2) & \hat{\Sigma}^K(x_1,x_2) \\ 0 & \hat{\Sigma}^R(x_1,x_2) \end{pmatrix}. \tag{4.37}$$

With these definitions, we can again write the Dyson equation using the integral bullet product notation as

$$\check{G}(x_1,x_2) = \check{G}^0(x_1,x_2) + \check{G}^0(x_1,x_4)\bullet\check{\Sigma}(x_4,x_3)\bullet\check{G}(x_3,x_2), \tag{4.38}$$

where $\check{G}^0$ is the non-interacting Green's function in Nambu⊗spin space. The free electron propagator in spin-space is denoted $\hat{G}_{(0)}$. Its inverse defines it

$$\hat{G}^{-1}_{(0)}(\boldsymbol{r}_i,t_i) = i\hat{\tau}_3\,\partial_{t_i} + \frac{\nabla^2_{\boldsymbol{r_i}}}{2m} + \mu. \tag{4.39}$$

Acting on the non-interacting Green's function in Nambu⊗Spin space, we get a Dirac-delta spike,

$$\hat{G}^{-1}_{(0)}(x_1)\check{G}^{(0)}(x_1,x_2) = \delta^4(x_1 - x_2). \tag{4.40}$$

Next, we will act with the inverse free electron Green's function on the Dyson equation to write it in a simpler form. Acting with it from the left on both sides, we get

$$\hat{G}^{-1}_{(0)}(x_1)\check{G}(x_1,x_2) = \delta^4(x_1 - x_2) + \check{\Sigma}(x_1,x_3) \bullet \check{G}(x_3,x_2). \tag{4.41}$$

To find an equation with terms that cancel, we take the complex conjugate of the above equation, which gives

$$\check{G}(x_1,x_s)\overleftarrow{\hat{G}}^{-1}_{(0)}(x_2) = \delta^4(x_1 - x_2) + \check{G}(x_1,x_3) \bullet \check{\Sigma}(x_3,x_2), \tag{4.42}$$

where the arrow indicates that $\hat{G}^{-1}_{(0)}(x_2)$ acts to the left, as opposed to ordinary operators. It can be understood as taking the hermitian conjugate and operating with it from the left. Now, subtracting these from each other, we get the Gor'kov equation

$$\left[\hat{G}^{-1}_{(0)}(x_1,x_2) - \check{\Sigma}(x_1,x_2), \check{G}(x_1,x_2)\right]^{\bullet} = 0, \tag{4.43}$$

where the bullet commutator $[A,B]^{\bullet} \equiv A \bullet B - B \bullet A$ was inserted. Also, the operator $\hat{G}^{-1}_{(0)}(x_1,x_2)$ should be interepeted as acting on $x_1$ from the left and $x_2$ from the right. This will be the starting point for finding the equation of motion for the system. In order to simplify the calculations, we need to make certain assumptions and restrictions in the Green's function and derive self-energies. This will allow us to express the Gor'kov equation in a more manageable way. Although eq. (4.38) provides a complete description of the system, it is not straightforward to work with since the interactions and self-energies have not been specified yet. We will work on these aspects in the next subsections to simplify calculations.

## 4.2 Mixed representation and quasiclassical approximation

This section will present the quasiclassical approximation, which puts certain constraints on the propagator of the system. The Green's function describing the system oscillates as a function of the relative coordinate with a length on the scale of the Fermi wavelength, which is much smaller than the characteristic lengths in the problems we are studying, for instance, the superconducting coherence length. Thus, the two-electron wavefunctions we study mainly depend on the center-of-mass coordinate. Eilenberger [79] and Larkin [80] realized that for most problems, it is sufficient to integrate out the relative coordinate. In doing so, we are only studying the envelope of the quantum mechanical wave function. This approximation assumes that only particles with energies close to the Fermi surface contribute to physical processes. Therefore, we often only keep the direction of the momentum but set the magnitude to the Fermi momentum $k_F$. Note that this assumption restricts all physical predictions this theory gives to the Fermi surface.

In the quasiclassical approximation, we make a change of variables to a relative coordinate and a center-of-mass coordinate. To obtain the quasiclassical Green's function, we first define new variables

$$\boldsymbol{R} = \frac{1}{2}(\boldsymbol{r}_1 + \boldsymbol{r}_2), \qquad \boldsymbol{r} = \boldsymbol{r}_1 - \boldsymbol{r}_2, \qquad T = \frac{1}{2}(t_1 + t_2), \qquad t = t_1 - t_2. \tag{4.44}$$

As we have argued, integrating out the relative coordinates is often sufficient. Therefore, we introduce a new Green's function in which we Fourier transform of relative space and time coordinates,

$$\check{\mathcal{G}}(\boldsymbol{R},T,\boldsymbol{p},\mathcal{E}) = \int dt\, e^{i\mathcal{E}t} \int d^3r\, e^{-i\boldsymbol{p}\cdot\boldsymbol{r}}\, \check{G}(\boldsymbol{R},T,\boldsymbol{r},t). \tag{4.45}$$

We can use this Fourier-transformed Green's function to introduce the quasiclassical one. For this, we use the approximation discussed at the beginning of this section; we restrict the momentum $\boldsymbol{p}$ to be on the Fermi surface $\boldsymbol{p}_F$, only keeping its direction. Expressing this in terms of the Dirac-delta, we can write it as

$$\check{\mathcal{G}}(\boldsymbol{R},T,\boldsymbol{p},\mathcal{E}) = -i\pi\delta(\xi_{\boldsymbol{p}})\, \check{g}(\boldsymbol{R},T,\hat{\boldsymbol{p}}_F,\mathcal{E}). \tag{4.46}$$

The delta function helps pick the correct momentum from all kinetic energy possibilities. The quantity $\xi_p$ is the kinetic energy relative to the chemical potential $\xi_{\boldsymbol{p}} = \frac{\boldsymbol{p}^2}{2m} - \mu$, and $\hat{\boldsymbol{p}}_F = \frac{\boldsymbol{p}_F}{|\boldsymbol{p}_F|}$. Integrating eq. (4.46) on both sides gives an expression for the envelope function we are interested in

$$\check{g}(\boldsymbol{R},T,\hat{\boldsymbol{p}}_F,\mathcal{E}) = \frac{i}{\pi}\int d\xi_{\boldsymbol{p}}\, \check{\mathcal{G}}(\boldsymbol{R},T,\boldsymbol{p},\mathcal{E}). \tag{4.47}$$

This is the quasiclassical Green's function, which will be important later in this thesis. It is not well-behaved at high energies, so it is common in the literature to introduce a cutoff energy or replace the integral with a semicircle in the upper and lower plane [81]. The resulting quasiclassical Green's function is ordered similarly as before, namely

$$\check{g}(\boldsymbol{R},T,\hat{\boldsymbol{p}}_F,\mathcal{E}) = \begin{pmatrix} \hat{g}^A(\boldsymbol{R},T,\hat{\boldsymbol{p}}_F,\mathcal{E}) & \hat{g}^K(\boldsymbol{R},T,\hat{\boldsymbol{p}}_F,\mathcal{E}) \\ 0 & \hat{g}^R(\boldsymbol{R},T,\hat{\boldsymbol{p}}_F,\mathcal{E}) \end{pmatrix}. \tag{4.48}$$

The components of the above matrix can be expressed as 4x4 matrices with 2x2 quasiclassical Green's functions as components. These are

$$\hat{g}^{A,R}(\boldsymbol{R},T,\hat{\boldsymbol{p}}_F,\mathcal{E}) = \begin{pmatrix} \underline{g}^{A,R}(\boldsymbol{R},T,\hat{\boldsymbol{p}}_F,\mathcal{E}) & \underline{f}^{A,R}(\boldsymbol{R},T,\hat{\boldsymbol{p}}_F,\mathcal{E}) \\ -\underline{\tilde{f}}^{A,R}(\boldsymbol{R},T,\hat{\boldsymbol{p}}_F,\mathcal{E}) & -\underline{\tilde{g}}^{A,R}(\boldsymbol{R},T,\hat{\boldsymbol{p}}_F,\mathcal{E}) \end{pmatrix}, \tag{4.49}$$

$$\hat{g}^{K}(\boldsymbol{R},T,\hat{\boldsymbol{p}}_F,\mathcal{E}) = \begin{pmatrix} \underline{g}^{K}(\boldsymbol{R},T,\hat{\boldsymbol{p}}_F,\mathcal{E}) & \underline{f}^{K}(\boldsymbol{R},T,\hat{\boldsymbol{p}}_F,\mathcal{E}) \\ \underline{\tilde{f}}^{K}(\boldsymbol{R},T,\hat{\boldsymbol{p}}_F,\mathcal{E}) & \underline{\tilde{g}}^{K}(\boldsymbol{R},T,\hat{\boldsymbol{p}}_F,\mathcal{E}) \end{pmatrix}, \tag{4.50}$$

where $\tilde{\cdot}$ is an operation of complex conjugation $\cdot^*$ as well as transforming the energy as $\mathcal{E} \to -\mathcal{E}$. The signs are different from the ordinary Green's functions due to the tilde conjugation because of the Fourier transform. If we consider the transformation of the entire matrix, we can write it as

$$\check{g}(\boldsymbol{R},T,\hat{\boldsymbol{p}}_F,\mathcal{E}) = \frac{i}{\pi}\int d\xi_{\boldsymbol{p}} \int dt\, e^{i\mathcal{E}t} \int d^3r\, e^{-i\boldsymbol{p}\cdot\boldsymbol{r}}\, \check{G}(\boldsymbol{R}+\boldsymbol{r}/2,T+t/2;\boldsymbol{R}-\boldsymbol{r}/2,T-t/2). \tag{4.51}$$

Next, we consider only one of the elements. From the above transform, we see that the anomalous quasiclassical retarded Green's function is

$$\underline{f}^R(\boldsymbol{R},T,\hat{\boldsymbol{p}}_F,\mathcal{E}) = \frac{i}{\pi}\int d\xi_{\boldsymbol{p}} \int d^3r \int dt\, e^{i\mathcal{E}t - i\boldsymbol{p}\cdot\boldsymbol{r}}\, \underline{F}^R(\boldsymbol{R},T,\boldsymbol{r},t). \tag{4.52}$$

Taking the complex conjugate of the integral leaves us with

$$\underline{f}^R(\boldsymbol{R},T,\hat{\boldsymbol{p}}_F,\mathcal{E})^* = -\frac{i}{\pi}\int d\xi_{\boldsymbol{p}}\int d^3r\int dt\, e^{-i\mathcal{E}t-i\boldsymbol{p}\cdot\boldsymbol{r}}\underline{F}^R(\boldsymbol{R},T,\boldsymbol{r},t)^*. \tag{4.53}$$

If we now, however, change the sign in front of the integral, as well as the sign of the energy $\mathcal{E}\to-\mathcal{E}$, we get the desired form, namely a Fourier transform

$$-\underline{\tilde{f}}^R(\boldsymbol{R},T,\hat{\boldsymbol{p}}_F,\mathcal{E}) = \frac{i}{\pi}\int d\xi_{\boldsymbol{p}}\int d^3r\int dt\, e^{i\mathcal{E}t-i\boldsymbol{p}\cdot\boldsymbol{r}}\underline{F}^R(\boldsymbol{R},T,\boldsymbol{r},t)^*. \tag{4.54}$$

This Green's function is normalized such that the product with itself is unity.

$$\check{g}\check{g} = \begin{pmatrix}\hat{g}^A\hat{g}^A & \hat{g}^A\hat{g}^K+\hat{g}^K\hat{g}^R\\ 0 & \hat{g}^R\hat{g}^R\end{pmatrix} = \underline{\sigma}_0\otimes\hat{\tau}_0, \tag{4.55}$$

which can also be summarized by the conditions

$$\hat{g}^A\hat{g}^K = -\hat{g}^K\hat{g}^R, \qquad \hat{g}^A\hat{g}^A = \hat{g}^R\hat{g}^R = \hat{\tau}_0. \tag{4.56}$$

## 4.3 Self-energies

Until now, the self-energy $\check{\Sigma}$ has been left unspecified. The structure of the self-energy depends on the system and the kind of interactions that cause it. Therefore, there is not a general equation describing all kinds of self-energies. Presented here are the self-energies relevant to the physical systems we study. The first self-energy we can write down is that of a superconductor, which is defined by the superconducting order parameter,

$$\check{\Sigma}_{\mathrm{SC}} = \hat{\Delta} = \begin{pmatrix}0 & \underline{\Delta}\\ \underline{\Delta}^* & 0\end{pmatrix}, \tag{4.57}$$

where $\underline{\Delta} = \mathrm{antidiag}(\Delta,-\Delta)$ and $\Delta = g\langle\hat{\psi}_{1\downarrow}\hat{\psi}_{2\uparrow}\rangle$ with $g$ being a coupling strength coefficient. Since it describes the interaction between pairs of particles, it is on the antidiagonal. Generally, the order parameter is complex, and its magnitude describes the gap size in the superconducting state. It is an important quantity, as only energies above this gap can excite superconducting states. Since we will consider superconductors in proximity to ferromagnets, we need their self-energy as well. For weak ferromagnets, the self-energy can be written as

$$\check{\Sigma}_{\mathrm{FM}} = \boldsymbol{h}\cdot\hat{\boldsymbol{\sigma}}, \tag{4.58}$$

where $\boldsymbol{h}$ is the exchange field, and $\hat{\boldsymbol{\sigma}} = \mathrm{diag}(\boldsymbol{\sigma},\boldsymbol{\sigma}^*)$. The two self-energies presented are intrinsic to the materials. That means that they will be present regardless of impurities or other interactions.

Next, we will add the extrinsic contributions to the total self-energy $\check{\Sigma}$. First, we consider how particles scatter on impurities. We write the potential arising from non-magnetic impurities as

$$V_{\mathrm{imp}}(\boldsymbol{r}) = \sum_i U(\boldsymbol{r}-\boldsymbol{r}_i), \tag{4.59}$$

where $U(\boldsymbol{r}-\boldsymbol{r}_i)$ is the potential of an impurity located at $\boldsymbol{r}_i$. If we assume that the potential only is a small perturbation of the non-interacting Green's function, we can rewrite eq. (4.40) as

$$\left[\hat{G}^{-1}_{(0)}(\boldsymbol{r}_1) - \check{\tau}_0 V_{\text{imp}}(\boldsymbol{r}_1)\right] \check{G}(\boldsymbol{r}_1,\boldsymbol{r}_2) = \delta^3(\boldsymbol{r}_1-\boldsymbol{r}_2), \tag{4.60}$$

where we have suppressed the Fourier transform of the relative time coordinate to the quasiparticle energy $\mathcal{E}$, such that we write $\check{G}(\boldsymbol{r}_1,\boldsymbol{r}_2;\mathcal{E}) \equiv \check{G}(\boldsymbol{r}_1,\boldsymbol{r}_2)$ [82]. We can write this equation similarly to the Dyson equation. Therefore, we write it as

$$\check{G}(\boldsymbol{r}_1,\boldsymbol{r}_2) = \check{G}^{(0)}(\boldsymbol{r}_1,\boldsymbol{r}_2) + \int d^3r_3\, \check{G}^{(0)}(\boldsymbol{r}_1,\boldsymbol{r}_3)\, V_{\text{imp}}(\boldsymbol{r}_3)\, \check{G}(\boldsymbol{r}_3,\boldsymbol{r}_2), \tag{4.61}$$

which can be confirmed by inserting eq. (4.60) into eq. (4.61) [83]. The self-energies will act in the same space as our quasiclassical Green's function. Therefore, for later convenience, we perform a Fourier transformation to momentum space. We can write the Dyson equation as

$$\check{\mathcal{G}}(\boldsymbol{p}_1,\boldsymbol{p}_2) = \check{\mathcal{G}}^{(0)}(\boldsymbol{p}_1)\delta^3(\boldsymbol{p}_1-\boldsymbol{p}_2) + \check{\mathcal{G}}^{(0)}(\boldsymbol{p}_1)\int \frac{d^3p_3}{(2\pi)^3} V_{\text{imp}}(\boldsymbol{p}_1-\boldsymbol{p}_3)\, \check{\mathcal{G}}(\boldsymbol{p}_3,\boldsymbol{p}_2), \tag{4.62}$$

where we have transformed the impurity potential as $V_{\text{imp}}(\boldsymbol{q}) = \sum_i U(\boldsymbol{q}) e^{-i\boldsymbol{q}\cdot\boldsymbol{r}_i}$. We note that the Fourier transformed Green's function $\check{\mathcal{G}}$ is on either side of the equation. Therefore, one trick is to solve it iteratively. That means inserting the entire left-hand side into $\check{\mathcal{G}}(\boldsymbol{p}_3,\boldsymbol{p}_2)$ furthest to the right. This will, however, add another Green's function we need to insert. We denote these terms

$$\begin{aligned}
\check{\mathcal{G}}(\boldsymbol{p}_1,\boldsymbol{p}_2) &= \check{\mathcal{G}}^{(0)}(\boldsymbol{p}_1)\delta^3(\boldsymbol{p}_1-\boldsymbol{p}_2) + \check{\mathcal{G}}^{(0)}(\boldsymbol{p}_1) V_{\text{imp}}(\boldsymbol{p}_1-\boldsymbol{p}_2)\, \check{\mathcal{G}}^{(0)}(\boldsymbol{p}_2) \\
&\quad + \check{\mathcal{G}}^{(0)}(\boldsymbol{p}_1)\int \frac{d^3p_3}{(2\pi)^3} V_{\text{imp}}(\boldsymbol{p}_1-\boldsymbol{p}_3)\check{\mathcal{G}}^{(0)}(\boldsymbol{p}_3) V_{\text{imp}}(\boldsymbol{p}_3-\boldsymbol{p}_2)\check{\mathcal{G}}^{(0)}(\boldsymbol{p}_2) + \dots \\
&= \check{\mathcal{G}}^{(0)}(\boldsymbol{p}_1,\boldsymbol{p}_2) + \check{\mathcal{G}}^{(1)}(\boldsymbol{p}_1,\boldsymbol{p}_2) + \check{\mathcal{G}}^{(2)}(\boldsymbol{p}_1,\boldsymbol{p}_2) + \dots
\end{aligned} \tag{4.63}$$

This contains an infinite number of terms with no simple solution. However, we can assume that the density of impurities is large, so we average over them [82–84]. This will simplify the next steps. The impurity averaged Green's function is defined as

$$\langle \check{\mathcal{G}}(\boldsymbol{p}_1,\boldsymbol{p}_2)\rangle_{\text{imp}} = \prod_i \left(\frac{1}{V}\int d^3r_i\right) \check{\mathcal{G}}(\boldsymbol{p}_1,\boldsymbol{p}_2), \tag{4.64}$$

which effectively changes the impurity potentials with the averaged ones,

$$\langle V_{\text{imp}}(\boldsymbol{q})\rangle_{\text{imp}} = \left\langle \sum_i U(\boldsymbol{q}) e^{-i\boldsymbol{q}\cdot r_i}\right\rangle_{\text{imp}} = (2\pi)^3\, n_{\text{imp}}\, U(\boldsymbol{q})\delta^3(\boldsymbol{q}). \tag{4.65}$$

There are products of impurity potentials in the higher order terms in eq. (4.63). The number of factors of impurity potentials $n$ is proportional to the order we denoted in $\check{\mathcal{G}}^{(n)}$. We will truncate the self-energy in the second order. Thus, we only consider the product between two impurity potentials,

$$\begin{aligned}
\langle V_{\text{imp}}(\boldsymbol{p}_1) V_{\text{imp}}(\boldsymbol{p}_2)\rangle_{\text{imp}} &= U(\boldsymbol{p}_1)U(\boldsymbol{p}_2)\left[\left\langle \sum_i e^{-i(\boldsymbol{p}_1+\boldsymbol{p}_2)\cdot r_i}\right\rangle_{\text{imp}} + \left\langle \sum_{i\neq j} e^{-i\boldsymbol{p}_1\cdot r_i - i\boldsymbol{p}_2\cdot r_j}\right\rangle_{\text{imp}}\right] \\
&\approx U(\boldsymbol{p}_1)U(\boldsymbol{p}_2)\left[(2\pi)^3 n_{\text{imp}}\delta^3(\boldsymbol{p}_1-\boldsymbol{p}_2) + (2\pi)^6 n_{\text{imp}}^2 \delta^3(\boldsymbol{p}_1)\delta(\boldsymbol{p}_2)\right],
\end{aligned} \tag{4.66}$$

where the approximation $n_{\rm imp}(n_{\rm imp}+1) \approx n_{\rm imp}^2$ was made. This is consistent with the assumption of a high density of impurities.

For the next step, we will use the Feynman diagrammatic approach. Each diagram is associated with a mathematical translation as before. However, since the propagators are in momentum space, we have additional rules: 1) at each vertex the total momentum is conserved 2) with every propagator $\check{\mathcal{G}}^{(0)}(\boldsymbol{p}_1)$ there is a momentum integral 3) there is a factor $(2\pi)^3\delta^3(\boldsymbol{p}_1-\boldsymbol{p}_2)$ for every diagram. Following these rules, the Dyson equation (4.38) written with Feynman diagrams is

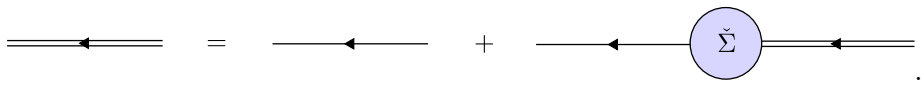


The self-energy takes the form

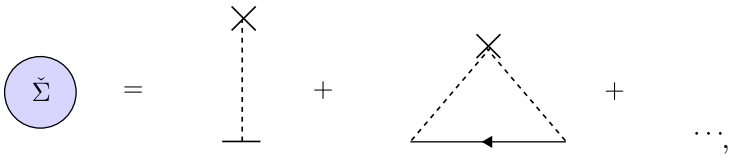


where we have only explicitly drawn contributions to the second order. The first term is a constant and can be discarded [83]. Thus, the self-energy to second order can be drawn as

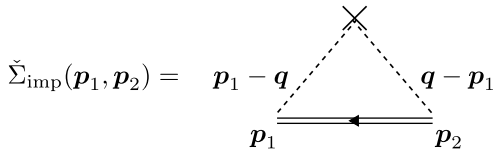


From this diagram, we can write the self-energy in momentum space as

$$\begin{aligned}\check{\Sigma}_{\rm imp}(\boldsymbol{p}_1,\boldsymbol{p}_2) &= n_{\rm imp}\int\frac{d^3q}{(2\pi)^3}U(\boldsymbol{p}_1-\boldsymbol{q})\check{\mathcal{G}}(\boldsymbol{q},\boldsymbol{q}-(\boldsymbol{p}_1-\boldsymbol{p}_2))U(\boldsymbol{q}-\boldsymbol{p}_1)\\ &= n_{\rm imp}\int\frac{d^3q}{(2\pi)^3}|U(\boldsymbol{p}-\boldsymbol{q})|^2\,\check{\mathcal{G}}\left(\boldsymbol{q}+\delta\boldsymbol{p}/2,\,\boldsymbol{q}-\delta\boldsymbol{p}/2\right),\end{aligned} \tag{4.67}$$

where $\boldsymbol{p}=(\boldsymbol{p}_1+\boldsymbol{p}_2)/2$ and $\delta\boldsymbol{p}=\boldsymbol{p}_1-\boldsymbol{p}_2$. In the mixed representation, we get that

$$\check{\Sigma}_{\rm imp}(\boldsymbol{R},T,\boldsymbol{p},\mathcal{E}) = n_{\rm imp}\int\frac{d^3q}{(2\pi)^3}\,|U(\boldsymbol{p}-\boldsymbol{q})|^2\,\check{\mathcal{G}}(\boldsymbol{R},T,\boldsymbol{q},\mathcal{E}). \tag{4.68}$$

Next, we rewrite the momentum integration measure in terms of the kinetic energy. As before, we write it as $\xi_q = q^2/2m$. We get

$$\begin{aligned}d^3q &= q^2\,dq\,d\Omega_q\\ &= q\,m\,d\xi_q\,d\Omega_q\\ &= \pi^2\,N(\xi_q)d\xi_q\,d\Omega_q\,,\end{aligned} \tag{4.69}$$

where we have used the density of states for a three-dimensional electron gas, which is

$$N(\mathcal{E}) = \frac{1}{2\pi^2}\,(2m)^{3/2}\,\sqrt{\mathcal{E}}. \tag{4.70}$$

In the quasiclassical approximation, we set the density of states to its value on the Fermi surface, that is, $N(\xi_q)\to N_F$. We also can assume that scattering potential in momentum

space is independent of the magnitude of $\boldsymbol{p}$, so we can write $U(\boldsymbol{p}-\boldsymbol{q}) \to U(\hat{\boldsymbol{p}}\cdot\hat{\boldsymbol{q}})$. We, therefore, place it outside of the kinetic energy integral. The integral now looks like

$$\begin{aligned}\check{\Sigma}_{\mathrm{imp}}(\boldsymbol{R},T,\boldsymbol{p},\mathcal{E}) &= \frac{n_{\mathrm{imp}}N_F}{2}\int\frac{d\Omega_q}{4\pi}\int d\xi_q\,|U(\boldsymbol{p}-\boldsymbol{q})|^2\,\check{\mathcal{G}}(\boldsymbol{R},T,\boldsymbol{q},\mathcal{E})\\ &= \frac{n_{\mathrm{imp}}N_F}{2}\int\frac{d\Omega_q}{4\pi}\,|U(\hat{\boldsymbol{p}}\cdot\hat{\boldsymbol{q}}_F)|^2\int d\xi_q\,\check{\mathcal{G}}(\boldsymbol{R},T,\boldsymbol{q},\mathcal{E})\\ &= -\frac{i\pi\,n_{\mathrm{imp}}N_F}{2}\int\frac{d\Omega_q}{4\pi}\,|U(\hat{\boldsymbol{p}}\cdot\hat{\boldsymbol{q}}_F)|^2\,\check{g}(\boldsymbol{R},T,\hat{\boldsymbol{q}}_F,\mathcal{E}).\end{aligned} \tag{4.71}$$

The only thing that remains is a spherical average of the quasiclassical Green's function. Since we have assumed that only energies at the Fermi level contribute to physical effects, the integral is taken here.

Lastly, we present the self-energy of spin-flip-scattering. We begin with a potential similar to the impurity scattering. However, we assume that this potential interacts with the spins. We write it as

$$V_{\mathrm{sf}}(\boldsymbol{r}) = \sum_i V(\boldsymbol{r}-\boldsymbol{r}_i). \tag{4.72}$$

For this type of scattering, we only present the result. It is quite similar to the impurity self-energy but needs to account for spin-flip-events. Also, here, we take the average $\langle\dots\rangle_{\mathrm{sf}}$ over spin-flip impurities. It is also assumed that the impurities are randomly distributed [85]. Thus, we can write the average magnitude of spins $\langle S_iS_j\rangle_{\mathrm{sf}} = S(S+1)\delta_{ij}/3$ [64]. We write the self-energy as

$$\begin{aligned}\check{\Sigma}_{\mathrm{sf}}(\boldsymbol{R},T,\boldsymbol{p},\mathcal{E}) &= \frac{n_{\mathrm{sf}}N_FS(S+1)}{12\pi}\int d\xi_q\int d\Omega_q\,|V(\hat{\boldsymbol{p}}\cdot\hat{\boldsymbol{q}})|^2\sum_i^3\hat{\alpha}_i\,\check{\mathcal{G}}(\boldsymbol{R},T,\boldsymbol{q},\mathcal{E})\,\hat{\alpha}_i\\ &= \frac{-in_{\mathrm{sf}}N_FS(S+1)}{12}\int d\Omega_q\,|V(\hat{\boldsymbol{p}}\cdot\hat{\boldsymbol{q}}_F)|^2\sum_i^3\hat{\alpha}_i\,\check{g}(\boldsymbol{R},T,\hat{\boldsymbol{q}}_F,\mathcal{E})\,\hat{\alpha}_i\,,\end{aligned} \tag{4.73}$$

where $\hat{\alpha}_i = \mathrm{diag}(\underline{\tau}_i, \underline{\tau}_i^T)$ and $n_{\mathrm{sf}}$ is the impurity density. The total self-energy, including both intrinsic and extrinsic contributions, is therefore

$$\check{\Sigma} = \check{\Sigma}_{\mathrm{SC}} + \check{\Sigma}_{\mathrm{FM}} + \check{\Sigma}_{\mathrm{imp}} + \check{\Sigma}_{\mathrm{sf}}\,. \tag{4.74}$$

This concludes the derivation of the necessary tools to develop the equations of motion. With the quasiclassical Green's functions and self-energies, we can derive the Eilenberger equation.

## 4.4 The Eilenberger equation

In this section, we will develop an equation of motion. In order to do so, we will change variables to those in eq. (4.44). This will let us write the Gor'kov equation in terms of the quasiclassical Green's function presented in section 4.2. We rewrite the Gor'kov equation in eq. (4.43) as

$$\left[\hat{G}^{-1}_{(0)}(x_1,x_2),\check{G}(x_1,x_2)\right]^{\bullet} = \left[\check{\Sigma}(x_1,x_2),\check{G}(x_1,x_2)\right]^{\bullet}\,, \tag{4.75}$$

and the inverse non-interacting Green's function is

$$\hat{G}^{-1}_{(0)}(x_1,x_2) = i\hat{\tau}_3\,\partial_{t_i} + \frac{\nabla^2_{\boldsymbol{r_i}}}{2m} + \mu. \tag{4.76}$$

The index in the derivatives is $i = 1$ when acting to the right and $i = 2$ when acting to the left. Expanding the equation above using the non-interacting Green's function and suppressing the internal variables $(x_1, x_2)$, it can be written as

$$i\hat{\tau}_3 \left(\partial_{t_1}\check{G}\right) + i\left(\partial_{t_2}\check{G}\right)\hat{\tau}_3 + \frac{1}{2m}\left(\nabla^2_{\boldsymbol{r_1}}\check{G} - \nabla^2_{\boldsymbol{r_2}}\check{G}\right) = \left[\check{\Sigma}, \check{G}\right]^\bullet. \tag{4.77}$$

Note the sign change of the second term in the commutator between the non-interacting inverse- and ordinary Green's function. Acting with the operator from the left is equivalent to taking the Hermitian conjugate of the operation from the right; therefore, the sign changed. At the next step of the derivation, we insert the center of mass and relative coordinate from the mixed representation. The spatial derivatives will change as follows

$$\begin{aligned}\nabla^2_{\boldsymbol{r}_1} - \nabla^2_{\boldsymbol{r}_2} &= \left(\frac{1}{4}\nabla^2_{\boldsymbol{R}} + \nabla_{\boldsymbol{R}}\cdot\nabla_{\boldsymbol{r}} + \nabla^2_{\boldsymbol{r}}\right) - \left(\frac{1}{4}\nabla^2_{\boldsymbol{R}} - \nabla_{\boldsymbol{R}}\cdot\nabla_{\boldsymbol{r}} + \nabla^2_{\boldsymbol{r}}\right) \\ &= 2\nabla_{\boldsymbol{R}}\cdot\nabla_{\boldsymbol{r}}.\end{aligned} \tag{4.78}$$

The time derivatives are similar in the mixed representation. The first time coordinate derivative is $\partial_{t_1} = \frac{1}{2}\partial_T + \partial_t$, and the second is $\partial_{t_2} = \frac{1}{2}\partial_T - \partial_t$. The temporal derivatives can be approximated as the derivative of the relative coordinate since it changes more rapidly compared to the center of mass one. Thus, inserting $\partial_T \approx 0$, we get

$$i\hat{\tau}_3 \left(\partial_t\check{G}\right) - i\left(\partial_t\check{G}\right)\hat{\tau}_3 + \frac{1}{m}\nabla_{\boldsymbol{R}}\cdot\nabla_{\boldsymbol{r}}\check{G} = \left[\check{\Sigma}, \check{G}\right]^\bullet. \tag{4.79}$$

Next, we will do a Fourier transformation to obtain a Green's function like in eq. (4.45). Evaluating the left-hand side, it transforms as

$$\begin{aligned}&\int dt\, e^{i\mathcal{E}t}\int d^3r\, e^{-i\boldsymbol{p}\cdot\boldsymbol{r}}\left(i\left[\hat{\tau}_3, \partial_t\check{G}(\boldsymbol{R}, T, \boldsymbol{r}, t)\right]^\bullet + \frac{1}{m}\nabla_{\boldsymbol{R}}\cdot\nabla_{\boldsymbol{r}}\check{G}(\boldsymbol{R}, T, \boldsymbol{r}, t)\right) \\ &\qquad = \int dt\, e^{i\mathcal{E}t}\int d^3r\, e^{-i\boldsymbol{p}\cdot\boldsymbol{r}}\left(\left[\mathcal{E}\hat{\tau}_3, \check{G}(\boldsymbol{R}, T, \boldsymbol{r}, t)\right]^\bullet + \frac{i}{m}\boldsymbol{p}\cdot\nabla_{\boldsymbol{R}}\check{G}(\boldsymbol{R}, T, \boldsymbol{r}, t)\right),\end{aligned} \tag{4.80}$$

where we used the method of partial integration and dropped the surface terms. Since the self-energies were found in the mixed representation, the Fourier transformation of the right-hand side is trivial. Replacing the Green's function $\check{G}(X, x)$ with $\check{\mathcal{G}}(X, P)$, so that we can write the equation of motion as

$$\left[\mathcal{E}\hat{\tau}_3, \check{\mathcal{G}}(\boldsymbol{R}, T, \boldsymbol{p}, \mathcal{E})\right]^\bullet + \frac{i}{m}\boldsymbol{p}\cdot\nabla_{\boldsymbol{R}}\check{\mathcal{G}}(\boldsymbol{R}, T, \boldsymbol{p}, \mathcal{E}) = \left[\check{\Sigma}, \check{\mathcal{G}}\right]^\bullet(\boldsymbol{R}, T, \boldsymbol{p}, \mathcal{E}). \tag{4.81}$$

It can be further simplified if we employ the approximation in eq. (B.15). Since we already have assumed that the center-of-mass coordinate $T$ varies slowly compared to the relative one, we apply $\partial_T \approx 0$ again. Thus, the bullet commutator reduces to the ordinary commutator. The details of this approximation can be found in appendix B. We also assume that all interesting phenomena are happening at the Fermi surface, thus fixing the magnitude of the momentum. Therefore, we can insert the quasiclassical Green's function from eq. (4.47). What we are left with is an equation capturing the behavior of the quasiclassical Green's function

$$\left[\mathcal{E}\hat{\tau}_3 - \check{\Sigma}, \check{g}\right] + iv_F\,\hat{\boldsymbol{p}}_F\cdot\nabla\,\check{g} = 0. \tag{4.82}$$

After simplifying the equation, we are left with what is known as the Eilenberger equation. Note that the only derivative in the equation is acting on the center of mass coordinate $\boldsymbol{R}$. Therefore, the Green's function might vary in space. However, since no time derivative exists, we are describing a stationary problem. In this thesis, we will focus on equilibrium systems, and therefore, the approximation $\partial_T \approx 0$ is appropriate.

## 4.5 The diffusive limit

In the previous section, we derived the Eilenberger equation. It describes the behavior of electrons and holes in a material. However, we have not specified any interactions or self-energies in its derivation. This section presents the diffusive limit, in which we derive an equation for dirty materials. Therefore, we will use the self-energies derived in section 4.3. In the dirty limit, we assume that the impurity self-energy $\check{\Sigma}_{\text{imp}}$ is dominant apart from the Fermi energy. It might seem contradictory to the derivation, where we implicitly assumed that the potential $V_{\text{imp}}$ was weak and truncated at the second order. It is not contradictory to have a strong self-energy despite a weak scattering potential, provided that the impurity density, $n_{\text{imp}}$, is high.

Assuming a high impurity density, we can assume they randomize the relative momentum direction. Therefore, the Green's function should be nearly isotropic. Thus, we can split the Green's function into a s- and p-wave part

$$\check{g} = \check{g}_s + \hat{\boldsymbol{p}}_F \cdot \check{g}_p, \tag{4.83}$$

where we assume $\check{g}_s >> \check{g}_p$. Since the Green's function still has to obey the normalization from eq. (4.55), we have that

$$(\check{g}_s + \hat{\boldsymbol{p}}_F \cdot \check{g}_p)(\check{g}_s + \hat{\boldsymbol{p}}_F \cdot \check{g}_p) \approx \check{g}_s\check{g}_s + \hat{\boldsymbol{p}}_F \cdot (\check{g}_s\check{g}_p + \check{g}_p\check{g}_s) = \underline{\sigma}_0 \otimes \hat{\tau}_0, \tag{4.84}$$

which means we can write

$$\check{g}_s\check{g}_s = \underline{\sigma}_0 \otimes \hat{\tau}_0, \qquad \check{g}_s\check{g}_p = -\check{g}_p\check{g}_s. \tag{4.85}$$

These expressions give a normalization condition for the s-wave contribution and a commutation relation $\{\check{g}_s, \check{g}_p\} = 0$ between the contributions. Next, we assume that the total quasiclassical Green's function does not contribute to the angular integrals of eqs. (4.71) and (4.73) [64]. Therefore, we relate those integrals to the scattering times $\tau_{\text{imp}}$ and $\tau_{\text{sf}}$. Next, we take an average over the momentum direction. The self-energies can therefore be approximated as

$$\check{\Sigma}_{\text{imp}} = -\frac{1}{2\tau_{\text{imp}}}\langle\check{g}\rangle_{\hat{\boldsymbol{p}}_F} \approx -\frac{1}{2\tau_{\text{imp}}}\check{g}_s, \tag{4.86}$$

$$\check{\Sigma}_{\text{sf}} = -\frac{i}{8\tau_{\text{sf}}}\sum_i^3 \hat{\alpha}_i \langle\check{g}\rangle_{\hat{\boldsymbol{p}}_F} \hat{\alpha}_i \approx -\frac{i}{8\tau_{\text{sf}}}\sum_i^3 \hat{\alpha}_i \check{g}_s \hat{\alpha}_i. \tag{4.87}$$

In the next step, we insert these self-energies into the Eilenberger equation from eq. (4.82). We separate the intrinsic and extrinsic self-energies and insert the quasiclassical Green's function from eq. (4.83). The Eilenberger equation can, therefore, be expressed as

$$\begin{aligned}\left[\mathcal{E}\hat{\tau}_3 - \hat{\Delta} - \boldsymbol{h}\cdot\hat{\boldsymbol{\sigma}}, \check{g}_s\right] + \hat{\boldsymbol{p}}_F \cdot \left[\mathcal{E}\hat{\tau}_3 - \hat{\Delta} - \boldsymbol{h}\cdot\hat{\boldsymbol{\sigma}}, \check{g}_p\right] + iv_F\,\hat{\boldsymbol{p}}_F \cdot \nabla(\check{g}_s + \hat{\boldsymbol{p}}_F \cdot \check{g}_p) \\ - \left[\check{\Sigma}_{\text{imp}}, \check{g}_s\right] - \hat{\boldsymbol{p}}_F \cdot \left[\check{\Sigma}_{\text{imp}}, \check{g}_p\right] - \left[\check{\Sigma}_{\text{sf}}, \check{g}_s\right] - \hat{\boldsymbol{p}}_F \cdot \left[\check{\Sigma}_{\text{sf}}, \check{g}_p\right] = 0,\end{aligned} \tag{4.88}$$

where the commutator $\left[\check{\Sigma}_{\text{imp}}, \check{g}_s\right]$ is zero. Please note that the next step involves two different actions; the first is collecting all the odd terms in $\hat{\boldsymbol{p}}_F$. The second is assumming that the impurity scattering is the dominant energy term, other than the Fermi energy. Therefore, we discard all terms except $\left[\check{\Sigma}_{\text{imp}}, \check{g}_p\right]$ and the that containing the Fermi velocity $v_F$. We can write these two actions as

$$\begin{aligned}0 &= \left[\mathcal{E}\hat{\tau}_3 - \hat{\Delta} - \boldsymbol{h}\cdot\hat{\boldsymbol{\sigma}}, \check{g}_p\right] + iv_F\,\nabla\check{g}_s - \left[\check{\Sigma}_{\text{sf}}, \check{g}_p\right] - \left[\check{\Sigma}_{\text{imp}}, \check{g}_p\right] \\ &\approx iv_F\,\nabla\check{g}_s - \left[\check{\Sigma}_{\text{imp}}, \check{g}_p\right].\end{aligned} \tag{4.89}$$

The above equation gives us a direct relationship between the s- and p-wave parts of the Green's function. To see this, we use the relation in eq. (4.85) to write out the commutator. This can be written as

$$iv_F \nabla \check{g}_s = -\frac{i}{2\tau_{\text{imp}}} [\check{g}_s, \check{g}_p] = -\frac{i}{\tau_{\text{imp}}} \check{g}_s \check{g}_p. \tag{4.90}$$

Acting on the above equation with $\check{g}_s$ from the left, we can deploy the normalization condition of the s-wave contribution $\check{g}_s \check{g}_s = 1$. This gives us the following expression for the p-wave contribution

$$\check{g}_p = -\tau_{\text{imp}} v_F \check{g}_s \nabla \check{g}_s. \tag{4.91}$$

Since we have collected all odd terms in $\hat{\boldsymbol{p}}_F$, the next step is to collect the even contributions. One can, in principle, relax the approximation that the spin-flip term if the term $\left[\check{\Sigma}_{\text{sf}}, \check{g}_s\right]$ is kept [75, 86]. In this thesis, we will not consider spin-flip scattering, and therefore we will neglect that term. Collecting all terms that are even in $\hat{\boldsymbol{p}}_F$, we have the equation

$$\left[\mathcal{E}\hat{\tau}_3 - \hat{\Delta} - \boldsymbol{h} \cdot \hat{\boldsymbol{\sigma}}, \check{g}_s\right] + iv_F \, \hat{\boldsymbol{p}}_F \cdot \nabla(\hat{\boldsymbol{p}}_F \cdot \check{g}_p) = 0. \tag{4.92}$$

We perform an average over the Fermi surface, which in practice means averaging over the momentum direction, which is randomized in the diffusive limit. The average of the even contribution yields

$$\left[\mathcal{E}\hat{\tau}_3 - \hat{\Delta} - \boldsymbol{h} \cdot \hat{\boldsymbol{\sigma}}, \check{g}_s\right] + \frac{iv_F}{3} \nabla \, \check{g}_p = 0. \tag{4.93}$$

We can now insert $\check{g}_p$ from eq. (4.91) to obtain the Usadel equation. We express it as

$$iD\nabla \left(\check{g}_s \nabla \check{g}_s\right) = \left[\mathcal{E}\hat{\tau}_3 - \hat{\Delta} - \boldsymbol{h} \cdot \hat{\boldsymbol{\sigma}}, \check{g}_s\right], \tag{4.94}$$

where $D = \frac{v_F^2 \tau_{\text{imp}}}{3}$ is the diffusion constant. Note that this equation only contains the s-wave part of the Green's function. Therefore, it is isotropic and can be preferable over the Eilenberger equation, which contains the full quasiclassical Green's function. It is, however, important to remember our approximations: We assumed that the impurity scattering self-energy dominated the commutator containing the quasiparticle energy, the superconducting gap, and the ferromagnetic self-energy. Therefore, the equation is unsuited for ferromagnets with a strong exchange-field $\boldsymbol{h}$.

There is an important difference between the Usadel and the Eilenberger equation. They can be used on opposite limits of the impurity density. This has direct consequences for what symmetries the superconducting order parameter can have. We began this section by assuming that $n_{\text{imp}} \gg 1$, which effectively made the pairing symmetry of the gap isotropic. In the Eilenberger equation, we did not specify the self-energies and can take $n_{\text{imp}} \approx 0$. Therefore, the Eilenberger equation can capture both s- and p-wave orbital symmetries, illustrated in fig. 1.1, while the Usadel equation is restricted to describing s-wave pairings.

## 4.6 Spin-orbit coupling

We are concerned with spin-orbit coupling since it can contribute to generating spin-polarized triplets in proximity systems. They can, for instance, be produced by having a varying SU(2) field, like the ferromagnet holmium, which has an intrinsic conical magnetization [9]. The rotating exchange field effectively creates a spin-orbit interaction for the electrons. A ferromagnet with geometric curvature can exhibit the same type of behavior [50, 51]. Another possibility is to have a misalignment of two different background SU(2) fields. Therefore, another possibility for generating long-range triplets in a ferromagnetic proximity system is to include spin-orbit coupling. If we require the Hamiltonian of the system to be SU(2) gauge invariant up to some arbitrary constant, we can transform the momentum as in classical mechanics, $\boldsymbol{p} \to \boldsymbol{p} - \hat{A}$. If the spin-orbit coupling is present in the form of a SU(2) gauge field, we need to replace all derivatives by their covariant counterpart [71], as we did in eq. (3.38). Thus, the Usadel equation becomes

$$iD\tilde{\mathcal{D}}(\check{g}\tilde{\mathcal{D}}\check{g}) = \left[\mathcal{E}\hat{\tau}_3 - \hat{\Delta} - \boldsymbol{h}\cdot\hat{\boldsymbol{\sigma}},\ \check{g}\right] . \tag{4.95}$$

Note that the spin-orbit field has a 4x4 matrix form in Nambu⊗Spin space and a vector structure in geometrical space. It can be written as $\hat{A} = \mathrm{diag}(\boldsymbol{A}, -\boldsymbol{A}^*)$, where $\boldsymbol{A} = (\underline{A}_x, \underline{A}_y, \underline{A}_z)$ in a cartesian coordinates system [67]. The spin-orbit field may be different depending on the system and on the symmetry breaking from which it originates. First, we consider a form practical for studying thin films in proximity systems. The spin-orbit field is confined to the $xy$-plane and describes intrinsic Rashba–Dresselhaus couplings. We write the field as

$$\boldsymbol{A} = (\beta\underline{\sigma}_1 - \alpha\underline{\sigma}_2,\ \alpha\underline{\sigma}_1 - \beta\underline{\sigma}_2,\ 0), \tag{4.96}$$

where $\alpha$ is the Rashba coefficient, and $\beta$ is the Dresselhaus coefficient [67]. If we introduce the spin-orbit strength $a$ and angle $\chi$, we can in polar notation define $\alpha \equiv -a\sin\chi$ and $\beta \equiv a\cos\chi$, which means the total vector can be rewritten as

$$\boldsymbol{A} = a(\underline{\sigma}_1\cos\chi + \underline{\sigma}_2\sin\chi)\hat{\boldsymbol{e}}_x - a(\underline{\sigma}_x\sin\chi + \underline{\sigma}_2\cos\chi)\hat{\boldsymbol{e}}_y. \tag{4.97}$$

A Rashba spin-orbit coupling in the $z$-direction can be a suitable choice for nanowires. The spin-orbit vector can be written as [87]

$$\boldsymbol{A} = (0, 0, \alpha\underline{\sigma}_1 - \alpha\underline{\sigma}_2). \tag{4.98}$$

The two examples presented here describe kinds of intrinsic symmetry breaking. If the system also has geometrical curvature, we need to add the strain-induced spin-orbit coupling. As discussed in section 3.2, the strain-induced field will depend on the geometry.

## 4.7 Boundary conditions

There are numerous boundary conditions to choose from in the quasiclassical framework. In the ballistic case, the first description of the boundary conditions was formulated by Shelankov and by Zaitsev [88, 89] for spin-inactive interfaces. Later came formulations in both equilibrium [90, 91] and non-equilibrium [92] situations. Further generalizations included spin-active interfaces, formulated for equilibrium [93] and for non-equilibrium [94], and interfaces with diffusive scattering characteristics [95]. In the dirty limit, Kupriyanov and Lukichev derived a formulation appropriate for the tunneling limit [96]. This was generalized to arbitrary transmission by Nazarov [97]. A general formulation can be found in

ref. [98] which allows for complex interface spin textures in and out of equilibrium. This thesis will use the Kupriyanov and Lukichev boundary conditions, as they take a simple form. Including the SO-couping, they can be expressed as

$$\hat{g}_j^R \tilde{\mathcal{D}} \hat{g}_j^R = \frac{1}{2L_j\zeta_j} \left[\hat{g}_1^R, \hat{g}_2^R\right]. \tag{4.99}$$

where $L_j$ is the length of material $j$ and $\hat{g}_j^R$ is the retarded Green's function in material $j$. The quantity $\zeta_j = \frac{R_B}{R_J}$ is the barrier restance $R_B$ divided by the bulk resistance $R_j$. For vacuum, the boundary condition is given by

$$\tilde{\nabla} \hat{g}_j^R = 0. \tag{4.100}$$

We note that we have only expressed the boundary conditions in terms of $\hat{g}^R$. In this thesis, we will consider only equilibrium systems. To fully describe these systems, we only need the retarded Green's function.

## 4.8 Parametrization

To treat the Usadel equation numerically, we wish to parameterize it. There are several ways to do it, where the most commonly used are the $\theta$- and Riccati parametrization [81]. In the $\theta$-parametrization, $\underline{g}^R = \cosh(\theta)\underline{\sigma}_0$ and $\underline{f}^R = \sinh(\theta)e^{i\phi}\, i\underline{\sigma}_2$, where $\theta$, $\phi$ are position and energy dependent [85]. However, since the values are not bound, the solutions can be unstable. Therefore, we will use the Riccati parametrization. The retarded Green's function is

$$\hat{g}^R = \begin{pmatrix} \underline{g}^R & \underline{f}^R \\ -\underline{\tilde{f}}^R & -\underline{\tilde{g}}^R \end{pmatrix}, \tag{4.101}$$

where the tilde-conjugation is $\tilde{g}(\boldsymbol{R}, T, \hat{\boldsymbol{p}}_F, \mathcal{E}) = g^*(\boldsymbol{R}, T, \hat{\boldsymbol{p}}_F, -\mathcal{E})$. We also had the normalization condition $\hat{g}^R\hat{g}^R = \hat{\tau}_0$. If we find another matrix that satisfies all the necessary requirements of $\hat{g}^R$, the two should describe the same system. Therefore, we employ the Riccati parametrization defined by

$$\hat{g}^R = \begin{pmatrix} N & 0 \\ 0 & -\tilde{N} \end{pmatrix} \begin{pmatrix} 1+\gamma\tilde{\gamma} & 2\gamma \\ 2\tilde{\gamma} & 1+\tilde{\gamma}\gamma \end{pmatrix}, \tag{4.102}$$

where $N = \underline{N}$ and $\gamma = \underline{\gamma}$ are energy and position dependent. This reduces the problem from an equation with 4x4 matrices to 2x2 ones. The normalization matrices are defined as

$$N = (1-\gamma\tilde{\gamma})^{-1}, \qquad \tilde{N} = (1-\tilde{\gamma}\gamma)^{-1}. \tag{4.103}$$

We can express the Usadel equation using $\gamma$ with the above parametrization. The derivation, including spin-orbit coupling, is tedious, and we present only the result. A detailed derivation can be found in ref. [67]. We can write the Usadel equation for $\gamma$ and $\tilde{\gamma}$ separately for a superconductor-ferromagnet proximity system. In the superconductor, the equation becomes

$$D\left[(\nabla^2\gamma) + 2(\nabla\gamma)\tilde{N}\tilde{\gamma}(\nabla\gamma)\right] = -2i\mathcal{E}\gamma - i(\underline{\Delta} - \gamma\underline{\Delta}^*\gamma), \tag{4.104}$$

$$D\left[(\nabla^2\tilde{\gamma}) + 2(\nabla\tilde{\gamma})N\gamma(\nabla\tilde{\gamma})\right] = -2i\mathcal{E}\tilde{\gamma} + i(\underline{\Delta}^* - \tilde{\gamma}\underline{\Delta}\tilde{\gamma}), \tag{4.105}$$

where $\nabla(\cdot)$ is with respect to the center-of-mass coordinate. The Usadel equation in the ferromagnetic region takes the form

$$\begin{aligned} D\left[(\nabla^2\gamma) + 2(\nabla\gamma)\tilde{N}\tilde{\gamma}(\nabla\gamma)\right] =& -i\boldsymbol{h}\cdot(\gamma\boldsymbol{\sigma}^* - \boldsymbol{\sigma}\gamma) - 2i\mathcal{E}\gamma + 2iD(\boldsymbol{A} + \gamma\boldsymbol{A}^*\tilde{\gamma})N(\nabla\gamma) \\ &+ 2iD(\nabla\gamma)\tilde{N}(\boldsymbol{A}^* + \tilde{\gamma}\boldsymbol{A}\gamma) + D(\boldsymbol{A}^2\gamma - \gamma(\boldsymbol{A}^*)^2) \\ &+ 2D(\boldsymbol{A}\gamma + \gamma\boldsymbol{A}^*)\tilde{N}(\boldsymbol{A}^* + \tilde{\gamma}\boldsymbol{A}\gamma), \end{aligned} \tag{4.106}$$

$$\begin{aligned} D\left[(\nabla^2\tilde{\gamma}) + 2(\nabla\tilde{\gamma})N\gamma(\nabla\tilde{\gamma})\right] =& i\boldsymbol{h}\cdot(\tilde{\gamma}\boldsymbol{\sigma} - \boldsymbol{\sigma}^*\tilde{\gamma}) - 2i\mathcal{E}\tilde{\gamma} - 2iD(\boldsymbol{A}^* + \tilde{\gamma}\boldsymbol{A}\gamma)\tilde{N}(\nabla\tilde{\gamma}) \\ &- 2iD(\nabla\tilde{\gamma})N(\boldsymbol{A} + \gamma\boldsymbol{A}^*\tilde{\gamma}) + D((\boldsymbol{A}^*)^2\tilde{\gamma} - \tilde{\gamma}\boldsymbol{A}^2) \\ &+ 2D(\boldsymbol{A}^*\tilde{\gamma} + \tilde{\gamma}\boldsymbol{A})N(\boldsymbol{A} + \gamma\boldsymbol{A}^*\tilde{\gamma})\,. \end{aligned} \tag{4.107}$$

The four equations above describe what is happening within the materials. Using the Riccati parametrization, we can also write the boundary conditions. When defining $\Omega_j = 1/L_j\zeta_j$, the Kupriyanov-Lukichev boundary conditions can be summarized as

$$(\nabla\gamma_1) - i(\boldsymbol{A}\gamma_1 + \gamma_1\boldsymbol{A}^*) = \Omega_1(1 - \gamma_1\tilde{\gamma}_2)N_2(\gamma_2 - \gamma_1), \tag{4.108}$$

$$(\nabla\gamma_2) - i(\gamma_2\boldsymbol{A}^* + \boldsymbol{A}\gamma_2) = \Omega_2(1 - \gamma_2\tilde{\gamma}_1)N_1(\gamma_2 - \gamma_1). \tag{4.109}$$

When against vacuum, the right-hand side goes to zero as $\Omega_j \to 0$. The indexes $i$ in $\gamma_i$ refer to the materials on either side of the interface. Thus, to solve the Usadel equation in one material, we need to know the solution on the other side of the interface. One could solve the two sides iteratively, but we are mainly interested in the solution in the material next to the superconductor. Thus, we assume a bulk solution in the superconductor and only find the Green's function in the other material. The bulk solution can be found analytically by realizing that the derivatives on the left-hand side in eq. (4.104) vanish since they are with respect to the center-of-mass coordinate. The equation becomes

$$2\mathcal{E}\begin{pmatrix}\gamma_{\alpha\alpha} & \gamma_{\alpha\beta}\\ \gamma_{\beta\alpha} & \gamma_{\beta\beta}\end{pmatrix} = \begin{pmatrix}\Delta^*(\gamma_{\alpha\alpha}\gamma_{\beta\alpha} - \gamma_{\alpha\alpha}\gamma_{\alpha\beta}) & \Delta^*(\gamma_{\alpha\alpha}\gamma_{\beta\beta} - \gamma_{\alpha\beta}^2) - \Delta\\ \Delta^*(\gamma_{\beta\alpha}^2 - \gamma_{\alpha\alpha}\gamma_{\beta\beta}) + \Delta & \Delta^*(\gamma_{\beta\alpha}\gamma_{\beta\beta} - \gamma_{\alpha\beta}\gamma_{\beta\beta})\end{pmatrix}. \tag{4.110}$$

It can be shown that $\gamma_{\alpha\alpha} = \gamma_{\beta\beta} = 0$ from the relations of the matrices above. Hence, the solutions to the quadratic equations for $\gamma_{\alpha\beta}$ and $\gamma_{\beta\alpha}$ gives

$$\gamma_{\alpha\beta} = \frac{-\mathcal{E} + \sqrt{\mathcal{E}^2 - |\Delta|^2}}{\Delta^*} = -\gamma_{\beta\alpha}. \tag{4.111}$$

The elements of the normalization matrix $N^{-1} = 1 - \gamma\tilde{\gamma}$ are equal and can be expressed in terms of the quadratic equations above. We find that

$$1 - \gamma_{\alpha\beta}\tilde{\gamma}_{\beta\alpha} = \frac{-2\mathcal{E}^2 + 2\mathcal{E}\sqrt{\mathcal{E}^2 - |\Delta|^2} + 2|\Delta|^2}{|\Delta|^2} = 1 - \tilde{\gamma}_{\alpha\beta}\gamma_{\beta\alpha}. \tag{4.112}$$

Now we can express the first element of the total retarded ordinary and anomalous BCS Green's functions as

$$\underline{g}^R_{\mathrm{BCS}} = \frac{\mathcal{E}}{\sqrt{\mathcal{E}^2 - |\Delta|^2}}, \qquad \underline{f}^R_{\mathrm{BCS}} = \frac{\underline{\Delta}}{\sqrt{\mathcal{E}^2 - |\Delta|^2}}. \tag{4.113}$$

If we write the gap $\underline{\Delta} = |\Delta|e^{i\phi}i\underline{\sigma}_2$, and introduce $\theta = \operatorname{arctanh}(|\Delta|/\mathcal{E})$, we can write the $\gamma$ matrices in terms of hyperbolic functions [99]. They become

$$\gamma_{\mathrm{BCS}} = \frac{\sinh\theta}{\cosh\theta + 1}e^{i\phi}i\underline{\sigma}_2, \qquad \tilde{\gamma}_{\mathrm{BCS}} = -\frac{\sinh\theta}{\cosh\theta + 1}e^{-i\phi}i\underline{\sigma}_2\,. \tag{4.114}$$

With this, we have a theory to describe proximity systems in the diffusive limit. We have also developed a suitable expression for the Usadel equation for numerical implementation and found the bulk superconductor solution, which will be used in the boundary conditions.

## 4.9 Physical observables

To make experimental predictions, we need to relate the Green's function to physical observables. We will present the density of states, which can directly be related to triplet correlations. We also present the expression for the charge current.

### 4.9.1 Density of states

As we have discussed, the retarded Green's function is directly related to the density of states. It can be seen from the fact that the elements on the diagonal are related to $\langle\psi_\sigma^\dagger(\boldsymbol{R},\mathcal{E})\psi_\sigma(\boldsymbol{R},\mathcal{E})\rangle$. We express the normalized density of states as

$$D(\boldsymbol{R},\mathcal{E}) = \frac{1}{2}\mathfrak{Re}\{\mathrm{Tr}\big[\underline{g}^R(\boldsymbol{R},\mathcal{E})\big]\}\,. \tag{4.115}$$

The value at zero energy, $D(\boldsymbol{R},0)$ is directly related to the relation between singlets and triplets. The singlets reduce the available states, while the triplets increase it. This can be illustrated in the weak proximity limit. Before going to this limit, we introduce the $\boldsymbol{d}$ vector. From this vector, we may extract the short- and long-ranged triplet components of the Green's function as well. It can be defined by rewriting the anomalous Green's function as

$$\underline{f}^R = (f_0 + \boldsymbol{d}\cdot\boldsymbol{\sigma})\; i\underline{\sigma}_2, \tag{4.116}$$

where $\boldsymbol{d} = (d_x, d_y, d_z)$. In a ferromagnet with an exchange-field $\boldsymbol{h}$, this decomposition makes the short-ranged triplet component $d_{||} = \boldsymbol{d}\cdot\hat{\boldsymbol{h}}$ and the long-ranged $d_\perp = |\boldsymbol{d}\times\hat{\boldsymbol{h}}|$. This notation may be confusing because the $\boldsymbol{d}$-vector projection parallel to $\boldsymbol{h}$ describes short-ranged triplets. However, when the spins are parallel to $\boldsymbol{h}$ we have long-ranged triplets, described by the projection of $\boldsymbol{d}$ perpendicular to the exchange field $\boldsymbol{h}$. Generally, the $\boldsymbol{d}$-vector describes triplet correlations with spin-polarization perpendicular to itself.

Getting back to the zero energy density of states, we use the Riccati parametrization. In the weak proximity limit, we assume that $|\gamma_{\alpha\beta}| \ll 1$ [52]. Therefore, we may neglect terms of order $\mathcal{O}(\gamma^2)$ and take $N \approx 1$. We can write the zero energy density in the weak proximity limit [64] as

$$D(\boldsymbol{R},0) = 1 - \frac{|f_s(\boldsymbol{R},0)|^2}{2} + \frac{|\boldsymbol{d}(\boldsymbol{R},0)|^2}{2}\,. \tag{4.117}$$

If we have a normal metal, both the singlet and triplet contributions are zero. This yields the normal metal density of states, one everywhere. If we have a bulk superconductor, the singlet contribution cancels the 1, such that we get a gap in the density of states. If $D(\boldsymbol{R},0) > 1$ the triplet correlations dominate.

### 4.9.2 Charge current density

The charge current density is related to the change of the Keldysh component of the Green's function [75]. Using the density of states at the Fermi surface and the diffusion constant, we can write the charge current density as

$$\boldsymbol{j}(\boldsymbol{R},T) = \frac{eN_F D}{4}\int d\mathcal{E}\;\mathrm{Tr}\Big[\hat{\tau}_3(\hat{g}\tilde{\mathcal{D}}\hat{g})^K\Big]\,, \tag{4.118}$$

where we trace the component in the Keldysh index $(\hat{g}\tilde{\mathcal{D}}\hat{g})^K = (\hat{g}^R\tilde{\mathcal{D}}\hat{g}^K) + (\hat{g}^K\tilde{\mathcal{D}}\hat{g}^A)$. In equilibrium, the retarded and advanced Green's functions are related to the Keldysh

component and each other. Since we are interested in equilibrium situations only, we can employ the relations in eq. (4.28) to write

$$\boldsymbol{j}(\boldsymbol{R},T) = \frac{eN_F D}{4}\int d\mathcal{E}\ \tanh\!\left(\frac{\beta\mathcal{E}}{2}\right)\mathrm{Tr}\Big[\hat{\tau}_3\big(\hat{g}^R\tilde{\mathcal{D}}\hat{g}^R + (\hat{\tau}_3\hat{g}^R\tilde{\mathcal{D}}\hat{g}^R\hat{\tau}_3)^\dagger\big)\Big]\,. \tag{4.119}$$

This concludes the chapter about Green's functions, where we have developed the relevant equations of motion and expressions for physical observables.

# Chapter 5

# Lattice models

This chapter will explore the framework which discretizes a problem onto a specific lattice. The advantage of this method, in contrast to the quasiclassical theory presented previously in this thesis, is that the length scales and self-energy magnitudes are not limiting [100]. The method presented here is often referred to as the Bogoliubov-de Gennes after the book "Superconductivity of metals and alloys" written by de Gennes [101]. Our method is based on the approach described in Chapter 2 of ref. [102], and similar methods can be found in refs. [100, 103, 104]. We will derive a tight-binding Hamiltonian, to which we then introduce a lattice.

## 5.1 Derivation of the tight-binding model

We begin with a general continuum Hamiltonian and derive the discretized counterpart, as well as other useful relations and equations for numerical calculations within the tight-binding formulation. Since this thesis is focused on superconductivity, we begin with a Hamiltonian consisting of a single-particle term and a two-particle interaction term

$$\begin{aligned}\mathcal{H} =& \sum_{\sigma\sigma'} \int d\boldsymbol{r}\; \psi^\dagger_\sigma(\boldsymbol{r}) h_{\sigma\sigma'}(\boldsymbol{r}) \psi_{\sigma'}(\boldsymbol{r}) \\ &+ \sum_{\sigma\sigma'} \int\int d\boldsymbol{r}\, d\boldsymbol{r}'\; \psi^\dagger_\sigma(\boldsymbol{r}) \psi^\dagger_{\sigma'}(\boldsymbol{r}') V_{\sigma\sigma'}(\boldsymbol{r},\boldsymbol{r}') \psi_{\sigma'}(\boldsymbol{r}') \psi_\sigma(\boldsymbol{r}) \,, \end{aligned} \tag{5.1}$$

where the spin-indices in $h_{\sigma\sigma'}$ allow for spin-flip effects and ferromagnetism for instance. It also allows for spin-orbit interactions, which we have shown is an integral part of discussing curvature effects. Next, we introduce Wannier orbitals $w(\boldsymbol{r}-\boldsymbol{R}_i)$, which describe electrons that are localized around ionic lattice sites located at $\boldsymbol{R}_i$. A qualitative picture of the spatial part of $w(\boldsymbol{r}-\boldsymbol{R}_i)$ can be seen in fig. 5.1. These form a complete orthonormal basis. That means

$$\int d\boldsymbol{r}\; w^*(\boldsymbol{r}-\boldsymbol{R}_i)\, w(\boldsymbol{r}-\boldsymbol{R}_j) = \delta_{ij} \,, \tag{5.2}$$

and that the field operators can be written as

$$\psi_\sigma(\boldsymbol{r}) = \sum_i w(\boldsymbol{r}-\boldsymbol{R}_i)\, c_{i\sigma}, \qquad \psi^\dagger_{\sigma'}(\boldsymbol{r}') = \sum_j w^*(\boldsymbol{r}'-\boldsymbol{R}_j)\, c^\dagger_{j\sigma} \,. \tag{5.3}$$

The operators $c^\dagger_{i\sigma}$ and $c_{i\sigma}$ create and annihilate a particle at lattice site $i$ respectively and obey the usual fermionic anti-commutation relations in eq. (2.1). Next, we use these

orbitals to map the continuous Hamiltonian to a lattice by considering one term at a time. Beginning with the non-interacting part, we can write

$$\begin{aligned}\mathcal{H}_0 &= \sum_{\sigma\sigma'} \int d\boldsymbol{r}\, \psi^\dagger_\sigma(\boldsymbol{r}) \left(-\frac{\hbar^2}{2m}\nabla^2 - \mu(\boldsymbol{r})\right) \delta_{\sigma\sigma'}\, \psi_{\sigma'}(\boldsymbol{r}) \\ &= \sum_{ij} c^\dagger_{i\sigma} c_{j\sigma} \int d\boldsymbol{r}\, w^*(\boldsymbol{r}-\boldsymbol{R}_i) \left(-\frac{\hbar^2}{2m}\nabla^2 - \mu(\boldsymbol{r})\right) w(\boldsymbol{r}-\boldsymbol{R}_j)\,. \end{aligned} \tag{5.4}$$

To simplify this expression, we assume that the spatial part of the Wannier orbitals decays rapidly away from each lattice site, as illustrated in fig. 5.1. Thus, we see that the orbitals evaluate to zero far away. Doing integration by parts in eq. (5.4), we get

$$\begin{aligned}\mathcal{H}_0 &= -\sum_{i\sigma} \mu_i c^\dagger_{i\sigma} c_{i\sigma} - \sum_{ij\sigma} c^\dagger_{i\sigma} c_{j\sigma} \frac{\hbar^2}{2m} \Big\{ w^*(\boldsymbol{r}-\boldsymbol{R}_i)\nabla w(\boldsymbol{r}-\boldsymbol{R}_j)\Big|_{\boldsymbol{r}\to\pm\infty} \\ &\qquad\qquad - \int d\boldsymbol{r}\, [\nabla w(\boldsymbol{r}-\boldsymbol{R}_i)]^*\, \nabla w(\boldsymbol{r}-\boldsymbol{R}_j) \Big\} \\ &= -\sum_{i\sigma} \mu_i c^\dagger_{i\sigma} c_{i\sigma} - \sum_{\langle ij\rangle\sigma} t_{ij} c^\dagger_{i\sigma} c_{j\sigma}\,, \end{aligned} \tag{5.5}$$

where we have used the idea that the orbitals are vanishing infinitely far away. We have also inserted $t_{ij}$ as the hopping integral as the orbitals may overlap, which gives rise to a finite tunneling amplitude for electrons to neighboring ions. However, we assume that only nearest neighbors have a substantial contribution, and thus $t_{ij}$ is only finite for $j = i \pm 1$. We will later rewrite the Hamiltonian and return to Nambu⊗Spin space, and therefore already note that $t^*_{ij} = t_{ji}$, which can be seen directly from the integral.

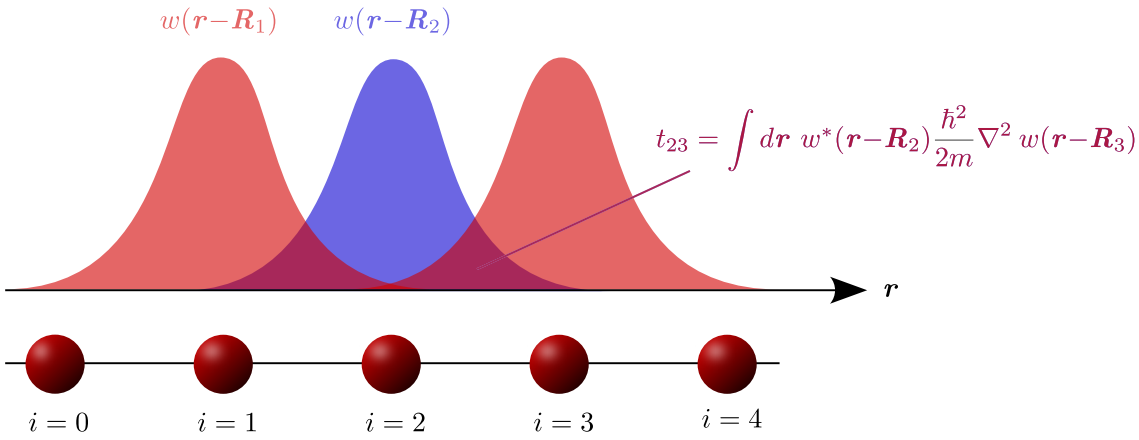


Figure 5.1: A qualitative picture of the spatial part of the electron wavefunction described by the Wannier orbitals. The overlapping regions give tunneling amplitudes between sites. In the nearest neighbor approximation, we assume $t_{ij}$ is non-negligible for $j = i \pm 1$.

Next, we consider how the spin-orbit interaction is mapped. We consider spin-orbit an effective background SU(2) field [71]. Thus, we write the spin-orbit part of the Hamiltonian as

$$\begin{aligned}\mathcal{H}_{soc} &= \sum_{\sigma\sigma'} \int d\boldsymbol{r}\, \psi^\dagger_\sigma(\boldsymbol{r}) \frac{i}{m} \boldsymbol{A}_{\sigma\sigma'} \cdot \nabla \psi_{\sigma'}(\boldsymbol{r}) \\ &= \sum_{ij\sigma\sigma'} c^\dagger_{i\sigma} c_{j\sigma'} \frac{i}{m} \boldsymbol{A}_{\sigma\sigma'} \cdot \int d\boldsymbol{r} w^*(\boldsymbol{r} - \boldsymbol{R}_i) \nabla w(\boldsymbol{r} - \boldsymbol{R}_j) \\ &= \sum_{\langle ij\rangle\sigma\sigma'} \alpha^{\sigma\sigma'}_{ij} c^\dagger_{i\sigma} c_{j\sigma'} \,, \end{aligned} \tag{5.6}$$

where the integral $\alpha^{\sigma\sigma'}_{ij}$ can be interpreted as a spin-dependent hopping term between neighboring ions. This term can be added to the hopping, rewriting it as $t^{\sigma\sigma'}_{ij} = t_{ij} + \alpha^{\sigma\sigma'}_{ij}$, which is not uncommon. However, we will keep it as a separate term. Considering the conjugate again, we start by noting that the spin-orbit field is Hermitian, which means $\boldsymbol{A}^*_{\sigma\sigma'} = \boldsymbol{A}_{\sigma'\sigma}$. We relate the integral over the Wannier orbitals to the nearest neighbor vector $\boldsymbol{d}_{ij}$ which changes sign for hopping in opposite directions, $\boldsymbol{d}_{ij} = -\boldsymbol{d}_{ji}$. Therefore, we write the spin-orbit term as $\alpha^{\sigma\sigma'}_{ij} = i\alpha\, \boldsymbol{n} \cdot (\boldsymbol{\sigma} \times \boldsymbol{d}_{ij})^{\sigma\sigma'}$, where the vector $\boldsymbol{n}$ is the direction of symmetry breaking. For later use, we define a vector $\boldsymbol{a}$ associated with the spin-orbit

$$\alpha^{\sigma\sigma'}_{ij} = \boldsymbol{a}^{\sigma\sigma'}_{ij} \cdot \boldsymbol{d}_{ij} \,. \tag{5.7}$$

It also lets us write down

$$\alpha^{\sigma\sigma'}_{ij} = \left(\alpha^{\sigma'\sigma}_{ji}\right)^* \,, \qquad \boldsymbol{a}^{\sigma\sigma'}_{ij} = -\left(\boldsymbol{a}^{\sigma'\sigma}_{ji}\right)^* = -\left(\boldsymbol{a}^{\sigma'\sigma}_{ij}\right)^* \,, \tag{5.8}$$

which will be used later in the derivation. For more details about the relationship between the Wannier orbitals and the nearest neighbor vectors, see appendix C.1.

Lastly, we consider the superconducting interaction part of the Hamiltonian. This interaction is realized through a two-particle attractive potential and can be written as

$$\begin{aligned}\mathcal{H}_s &= -\int d\boldsymbol{r}\, U(\boldsymbol{r}) \psi^\dagger_\downarrow(\boldsymbol{r}) \psi^\dagger_\uparrow(\boldsymbol{r}') \psi_\uparrow(\boldsymbol{r}') \psi_\downarrow(\boldsymbol{r}) \\ &= -\int d\boldsymbol{r} \left\{ \Delta(\boldsymbol{r}) \psi^\dagger_\downarrow(\boldsymbol{r}) \psi^\dagger_\uparrow + \Delta^*(\boldsymbol{r}) \psi_\uparrow(\boldsymbol{r}) \psi_\downarrow + U(\boldsymbol{r}) \langle \psi^\dagger_\downarrow(\boldsymbol{r}) \psi^\dagger_\uparrow(\boldsymbol{r})\rangle \langle \psi_\uparrow(\boldsymbol{r}) \psi_\downarrow(\boldsymbol{r})\rangle \right\} , \end{aligned} \tag{5.9}$$

where we have inserted the mean-field ansatz $\Delta(\boldsymbol{r}) = U(\boldsymbol{r}) \langle \psi_\uparrow(\boldsymbol{r}) \psi_\downarrow(\boldsymbol{r})\rangle$. Commutating the field operators and inserting the Wannier orbitals as before, we obtain

$$\begin{aligned}\mathcal{H}_s &= \sum_{ij} \Big\{ c^\dagger_{i\uparrow} c^\dagger_{j\downarrow} \int d\boldsymbol{r} \Delta(\boldsymbol{r}) w^*(\boldsymbol{r} - \boldsymbol{R}_i) w^*(\boldsymbol{r} - \boldsymbol{R}_j) \\ &\qquad + c_{i\downarrow} c_{j\uparrow} \int d\boldsymbol{r} \Delta^*(\boldsymbol{r}) w(\boldsymbol{r} - \boldsymbol{R}_i) w(\boldsymbol{r} - \boldsymbol{R}_j) \Big\} \\ &= \sum_i \left( \Delta_i c^\dagger_{i\uparrow} c^\dagger_{i\downarrow} + \Delta^*_i c_{i\downarrow} c_{i\uparrow} \right) \,, \end{aligned} \tag{5.10}$$

where we have used that $\Delta_{ij} \approx \Delta_i \delta_{ij}$. This implies that we assume $\Delta(\boldsymbol{r})$ varies slowly compared to the strongly localized Wannier orbitals. Therefore, the integral above only

gives a non-negligible contribution when $i = j$. We have not considered the last term in eq. (5.9). Mapping it to a lattice, the integral gives

$$\begin{aligned}\mathcal{E}_0 &= -\int d\boldsymbol{r}\, U(\boldsymbol{r})\langle\psi_\downarrow^\dagger(\boldsymbol{r})\psi_\uparrow^\dagger(\boldsymbol{r})\rangle\langle\psi_\uparrow(\boldsymbol{r})\psi_\downarrow(\boldsymbol{r})\rangle \\ &= -\int d\boldsymbol{r}\, U(\boldsymbol{r})\frac{\Delta(\boldsymbol{r})}{U(\boldsymbol{r})}\frac{\Delta^*(\boldsymbol{r})}{U(\boldsymbol{r})} \\ &= \sum_i \frac{|\Delta_i|^2}{U_i}\,. \end{aligned} \tag{5.11}$$

Collecting all terms, we have a Hamiltonian that describes free electrons, possible spin-dependent hopping between sites, and superconducting pairwise interactions on a discretized lattice. It can be written as

$$\begin{aligned}\mathcal{H} = \mathcal{E}_0 &- \sum_{i\sigma}\mu_i c_{i\sigma}^\dagger c_{i\sigma} - \sum_{\langle ij\rangle\sigma\sigma'}\left(t_{ij}\delta_{\sigma\sigma'} + \alpha_{ij}^{\sigma\sigma'}\right)c_{i\sigma}^\dagger c_{j\sigma'} \\ &+ \sum_i\left(\Delta_i c_{i\uparrow}^\dagger c_{i\downarrow}^\dagger + \Delta_i^* c_{i\downarrow}c_{i\uparrow}\right)\,. \end{aligned} \tag{5.12}$$

As in the quasiclassical theory, we introduce a basis such that our Hamiltonian is written in Nambu⊗Spin space. We choose the same basis as previously, namely

$$\hat{c}_i^\dagger = \begin{pmatrix} c_{i\uparrow}^\dagger, & c_{i\downarrow}^\dagger, & c_{i\uparrow}, & c_{i\downarrow}\end{pmatrix}\,. \tag{5.13}$$

We do a trick to reconcile the Hamiltonian we already have with the newly chosen basis. We will rewrite the Hamiltonian using the fermionic anti-commutation relations in eq. (2.1), and then collect all constant terms, not involving creation or annihilation operators, into the constant $\mathcal{E}$. We will discard this constant when introducing the lattice space, as it does not change the system's dynamics. We can write the total Hamiltonian as

$$\begin{aligned}\mathcal{H} = \ \mathcal{E} &- \frac{1}{2}\sum_{i\sigma}\mu_i\left(c_{i\sigma}^\dagger c_{i\sigma} - c_{i\sigma}c_{i\sigma}^\dagger\right) \\ &- \frac{1}{2}\sum_{\langle ij\rangle\sigma}\left(t_{ij}c_{i\sigma}^\dagger c_{j\sigma} - t_{ji}c_{i\sigma}c_{j\sigma}^\dagger\right) \\ &- \frac{1}{2}\sum_{\langle ij\rangle\sigma\sigma'}\left(\alpha_{ij}^{\sigma\sigma'}c_{i\sigma}^\dagger c_{j\sigma'} - \alpha_{ji}^{\sigma'\sigma}c_{i\sigma}c_{j\sigma'}^\dagger\right) \\ &+ \frac{1}{2}\sum_i\left(\Delta_i(c_{i\uparrow}^\dagger c_{i\downarrow}^\dagger - c_{i\downarrow}^\dagger c_{i\uparrow}^\dagger) + \Delta_i^*(c_{i\downarrow}c_{i\uparrow} - c_{i\uparrow}c_{i\downarrow})\right)\,. \end{aligned} \tag{5.14}$$

Using the Nambu spinor, we can write it much more compactly, which will be the starting point when introducing the actual lattice

$$\mathcal{H} = \ \mathcal{E} - \frac{1}{2}\sum_{ij}\hat{c}_i^\dagger\hat{H}_{ij}\hat{c}_j\,, \tag{5.15}$$

$$\hat{H}_{ij} = \begin{pmatrix} \mu_i\delta_{ij} + t_{ij} + \alpha_{ij}^{\uparrow\uparrow} & \alpha_{ij}^{\uparrow\downarrow} & 0 & \Delta_i\delta_{ij} \\ \alpha_{ij}^{\downarrow\uparrow} & \mu_i\delta_{ij} + t_{ij} + \alpha_{ij}^{\downarrow\downarrow} & -\Delta_i\delta_{ij} & 0 \\ 0 & -\Delta_i^*\delta_{ij} & -\mu_i\delta_{ij} - t_{ji} - \alpha_{ji}^{\uparrow\uparrow} & -\alpha_{ji}^{\downarrow\uparrow} \\ \Delta_i^*\delta_{ij} & 0 & -\alpha_{ji}^{\uparrow\downarrow} & -\mu_i\delta_{ij} - t_{ji} - \alpha_{ji}^{\uparrow\uparrow} \end{pmatrix}\,. \tag{5.16}$$

## 5.2 Periodic boundary condictions

The Hamiltonian derived in the previous subsection is valid for systems of any dimension. In this thesis, we will only consider the case of one- and two-dimensional lattices. In the first case, we only apply periodic boundary conditions when investigating a closed ring or ellipse, which will be specified in the results. In that case, the only ingredient needed is a hopping between the first and the last lattice site. When investigating systems in two dimensions, we can apply periodic boundary conditions in the direction without any material change, which we label $y$. The equations needed for that are derived in this section. This allows us to model a large system using only a few lattice points. Therefore, we can write the fermionic operators as the following Fourier transforms

$$c_{i,\sigma} = \frac{1}{\sqrt{N_y}} \sum_{k_y} c_{i_x,k_y,\sigma} e^{ik_y i_y} \,, \tag{5.17}$$

$$c^\dagger_{i,\sigma} = \frac{1}{\sqrt{N_y}} \sum_{k_y} c^\dagger_{i_x,k_y,\sigma} e^{-ik_y i_y} \,. \tag{5.18}$$

The sum over $k_y$ is restricted to the first Brillouin zone, which is $k_y \in (-\pi, \pi]$. The values that $k_y$ can take are also restricted by the periodic boundary conditions and the number of lattice points in the $y$- direction. The momentum can only take values $k_y = 2\pi n/N_y$, where $n$ is an integer [105]. We also want to note the relation

$$\frac{1}{N_y} \sum_{i_y} e^{i(k_y - k'_y) i_y} = \delta_{k_y,k'_y} \,, \tag{5.19}$$

which will be important when changing the fermionic operators. To begin with, we which to rewrite the Hamiltonian in eq. (5.14) using the operators $c_{i_x,k_y,\sigma}$ and $c^\dagger_{i_x,k_y,\sigma}$. We will go through the calculation of each term explicitly. Beginning with the first sum, containing the chemical potential, we get

$$\begin{aligned}
&\sum_{i\sigma} \mu_i \left( c^\dagger_{i\sigma} c_{i\sigma} - c_{i\sigma} c^\dagger_{i\sigma} \right) \\
&= \frac{1}{N_y} \sum_{i_x,i_y,\sigma} \sum_{k_y,k'_y} \mu_{i_x,k_y} \left( c^\dagger_{i_x,k_y,\sigma} c_{i_x,k'_y,\sigma} e^{i(k'_y - k_y) i_y} - c_{i_x,k_y,\sigma} c^\dagger_{i_x,k'_y,\sigma} e^{i(k_y - k'_y) i_y} \right) \\
&= \sum_{i_x,k_y,\sigma} \left( \mu_{i_x,k_y}\, c^\dagger_{i_x,k_y,\sigma} c_{i_x,k_y,\sigma} - \mu_{i_x,-k_y}\, c_{i_x,-k_y,\sigma} c^\dagger_{i_x,-k_y,\sigma} \right) \,.
\end{aligned} \tag{5.20}$$

In the second term, we have the nearest neighbor hopping. We will split the sum into hopping in the $x$- and $y$-direction for reasons that will become clear shortly. Starting with hopping in the $x$-direction, we get

$$\begin{aligned}
&\sum_{\langle ij \rangle_x,\sigma} \left( t_{ij} c^\dagger_{i\sigma} c_{j\sigma} - t_{ji} c_{i\sigma} c^\dagger_{j\sigma} \right) \\
&= \frac{1}{N_y} \sum_{\langle i_x j_x \rangle, i_y,\sigma} \sum_{k_y,k'_y} \left( t_{i_x,j_x,k_y} c^\dagger_{i_x,k_y,\sigma} c_{j_x,k'_y,\sigma} e^{i(k'_y - k_y) i_y} - t_{j_x,i_x,k_y} c_{i_x,k_y,\sigma} c^\dagger_{j_x,k'_y,\sigma} e^{i(k_y - k'_y) i_y} \right) \\
&= \sum_{\langle i_x j_x \rangle, k_y,\sigma} \left( t_{i_x,j_x,k_y} c^\dagger_{i_x,k_y,\sigma} c_{j_x,k_y,\sigma} - t_{j_x,i_x,-k_y} c_{i_x,-k_y,\sigma} c^\dagger_{j_x,-k_y,\sigma} \right) \,,
\end{aligned} \tag{5.21}$$

which has the same form as the previous hopping term. However, in the $y$-direction, we will get a hopping described by an onsite formulation modulated by $k_y$. In this direction,

we need to write out both directions of hopping. We get

$$
\begin{aligned}
&\sum_{\langle ij\rangle_y,\sigma}\left(t_{ij}c^\dagger_{i\sigma}c_{j\sigma}-t_{ji}c_{i\sigma}c^\dagger_{j\sigma}\right)\\
&=\frac{1}{N_y}\sum_{i_x,i_y,\sigma}\sum_{k_y,k'_y}\sum_{\pm}\Bigg(t_{i_x,i_x,k_y}c^\dagger_{i_x,k_y,\sigma}c_{i_x,k'_y,\sigma}e^{-ik_yi_y+ik'_y(i_y\pm1)}\\
&\qquad\qquad -t_{i_x,i_x,k_y}c_{i_x,k_y,\sigma}c^\dagger_{i_x,k'_y,\sigma}e^{ik_yi_y-ik'_y(i_y\pm1)}\Bigg)\\
&=\frac{1}{N_y}\sum_{i_x,i_y,\sigma}\sum_{k_y,k'_y}\sum_{\pm}\Bigg(t_{i_x,i_x,k_y}e^{\pm ik'_y}c^\dagger_{i_x,k_y,\sigma}c_{i_x,k'_y,\sigma}e^{i(k'_y-k_y)i_y}\\
&\qquad\qquad -t_{i_x,i_x,k_y}e^{\mp ik'_y}c_{i_x,k_y,\sigma}c^\dagger_{i_x,k'_y,\sigma}e^{i(k_y-k'_y)i_y}\Bigg)\\
&=\sum_{i_x,k_y,\sigma}\sum_{\pm}\left(t_{i_x,i_x,k_y}e^{\pm ik_y}c^\dagger_{i_x,k_y,\sigma}c_{i_x,k_y,\sigma}-t_{i_x,i_x,k_y}e^{\mp ik_y}c_{i_x,k_y,\sigma}c^\dagger_{i_x,k_y,\sigma}\right)\\
&=\sum_{i_x,k_y,\sigma}2\cos k_y\,\left(t_{i_x,i_x,k_y}\,c^\dagger_{i_x,k_y,\sigma}c_{i_x,k_y,\sigma}-t_{i_x,i_x,-k_y}\,c_{i_x,-k_y,\sigma}c^\dagger_{i_x,-k_y,\sigma}\right),
\end{aligned}
\tag{5.22}
$$

where $t_{i_x,i_x,k_y}$ is the hopping integral for neighboring sites in the $y$-direction. Next, we see how the spin-orbit hopping term transforms. Again, we consider separately hopping in the $x$- and $y$-direction. We begin with

$$
\begin{aligned}
&\sum_{\langle ij\rangle_x,\sigma,\sigma'}\left(\alpha^{\sigma\sigma'}_{ij}c^\dagger_{i\sigma}c_{j\sigma'}-\alpha^{\sigma'\sigma}_{ji}c_{i\sigma}c^\dagger_{j\sigma'}\right)\\
&=\frac{1}{N_y}\sum_{i_x,j_x,i_y}\sum_{\sigma,\sigma'}\sum_{k_y,k'_y}\Bigg(\alpha^{\sigma\sigma'}_{i_x,j_x}c^\dagger_{i_x,k_y,\sigma}c_{j_x,k'_y,\sigma'}e^{i(k'_y-k_y)i_y}\\
&\qquad\qquad -\alpha^{\sigma'\sigma}_{j_x,i_x}c_{i_x,k_y,\sigma}c^\dagger_{j_x,k'_y,\sigma'}e^{i(k_y-k'_y)i_y}\Bigg)\\
&=\sum_{i_x,j_x,k_y,\sigma,\sigma'}\left(\alpha^{\sigma\sigma'}_{i_x,j_x}c^\dagger_{i_x,k_y,\sigma}c_{j_x,k_y,\sigma'}-\alpha^{\sigma'\sigma}_{j_x,i_x}c_{i_x,k_y,\sigma}c^\dagger_{j_x,k_y,\sigma'}\right).
\end{aligned}
\tag{5.23}
$$

Following the same procedure as in eq. (5.22), we get

$$
\begin{aligned}
&\sum_{\langle ij\rangle_y,\sigma,\sigma'}\left(\alpha^{\sigma\sigma'}_{ij}c^\dagger_{i\sigma}c_{j\sigma'}-\alpha^{\sigma'\sigma}_{ji}c_{i\sigma}c^\dagger_{j\sigma'}\right)\\
&=\frac{1}{N_y}\sum_{i_x,i_y}\sum_{\sigma,\sigma'}\sum_{k_y,k'_y}\sum_{\pm}\pm\Bigg(a^{\sigma\sigma'}_{i_x,i_x}c^\dagger_{i_x,k_y,\sigma}c_{i_x,k'_y,\sigma'}e^{-ik_yi_y+ik'_y(i_y\pm1)}\\
&\qquad\qquad -a^{\sigma'\sigma}_{i_x,i_x}c_{i_x,k_y,\sigma}c^\dagger_{i_x,k'_y,\sigma'}e^{ik_yi_y-ik'_y(i_y\pm1)}\Bigg)\\
&=\frac{1}{N_y}\sum_{i_x,i_y}\sum_{\sigma,\sigma'}\sum_{k_y,k'_y}\sum_{\pm}\pm\Bigg(a^{\sigma\sigma'}_{i_x,i_x}e^{\pm ik'_y}c^\dagger_{i_x,k_y,\sigma}c_{i_x,k'_y,\sigma'}e^{i(k'_y-k_y)i_y}\\
&\qquad\qquad -a^{\sigma'\sigma}_{i_x,i_x}e^{\mp ik'_y}c_{i_x,k_y,\sigma}c^\dagger_{i_x,k'_y,\sigma'}e^{i(k_y-k'_y)i_y}\Bigg)\\
&=\sum_{i_x,k_y}\sum_{\sigma,\sigma'}\sum_{\pm}\pm\left(a^{\sigma\sigma'}_{i_x,i_x}e^{\pm ik_y}c^\dagger_{i_x,k_y,\sigma}c_{i_x,k_y,\sigma'}-a^{\sigma'\sigma}_{i_x,i_x}e^{\mp ik_y}c_{i_x,k_y,\sigma}c^\dagger_{i_x,k_y,\sigma'}\right)\\
&=\sum_{i_x,k_y}\sum_{\sigma,\sigma'}2i\sin k_y\,\left(a^{\sigma\sigma'}_{i_x,i_x}c^\dagger_{i_x,k_y,\sigma}c_{i_x,k_y,\sigma'}+a^{\sigma'\sigma}_{i_x,i_x}c_{i_x,-k_y,\sigma}c^\dagger_{i_x,-k_y,\sigma'}\right),
\end{aligned}
\tag{5.24}
$$

where $a_{i_x,i_x}$ is the spin-dependent hopping in the $y$-direction. Also, note that a $\pm$ was added to account for the hopping in the two opposite directions along the $y$-axis. It comes directly from the component $d_{ij}^{y}$ of the nearest neighbor vector. Finally, the superconducting term transforms as

$$\begin{aligned}
&\sum_{i,\sigma}\left(\sigma\Delta_i c_{i,\sigma}^{\dagger}c_{i,-\sigma}^{\dagger}-\sigma\Delta_i^{*}c_{i,\sigma}c_{i,-\sigma}\right)\\
&=\frac{1}{N_y}\sum_{i_x,i_y,\sigma}\sum_{k_y,k_y'}\Big(\sigma\Delta_{i_x,k_y}c_{i_x,k_y,\sigma}^{\dagger}c_{i_x,k_y',-\sigma}^{\dagger}e^{-i(k_y+k_y')i_y}\\
&\qquad\qquad-\sigma\Delta_{i_x,k_y}^{*}c_{i_x,k_y,\sigma}c_{i_x,k_y',-\sigma}e^{i(k_y+k_y')i_y}\Big)\\
&=\sum_{i_x,k_y}\left(\sigma\Delta_{i_x,k_y}c_{i_x,k_y,\sigma}^{\dagger}c_{i_x,-k_y,-\sigma}^{\dagger}-\sigma\Delta_{i_x,k_y}^{*}c_{i_x,k_y,\sigma}c_{i_x,-k_y,-\sigma}\right)\,. \qquad (5.25)
\end{aligned}$$

Collecting all the terms above, we can rewrite the Hamiltonian in eq. (5.14) to have periodic boundary conditions. We write it as

$$\begin{aligned}
\mathcal{H}=\mathcal{E}&-\frac{1}{2}\sum_{i_x,k_y,\sigma}\left(\mu_{i_x,k_y}\,c_{i_x,k_y,\sigma}^{\dagger}c_{i_x,k_y,\sigma}-\mu_{i_x,-k_y}\,c_{i_x,-k_y,\sigma}c_{i_x,-k_y,\sigma}^{\dagger}\right)\\
&-\frac{1}{2}\sum_{\langle i_xj_x\rangle,k_y,\sigma}\left(t_{i_x,j_x,k_y}c_{i_x,k_y,\sigma}^{\dagger}c_{j_x,k_y,\sigma}-t_{j_x,i_x,-k_y}c_{i_x,-k_y,\sigma}c_{j_x,-k_y,\sigma}^{\dagger}\right)\\
&-\frac{1}{2}\sum_{i_x,k_y,\sigma}2\cos k_y\,\left(t_{i_x,i_x,k_y}\,c_{i_x,k_y,\sigma}^{\dagger}c_{i_x,k_y,\sigma}-t_{i_x,i_x,-k_y}\,c_{i_x,-k_y,\sigma}c_{i_x,-k_y,\sigma}^{\dagger}\right)\\
&-\frac{1}{2}\sum_{\langle i_xj_x\rangle,k_y,\sigma,\sigma'}\left(\alpha_{i_x,j_x}^{\sigma\sigma'}c_{i_x,k_y,\sigma}^{\dagger}c_{j_x,k_y,\sigma'}-\alpha_{j_x,i_x}^{\sigma'\sigma}c_{i_x,-k_y,\sigma}c_{j_x,-k_y,\sigma'}^{\dagger}\right)\\
&-\frac{1}{2}\sum_{i_x,k_y}\sum_{\sigma,\sigma'}2i\sin k_y\,\left(a_{i_x,i_x}^{\sigma\sigma'}c_{i_x,k_y,\sigma}^{\dagger}c_{i_x,k_y,\sigma'}+a_{i_x,i_x}^{\sigma'\sigma}c_{i_x,-k_y,\sigma}c_{i_x,-k_y,\sigma'}^{\dagger}\right)\\
&+\frac{1}{2}\sum_{i_x,k_y,\sigma}\left(\sigma\Delta_{i_x,k_y}c_{i_x,k_y,\sigma}^{\dagger}c_{i_x,-k_y,-\sigma}^{\dagger}-\sigma\Delta_{i_x,k_y}^{*}c_{i_x,k_y,\sigma}c_{i_x,-k_y,-\sigma}\right)\,. \qquad (5.26)
\end{aligned}$$

Note that, with this form, we allow there to be a momentum dependence in either direction in the spin-orbit coupling. Thus, the matrix $\alpha_{i_x,i_x}$ is not equal to $\alpha_{i_x,j_x}$ with $i_x=j_x$, since these are related to a momentum dependence in the $y$- and $x$-direction, respectively. If we choose a new basis, the above equation can be rewritten to the same form as eq. (5.15). If we choose the new basis

$$\hat{B}_{i_x,k_y}^{\dagger}=\begin{pmatrix}c_{i_x,k_y,\uparrow}^{\dagger} & c_{i_x,k_y,\downarrow}^{\dagger} & c_{i_x,-k_y,\uparrow} & c_{i_x,-k_y,\downarrow}\end{pmatrix}\,. \qquad (5.27)$$

With this basis, we can again write the Hamiltonian compactly as

$$\mathcal{H}=\mathcal{E}-\frac{1}{2}\sum_{i_x,j_x,k_y}\hat{B}_{i_x,k_y}^{\dagger}\hat{H}_{i_x,j_x,k_y}\hat{B}_{j_x,k_y}\,, \qquad (5.28)$$

where

$$\hat{H}_{i_x,j_x,k_y} = \begin{pmatrix} \epsilon_{i_x,j_x,k_y} + \lambda^{\uparrow\uparrow}_{i_x,j_x,k_y} & \lambda^{\uparrow\downarrow}_{i_x,j_x,k_y} & 0 & \Delta_{i_x,k_y}\delta_{i_x,j_x} \\ \lambda^{\downarrow\uparrow}_{i_x,j_x,k_y} & \epsilon_{i_x,j_x,k_y} + \lambda^{\downarrow\downarrow}_{i_x,j_x,k_y} & -\Delta_{i_x,k_y}\delta_{i_x,j_x} & 0 \\ 0 & -\Delta^*_{i_x,-k_y}\delta_{i_x,j_x} & -\epsilon_{j_x,i_x,-k_y} - \lambda^{\uparrow\uparrow}_{j_x,i_x,-k_y} & -\lambda^{\downarrow\uparrow}_{j_x,i_x,-k_y} \\ \Delta^*_{i_x,-k_y}\delta_{i_x,j_x} & 0 & -\lambda^{\uparrow\downarrow}_{j_x,i_x,-k_y} & -\epsilon_{j_x,i_x,-k_y} - \lambda^{\downarrow\downarrow}_{j_x,i_x,-k_y} \end{pmatrix}, \tag{5.29}$$

and

$$\epsilon_{i_x,j_x,k_y} = \Big(2\cos k_y\, t_{i_x,i_x,k_y} + \mu_{i_x,k_y}\Big)\delta_{i_x,j_x} + t_{i_x,j_x,k_y}\delta_{i_x,j_x\pm1}\,, \tag{5.30}$$

$$\lambda^{\sigma\sigma'}_{i_x,j_x,k_y} = 2\sin k_y\, a^{\sigma\sigma'}_{i_x,i_x}\delta_{i_x,j_x} + a^{\sigma\sigma'}_{i_x,j_x}(\delta_{i_x,j_x+1} - \delta_{i_x,j_x-1})\,. \tag{5.31}$$

To conclude, we have derived a tight-binding Hamiltonian for a square lattice with periodic boundary conditions in the $y$-direction. Next, we will express the Hamiltonian as a single matrix in lattice space.

## 5.3 Matrix equations in lattice space

To make predictions about observables, we formulate the theory so that it can be solved numerically. To write the problem even more compactly, we introduce an operator $W_{k_y}$ [104], a column vector where each element is a Nambu spinor at a different lattice site. The vector and its hermitian conjugate can be written as

$$W_{k_y} = \begin{pmatrix} \hat{B}_{1,k_y} \\ \hat{B}_{2,k_y} \\ \hat{B}_{3,k_y} \\ \vdots \\ \hat{B}_{N_x,k_y} \end{pmatrix}, \qquad W^\dagger_{k_y} = \begin{pmatrix} \hat{B}^\dagger_{1,k_y} & \hat{B}^\dagger_{2,k_y} & \hat{B}^\dagger_{3,k_y} & \dots & \hat{B}^\dagger_{N_x,k_y} \end{pmatrix}, \tag{5.32}$$

where $N_x$ is the number of lattice sites in the $x$-direction. This means that these are of length $4N_x$, since each Nambu spinor $\hat{B}_{i_x,k_y}$ contains four elements, as seen in eq. (5.27). Similiarily, we can sort all Hamiltonians $\hat{H}_{i_x,j_x,k_y}$ into a $4N_x \times 4N_x$ matrix $H_{k_y}$. This matrix will have the following structure

$$H_{k_y} = \begin{pmatrix} \hat{H}_{1,1,k_y} & \hat{H}_{1,2,k_y} & \hat{H}_{1,3,k_y} & \dots & \hat{H}_{1,N_x,k_y} \\ \hat{H}_{2,1,k_y} & \hat{H}_{2,2,k_y} & \hat{H}_{2,3,k_y} & \dots & \hat{H}_{2,N_x,k_y} \\ \hat{H}_{3,1,k_y} & \hat{H}_{3,2,k_y} & \hat{H}_{3,3,k_y} & \dots & \hat{H}_{3,N_x,k_y} \\ \vdots & \vdots & \vdots & \ddots & \vdots \\ \hat{H}_{N_x,1,k_y} & \hat{H}_{N_x,2,k_y} & \hat{H}_{N_x,3,k_y} & \dots & \hat{H}_{N_x,N_x,k_y} \end{pmatrix}. \tag{5.33}$$

As before, the indices describe hopping between lattice site $i_x$ and $j_x$ in $\hat{H}_{i_x,j_x,k_y}$. This means the diagonal are onsite terms, while the off-diagonals describe hopping. The first off-diagonal elements are nearest neighbors, and the second off-diagonal elements are next-nearest neighbors. Discarding the constant energy term $\mathcal{E}$, the Hamiltonian describing system can be written as

$$\mathcal{H} = -\frac{1}{2}\sum_{k_y} W^\dagger_{k_y} H_{k_y} W_{k_y}. \tag{5.34}$$

### 5.3.1 Particle-hole symmetry

The end goal is to diagonalize our Hamiltonian and make predictions using the eigenenergies and new quasiparticle operators. There is, however, a point to be made about the signs of the eigenenergies, which relates to a particle-hole symmetry [103]. We define our eigenenergies by the eigenvalue problem

$$H_{k_y}\Phi_{n,k_y} = \mathcal{E}_{n,k_y}\Phi_{n,k_y}\ , \tag{5.35}$$

where $\Phi_{n,k_y}$ is a $4N_x$-element eigenvector given by $\Phi^\dagger_{n,k_y} = \begin{pmatrix}\hat{\phi}^\dagger_{1,n,k_y} & \hat{\phi}^\dagger_{2,n,k_y} & \dots & \hat{\phi}^\dagger_{N_x,n,k_y}\end{pmatrix}$. This means that the problem can be rewritten for each lattice site $i_x$ and momentum index $k_y$, namely

$$\sum_{j_x}\hat{H}_{i_x,j_x,k_y}\hat{\phi}_{j_x,n,k_y} = \mathcal{E}_{n,k_y}\hat{\phi}_{i_x,n,k_y}. \tag{5.36}$$

The eigenvectors can be written in terms of their elements. It has four entries, where the first two effectively correspond to a particle spinor and the last two a hole spinor. We denote these elements

$$\hat{\phi}^\dagger_{i_x,n,k_y} = \begin{pmatrix}u^*_{i_x,n,k_y} & v^*_{i_x,n,k_y} & w^*_{i_x,n,k_y} & x^*_{i_x,n,k_y}\end{pmatrix}\ . \tag{5.37}$$

If we explicitly write out the matrix equation in eq. (5.35), we see the particle-hole symmetry in the Hamiltonian, where the top rows are related to the bottom ones through complex conjugation. We will show that this also results in a similar symmetry in the eigenenergies. We begin by writing out the four equations for each element separately, which gives

$$\Delta_{i_x,k_y}x_{i_x,n,k_y} + \sum_{j_x}\left[\left(\epsilon_{i_x,j_x,k_y} + \lambda^{\uparrow\uparrow}_{i_x,j_x,k_y}\right)u_{j_x,n,k_y} + \lambda^{\uparrow\downarrow}_{i_x,j_x,k_y}v_{j_x,n,k_y}\right] = \mathcal{E}_{n,k_y}u_{i_x,n,k_y}, \tag{5.38}$$

$$-\Delta_{i_x,k_y}w_{i_x,n,k_y} + \sum_{j_x}\left[\left(\epsilon_{i_x,j_x,k_y} + \lambda^{\downarrow\downarrow}_{i_x,j_x,k_y}\right)v_{j_x,n,k_y} + \lambda^{\downarrow\uparrow}_{i_x,j_x,k_y}u_{j_x,n,k_y}\right] = \mathcal{E}_{n,k_y}v_{i_x,n,k_y}, \tag{5.39}$$

$$-\Delta^*_{i_x,-k_y}v_{i_x,n,k_y} - \sum_{j_x}\left[\left(\epsilon_{j_x,i_x,-k_y} + \lambda^{\uparrow\uparrow}_{j_x,i_x,-k_y}\right)w_{j_x,n,k_y} + \lambda^{\downarrow\uparrow}_{j_x,i_x,-k_y}x_{j_x,n,k_y}\right] = \mathcal{E}_{n,k_y}w_{i_x,n,k_y}, \tag{5.40}$$

$$\Delta^*_{i_x,-k_y}u_{i_x,n,k_y} - \sum_{j_x}\left[\left(\epsilon_{j_x,i_x,-k_y} + \lambda^{\downarrow\downarrow}_{j_x,i_x,-k_y}\right)x_{j_x,n,k_y} + \lambda^{\uparrow\downarrow}_{j_x,i_x,-k_y}w_{j_x,n,k_y}\right] = \mathcal{E}_{n,k_y}x_{i_x,n,k_y}. \tag{5.41}$$

To gain insight into the particle-hole symmetry, we complex conjugate the equations for the last two elements and let $k_y \to -k_y$. This gives

$$\Delta_{i_x,k_y} x_{i_x,n,k_y} + \sum_{j_x} \left[ \left( \epsilon_{i_x,j_x,k_y} + \lambda^{\uparrow\uparrow}_{i_x,j_x,k_y} \right) u_{j_x,n,k_y} + \lambda^{\uparrow\downarrow}_{i_x,j_x,k_y} v_{j_x,n,k_y} \right] = \mathcal{E}_{n,k_y} u_{i_x,n,k_y}, \tag{5.42}$$

$$-\Delta_{i_x,k_y} w_{i_x,n,k_y} + \sum_{j_x} \left[ \left( \epsilon_{i_x,j_x,k_y} + \lambda^{\downarrow\downarrow}_{i_x,j_x,k_y} \right) v_{j_x,n,k_y} + \lambda^{\downarrow\uparrow}_{i_x,j_x,k_y} u_{j_x,n,k_y} \right] = \mathcal{E}_{n,k_y} v_{i_x,n,k_y}, \tag{5.43}$$

$$\Delta_{i_x,k_y} v^*_{i_x,n,-k_y} + \sum_{j_x} \left[ \left( \epsilon_{i_x,j_x,k_y} + \lambda^{\uparrow\uparrow}_{i_x,j_x,k_y} \right) w^*_{j_x,n,-k_y} + \lambda^{\uparrow\downarrow}_{i_x,j_x,k_y} x^*_{j_x,n,-k_y} \right] = -\mathcal{E}_{n,-k_y} w^*_{i_x,n,-k_y}, \tag{5.44}$$

$$-\Delta_{i_x,k_y} u^*_{i_x,n,-k_y} + \sum_{j_x} \left[ \left( \epsilon_{i_x,j_x,k_y} + \lambda^{\downarrow\downarrow}_{i_x,j_x,k_y} \right) x^*_{j_x,n,-k_y} + \lambda^{\downarrow\uparrow}_{i_x,j_x,k_y} w^*_{j_x,n,-k_y} \right] = -\mathcal{E}_{n,-k_y} x^*_{i_x,n,-k_y}. \tag{5.45}$$

From the above equations, we can identify the eigenvector

$$\Phi_{n,k_y} = \begin{pmatrix} u_{1,n,k_y} & v_{1,n,k_y} & w_{1,n,k_y} & x_{1,n,k_y} & u_{2,n,k_y} & v_{2,n,k_y}, \ldots \end{pmatrix}^T , \tag{5.46}$$

which corresponds to the the positive eigenvalues $+\mathcal{E}_{n,k_y}$. In addition to this vector, there must be another eigenvector

$$\Psi_{n,-k_y} = \begin{pmatrix} w^*_{1,n,-k_y} & x^*_{1,n,-k_y} & u^*_{1,n,-k_y} & v^*_{1,n,-k_y} & w^*_{2,n,-k_y} & x^*_{2,n,-k_y}, \ldots \end{pmatrix}^T , \tag{5.47}$$

associated with the negative eigenvalues $-\mathcal{E}_{n,-k_y}$. All the eigenvalues of eq. (5.35) can thus be written as $\mathcal{E}_{1,k_y}, \ldots, \mathcal{E}_{2N_x,k_y}, -\mathcal{E}_{1,-k_y}, \ldots, -\mathcal{E}_{2N_x,-k_y}$. The eigenvalues always come in pairs since there are two linearly independent eigenvectors. For the $k_y = 0$ case we can write $\mathcal{E}_{n,0} = -\mathcal{E}_{n+2N_x,0}$. The eigenvector components for the zero momentum are related through

$$\begin{aligned} u_{i_x,n,0} &= v^*_{i_x,n+2N_x,0}, \qquad & w_{i_x,n,0} &= x^*_{i_x,n+2N_x,0} , \\ v_{i_x,n,0} &= u^*_{i_x,n+2N_x,0}, \qquad & x_{i_x,n,0} &= w^*_{i_x,n+2N_x,0} . \end{aligned} \tag{5.48}$$

This observation will be important when we use the eigenvectors to express expectation values since we should only use linearly independent operators. To do this, we will use the zero momentum relations above and the relationship between eqs. (5.46) and (5.47).

### 5.3.2 Diagonalization

Next, we attack the actual problem at hand, diagonalizing our Hamiltonian. First, we make a note that $H_{k_y}$ is Hermitian since $\hat{H}_{i_x,j_x,k_y}$ is. Thus, we can diagonalize the matrix by using the eigenvectors we previously found. The diagonalization looks like

$$H_{k_y} = P_{k_y} D_{k_y} P^{-1}_{k_y} = P_{k_y} D_{k_y} P^{\dagger}_{k_y}, \tag{5.49}$$

where $P_{k_y} = \begin{bmatrix} \Phi_{1,k_y} & \Phi_{2,k_y} & \ldots & \Phi_{4N_x,k_y} \end{bmatrix}$ is a block matrix and $D_{k_y} = \text{diag}\left( \mathcal{E}_{1,k_y}, \mathcal{E}_{2,k_y}, \ldots, \mathcal{E}_{4N_x,k_y} \right)$ is a diagonal matrix. Inserting this diagonalization into eq. (5.34) we get

$$\mathcal{H} = -\frac{1}{2} \sum_{n,k_y} \mathcal{E}_{n,k_y} \gamma^{\dagger}_{n,k_y} \gamma_{n,k_y} , \tag{5.50}$$

where $\gamma_{n,k_y}$ is the nth element of the new quasiparticle operators we define by $\gamma^\dagger_{k_y} = W^\dagger_{k_y} P_{k_y}$ and $\gamma_{k_y} = P^{-1}_{k_y} W_{k_y}$. We note that the new quasiparticle operators do obey the usual fermionic anti-commutation relations in eq. (2.1). To see how the new operators are related to the old ones, we explicitly write out the relation

$$\begin{pmatrix} \gamma_{1,k_y} \\ \vdots \\ \gamma_{4N_x,k_y} \end{pmatrix} = \begin{pmatrix} u_{1,1,k_y} & \cdots & u_{1,4N_x,k_y} \\ v_{1,1,k_y} & \cdots & v_{1,4N_x,k_y} \\ w_{1,1,k_y} & \cdots & w_{1,4N_x,k_y} \\ x_{1,1,k_y} & \cdots & x_{1,4N_x,k_y} \\ \vdots & \ddots & \vdots \\ u_{N_x,1,k_y} & \cdots & u_{N_x,4N_x,k_y} \\ v_{N_x,1,k_y} & \cdots & v_{N_x,4N_x,k_y} \\ w_{N_x,1,k_y} & \cdots & w_{N_x,4N_x,k_y} \\ x_{N_x,1,k_y} & \cdots & x_{N_x,4N_x,k_y} \end{pmatrix}^\dagger \begin{pmatrix} c_{1,k_y,\uparrow} \\ c_{1,k_y,\downarrow} \\ c^\dagger_{1,-k_y,\uparrow} \\ c^\dagger_{1,-k_y,\downarrow} \\ \vdots \\ c_{N_x,k_y,\uparrow} \\ c_{N_x,k_y,\downarrow} \\ c^\dagger_{N_x,-k_y,\uparrow} \\ c^\dagger_{N_x,-k_y,\downarrow} \end{pmatrix}, \tag{5.51}$$

which can be written more concisely as

$$\gamma_{n,k_y} = \sum_{i_x} \left( u^*_{i_x,n,k_y} c_{i_x,k_y,\uparrow} + v^*_{i_x,n,k_y} c_{i_x,k_y,\downarrow} + w^*_{i_x,n,k_y} c^\dagger_{i_x,-k_y,\uparrow} + x^*_{i_x,n,k_y} c^\dagger_{i_x,-k_y,\downarrow} \right) . \tag{5.52}$$

Because of the symmetry arguments from before, there must be another eigenvector $\Psi_{n,-k_y}$ with eigenvalues $-\mathcal{E}_{n,-k_y}$. Doing the same calculation with the block matrix $P = \begin{bmatrix} \Psi_{1,-k_y} & \Psi_{2,-k_y} & \dots & \Psi_{4N_x,-k_y} \end{bmatrix}$ gives the new quasiparticle

$$\gamma_{m,k_y} = \sum_{j_x} \left( w_{j_x,m,-k_y} c_{j_x,k_y,\uparrow} + x_{j_x,m,-k_y} c_{j_x,k_y,\downarrow} + u_{j_x,m,-k_y} c^\dagger_{j_x,-k_y,\uparrow} + v_{j_x,m,-k_y} c^\dagger_{j_x,-k_y,\downarrow} \right) , \tag{5.53}$$

which is not independent of those from the first eigenvector $\Phi_{n,k_y}$. If we take the hermitian conjugate and transform $k_y \to -k_y$, we see they are related

$$\gamma^\dagger_{m,-k_y} = \sum_{j_x} \left( w^*_{j_x,m,k_y} c^\dagger_{j_x,-k_y,\uparrow} + x^*_{j_x,m,k_y} c^\dagger_{j_x,-k_y,\downarrow} + u^*_{j_x,m,k_y} c_{j_x,k_y,\uparrow} + v^*_{j_x,m,k_y} c_{j_x,k_y,\downarrow} \right) = \gamma_{m,k_y} . \tag{5.54}$$

This means that the quasiparticle operators stemming from the two eigenvectors $\Phi_{n,k_y}$ and $\Psi_{n,-k_y}$ with opposite signed energy spectrums are related through $\gamma_{n,k_y} = \gamma^\dagger_{n,-k_y}$. This also means that they are not independent. It can be understood from the interpretation that removing a Bogoliubov quasiparticle $\gamma_{n,k_y}$ with energy $\mathcal{E}_{n,k_y}$ is the same as creating a Bogoliubov hole $\gamma^\dagger_{n,-k_y}$ with energy $-\mathcal{E}_{n,-k_y}$ [103]. Conversely, we may also write the old operators in terms of the new ones. They are related through

$$c_{i_x,k_y,\uparrow} = \sum_n u_{i_x,n,k_y} \gamma_{n,k_y} , \qquad c_{i_x,k_y,\downarrow} = \sum_n v_{i_x,n,k_y} \gamma_{n,k_y} , \tag{5.55}$$

$$c^\dagger_{i_x,-k_y,\uparrow} = \sum_n w_{i_x,n,k_y} \gamma_{n,k_y} , \qquad c^\dagger_{i_x,-k_y,\downarrow} = \sum_n x_{i_x,n,k_y} \gamma_{n,k_y} . \tag{5.56}$$

We are, however, not quite finished with the diagonalization. In eq. (5.50) we have written the diagonalized Hamiltonian in terms of linear dependent eigenvectors $\gamma_{n,k_y}$ and $\gamma_{n,-k_y}$ since the momentum sum covers the entire Brillouin zone. Therefore, we want to express

it in terms of linearly independent vectors. To do so we split the sum into its positive, negative, and zero momentum contributions. Therefore, we can write

$$\begin{aligned}
\mathcal{H} =& -\frac{1}{2}\sum_{n,k_y}\mathcal{E}_{n,k_y}\gamma^\dagger_{n,k_y}\gamma_{n,k_y} \\
=& -\frac{1}{2}\sum_{n,k_y>0}\mathcal{E}_{n,k_y}\gamma^\dagger_{n,k_y}\gamma_{n,k_y} - \frac{1}{2}\sum_{n,k_y<0}\mathcal{E}_{n,k_y}\gamma^\dagger_{n,k_y}\gamma_{n,k_y} \\
& -\frac{1}{2}\sum_{n=1}^{2N_x}\mathcal{E}_{n,0}\gamma^\dagger_{n,0}\gamma_{n,0} - \frac{1}{2}\sum_{n=2N_x+1}^{4N_x}\mathcal{E}_{n,0}\gamma^\dagger_{n,0}\gamma_{n,0} \\
=& -\frac{1}{2}\sum_{n,k_y>0}\mathcal{E}_{n,k_y}\gamma^\dagger_{n,k_y}\gamma_{n,k_y} - \frac{1}{2}\sum_{n,k_y>0}\mathcal{E}_{n,-k_y}\gamma^\dagger_{n,-k_y}\gamma_{n,-k_y} \\
& -\frac{1}{2}\sum_{n=1}^{2N_x}\mathcal{E}_{n,0}\gamma^\dagger_{n,0}\gamma_{n,0} - \frac{1}{2}\sum_{n=1}^{2N_x}(-\mathcal{E}_{n,0})\gamma_{n,0}\gamma^\dagger_{n,0} \\
=& -\sum_{n,k_y>0}\mathcal{E}_{n,k_y}\gamma^\dagger_{n,k_y}\gamma_{n,k_y} - \sum_{\mathcal{E}_n\geq 0}\mathcal{E}_{n,0}\gamma^\dagger_{n,0}\gamma_{n,0}\,.
\end{aligned} \tag{5.57}$$

In this derivation, we used the relations between pairs of eigenvalues $\mathcal{E}_{n,k_y} = -\mathcal{E}_{n,-k_y}$ and $\mathcal{E}_{n,0} = -\mathcal{E}_{n+2N_x,0}$. We also used the anti-commutation relations for the quasiparticle operators and discarded the constant term from the commutation. As it turns out, the above splitting of the sum will be done multiple times in the next section. Therefore, it is natural to define a new sum to keep everything tidy,

$$\sum_{n,k_y}{}' = \sum_{n,k_y>0} + \sum_{\mathcal{E}_n\geq 0,k_y=0}\,. \tag{5.58}$$

It is important to note that we have not considered the end of the Brillouin zone, $k_y = \pi$. As we have stated, the momentum index will be in $k_y \in (-\pi, \pi]$. The values are also restricted by $k_y = 2\pi n/N_y$, where $n$ is an integer. This means that there is an extra value in the positive momentum sum for an even $N_y$ that needs to be taken care of. For the sake of simplicity, we will only consider odd $N_y$ systems.

## 5.4 Observables and expectation values

This section will give expressions for different physical observables and expectation values. These expressions will be based on the Bogoliubov quasiparticles and their eigenenergies. Thus, in the following subsections, we assume the Hamiltonian can be diagonalized and that all eigenvalues and eigenvectors are known. In this section, we outline how the derivation is performed and simply state the results. The total derivations can be found in appendix D.

### 5.4.1 Superconducting gap

For the numerical implementation, we need to find an expression for the superconducting gap to solve the system self-consistently. We use the above relations between electron creation and annihilation operators $c^\dagger_{i_x,\pm k_y,\sigma}$, $c_{i_x,\pm k_y,\sigma}$ and the quasiparticle operators $\gamma_{n,k_y}$.

If we take the mean gap in the $y$-direction, we can write

$$\begin{aligned}\Delta_{i_x} &= \frac{1}{N_y}\sum_{i_y}\frac{U_i}{2}\left[\langle c_{i,\uparrow}c_{i,\downarrow}\rangle - \langle c_{i,\downarrow}c_{i,\uparrow}\rangle\right] \\ &= \frac{U_{i_x}}{2N_y}\sum_{n,k_y}{}'\left[x^*_{i_x,n,k_y}u_{i_x,n,k_y} - w^*_{i_x,n,k_y}v_{i_x,n,k_y}\right]\tanh\big(\beta\mathcal{E}_{n,k_y}\big)\,,\end{aligned} \tag{5.59}$$

where we have used that $\langle\gamma^\dagger_{n,k_y}\gamma_{m,k_y}\rangle = f(2\mathcal{E}_{n,k_y})\delta_{n,m}$ [100]. Conversely, for the hermitian conjugated operators $\langle\gamma_{n,k_y}\gamma^\dagger_{m,k_y}\rangle = f(-2\mathcal{E}_{n,k_y})\delta_{n,m} = \big[1 - f(2\mathcal{E}_{n,k_y})\big]\,\delta_{n,m}$. The function $f(2\mathcal{E}_{n,k_y})$ is the Fermi-Dirac distribution function given by

$$f(2\mathcal{E}_{n,k_y}) = \frac{1}{e^{2\beta\mathcal{E}_{n,k_y}}+1}, \tag{5.60}$$

with the inverse temperature $\beta = 1/k_BT$. Using the distribution and the eigenvalues found from diagonalizing the Hamiltonian lets us write physical quantities and expectation values, which we will use in the following subsections.

We wish to make a comment about the choice of prefactors for the eigenvalues. In more recent publications [106–108], one might find that $f(\mathcal{E}_{n,k_y})$ has been used. We choose to ignore the common prefactor in the Hamiltonian we diagonalize. Therefore, we get an expectation value of $f(2\mathcal{E}_{n,k_y})$. If we ignore the factor $(-1/2)$ in eq. (5.34), we can summarize the diagonalization procedure as

$$\mathcal{H} = \sum_{k_y} W^\dagger_{k_y}H_{k_y}W_{k_y} = \sum_{n,k_y}{}'\,2\mathcal{E}_{n,k_y}\gamma^\dagger_{n,k_y}\gamma_{n,k_y}\,. \tag{5.61}$$

### 5.4.2 Singlet and triplet amplitudes

In proximity systems and curved geometries, the Cooper pairs may be converted to other pairing symmetries, such as spin-triplet Cooper pairs. However, there are certain constraints these conversions must obey. If we write a general pairing amplitude as a two-fermion correlation function

$$\Delta_{\sigma\sigma',ab}(\boldsymbol{r},t) = \langle T\, c_{\sigma a}(\boldsymbol{r},t)c_{\sigma' b}(0,0)\rangle\,, \tag{5.62}$$

where $T$ is the time ordering operator and where we have allowed for pairings at different times [109]. The indices $\sigma,\sigma'$ are spin indices and $a,b$ denote the orbital and band degree of freedom. Since the superconductivity is related to the fermion correlation function, it cannot violate Fermi statistics. The symmetry constraints from permuting the operators can be summarized as follows: If we consider the permutations of the spin $S$, the relative coordinate $P^*$, the orbital index $O$, and the relative time $T^*$, they are constrained by

$$S\Delta_{\sigma\sigma',ab}(\boldsymbol{r},t)S^{-1} = \Delta_{\sigma'\sigma,ab}(\boldsymbol{r},t)\,, \qquad P^*\Delta_{\sigma\sigma',ab}(\boldsymbol{r},t)P^{*-1} = \Delta_{\sigma\sigma',ab}(-\boldsymbol{r},t)\,, \tag{5.63}$$

$$O\Delta_{\sigma\sigma',ab}(\boldsymbol{r},t)O^{-1} = \Delta_{\sigma\sigma',ba}(\boldsymbol{r},t)\,, \qquad T^*\Delta_{\sigma\sigma',ab}(\boldsymbol{r},t)T^{*-1} = \Delta_{\sigma\sigma',ab}(\boldsymbol{r},-t)\,. \tag{5.64}$$

Vadim L. Berezinskii showed that combining these four permutations should result in an overall sign change of the order parameter [110]. We can write it as

$$SP^*OT^*\,\Delta_{\sigma\sigma',ab}(\boldsymbol{r},t) = -\Delta_{\sigma\sigma',ab}(\boldsymbol{r},t)\,. \tag{5.65}$$

We note that $T^*$ is not the entire time reversal operator, as it only permutes the relative time coordinate [109]. The same is true for the coordinate permutation $P^*$ since it only permutes the relative coordinate between the two particles and does not invert the full space. Still, the product must be $SP^*OT^* = -1$, as well as $S^2 = P^{*2} = O^2 = T^{*2} = 1$. For example, take the singlet even-frequency Cooper pair $\uparrow\downarrow - \downarrow\uparrow$, which changes sign under the spin permutation $S$. The same is not true for the triplets $\uparrow\downarrow + \downarrow\uparrow$, $\uparrow\uparrow$, and $\downarrow\downarrow$, so one of the other permutations must be negative. They can, for instance, be odd in their spatial part and, therefore, have a p-wave orbital symmetry.

The different types of order parameters take different forms. We will investigate s- and p-wave pairings in later chapters. Thus, we need an expression for those amplitudes. We begin with the s-wave singlet, again taking the mean in the $y$-direction we get

$$\mathcal{S}_{i_x,0} = \frac{1}{2N_y} {\sum_{n,k_y}}' \left[ x^*_{i_x,n,k_y} u_{i_x,n,k_y} - w^*_{i_x,n,k_y} v_{i_x,n,k_y} \right] \tanh\left(\beta \mathcal{E}_{n,k_y}\right). \tag{5.66}$$

This is an onsite pairing amplitude and, as discussed, is odd under permutation in the spin index. Next, we consider the p-wave triplets, which are odd in the spatial part. Thus, we have six different p-wave amplitudes, the threefold degeneracy of the spin in both the $x$- and $y$-direction. We begin with the px-wave amplitudes, which are

$$\begin{aligned} \mathcal{P}^x_{i_x,0} = \frac{1}{2N_y} {\sum_{n,k_y}}' \sum_{\pm} \pm \Big[ &\left( x^*_{i_x\pm1,n,k_y} u_{i_x,n,k_y} + w^*_{i_x\pm1,n,k_y} v_{i_x,n,k_y} \right) f(-2\mathcal{E}_{n,k_y}) \\ &+ \left( x^*_{i_x,n,k_y} u_{i_x\pm1,n,k_y} + w^*_{i_x,n,k_y} v_{i_x\pm1,n,k_y} \right) f(2\mathcal{E}_{n,k_y}) \Big], \end{aligned} \tag{5.67}$$

$$\mathcal{P}^x_{i_x,\uparrow} = \frac{1}{2N_y} {\sum_{n,k_y}}' \sum_{\pm} \pm \left[ w^*_{i_x,n,k_y} u_{i_x\pm1,n,k_y} f(2\mathcal{E}_{n,k_y}) + w^*_{i_x\pm1,n,k_y} u_{i_x,n,k_y} f(-2\mathcal{E}_{n,k_y}) \right], \tag{5.68}$$

$$\mathcal{P}^x_{i_x,\downarrow} = \frac{1}{2N_y} {\sum_{n,k_y}}' \sum_{\pm} \pm \left[ x^*_{i_x,n,k_y} v_{i_x\pm1,n,k_y} f(2\mathcal{E}_{n,k_y}) + x^*_{i_x\pm1,n,k_y} v_{i_x,n,k_y} f(-2\mathcal{E}_{n,k_y}) \right]. \tag{5.69}$$

The $\pm$ in the expression above was added since the lobes of the p-wave orbital have opposite signs. Thus, without it, they cancel, and we are left with zero. For the remaining amplitudes, we add the $\pm$ as well. The py-wave amplitudes take a somewhat different form because of the periodic boundary conditions. They are

$$\mathcal{P}^y_{i_x,0} = \frac{-i}{N_y} {\sum_{n,k_y}}' \sin(k_y) \left[ x^*_{i_x,n,k_y} u_{i_x,n,k_y} + w^*_{i_x,n,k_y} v_{i_x,n,k_y} \right] \tanh\left(\beta \mathcal{E}_{n,k_y}\right), \tag{5.70}$$

$$\mathcal{P}^y_{i_x,\uparrow} = \frac{-2i}{N_y} {\sum_{n,k_y}}' \sin(k_y) w^*_{i_x,n,k_y} u_{i_x,n,k_y} \tanh\left(\beta \mathcal{E}_{n,k_y}\right), \tag{5.71}$$

$$\mathcal{P}^y_{i_x,\downarrow} = \frac{-2i}{N_y} {\sum_{n,k_y}}' \sin(k_y) x^*_{i_x,n,k_y} v_{i_x,n,k_y} \tanh\left(\beta \mathcal{E}_{n,k_y}\right). \tag{5.72}$$

### 5.4.3 Charge current

In this subsection we will give a general expression for the charge current. The specific form changes based on the spin-orbit interaction. To obtain an expression for the current,

we begin with the charge continuity equation [104], which is

$$\partial_t \rho_i = -\nabla \cdot \boldsymbol{j}_i \,, \tag{5.73}$$

where $\rho_i$ is the charge density, and $\boldsymbol{j}_i$ is the current density at site $i$. It can be rewritten using Heisenberg's equation of motion. This relates the charge $Q_i = \sum_\sigma c^\dagger_{i,\sigma} c_{i,\sigma}$ to the Hamiltonian of the system by

$$\sum_m I_{i,m} = -i\,[\mathcal{H},\, Q_i]\,, \tag{5.74}$$

where $\mathcal{H}$ is the Hamiltonian given in eq. (5.12) not assuming periodic boundary conditions, and $I_{i,m}$ is the is the current flowing out of surface $m$. The full derivation of the charge current is given in appendix D.3. We find that a general expression for the charge current in the $x$-direction is given by

$$\begin{aligned}
\langle I^x_{i_x} \rangle =& \frac{-2t}{N_y} \sum_{\pm} {\sum_{n,k_y}}' \pm \Big[ \mathfrak{Im}\{u^*_{i_x\pm1,n,k_y} u_{i_x,n,k_y} + v^*_{i_x\pm1,n,k_y} v_{i_x,n,k_y}\} f(2\mathcal{E}_{n,k_y}) \\
&\qquad - \mathfrak{Im}\{w^*_{i_x\pm1,n,k_y} w_{i_x,n,k_y} + x^*_{i_x\pm1,n,k_y} x_{i_x\,n,k_y}\} f(-2\mathcal{E}_{n,k_y}) \Big] \\
&+ \frac{2}{N_y} \sum_{\pm} {\sum_{n,k_y}}' \Big[ \mathfrak{Im}\{a^{\uparrow\uparrow}_{i_x\pm1,i_x} u^*_{i_x\pm1,n,k_y} u_{i_x,n,k_y} + a^{\uparrow\downarrow}_{i_x\pm1,i_x} u^*_{i_x\pm1,n,k_y} v_{i_x,n,k_y} \\
&\qquad + a^{\downarrow\uparrow}_{i_x\pm1,i_x} v^*_{i_x\pm1,n,k_y} u_{i_x,n,k_y} + a^{\downarrow\downarrow}_{i_x\pm1,i_x} v^*_{i_x\pm1,n,k_y} v_{i_x,n,k_y}\} f(2\mathcal{E}_{n,k_y}) \\
&\quad + \mathfrak{Im}\{a^{\uparrow\uparrow}_{i_x\pm1,i_x} w^*_{i_x,n,k_y} w_{i_x\pm1,n,k_y} + a^{\uparrow\downarrow}_{i_x\pm1,i_x} x^*_{i_x,n,k_y} w_{i_x\pm1,n,k_y} \\
&\qquad + a^{\downarrow\uparrow}_{i_x\pm1,i_x} w^*_{i_x,n,k_y} x_{i_x\pm1,n,k_y} + a^{\downarrow\downarrow}_{i_x\pm1,i_x} x^*_{i_x,n,k_y} x_{i_x\pm1,n,k_y}\} f(-2\mathcal{E}_{n,k_y}) \Big].
\end{aligned} \tag{5.75}$$

### 5.4.4 Spin current

The spin current can be found the same way as the charge current, starting from the continuity equation. The details of the derivation are given in appendix D.4. There, we find that the $z$-component of a spin-current in the $x$-direction is

$$\begin{aligned}
\langle I^{x,z}_{S,i_x} \rangle =& \frac{-2t}{N_y} \sum_{\pm} {\sum_{n,k_y}}' \pm \Big[ \mathfrak{Im}\{u^*_{i_x\pm1,n,k_y} u_{i_x,n,k_y} - v^*_{i_x\pm1,n,k_y} v_{i_x,n,k_y}\} f(2\mathcal{E}_{n,k_y}) \\
&\qquad - \mathfrak{Im}\{w^*_{i_x\pm1,n,k_y} w_{i_x,n,k_y} - x^*_{i_x\pm1,n,k_y} x_{i_x,n,k_y}\} f(-2\mathcal{E}_{n,k_y}) \Big] \\
&+ \frac{2}{N_y} \sum_{\pm} {\sum_{n,k_y}}' \Big[ \mathfrak{Im}\{a^{\uparrow\uparrow}_{i_x\pm1,i_x} u^*_{i_x\pm1,n,k_y} u_{i_x,n,k_y} - a^{\uparrow\downarrow}_{i_x\pm1,i_x} u^*_{i_x\pm1,n,k_y} v_{i_x,n,k_y} \\
&\qquad + a^{\downarrow\uparrow}_{i_x\pm1,i_x} v^*_{i_x\pm1,n,k_y} u_{i_x,n,k_y} - a^{\downarrow\downarrow}_{i_x\pm1,i_x} v^*_{i_x\pm1,n,k_y} v_{i_x,n,k_y}\} f(2\mathcal{E}_{n,k_y}) \\
&\quad + \mathfrak{Im}\{a^{\uparrow\uparrow}_{i_x\pm1,i_x} w^*_{i_x,n,k_y} w_{i_x\pm1,n,k_y} - a^{\uparrow\downarrow}_{i_x\pm1,i_x} x^*_{i_x,n,k_y} w_{i_x\pm1,n,k_y} \\
&\qquad + a^{\downarrow\uparrow}_{i_x\pm1,i_x} w^*_{i_x,n,k_y} x_{i_x\pm1,n,k_y} - a^{\downarrow\downarrow}_{i_x\pm1,i_x} x^*_{i_x,n,k_y} x_{i_x\pm1,n,k_y}\} f(-2\mathcal{E}_{n,k_y}) \Big].
\end{aligned} \tag{5.76}$$

### 5.4.5 Spin magnetization

In this subsection, we present the expressions for the amplitude of the spin magnetization. We can generally write it as $\boldsymbol{S}_i = \langle c^\dagger_{i,\alpha} \boldsymbol{\sigma}^{\alpha\beta} c_{i,\beta} \rangle$, where we have neglected constant prefactors. Taking the mean in the $y$-direction as before, the amplitudes become

$$S^x_{i_x} = \frac{2}{N_y} {\sum_{n,k_y}}' \left[ \mathfrak{Re}\{u^*_{i_x,n,k_y} v_{i_x,n,k_y}\}\, f(2\mathcal{E}_{n,k_y}) + \mathfrak{Re}\{x^*_{i_x,n,k_y} w_{i_x,n,k_y}\}\, f(-2\mathcal{E}_{n,k_y}) \right], \tag{5.77}$$

$$S^y_{i_x} = \frac{2}{N_y} {\sum_{n,k_y}}' \left[ \mathfrak{Im}\{u^*_{i_x,n,k_y} v_{i_x,n,k_y}\}\, f(2\mathcal{E}_{n,k_y}) + \mathfrak{Im}\{x^*_{i_x,n,k_y} w_{i_x,n,k_y}\}\, f(-2\mathcal{E}_{n,k_y}) \right], \tag{5.78}$$

$$S^z_{i_x} = \frac{2}{N_y} {\sum_{n,k_y}}' \left[ \left(|u_{i_x,n,k_y}|^2 - |v_{i_x,n,k_y}|^2\right)\, f(2\mathcal{E}_{n,k_y}) + \left(|w_{i_x,n,k_y}|^2 - |x_{i_x,n,k_y}|^2\right)\, f(-2\mathcal{E}_{n,k_y}) \right]. \tag{5.79}$$

It is also possible to express the spin magnetization in curvilinear coordinates, not the lab frame since these might be more intuitive. It can be done in two ways: We take the elements of $\boldsymbol{S}_i$ in the lab frame and change the basis using the parametrization. Alternatively, the Pauli-vector can be replaced by the curvilinear one, such that $S^{T,N,B}_i = \langle c^\dagger_{i,\alpha} \sigma^{\alpha\beta}_{T,N,B} c_{i,\beta} \rangle$. In a circular geometry, we can write them as

$$S^T_{i_s} = \frac{-2}{N_b} {\sum_{m,k_b}}' \left[ \mathfrak{Im}\{v^*_{i_s,m,k_b} u_{i_s,m,k_b} e^{i\kappa i_s}\}\, f(2\mathcal{E}_{m,k_b}) + \mathfrak{Im}\{w^*_{i_s,m,k_b} x_{i_s,m,k_b} e^{i\kappa i_s}\}\, f(-2\mathcal{E}_{m,k_b}) \right], \tag{5.80}$$

$$S^N_{i_s} = \frac{-2}{N_b} {\sum_{m,k_b}}' \left[ \mathfrak{Re}\{u^*_{i_s,m,k_b} v_{i_s,m,k_b} e^{-i\kappa i_s}\}\, f(2\mathcal{E}_{m,k_b}) + \mathfrak{Im}\{x^*_{i_s,m,k_b} w_{i_s,m,k_b} e^{-i\kappa i_s}\}\, f(-2\mathcal{E}_{m,k_b}) \right], \tag{5.81}$$

$$S^B_{i_s} = \frac{2}{N_b} {\sum_{m,k_b}}' \left[ \left(|u_{i_s,m,k_b}|^2 - |v_{i_s,m,k_b}|^2\right)\, f(2\mathcal{E}_{m,k_b}) + \left(|w_{i_s,m,k_b}|^2 - |x_{i_s,m,k_b}|^2\right)\, f(-2\mathcal{E}_{m,k_b}) \right]. \tag{5.82}$$

Note that here, $i_s$ in the exponents should be interpreted as the arc length coordinate associated with the lattice index. That means that the left-most lattice point $i_s = 1$ should be interpreted as zero, and the right-most $i_s = N_s$ should be interpreted as one.

### 5.4.6 Local density of states

From the derivation of the magnetization in the $z$-direction, we know that the densities of spin-up and spin-down particles is

$$\langle n_{i_x,\uparrow} \rangle = \frac{1}{N_y} {\sum_{n,k_y}}' \left[ |u_{i_x,n,k_y}|^2 f(2\mathcal{E}_{n,k_y}) + |w_{i_x,n,k_y}|^2 f(-2\mathcal{E}_{n,k_y}) \right], \tag{5.83}$$

$$\langle n_{i_x,\downarrow} \rangle = \frac{1}{N_y} {\sum_{n,k_y}}' \left[ |v_{i_x,n,k_y}|^2 f(2\mathcal{E}_{n,k_y}) + |x_{i_x,n,k_y}|^2 f(-2\mathcal{E}_{n,k_y}) \right]. \tag{5.84}$$

We can use these to express the local density of states [102, 107] as

$$D_{i_x}(\mathcal{E}) = \frac{1}{N_y} \sum_{n,k_y}{}' \Big[ \left( |u_{i_x,n,k_y}|^2 + |v_{i_x,n,k_y}|^2 \right) \delta(\mathcal{E} - \mathcal{E}_{n,k_y}) + \left( |w_{i_x,n,k_y}|^2 + |x_{i_x,n,k_y}|^2 \right) \delta(\mathcal{E} + \mathcal{E}_{n,k_y}) \Big] . \tag{5.85}$$

Note that the above expression assumes $T = 0$, such that the derivative of the Fermi-Dirac distribution becomes a Dirac-delta. However, for the numerical simulations, we approximate the Dirac-delta function as

$$\delta(\mathcal{E}) \approx \frac{1}{\pi} \frac{\Gamma}{\Gamma^2 + \mathcal{E}^2} , \tag{5.86}$$

where we choose a sensible value for $\Gamma$, such that the local density of states gives a reasonable smooth curve. It should at least be an order of magnitude less than the scale of the difference of energy eigenenergies.

# Chapter 6

# One-dimensional systems

This chapter will investigate one-dimensional systems using both the quasiclassical theory and Bogoliubov-de-Gennes framework. These are rarely compared since they are mainly used to describe systems in the dirty and clean limit, respectively. However, one can make predictions using both, and they have their strengths and weaknesses. While the quasiclassical theory predicts continuous functions in real space, lattice models only give expectation values on lattice sites. It can be viewed as both a strength and a weakness of the quasiclassical theory; while the continuous functions are easy to work with, they are limited by the length scales and self-energies of the system. Effects that take place at interatomic distances may be washed out. In that case, it can be helpful to use lattice models like the Bogoliubov-de-Gennes method.

## 6.1 Straight ferromagnet proximity systems

To build an intuition for the interplay of ferromagnetism and spin-orbit coupling in proximity systems, we solve the Usadel equation numerically for superconductor-ferromagnet bilayers and for Josephson junctions without curvature. We present the density of states as a physical observable. The systems we consider are similar to those in ref. [67], and the analysis can reproduce their results. We use the parametrization given in section 4.8 to solve the problem numerically. Details concerning the implementation can be found in appendix E.1. The results are obtained with $L_F/\xi_S = 0.5$, and we normalize energies to the gap magnitude $\Delta$. For the spin-orbit field, we take the expression given in eq. (4.96), a combination of Rashba and Dresselhaus. The factors $\alpha$, $\beta$ are normalized to the inverse of the length of the ferromagnet, and we use the shorthand $\alpha = 1$ for $\alpha L_F = 1$. We start by considering an S-F bilayer, and we use the Kupriyanov-Lukichev boundary conditions with the bulk superconductor solution on one side of the ferromagnetic and vacuum on the other. We illustrate the density of states at the center of the ferromagnet. In fig. 6.1, we can see that the triplet pairings dominate. It can be seen from the zero energy peak, which, according to eq. (4.117), tells us that if $D(0) > 1$, we have more triplets than singlet correlations.

Next, we consider a S-F-S Josephson junction. All the values are kept the same as for the bilayer, and we assume the magnitude of the gaps of the superconductors to be equal. However, in the Kupriyanov-Lukichev boundary conditions, we apply a phase to the two bulk superconductors. The density of states in the F-layer will depend on the superconductors' phase difference. We denote this phase difference $\phi$. The phases of the first and second superconductors are chosen to share the total phase difference equally. This is for numerical stability, and $\phi$ could, in principle, be distributed arbitrarily and yield the same

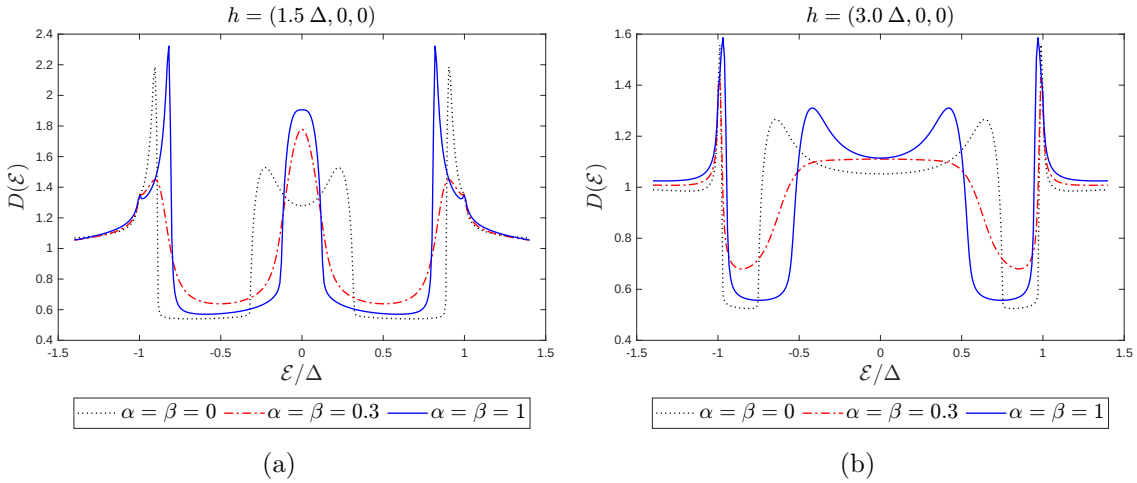


(a) (b)

Figure 6.1: The normalized density of states is plotted for an increasing exchange field and increasing spin-orbit coupling in an S-F bilayer. Slightly increasing the exchange field can suppress the mixing significantly. Then, the density of states goes towards that of a normal metal. The values are taken from the center of the ferromagnet.

results. Again, we show the density of states at the center of the ferromagnet. It can be shown that the density of states remains the same throughout the magnet's length. In fig. 6.2, we illustrate that both the phase and spin-orbit coupling can be detrimental to the generation of triplets. When the singlets dominate, we see that there is a mini-gap opening. When such a minigap is present, the ferromagnet mimics the behavior of the bulk superconductors. Increasing the exchange field would take it beyond a resonant condition [111, 112] where the minigap would vanish and increasing the phase difference would increase the density of states towards that of a normal metal [113].

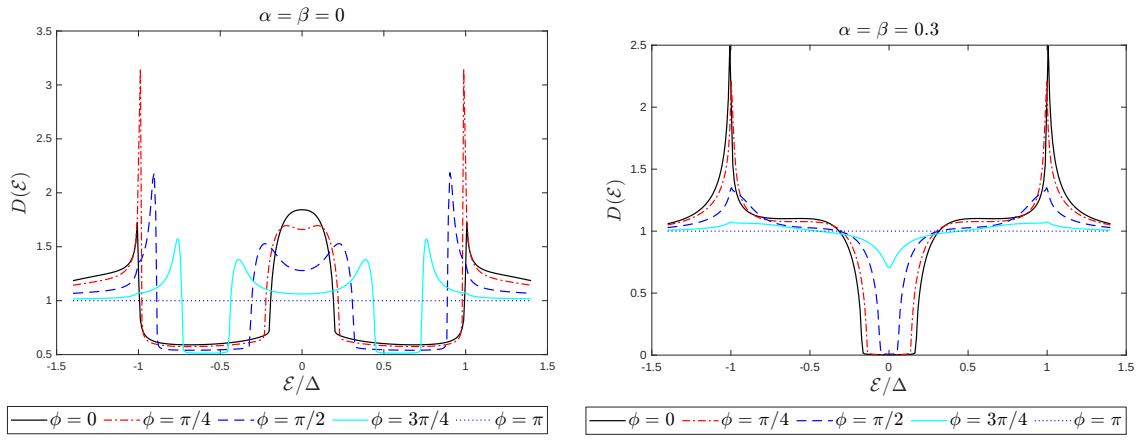


(a) (b)

Figure 6.2: The figures show the normalized density of states $D(\mathcal{E})$ for a Josephson junction with an exchange field in the $z$-direction, $\boldsymbol{h} = (0, 0, 1.5\Delta)$. The density of states is normalized to the gap parameter $\Delta$. The mini-gap in the ferromagnet grows with an increase in the spin-orbit coupling, which is normalized to the inverse of the length of the ferromagnet $1/L_F$. Also, when the two superconductors reach a phase difference of $\phi = \pi$, the density of states reaches that of a normal metal.

## 6.2 Usadel in curvilinear coordinates

We have solved the Usadel equation in straight S-F and S-F-S systems, but the complexity increases as we introduce curvature. We will apply the curvilinear coordinates to the equation since we expect that altering the geometry of the ferromagnet will affect the triplet generation. To consider the geometry and the SU(2) spin-orbit gauge field, we have to change the derivatives in the equation with the space-gauge covariant derivative to have a consistent theory. Using the definition in eq. (3.38), we can write the Usadel equation as

$$iD_F\mathcal{G}^{\lambda\mu}\tilde{\mathcal{D}}_\lambda\left(\hat{g}_R\tilde{\mathcal{D}}_\mu\hat{g}_R\right)=\left[\mathcal{E}\hat{\tau}_3-\hat{\Delta}-\mathcal{G}^{\lambda\mu}h_\lambda\sigma_\mu,\hat{g}_R\right]. \tag{6.1}$$

This is the Usadel equation in its most general form, where the geometry and spin-orbit field still need to be specified. Therefore, even the equation in Cartesian coordinates for a straight wire is a special case of the above. We can express the equation in the Frenet-Serret frame without specifying the curvature and torsion. In that case, we have $\kappa(s),\tau(s)\neq 0$ and include the derivatives in the normal and binormal direction. The left-hand side becomes

$$iD_F\mathcal{G}^{\lambda\mu}\tilde{\mathcal{D}}_\lambda\left(\hat{g}_R\tilde{\mathcal{D}}_\mu\hat{g}_R\right)=iD_F\mathcal{G}^{\lambda\mu}\tilde{\partial}_\lambda\left(\hat{g}_R\tilde{\partial}_\mu\hat{g}_R\right)-iD_F\mathcal{G}^{\lambda\mu}\Gamma^\nu_{\lambda\mu}\left(\hat{g}_R\tilde{\partial}_\nu\hat{g}_R\right), \tag{6.2}$$

where we have not written out the dependence on $A_\lambda$ explicitly. To get a clearer idea of how the choice of a system affects the equations, we write out both terms without using the Einstein summation notation. For a curved, 3-dimensional surface, the first and second terms are, respectively

$$\begin{aligned}iD_F\mathcal{G}^{\lambda\mu}\tilde{\partial}_\lambda\left(\hat{g}_R\tilde{\partial}_\mu\hat{g}_R\right)=\frac{iD_F}{\eta(s,n)^2}\Big\{&\tilde{\partial}_s(\hat{g}_R\tilde{\partial}_s\hat{g}_R)+b\tau(s)\tilde{\partial}_s(\hat{g}_R\tilde{\partial}_n\hat{g}_R)-n\tau(s)\tilde{\partial}_s(\hat{g}_R\tilde{\partial}_b\hat{g}_R)\\&+b\tau(s)\tilde{\partial}_n(\hat{g}_R\tilde{\partial}_s\hat{g}_R)+\left[\eta(s,n)^2+b^2\tau(s)^2\right]\tilde{\partial}_n(\hat{g}_R\tilde{\partial}_n\hat{g}_R)\\&-nb\tau(s)^2\tilde{\partial}_n(\hat{g}_R\tilde{\partial}_b\hat{g}_R)-n\tau(s)\tilde{\partial}_b(\hat{g}_R\tilde{\partial}_s\hat{g}_R)\\&-nb\tau(s)^2\tilde{\partial}_b(\hat{g}_R\tilde{\partial}_n\hat{g}_R)+\left[\eta(s,n)^2+n^2\tau(s)^2\right]\tilde{\partial}_b(\hat{g}_R\tilde{\partial}_b\hat{g}_R)\Big\},\end{aligned} \tag{6.3}$$

$$\begin{aligned}iD_F\mathcal{G}^{\lambda\mu}\Gamma^\nu_{\lambda\mu}\left(\hat{g}_R\tilde{\partial}_\nu\hat{g}_R\right)=\frac{iD_F}{\eta(s,n)^3}\Big\{&(\hat{g}_R\tilde{\partial}_s\hat{g}_R)\left[\partial_s\eta(s,n)-b\tau(s)\kappa(s)\right]\\&+(\hat{g}_R\tilde{\partial}_n\hat{g}_R)\left[-\eta(s,n)^2\partial_n\eta(s,n)+b\partial_s\big(\eta(s,n)\tau(s)\big)\right.\\&\qquad\left.+(n^2-b^2)\kappa(s)\tau(s)^2+n\tau(s)^2\right]\\&+(\hat{g}_R\tilde{\partial}_b\hat{g}_R)\left[n\tau(s)\partial_s\eta(s,n)-n\eta(s,n)\partial_s\tau(s)+b\tau(s)^2\right]\Big\}.\end{aligned} \tag{6.4}$$

Next, we consider an in-plane curved ferromagnetic wire sandwiched between two bulk superconductors. In the language of curvilinear coordinates, the in-plane curvature means no torsion $\tau(s)=0$. Assuming a one-dimensional nanowire means we set $n,b=0$ in the equations we have developed above. The second term containing the Christoffel symbols vanishes completely. The only terms that remain in the Usadel equation are

$$iD_F\tilde{\partial}_s(\hat{g}_R\tilde{\partial}_s\hat{g}_R)=\left[\mathcal{E}\hat{\tau}_3-\hat{\Delta}-\boldsymbol{h}\cdot\boldsymbol{\sigma},\hat{g}_R\right], \tag{6.5}$$

since also the contravariant metric tensor $\mathcal{G}^{\lambda\mu}$ reduces to the identity matrix. The magnetization $\boldsymbol{M} = \boldsymbol{h} \cdot \boldsymbol{\sigma}$ is expressed in curvilinear components. That means that $\boldsymbol{h} = (h_T, h_N, h_B)$ and $\boldsymbol{\sigma} = (\sigma_T, \sigma_N, \sigma_B)$, where still $\sigma_{T,N,B} = \boldsymbol{\sigma} \cdot \{\hat{\mathcal{T}}(s), \hat{\mathcal{N}}(s), \hat{\mathcal{B}}(s)\}$, and thus are dependent on where along the wire we look. This looks exactly like the straight problem, so we can immediately write down the Riccati parametrization for the curved problem

$$\begin{aligned}\partial_s^2\gamma + 2(\partial_s\gamma)\tilde{N}\tilde{\gamma}(\partial_s\gamma) = &-2i\frac{\mathcal{E}}{D_F}\gamma - \frac{i\boldsymbol{h}}{D_F}\cdot(\gamma\boldsymbol{\sigma}^* - \boldsymbol{\sigma}\gamma) - i\big[(\partial_s A_T)\gamma + \gamma(\partial_s A_T^*)\big] \\ &+ \boldsymbol{A}^2\gamma - \gamma(\boldsymbol{A}^*)^2 + 2(\boldsymbol{A}\gamma + \gamma\boldsymbol{A}^*)\tilde{N}(\boldsymbol{A}^* + \tilde{\gamma}\boldsymbol{A}\gamma) \\ &+ 2i\big[(A_T + \gamma A_T^*\tilde{\gamma})N(\partial_s\gamma) + (\partial_s\gamma)\tilde{N}(A_T^* + \tilde{\gamma}A_T\gamma)\big]. \end{aligned} \tag{6.6}$$

Note that this is the equation for the ferromagnet and that we have inserted that the spin-orbit field only has a tangential direction. Since we assume weak proximity, we apply the bulk solution on both sides and do not present the equations for the superconductor. The boundary conditions for the ferromagnet are

$$\partial_I\gamma = \Omega_F(1 - \gamma\tilde{\gamma}_s)N_s(\gamma - \gamma_s) + iA_T\gamma + i\gamma A_T^*, \tag{6.7}$$

$$\partial_I\tilde{\gamma} = \Omega_F(1 - \tilde{\gamma}\gamma_s)\tilde{N}_s(\tilde{\gamma} - \tilde{\gamma}_s) - iA_T^*\tilde{\gamma} - i\tilde{\gamma}A_T, \tag{6.8}$$

where $\partial_I$ is the gradient at the interface and $\gamma_s$ is the gamma matrix for the BCS bulk solution. We are mainly concerned with the weak link in this example because the exchange field direction changes as we introduce curvature. We consider the exchange field to be parallel to the tangential vector $\boldsymbol{h}(s) = h\hat{\mathcal{T}}(s)$. This is how the field is expected to orient in a curved, one-dimensional structure [114]. If we map the curved ferromagnet to a straight wire, it is equivalent to a rotating exchange field. Electrons traveling through the ferromagnet will experience a varying magnetic field, equivalent to a spin-orbit coupling. We will refer to this effect as the curvature-induced spin-orbit coupling, not to be confused with the strain-induced one. Therefore, we expect the rotating field to create triplet correlations within the wire. In fig. 6.3, we show the density of states from the center of the ferromagnet for three different curvatures and two different lengths $L_F$. In both cases, the curvature creates a zero-bias conductance peak, which can be tuned with the curvature. Even for a longer junction $L_F = 2\xi_s$, where the density of states begins to resemble that of a normal metal, one can make a triplet contribution easily detectable [115].

The previous section established that combining the exchange field in the ferromagnet and intrinsic spin-orbit can enhance or degrade the proximity effect. Therefore, it is natural to assume that the same is true for a bent ferromagnet. In fig. 6.4, we show a setup where the strain- and curvature-induced spin-orbit interaction acts as a source for triplets. The intrinsic spin-orbit coupling through $\alpha_B$ has the opposite effect. There is a small peak at zero energy without curvature seen in fig. 6.4b, but the peaks in fig. 6.3a are suppressed as the curvature is introduced. Although the peaks have vanished, triplet pairings are still present. This can again be argued from the fact that $D(0) > 1$ in fig. 6.4b. It can also be seen in the weak proximity equations. The triplet correlations vanish entirely for high curvatures, and a minimap opens in the density of states. In fig. 6.5, we show how the curvature kills the triplet correlations in a ferromagnet with Rashba spin-orbit coupling. We have neglected the strain-induced spin-orbit coupling since it is additive to the curvature-induced one. We can show this if we go to the weak proximity limit and linearize the Usadel equation.

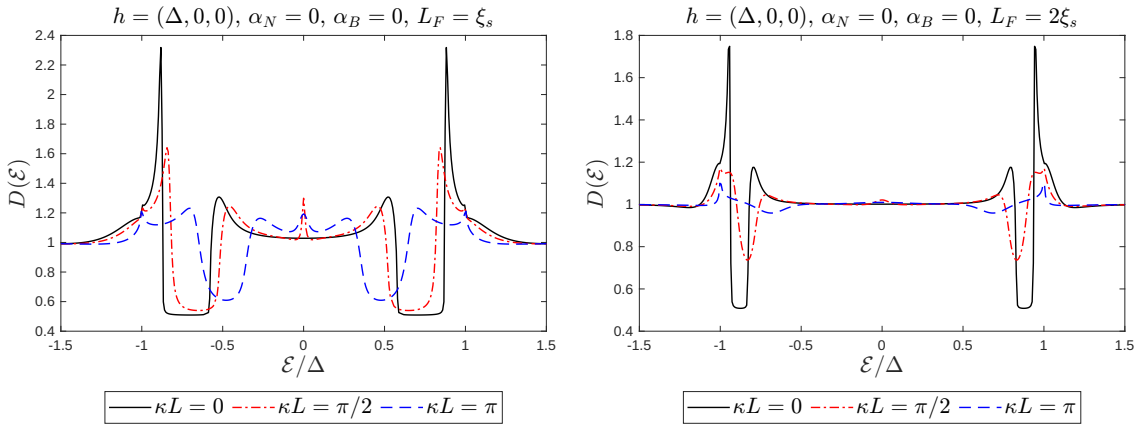


(a) (b)

Figure 6.3: The density of states $D(\mathcal{E})$ for a curved ferromagnet without intrinsic or strain-induced spin-orbit coupling. (a) Shows the density for a ferromagnet with the same length as the coherence length and (b) twice the coherence length. The exchange field points in the tangential direction $\hat{\mathcal{T}}(s)$ and is normalized to the gap magnitude. The energies $\mathcal{E}$ are also normalized to $\Delta$.

In the weak proximity limit, we assume that $|\gamma_{\alpha\beta}| \ll 1$, which means we can set $N \approx 1$. We use the same expression as before for the anomalous Green's function $\underline{f}^R$, given in eq. (4.116). However, we now change to the curvilinear coordinates, which is realized by switching expressing $\boldsymbol{d} = (d_T, d_N, d_B)$ and $\boldsymbol{\sigma} = (\sigma_T, \sigma_N, \sigma_B)$. Using the curvilinear coordinates given in eq. (3.53), we can write the $\gamma = \underline{f}^R/2$ matrix as

$$\gamma = \frac{1}{2}\begin{pmatrix} (id_T + d_N)e^{-i\kappa s} & d_B + f_0 \\ d_B - f_0 & (id_T - d_N)e^{i\kappa s} \end{pmatrix} . \tag{6.9}$$

Since we are considering an exchange field with only one directional component, it is straightforward to identify the short- and long-ranged triplet components. As mentioned, the $\boldsymbol{d}$-vector components describe triplets with a finite spin projection in the plane perpendicular to itself. The spins parallel to the exchange field have a longer diffusion length and describe the long-ranged triplets. The long-ranged triplets are associated with $d_N$ and $d_B$ for an exchange field in the tangential direction. The spins perpendicular to the exchange field are described by $d_T$. If we insert the expression for $\gamma$ in the weak proximity limit, we can write down a linearized version of the Usadel equation. This lets us see directly how the $\boldsymbol{d}$-vector components are affected by tuning the curvature and spin-orbit factors $\alpha_N$ and $\alpha_B$. The weak proximity equations in the curved ferromagnet become [51]

$$\frac{iD_F}{2}\partial_s^2 d_T - iD_F(\kappa + 2\alpha_N)\partial_s d_N - 2iD_F\alpha_B\partial_s d_B = f_0 h_T + \left\{\mathcal{E} + \frac{iD_F}{2}\left[(\kappa + 2\alpha_N)^2 + 4\alpha_B^2\right]\right\} d_T , \tag{6.10}$$

$$\frac{iD_F}{2}\partial_s^2 d_N + iD_F(\kappa + 2\alpha_N)\partial_s d_T = \left\{\mathcal{E} + \frac{iD_F}{2}(\kappa + 2\alpha_N)^2\right\} d_N - iD_F\alpha_B(\kappa + 2\alpha_N) d_N , \tag{6.11}$$

$$\frac{iD_F}{2}\partial_s^2 d_B + 2iD_F\alpha_B\partial_s d_T = \left\{\mathcal{E} + 2iD_F\alpha_B^2\right\} d_B - iD_F\alpha_B(\kappa + 2\alpha_N) d_N , \tag{6.12}$$

$$\frac{iD_F}{2}\partial_s^2 f_0 = \mathcal{E} f_0 + h_T d_T . \tag{6.13}$$

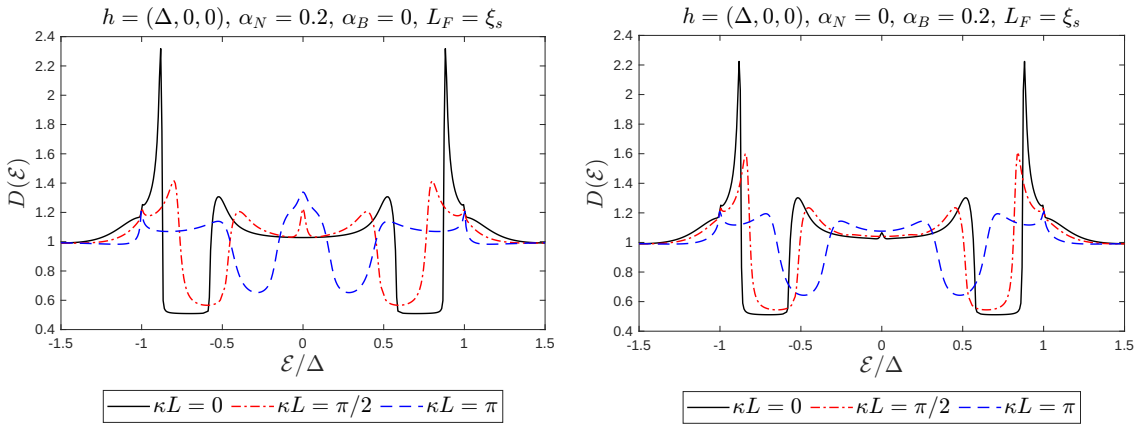


(a) (b)

Figure 6.4: Density of states $D(\mathcal{E})$ for a curved ferromagnet with (a) curvature-induced spin-orbit coupling and (b) intrinsic spin-orbit coupling. The exchange field points in the tangential direction $\hat{\mathcal{T}}(s)$ and is normalized to the gap magnitude. The energies are also normalized to $\Delta$. The ferromagnet has the same length as the coherence length, $L_F = \xi_s$.

These equations describe how the spin-singlet to triplet conversion occurs in the ferromagnet. Starting from eq. (6.13), it represents spin-singlets from the superconductors injected into the ferromagnet. These are then converted to short-ranged triplets $d_T$ due to the exchange field $\boldsymbol{h} = h_T\hat{\mathcal{T}}(s)$. The remaining equations describe how short-ranged triplets can be converted to long-ranged triplets and how all components diffuse through the ferromagnet. These two physical effects can be associated with the first-order derivative terms and an additional imaginary component to the triplet energy [71]. The first derivatives describe the rotation of superconducting triplet correlations as they move along the ferromagnet. Naturally, this is called spin precession. The spin-relaxation from the imaginary contribution to the energy is due to the high impurity density. Since the quasiparticles scatter often, their spin information is gradually lost when traversing the ferromagnet. Therefore, both the curvature and the spin-orbit coupling can be a source of long-range triplet generation independent of each other. It is also clear that without an exchange field $\boldsymbol{h}$, we cannot convert singlets to short-ranged triplets. Consequently, there will not be any long-ranged triplet correlations either. We do not expect to find any triplet correlations if we use the Usadel equation and Kupriyanov-Lukichev boundary condition to describe a curved superconductor-normal metal-superconductor junction. However, the interface between a superconductor and normal metal with spin-orbit coupling should be sufficient to create triplet pairings [116–120]. Note that these might have different orbital symmetries and cannot be captured by the Usadel equation.

Curvature in the S-F-S junction can also induce a $0-\pi$ transition [50], which is schematically drawn in fig. 1.5. As previously mentioned, the current in a Josephson junction is dependent on the phase difference between the superconductors, and we generally have $I(\phi) = I_0\sin(\phi)$ for the 0-state. It is possible to affect the relation to get a $\pi$-state [44, 121], where the current is $I(\phi) = I_0\sin(\phi + \pi)$. In fig. 6.6, we show the transition for the critical current $I(\pi/2)$ for different lengths of the ferromagnet. At $\kappa L_F = 0$ the junction is in the 0 state, and after the current vanishes, it has the opposite direction; it is in the $\pi$ state. To understand how the transition appears, we consider the singlet and triplet contributions to the current. It can be shown that for $\kappa = 0$, the contributions to the charge current from the singlets and triplets have opposite signs. In the absence of spin-

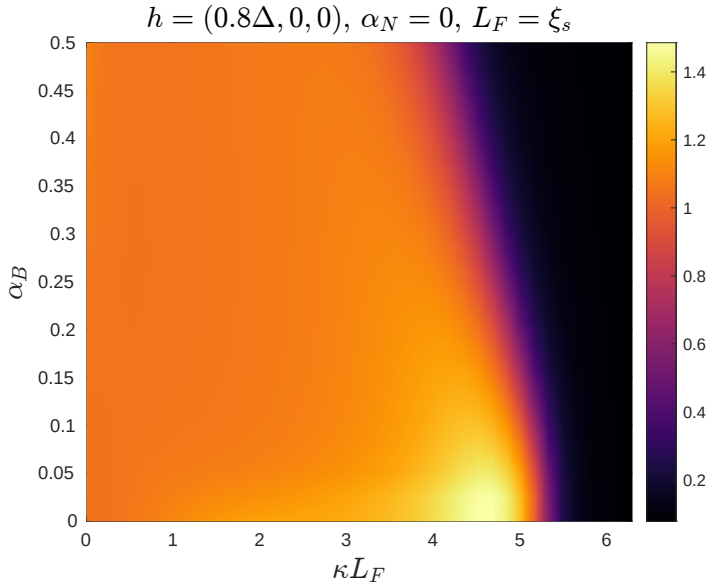


Figure 6.5: The zero energy density of states $D(0)$ as a function of the Rasbha spin-otbit strength $\alpha_B$ and the curvature $\kappa L_F$. The singlet correlations dominate for large curvatures, $D(0) < 1$ and a minigap opens in the ferromagnet. The temperature is $T = 0.005T_c$ and the interface resistance $\zeta = 3$.

orbit coupling, there is no mechanism for spin-precession in the straight case, which can be seen from the weak proximity equations. Therefore, the only triplet contribution to the charge current is from the tangential $\boldsymbol{d}$-vector component $d_T$. Generally, this contribution is bigger than the singlet one. Introducing curvature creates a non-zero long-range $d_N$ component, which contributes with a current in the opposite direction as $d_T$. The sign of the singlet current contribution is unaffected by the curvature. Increasing the curvature enough, the singlet and $d_N$ contribution surpasses the $d_T$ contribution, and the total current switches direction. The total singlet and triplet currents have the same sign for a half-circle. Therefore, the magnitude of the total charge current is greater in the $\pi$ state than in the 0 state. Note that the length of the ferromagnet can affect for which curvature the transition takes place, as seen in fig. 6.6. This is because changing the length of the weak link can also induce a $0 - \pi$ transition [122, 123]. Changing the length is, however, unsuitable for device implementation, as one would need to prepare multiple samples. That is why ref. [50] proposes to curve the ferromagnet in situ, which makes for a much easier device implementation.

## 6.3 Triplet pairings in nanowire

Although we cannot find triplet pairings by solving the Usadel equation for a superconductor-normal metal-superconductor junction, they should be present. This section presents a short analytical derivation of the triplet components we predict to be in a curved wire. We begin with the Hamiltonian for a nanowire, including curvature and torsion, as well as both intrinsic and curvature-induced spin-orbit interactions from before. For now, if we disregard superconductivity, the Hamiltonian is given in eq. (3.43). If we consider a one-dimensional curved nanowire without an intrinsic spin-orbit interaction, which means

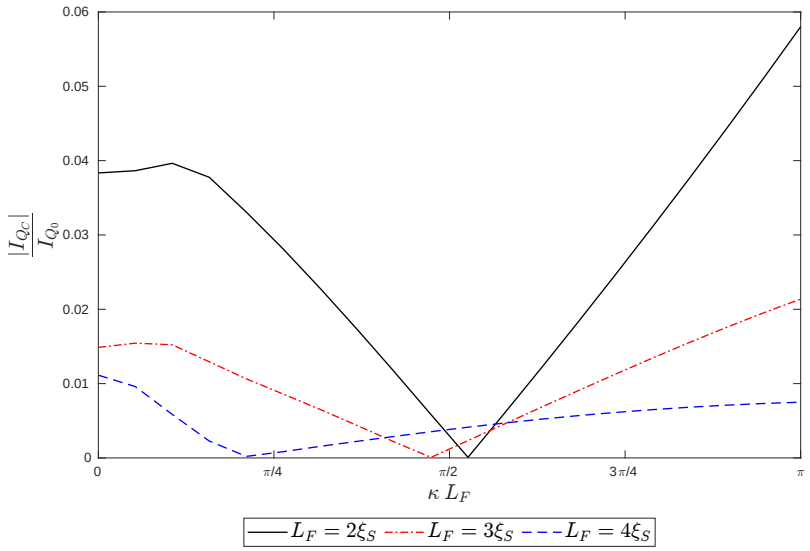


Figure 6.6: Magnitude of the critical current for an increasing curvature and varying lengths $L_F$. The exchange field is in the tangential direction $\boldsymbol{h}(s) = h\hat{\mathcal{T}}(s)$, the temperature is $T = 0.005T_c$, the interface resistance $\zeta = 3$, and $\alpha_N = \alpha_B = 0$. The curvature and rotating exchange field induce a $0 - \pi$ transition. Reproduction of results from ref. [50].

setting $\tau(s)$, $\alpha_B = 0$, we are left with

$$\begin{aligned}\mathcal{H} =& -\frac{\hbar^2}{2m}\left(\partial_s^2 + \frac{\kappa(s)^2}{4}\right) - \frac{i\hbar}{m}\alpha_N \underline{\sigma}_B \partial_s \\ =& \frac{\hbar^2}{2m}\left(\boldsymbol{k}^2 - \frac{\kappa(s)^2}{4}\right) + \frac{\hbar}{m}\alpha_N \underline{\sigma}_B \boldsymbol{k} \\ =& \xi_{\boldsymbol{k}} + \tilde{\alpha}_N \underline{\sigma}_B \boldsymbol{k}, \end{aligned} \tag{6.14}$$

where we used that $\boldsymbol{k} = -i\partial_s$ and discarded the $\kappa^2$ term because this acts as a potential due to the curvature and only gives a constant shift to the overall energy. Next, we combine the curvature Hamiltonian above and the mean-field BCS Hamiltonian. The spin-orbit interaction due to curvature acts as a spin-splitting potential [124], and the Hamiltonian we get is

$$\begin{aligned}\mathcal{H} =& \sum_{\boldsymbol{k}\,\sigma}\left[\left(\xi_{\boldsymbol{k}} + \sigma\tilde{\alpha}_N\boldsymbol{k}\right) c^\dagger_{\boldsymbol{k}\,\sigma} c_{\boldsymbol{k}\,\sigma} + \left(\xi_{\boldsymbol{k}} - \sigma\tilde{\alpha}_N\boldsymbol{k}\right) c^\dagger_{-\boldsymbol{k}\,\sigma} c_{-\boldsymbol{k}\,\sigma}\right] \\ &+ \sum_{\boldsymbol{k}\,\sigma}\left[\sigma\Delta c^\dagger_{\boldsymbol{k}\,\sigma} c^\dagger_{-\boldsymbol{k}\,-\sigma} + \sigma\Delta^* c_{-\boldsymbol{k}\,-\sigma} c_{\boldsymbol{k}\,\sigma}\right]. \end{aligned} \tag{6.15}$$

Next, we reintroduce the Nambu⊗Spin-space spinors $\boldsymbol{\Psi}_{\boldsymbol{k}}$ in momentum space with the creation and annihilation operators $c^\dagger_{\boldsymbol{k}\,\sigma}$ and $c_{\boldsymbol{k}\,\sigma}$. We use some of the fermionic commutation relations of the electron operators given in eq. (2.1) to rewrite the Hamiltonian. This is the same procedure as in section 5.1, and means we can write it as

$$\mathcal{H} = \sum_{\boldsymbol{k}} \boldsymbol{\Psi}^\dagger_{\boldsymbol{k}} \begin{pmatrix} \xi_{\boldsymbol{k}} + \tilde{\alpha}_N\boldsymbol{k} & 0 & 0 & \Delta \\ 0 & \xi_{\boldsymbol{k}} - \tilde{\alpha}_N\boldsymbol{k} & -\Delta & 0 \\ 0 & -\Delta^* & -\xi_{\boldsymbol{k}} + \tilde{\alpha}_N\boldsymbol{k} & 0 \\ \Delta^* & 0 & 0 & -\xi_{\boldsymbol{k}} - \tilde{\alpha}_N\boldsymbol{k} \end{pmatrix} \Psi^\dagger_{\boldsymbol{k}}, \tag{6.16}$$

where we neglected the constant terms and prefactors from the commutations performed. To find the dispersion relation, we find the eigenvalues $\lambda$ of $\hat{h}_{\boldsymbol{k}}$, we solve the equation

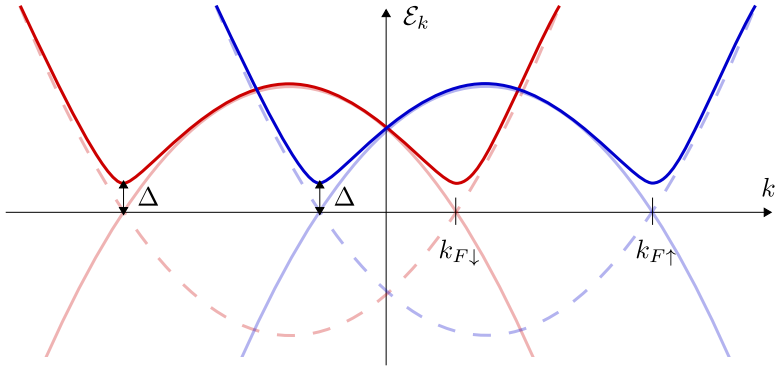


Figure 6.7: Band structure with the curvature induced spin-orbit interaction. Here, it showcases a horizontal shift, lifting the twofold degeneracy. The faded, dashed (full) lines show the two spin species' normal-state electron (hole) band structures. The lines are the eigenenergies $\mathcal{E}_{\pm k}$, and the shifted Fermi momentum $k_{F\sigma}$ are shown.

$|\hat{h}_{\boldsymbol{k}} - \lambda I| = 0$. This yields a quadratic equation where the solutions are the energy spectrum. We rename the eigenvalues $\lambda \to \mathcal{E}$. We see that they induce a horizontal shift in bands, lifting the spin degeneracy. The eigenenergies are

$$\mathcal{E}_{\boldsymbol{k}} = \pm\sqrt{(\xi_{\boldsymbol{k}} - \tilde{\alpha}_N \boldsymbol{k})^2 + |\Delta|^2}\,, \tag{6.17}$$

$$\mathcal{E}_{-\boldsymbol{k}} = \pm\sqrt{(\xi_{\boldsymbol{k}} + \tilde{\alpha}_N \boldsymbol{k})^2 + |\Delta|^2}\,, \tag{6.18}$$

where we have shown a qualitative picture of the upper sign in fig. 6.7. Next, we can find the Green's function by taking the inverse of the Gaussian action $(i\omega - \mathcal{H})$ in Matsubara space [125], which gives

$$\hat{\mathcal{G}}(\boldsymbol{k}, i\omega) = \left[i\omega\,\hat{\tau}_0 - \hat{h}_{\boldsymbol{k}}\right]^{-1} \tag{6.19}$$

$$= \begin{pmatrix} \frac{-\eta^+_{\boldsymbol{k}} - i\omega}{-(i\omega)^2 + (\eta^+_{\boldsymbol{k}})^2 + |\Delta|^2} & 0 & 0 & \frac{-\Delta}{-(i\omega)^2 + (\eta^+_{\boldsymbol{k}})^2 + |\Delta|^2} \\ 0 & \frac{-\eta^-_{\boldsymbol{k}} - i\omega}{-(i\omega)^2 + (\eta^-_{\boldsymbol{k}})^2 + |\Delta|^2} & \frac{\Delta}{-(i\omega)^2 + (\eta^-_{\boldsymbol{k}})^2 + |\Delta|^2} & 0 \\ 0 & \frac{\Delta^*}{-(i\omega)^2 + (\eta^-_{\boldsymbol{k}})^2 + |\Delta|^2} & \frac{\eta^-_{\boldsymbol{k}} - i\omega}{-(i\omega)^2 + (\eta^-_{\boldsymbol{k}})^2 + |\Delta|^2} & 0 \\ \frac{-\Delta^*}{-(i\omega)^2 + (\eta^+_{\boldsymbol{k}})^2 + |\Delta|^2} & 0 & 0 & \frac{\eta^+_{\boldsymbol{k}} - i\omega}{-(i\omega)^2 + (\eta^+_{\boldsymbol{k}})^2 + |\Delta|^2} \end{pmatrix},$$

where we have defined $\eta^{\pm}_{\boldsymbol{k}} \equiv \xi_k \pm \tilde{\alpha}_N \boldsymbol{k}$. Note that the denominators are unequal and must be left inside the matrix. We can directly read off the anomalous Green's function elements related to the singlet and triplet pairing amplitudes. They are

$$F_{\uparrow\downarrow}(\boldsymbol{k}, i\omega) = +\frac{\Delta}{(i\omega)^2 - (\xi_{\boldsymbol{k}} + \tilde{\alpha}_N \boldsymbol{k})^2 - |\Delta|^2}\,, \tag{6.20}$$

$$F_{\downarrow\uparrow}(\boldsymbol{k}, i\omega) = -\frac{\Delta}{(i\omega)^2 - (\xi_{\boldsymbol{k}} - \tilde{\alpha}_N \boldsymbol{k})^2 - |\Delta|^2}\,. \tag{6.21}$$

Because $F_{\uparrow\downarrow} + F_{\downarrow\uparrow} \neq 0$, this indicates that there exist p-wave pairings in the system. However, we do note that this alone is an insufficient requirement to produce measurable p-wave triplet Cooper pairs [124]. Even in the absence of a finite magnetization, there is an equilibrium spin-current with a relative momentum shift due to the spin-orbit coupling [126, 127]. If the phase difference between the singlet and triplets is different from $\pi/2$, the requirements to obtain a finite magnetization are met [100].

## 6.4 Eilenberger in curvilinear coordinates

The Usadel equation is a specific case of the equations of motion in the dirty limit. We expect the high impurity density to kill all p-wave correlations. It is likely not the best-suited formalism to look for these correlations. Whereas curvature effects have been studied using the Usadel equation [50–54], introducing the curvilinear coordinates to the Eilenberger equation is novel. We begin with the expression in eq. (4.82). Since we want to introduce curvature, we go to a covariant form, thus rewriting the dot product as $\hat{\boldsymbol{p}}_F \cdot \nabla_{\boldsymbol{R}} = \mathcal{G}^{\lambda\mu}\hat{p}_\lambda^F \tilde{\partial}_\mu$. Now, we apply the same procedure as in the previous subsection: changing the derivatives with their space-gauge covariant counterparts. We can collect all terms constant in $\check{g}$ on the right-hand side and the derivative on the left. Including the spin-orbit field $A_\mu$ implicitly contained in the partial derivative $\tilde{\partial}_\mu$, the equation takes the form

$$v_F\, \mathcal{G}^{\lambda\mu}\, \hat{p}_\lambda^F\, \partial_\mu\, \check{g} = v_F\, \mathcal{G}^{\lambda\mu}\, \hat{p}_\nu^F\, \Gamma^\nu_{\lambda\mu}\, \check{g} + i\left[\mathcal{E}\hat{\tau}_3 - \check{\Sigma} + v_F\, \mathcal{G}^{\lambda\mu}\, \hat{p}_\lambda^F\, \hat{A}_\mu, \check{g}\right]. \tag{6.22}$$

Beginning with the term on the right-hand side of the above equation, we write out all terms explicitly. We get

$$\begin{aligned} v_F\, \mathcal{G}^{\lambda\mu}\, \hat{p}_\lambda^F\, \partial_\mu\, \check{g} =& \frac{v_F}{\eta(s,n)^2}\left(\hat{p}_s^F + b\tau(s)\, \hat{p}_n^F - n\tau(s)\, \hat{p}_b^F\right)\, \partial_s \check{g} \\ &+ \frac{v_F}{\eta(s,n)^2}\left(b\tau(s)\, \hat{p}_s^F + [\eta(s,n)^2 + b^2\tau(s)^2]\, \hat{p}_n^F - nb\tau(s)^2\, \hat{p}_b^F\right)\partial_n \check{g} \\ &+ \frac{v_F}{\eta(s,n)^2}\left(-n\tau(s)\, \hat{p}_s^F - nb\tau(s)^2\, \hat{p}_n^F + [\eta(s,n)^2 + n^2\tau(s)^2]\, \hat{p}_b^F\right)\partial_b \check{g}\,, \end{aligned} \tag{6.23}$$

$$\begin{aligned} v_F\, \mathcal{G}^{\lambda\mu}\, \hat{p}_\nu^F\, \Gamma^\nu_{\lambda\mu}\, \check{g} =& \frac{v_F}{\eta(s,n)^3}\, \hat{p}_s^F\left[\partial_s\eta(s,n) - b\tau(s)\kappa(s)\right]\check{g} \\ &+ \frac{v_F}{\eta(s,n)^3}\, \hat{p}_n^F\big[-\eta(s,n)^2\partial_n\eta(s,n) + b\partial_s(\eta(s,n)\tau(s)) \\ &\qquad + \kappa(s)\zeta(s,n,b)^2 - 2b^2\tau(s)^2\kappa(s) + n\tau(s)^2\big]\check{g} \\ &+ \frac{v_F}{\eta(s,n)^3}\, \hat{p}_b^F\left[n\tau(s)\partial_s\eta(s,n) - n\eta(s,n)\partial_s\tau(s) + b\tau(s)^2\right]\check{g}\,, \end{aligned} \tag{6.24}$$

$$\left[\mathcal{E}\hat{\tau}_3 - \check{\Sigma} + v_F\, \mathcal{G}^{\lambda\mu}\, \hat{p}_\lambda^F\, \hat{A}_\mu, \check{g}\right] = \left[\mathcal{E}\hat{\tau}_3 - \check{\Sigma} + \frac{v_F}{\eta(s,n)^2}\left(\hat{p}_s^F + b\tau(s)\, \hat{p}_n^F - n\tau(s)\hat{p}_b^F\right)\hat{A}_T,\ \check{g}\right]. \tag{6.25}$$

Now, we apply the above equation to a 1D nanowire. Thus, we assume an infinite well trapping the particles to one dimension and setting the curvilinear coordinates $n$ and $b$ to zero. This also means that there will not be any changes along the normal and binormal direction either, so we set $\partial_{n,b} = 0$. The resulting equation is thus

$$\xi v_F \partial_s \check{g} = i\left[\mathcal{E}\hat{\tau}_3 - \hat{\Delta} + \xi v_F \hat{A}_T,\ \check{g}\right], \tag{6.26}$$

where $\xi = \hat{p}_F = \pm 1$. Note that we have used the spin-orbit field from eq. (3.48), which only has a tangential component, $\hat{A}_T = \mathrm{diag}(\underline{A}_T, -\underline{A}_T^*)$, $A_T = \alpha_N \underline{\sigma}_B - \alpha_B \underline{\sigma}_N$. The constant $\alpha_B$ is the intrinsic Rashba spin-orbit coupling, and $\alpha_N \propto \kappa(s)$ is the strain-induced spin-orbit coupling. We assume that the system is in equilibrium and thus only consider the retarded Green's function. We again introduce the parametrization in eq. (4.102). The

Eilenberger equation for a curved superconductor expressed in the Ricatti parametrization can therefore be summarized as

$$\partial_s\gamma = \frac{2i\mathcal{E}}{\xi v_F}\,\gamma + \frac{i}{\xi v_F}\big(\underline{\Delta} - \gamma\underline{\Delta}^*\gamma\big) + i\big(\gamma\underline{A}_T^* + \underline{A}_T\gamma\big), \tag{6.27}$$

$$\partial_s\tilde{\gamma} = \frac{2i\mathcal{E}}{\xi v_F}\,\tilde{\gamma} - \frac{i}{\xi v_F}\big(\underline{\Delta}^* - \tilde{\gamma}\underline{\Delta}\tilde{\gamma}\big) - i\big(\tilde{\gamma}\underline{A}_T + \underline{A}_T^*\tilde{\gamma}\big). \tag{6.28}$$

As the boundary conditions, we set $\partial_s\gamma = \partial_s\tilde{\gamma} = 0$ at both ends of the superconductor. To calculate the density of states, we have used the expression below to include both possible directions of the Fermi momentum [128]. Otherwise it resembles that in eq. (4.115). We get that

$$N(\mathcal{E}) = \frac{1}{4}\sum_{\xi=\pm1}\mathfrak{Re}\big\{\mathrm{Tr}[N(1+\gamma\tilde{\gamma})]\big\}\,. \tag{6.29}$$

When solving this version of the Eilenberger equation numerically, we find no trace of triplet pairings. This is likely because of the boundary conditions we have chosen. Setting the derivative in the endpoints to zero effectively sets it to zero everywhere. Thus, we are solving only the commutator in eq. (6.26), which is the equation for a bulk superconductor. That would explain why we only get a superconductor density of states for all $\kappa$ values. Two different approaches could potentially alter the result of this analysis. First, one could change the boundary conditions to something more fitting. This can be another type of boundary condition or making an uncurved bulk BCS-curved superconductor-uncurved bulk BCS type of junction. The second is to change the method. Namely, using a lattice model instead of the quasiclassical theory. This is what the next section will discuss.

## 6.5 Curved superconductors

This section presents the analysis done on curved superconductors. We will use the lattice model presented in chapter 5, which is highly flexible and well-suited for exploring p-wave contributions. Using this method, we solve the gap self-consistently, which lets us determine if there are changes to its magnitude and orbital symmetry. We will begin by writing down the Hamiltonian containing terms for intrinsic and strain-induced spin-orbit coupling. A similar model has been considered in ref. [42] where they have neglected strain-induced effects. We continue to use curvilinear coordinates in this chapter, and thus, the Hamiltonian can be written as

$$\begin{aligned}\mathcal{H} = &\sum_{\sigma\sigma'}\int ds\, c_\sigma^\dagger(s)\Big\{\Big(-\frac{\hbar^2\partial_s^2}{2m} - \mu\Big)\\ &+ \frac{i\alpha_B}{2}\Big(\sigma_N(s)\,\partial_s + \partial_s\,\sigma_N(s)\Big) - \frac{i\alpha_N}{2}\Big(\sigma_B(s)\,\partial_s + \partial_s\,\sigma_B(s)\Big)\Big\}c_{\sigma'}(s)\\ &+ \int ds\,\Big[\Delta(s)c_\uparrow^\dagger(s)c_\downarrow^\dagger(s) + \Delta^*(s)c_\downarrow(s)c_\uparrow(s)\Big]\,.\end{aligned} \tag{6.30}$$

In the above, the arclength $s$ is a continuous variable in the tangential direction. To be able to apply this Hamiltonian to an actual lattice, it needs to be discretized. Applying a discretization scheme, we arrive at the Hamiltonian

$$\mathcal{H} = -\mu\sum_{i\sigma}c_{i\sigma}^\dagger c_{i\sigma} - \sum_{\langle ij\rangle\sigma\sigma'}\big(t\delta_{\sigma\sigma'} + \alpha_{ij}^{\sigma\sigma'}\big)c_{i\sigma}^\dagger c_{j\sigma'} + \sum_i\Big(\Delta_i c_{i\uparrow}^\dagger c_{i\downarrow}^\dagger + \Delta_i^* c_{i\downarrow}c_{i\uparrow}\Big)\,, \tag{6.31}$$

where the indexes $i$ and $j$ refer to the site at $s_i$ and $s_j$ respectively. The spin index $\sigma\sigma'$ refers to the different indexes in the matrix structure. We find that the spin-orbit hopping term becomes

$$a_{ij} = \frac{i\alpha_B}{4}\big[\sigma_N(s_i) + \sigma_N(s_j)\big] - \frac{i\alpha_N}{4}\big[\sigma_B(s_i) + \sigma_B(s_j)\big] \,, \tag{6.32}$$

where $a_{ij}$ is related to the spin-orbit hopping amplitude through the expression in eq. (5.7). The details of the discretization can be found in appendix C. The curvilinear Pauli matrices $\sigma_N$, $\sigma_B$ and curvature $\kappa$ are decided by the shape of the system we are examining. To begin with, we will consider a curved semiconductor placed on a superconductor such that it becomes superconducting through the proximity effect. The semiconductor is assumed to have an intrinsic Rashba spin-orbit coupling $\alpha_B$, because of the breaking of the surface inversion symmetry [36].

We start by considering a wire with circular curvature, so we choose the parametrization given in eq. (3.49), where $\kappa \in [0, 2\pi/L)$. On a lattice, this means $\kappa \in [0, 2\pi/N)$, where $N$ is the number of total lattice sites. We find the order parameter $\Delta$ self-consistently using the numerical implementation detailed in appendix E.1. We obtain the results shown in fig. 6.8 for a superconducting chain. Our figure shows that increasing a wire's curvature with considerable strain-induced spin-orbit coupling alters the order parameter magnitude. We have taken the mean of the magnitude of the order parameter for increasing chemical potential and curvature. These results are comparable with what Ying Zu-Jian et al. [47]. They analyze a superconducting ring with increasing Rashba spin-orbit coupling and increasing chemical potential. This example, however, only shows a wire with constant curvature. This will not alter the order parameter throughout the material. If we want to alter the order parameter locally, we must introduce non-constant curvature.

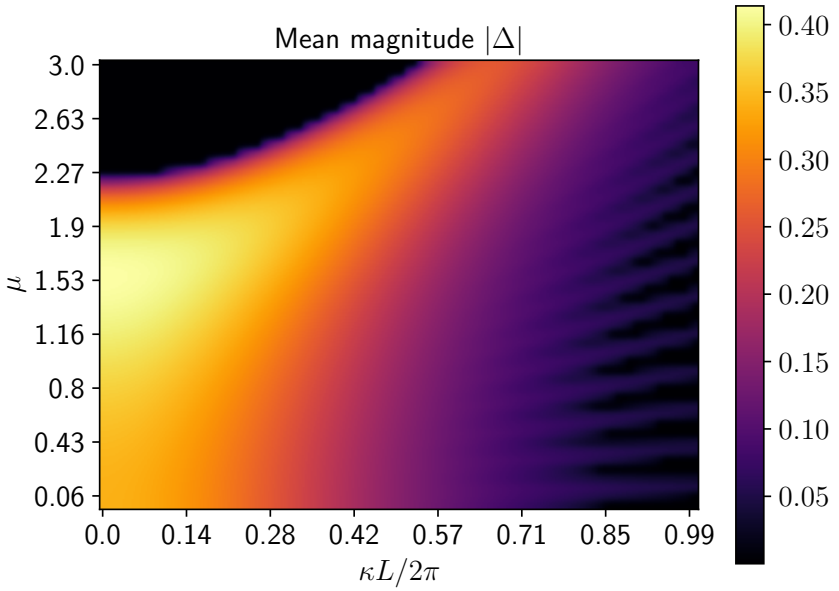


Figure 6.8: (b) Mean magnitude $|\Delta|$ for a curved superconductor, found for $N = 50$ sites, $U = 2.0$, and $T = 0.01$. We have only considered strain-induced spin-orbit coupling, so we have set $\alpha_B = 0$ and $\alpha_N = 0.6$ .

We begin by investigating how the non-constant curvature affects the order parameter through the intrinsic spin-orbit coupling. We assume the semiconductor is shaped like a circle, which we can deform to get an ellipse. Since the wire is circular before we squeeze it, we have $\kappa = 2\pi/N$. This means that the curvilinear Pauli matrices do a full rotation in the lab frame when traversing the wire we are considering. Therefore, in this case, we must connect the first and last sites using a hopping term in our Hamiltonian. This will be the total Hamiltonian's upper right and lower left blocks. We set $\alpha_B = 2$ and $\alpha_N = 0$. The Rashba spin-orbit coupling has Pauli matrices that do not rotate constantly, and this alters the gap $\Delta$ locally. The chemical potential $\mu$ decides if the gap experiences an enhancement or decreases. In fig. 6.9a, we show how the singlet pairing $|\mathcal{S}_0|$ is affected close to the ellipse vertex at $i_s = 50$ for a ring with $N = 100$ sites. For $b/a = 0.1$ the chemical potential below two will enhance the order parameter, while it will decrease above. The gap has vanished everywhere for $\mu = 3$, consistent with the findings in ref. [47]. The gap survives for such high fillings because of the bandwidth enlargement caused by the high spin-orbit coupling $\alpha_B$.

In addition to altering the singlet order parameter, the curvature induces a p-wave pairing at the vertex. In fig. 6.9b, we show the zero-projection p-wave triplet $|\mathcal{P}_0|$ for different chemical potentials. Triplet pairings can arise due to the spin-orbit coupled semiconductor in proximity with an s-wave superconductor [129]. The oscillating singlet pairing in fig. 6.9a is also present in the p-wave pairing for low $\mu$. Both peak exactly at the ellipse vertex, where the curvature is the highest. This is due to a winding of the $\boldsymbol{d}$-vector around the wire [37]. For $b/a$ close to one, away from the vertex, the $\boldsymbol{d}$-vector lies in the plane, parallel to the effective magnetic field due to the spin-orbit coupling [130]. However, the direction changes close to $i_s = 50$, and as $|\mathcal{S}_0|$ is enhanced, so is $|\mathcal{P}_0|$. For low $b/a$ and high $\alpha_B$ the $\boldsymbol{d}$-vector will have high winding numbers when traversing the wire. The checkered pattern in fig. 6.9b is the changing spin-polarization of the p-wave correlations. The squeezing of a superconducting ring with negligible strain effects can directly alter the spin texture in the structure.

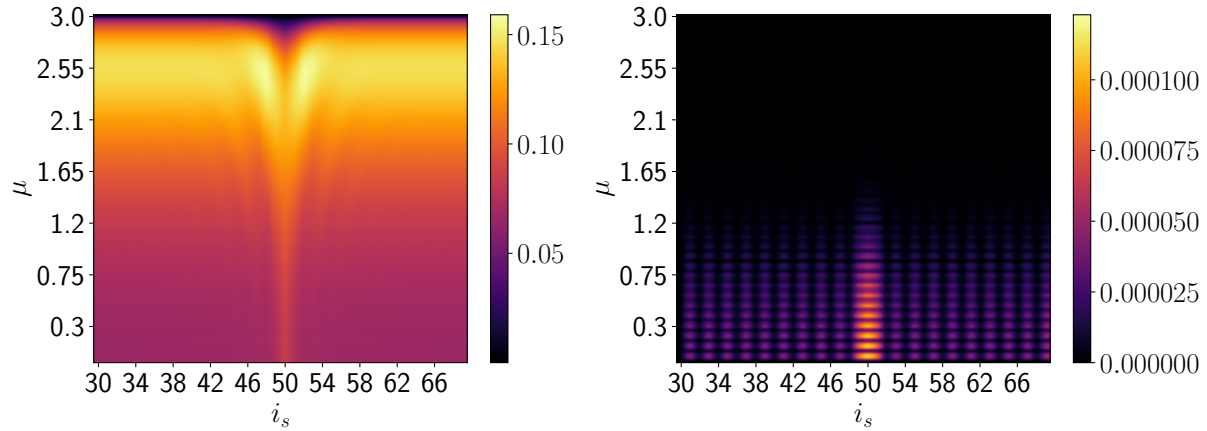


(a) (b)

Figure 6.9: (a) Singlet $|\mathcal{S}_0|$ and (b) triplet $|\mathcal{P}_0|$ for an ellipse with $b/a = 0.1$ and $N = 100$ sites. The curvature at the ellipse vertex alters the magnitude of the pairings. We have used $U = 2$, $\alpha_B = 2$, $a_N = 0$, and $T = 0.01$. (a) Reproduces the results in ref. [47].

Next, we consider the strain effects only, so we set $\alpha_B = 0$. We use the strain-induced spin-orbit factor in eq. (3.80). Therefore, we assume that the semiconductor shaped like a circle is unstrained. We can introduce strain in situ by squeezing it into an ellipse. Notably, there is most strain at the vertex, which reduces the local singlet order parameter $|\mathcal{S}_0|$. In this limit, where the intrinsic spin-orbit coupling is negligible, we don't have a winding of the $\boldsymbol{d}$-vector. This is because the intrinsic term $\alpha_B \sigma_N(i_s)$ is position-dependent in spin space, and $\alpha_N \sigma_B$ is not. Only the strain-induced factor $\alpha_N(i_s) = a_N \kappa(i_a)$ changes in magnitude locally. However, the spin-orbit coupling still creates $|\mathcal{P}_0|$ correlations, as shown in fig. 6.10. The triplets vanish as the gap closes for low $b/a$ fractions. This indicates that there is a conversion from $|\mathcal{S}_0| \to |\mathcal{P}_0|$, similar to the spin-mixing in S-F-S proximity systems. Therefore, creating a controlled localized p-wave order parameter in situ may be possible by geometrical curvature, such as an ellipse.

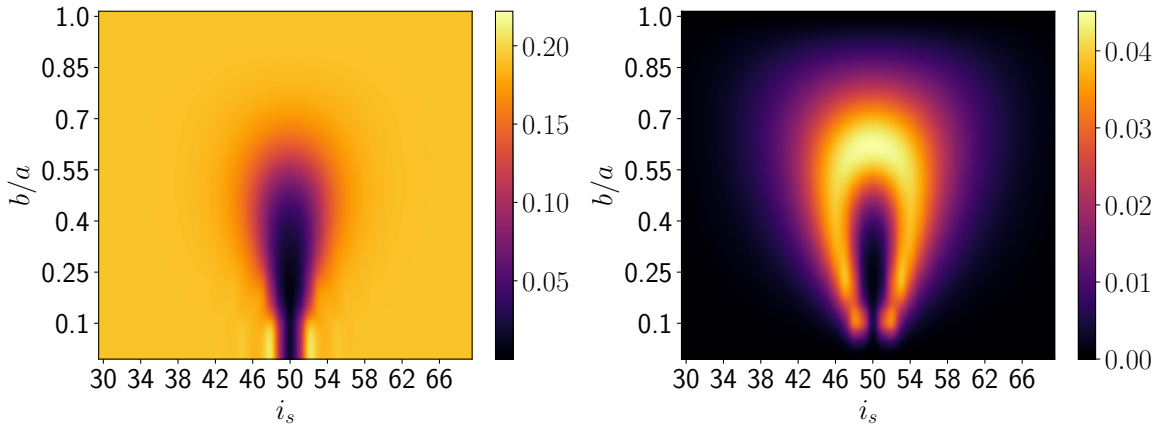


(a) (b)

Figure 6.10: (a) Singlet $|\mathcal{S}_0|$ and (b) p-wave triplet $|\mathcal{P}_0|$ for a ellipse with $N = 100$ sites. The curvature at the ellipse vertex ($i_s = 50$) decreases the singlet magnitude and induces a triplet pairing. We have used $U = 2$, $\alpha_B = 0$, $a_N = 0.5$, $\mu = 1$ and $T = 0.01$.

## 6.6 Josephson junction

Josephson junctions are interesting to study because of the current flowing between the superconductors, among other things. In this section, we will consider a junction where both the superconductors and the weak link are curved, as shown in fig. 6.11. We will consider a setup that allows us to have curvature in plane, and introduce torsion if we want to. In terms of the parameterizations presented in section 3.3, that means we analyze a helical junction. For a fixed number of turns $n$, there is a correspondence between the curvature $\kappa$ and the torsion $\tau$. The curvature and torsion are related through eq. (3.65). In the analysis presented in this section, we will vary both the number of turns and torsion, not keeping one fixed. Therefore, $\tau$ will, in the following, be normalized to a fraction of the in-plane circle with length $L$ and the number of turns. Thus, we write $\tau = 0.1 \times 2\pi n/L$ as $\tau = 0.1$. For $\tau = 1$, we obtain a straight wire with the tangential unit vector $\hat{\mathcal{T}}(s)$ pointing in the $z$-direction. We initialize the superconductors with an s-wave gap and with a constant phase throughout them. We use the Hamiltonian in eq. (6.31), and set $\Delta_i = 0$ inside the normal metal. More details about the implementation can be found in appendix E.

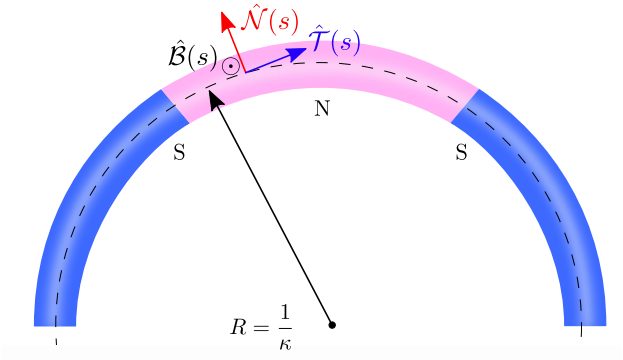


Figure 6.11: Schemtic illustration of a curved Josephson junction including the curvilinear coordinates and the curvature $\kappa$ and zero torsion $\tau$.

We can induce a $0-\pi$ transition in the clean, curved S-N-S junction. We consider a junction with $N_S = 50$ lattice sites in superconductors and $N_N = 11$ in the normal metal. For $\tau = 0$, we can show that the curvature induces the transition because of the strain-induced spin-orbit coupling. In fig. 6.12, we show the total charge current as a function of $\kappa$ and $\phi$. We use the expression in eq. (5.75) for the charge current. We also show the absolute value of the hopping and spin-orbit contributions from eqs. (D.23) and (D.26) in fig. 6.12a. The spin-orbit contribution has the opposite sign of the hopping illustrated in fig. 6.13, so as it becomes greater in magnitude, the $0-\pi$ transition takes place. The contribution $\langle I^s\rangle_\alpha$ grows in amplitude since the spin-orbit factor $\alpha_N = a_N\kappa$ increases with curvature. The current goes to zero for high curvatures because the $|\mathcal{S}_0|$ pairings vanish. The spin-orbit coupling enhances the oscillations always present at the ends of the superconductor [131], which kills the pairings in the normal metal. However, this is a finite-size effect and can be avoided by having more lattice sites in the superconductors. In fig. 6.14, we show the density of states in the center of the first superconductor for $N_S = 250$. The gap does not close entirely, which it does for $N_S = 50$.

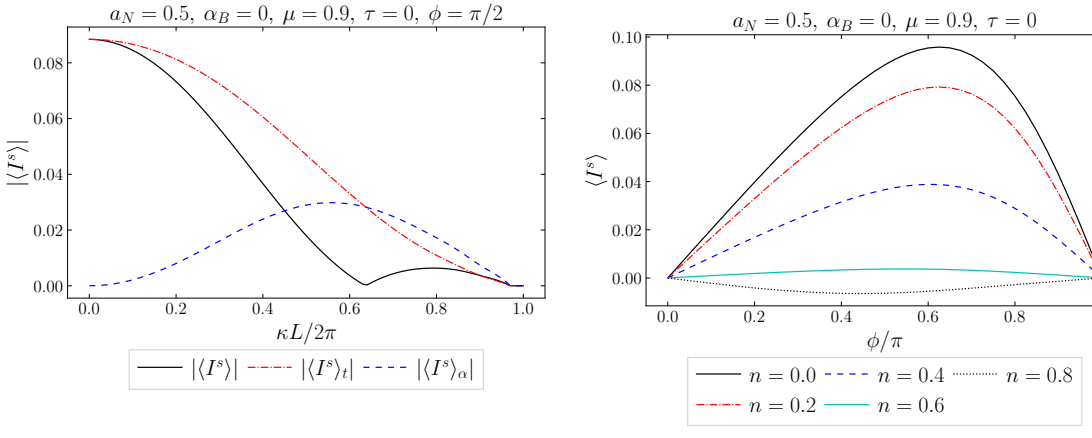


(a) (b)

Figure 6.12: The charge current at the center of the center of the normal metal. (a) The $0-\pi$ transition for the critical current, and (b) the current-phase relation for different curvatures. (a) We show the total charge current and the contributions from the hopping and spin-orbit terms. As $|\langle I^s\rangle_\alpha|$ becomes greater than $|\langle I^s\rangle_t|$, the current switches direction. We have used $U = 2$, $T = 0.05$, and $L$ for the length of the entire junction.

In fig. 6.13, we show the current phase relation for the different charge current contributions. Both have in common that higher harmonics contribute. The Josephson current can be written as a sine Fourier series $\sum_m \sin(m\phi)$, where the term with $m = 1$ usually has the most significant contribution. Both $\langle I^s \rangle_t$ and $\langle I^s \rangle_\alpha$ have higher harmonic contributions, $m > 1$, that change for increasing curvature. Past the $0 - \pi$ transition, the curves go from having tilt towards $\pi$ to tilting towards zero phase. Although it is not immediately apparent from fig. 6.13a, the line for $n = 0.8$ is skewed in the opposite direction compared to the rest. The line for $n = 0.8$ in fig. 6.13b exhibits this more clearly.

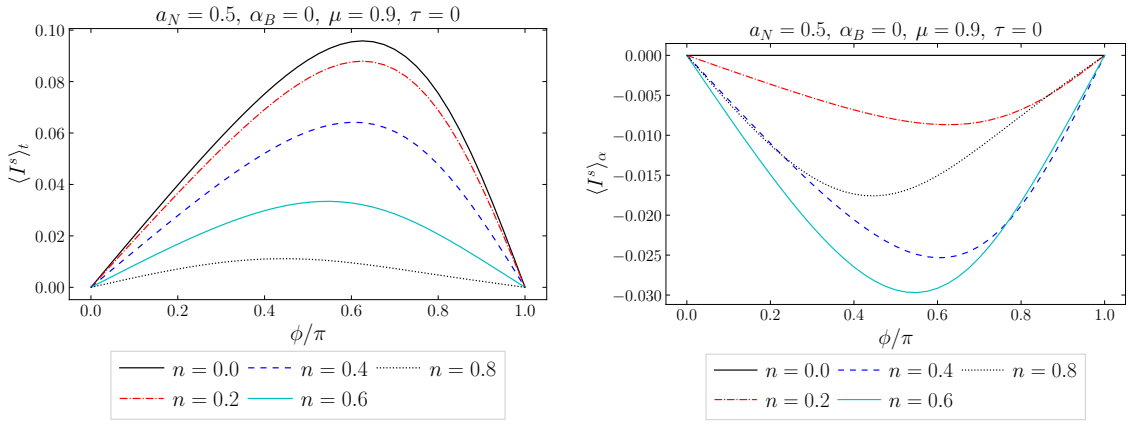


(a) (b)

Figure 6.13: The charge current contributions at the center of the center of the normal metal. (a) The contribution from the hopping term in the Hamiltonian, and (b) the contribution from the spin-orbit term. We have used $U = 2$ and $T = 0.05$.

The charge current through the normal metal can be associated with Andreev bound states. The electrons reflected at the interfaces are present in the density of states and have an energy dispersion that lies within the gap [132]. If we plot the density of states at the center of the normal metal, we see non-zero densities, which are the Andreev-bound states. In fig. 6.14, we show the density of states in the superconductors without the presence of the bound states. However, the inset shows the Hamiltonian eigenenergies, where the Andreev-bound states have the energies within the gap. These will be localized to the normal metal. The outer pair of the bound states disappears at the $0-\pi$ transitions because of the reduction in the band gap. The transition occurs at roughly $\kappa L \approx 0.64$ for these parameters, seen in fig. 6.12a and the inset in fig. 6.14. The bound states provide channels for the charge current, and as the curvature increases, it diminishes the gap, removing a channel. It can be argued that the skewness in the current-phase relations depends on higher harmonics and which channels contribute to the charge current [133].

By changing the pitch, tuning the $0-\pi$ is possible. To show this, we assume that an S-N-S junction can be manufactured as a helix without strain. It is unstrained until squeezed or stretched. We choose to have a helix without strain at $n = 2$ turns and $\tau = 0.5$, introducing strain by changing the torsion. The strain effects will be most significant when reducing the torsion since the curvature will be the highest. It is equivalent to squeezing a spring. Also, when the helix is stretched, it becomes strained, and the charge current is reduced. In fig. 6.15, we show how the junction responds to torsion. At $\tau = 0.5$, the current $\langle I^s \rangle$ and singlet pairing $|\mathcal{S}_0|$ are at their maximum since no strain exists. When compressing the helix enough, $\tau \approx 0.11$, we get a $0 - \pi$ transition.

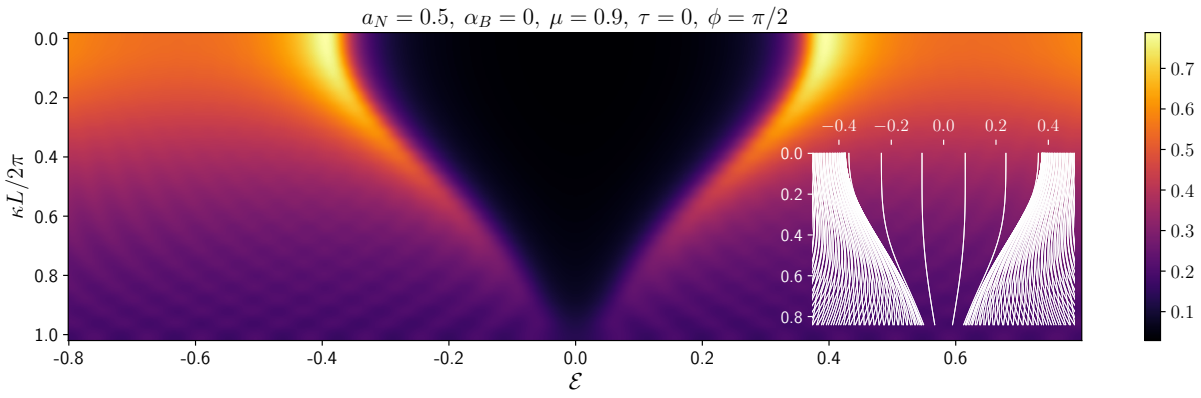


Figure 6.14: Density of state at the center of the first superconductor for increasing curvature $\kappa$. (inset) Shows the eigenenergies of the Hamiltonian for increasing curvature. We used $N_S = 250$, $N_N = 11$, $U = 2$, $T = 0.05$, and $L$ for the length of the entire junction.

As we established in the previous section, the strain-induced spin-orbit coupling can induce p-wave pairings. In fig. 6.15b, we show the correlations that are present at the center of the normal metal. For a junction curved in-plane, $\tau = 0$, we only get $\mathcal{P}_0$ correlations. This is related to the chosen spin-axis: we have chosen the spin-axis in the $z$-direction, which coincides with $\hat{\mathcal{B}}(s)$ in the $\tau = 0$ case. The spin-orbit term couples to $\sigma_B$, and so the p-wave pairings have no spin projection, $S_z = 0$. When we introduce torsion, the binormal unit vector gets a tilt and becomes a mix of all the Cartesian Pauli matrices, which can be seen in eq. (3.68). Figure 6.15b shows that close to the torsion without strain $\tau = 0.5$, we get more spin-polarized p-wave pairings since the helix is torsion-dominated. When we assumed that the strain was low for $\tau = 0.5$, we assumed the curvature was also low. Therefore, the $\kappa$-$\tau$ relation in eq. (3.65) is essentially shifted by $\tau = 0.5$ and $n = 2$. Hence, we go from torsion-dominated to curvature-dominated at $\tau = 1/\sqrt{2} - 1/2 \approx 0.21$. Here, the zero-projection triplet is larger $|\mathcal{P}_0| > |\mathcal{P}_\sigma|$, as shown in fig. 6.15. Consequently, torsion gives us a mechanism for controlling the type of induced p-wave pairings in the junction. Since the intrinsic Rasbha term couples to $\sigma_N$, it will also induce $\mathcal{P}_\sigma$ pairings. Therefore, if we have a helix, the intrinsic spin-orbit coupling is additive to the torsion. Therefore, we have not considered its contribution.

In conclusion, we can control the superconducting correlations with a helix. In-plane curvature creates $\mathcal{P}_0$ correlations, and spin-polarized $\mathcal{P}_\sigma$ correlations will be present if the system has intrinsic spin-orbit coupling. Alternatively, a helix with strain-induced spin-orbit coupling can create the same pairings. We can control the direction of the charge current by in-plane curvature or tuning the torsion of a helix. The transition happens when a channel in the Andreev bound states disappears, and the spin-orbit contribution to the current becomes greater than the hopping contribution. We should note that fig. 6.15 could be misleading because it appears that the $\mathcal{S}_0$ are responsible for the $\langle I^s \rangle_t$ current and the $\mathcal{P}_0$ pairings for the $\langle I^s \rangle_\alpha$ current. The hopping current is related to the singlet pairings, and as the gap decreases with curvature, so does the current contribution. The p-wave correlations and spin-orbit current contribution are not related to each other. However, both originate from the strain-induced term $\propto \alpha_N$. With only Rashba and without the strain-induced spin-orbit, the $\langle I^s \rangle_\alpha$ would remain constant. The same would apply to the gap and the hopping current contribution. Therefore, the strain-induced spin-orbit is crucial for controlling the effects discussed in this section.

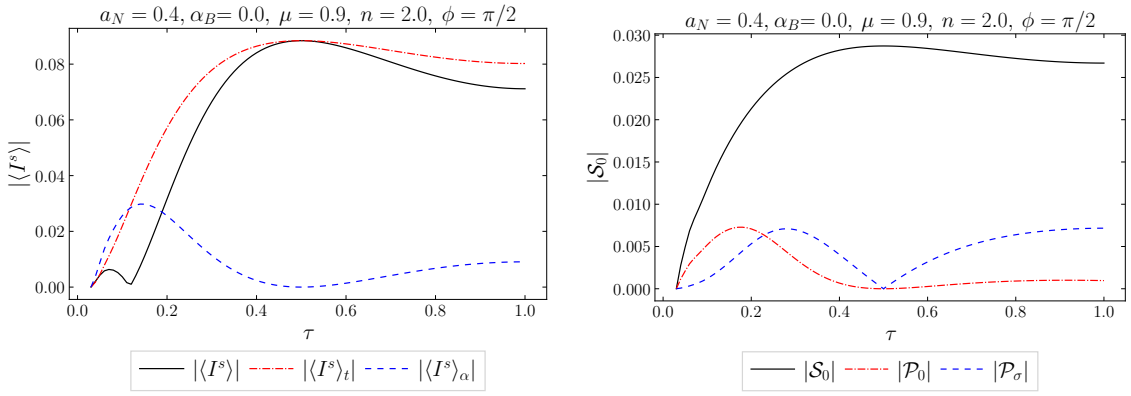


(a) (b)

Figure 6.15: (a) The total critical charge current and its contributions. (b) The s- and p-wave pairing correlations as a function of the torsion. We have assumed no strain at $n = 2$ and $\tau = 0.5$. The values are taken from the center of the normal metal, and we have used $N_S = 50$, $N_N = 11$, $U = 2$, and $T = 0.05$.

## 6.7 Dirty and clean limit

When comparing the dirty and clean limits, we found that we can induce p-wave pairings in the clean limit but not in the dirty when curving an s-wave superconductor. In the clean limit, we can control where the correlation is induced in the wire, depending on where it is considerably strained. We used an unstrained ring as an example; if it is squeezed into an ellipse, it has the highest strain and localized p-wave pairings at the vertices.

We have shown that we can induce $0 - \pi$ transitions in both limits. However, we need an exchange field in the dirty limit to change the spin axis and obtain spin rotation. The exchange field and the spin-mixing can generate a greater amount of triplet pairings. Therefore, in the dirty limit, they can dominate over the singlets. These can be curvature-induced, and the strain-induced spin-orbit is not necessary for the $0 - \pi$ transition. In the clean limit, the induced p-wave pairings are always a fraction of the s-wave and cannot dominate. On the other hand, the exchange field is not necessary to change the direction of the current. However, the strain-induced spin-orbit field is crucial.

# Chapter 7

# Two-dimensional Josephson junction

This chapter will present the results of curvature in two-dimensional systems. Solving quasiclassical equations in two dimensions is possible but requires the application of the method of finite elements [134, 135]. Creating such a numerical code can be cumbersome and is beyond the scope of this thesis. Therefore, all results in this chapter have been obtained using the Bogoliubov de Gennes method with periodic boundary conditions parallel to the interfaces or perpendicular to the curvature direction. Throughout this chapter, we will consider the geometry illustrated in fig. 7.1. In this geometry, we assume the junction has no thickness $n = 0$, but we keep the binormal coordinate $b$. Since the curvature is in the tangential direction, we apply periodic boundary conditions in the binormal.

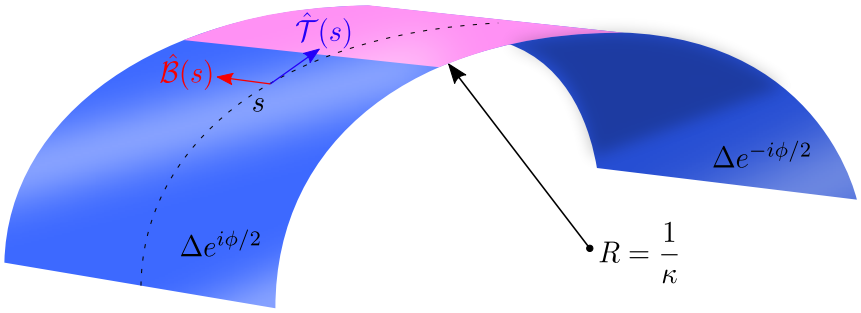


Figure 7.1: Curved two-dimensional Josephson junction. The curvature is given as the inverses of the radius $R$. The phase difference between the superconductors is $\phi$.

From eq. (3.48), we established that the curvature-induced spin-orbit field also has a binormal component. To keep things general, we keep the curvature-induced spin-orbit coupling $\alpha_N$ and denote the intrinsic $\alpha_R$. The intrinsic spin-orbit form comes from a lack of surface inversion symmetry. The symmetry breaking is in the normal direction, and we can write its Hamiltonian as

$$\mathcal{H}_R = -\frac{\alpha_R}{\hbar}(\boldsymbol{\sigma}\cdot\boldsymbol{p})\times\hat{\mathcal{N}}(s) = i\alpha_R\big(\sigma_B(s)\partial_s - \sigma_T(s)\partial_b\big)\,. \tag{7.1}$$

Since it is in the normal direction, it is additive to the strain-induced spin-orbit coupling. We could introduce a shifted curvature to the spin-orbit $\alpha_N = a_N\kappa \to a_N(\alpha_R/a_N + \kappa)$. However, we set $\alpha_R = 0$ since the effects of intrinsic only shift the curvature-induced ones.

This lets us write down a continuum expression for the Hamiltonian. We can express it as

$$\begin{aligned}\mathcal{H} = &\sum_{\sigma\sigma'} \iint ds\, db\, c^\dagger_\sigma(s,b) \left\{ \left( -\frac{\hbar^2}{2m}(\partial_s^2 + \partial_b^2) - \mu \right) \right. \\ &\left. + i\alpha_N \big(\sigma_B(s)\, \partial_s - \sigma_T(s)\, \partial_b\big) \right\} c_{\sigma'}(s,b) \\ &+ \iint ds\, db\, \Big[\Delta(s,b) c^\dagger_\uparrow(s,b) c^\dagger_\downarrow(s,b) + \Delta^*(s,b) c_\downarrow(s,b) c_\uparrow(s,b)\Big] \,,\end{aligned} \tag{7.2}$$

where we have discarded constant shifts to the energy. Applying a finite difference scheme in the tangential direction yields a similar expression for the spin-orbit term in the discretized Hamiltonian as in one dimension. However, we get an extra $\sin(k_b)\sigma_T$ for the spin-orbit interaction in the binormal direction. This is consistent with the result in eq. (5.26). A detailed derivation is given in appendix C.3.

## 7.1 Dispersion

The dispersion relation in two dimensions is expected to vary from the one dimensional given in eq. (6.17) since the spin-orbit, and therefore spin-splitting is different. We will compare the analytical dispersion with the Bogoliubov-de Gennes simulations. We consider the Hamiltonian presented above and the curvilinear Pauli matrices from eq. (3.53). We begin finding the analytical dispersion, so we denote the first integral in eq. (7.2) as $H_0(\boldsymbol{r})$ and $\boldsymbol{q} = \kappa\hat{\mathcal{T}}(s)$, which means $\boldsymbol{q}\cdot\boldsymbol{r} = \kappa s$. We propose a unitary transformation $\mathcal{U}$, and we choose $\mathcal{U}(\boldsymbol{r}) = \mathrm{diag}(i,\ ie^{-i\boldsymbol{q}\cdot\boldsymbol{r}},\ i,\ ie^{i\boldsymbol{q}\cdot\boldsymbol{r}})$. This unitary transformation will have the following effect on the spin element and the interaction part

$$H_0'(\boldsymbol{r}) = \begin{pmatrix} -\frac{\hbar^2}{2m}\nabla^2 - i\tilde{\alpha}_N\partial_s & \tilde{\alpha}_N\partial_b \\ -\tilde{\alpha}_N\partial_b & -\frac{\hbar^2}{2m}\left[(\partial_s + i\kappa)^2 + \partial_b^2\right] + i\tilde{\alpha}_N(\partial_s + i\kappa) \end{pmatrix}, \tag{7.3}$$

$$\Delta'(\boldsymbol{r}) = \begin{pmatrix} 0 & \Delta e^{-i\boldsymbol{q}\cdot\boldsymbol{r}} \\ -\Delta e^{-i\boldsymbol{q}\cdot\boldsymbol{r}} & 0 \end{pmatrix} = \Delta(\boldsymbol{r}) e^{-i\boldsymbol{q}\cdot\boldsymbol{r}} \,. \tag{7.4}$$

Next, we would like to Fourier transform the Hamiltonian. This is to be able to find the energy dispersion in terms of the momentum variables. We assume the real space spinor of the noninteracting part Fourier transforms into the spinor in section 6.3, with creation and annihilation operators $c^\dagger_{\pm\boldsymbol{k}}$ and $c_{\pm\boldsymbol{k}}$. Therefore, the Hamiltonian $H_0'$ describing the free electrons and spin-orbit coupling will become

$$\mathcal{H}_0(\boldsymbol{k}) = \begin{pmatrix} \xi_{\boldsymbol{k}} + \tilde{\alpha}_N k_s & -i\tilde{\alpha}_N k_b \\ i\tilde{\alpha}_N k_b & \xi_{\boldsymbol{k}} - (\tilde{\alpha}_N - \alpha_q)k_s + f(\kappa) \end{pmatrix},$$

where we have introduced the quantities $\alpha_q = \hbar^2\kappa/m$ and $f(\kappa) = \xi_{\boldsymbol{q}} - \tilde{\alpha}_N\kappa$. In the interaction part of the Hamiltonian, we get finite momentum pairs. Namely, the exponential with $\boldsymbol{q}\cdot\boldsymbol{r}$ shifts the Fourier transform integral over $\boldsymbol{k}$. Therefore, we can write this part of the Hamiltonian as

$$\mathcal{H}_{int}' = \sum_{\boldsymbol{k}} \left[ \Delta c^\dagger_{\boldsymbol{k}\uparrow} c^\dagger_{-\boldsymbol{q}-\boldsymbol{k}\downarrow} + \Delta^* c_{-\boldsymbol{q}-\boldsymbol{k}\downarrow} c_{\boldsymbol{k}\uparrow} - \Delta c^\dagger_{\boldsymbol{k}\downarrow} c^\dagger_{-\boldsymbol{q}-\boldsymbol{k}\uparrow} - \Delta^* c_{-\boldsymbol{q}-\boldsymbol{k}\uparrow} c_{\boldsymbol{k}\downarrow} \right]. \tag{7.5}$$

To express the interacting and non-interacting part using the same spinors, we shift the summation variable $\boldsymbol{k} \to \boldsymbol{k} - \boldsymbol{q}/2$ in $\mathcal{H}_0$ and its spinors. We assume that the shifted

variable stays within the first Brillouin zone. It lets us write the total Hamiltonian in the new basis as

$$\mathcal{H} = \sum_{\boldsymbol{k}} \hat{\Psi}^\dagger_{\boldsymbol{k}} \begin{pmatrix} \mathcal{H}_0(\boldsymbol{k}-\boldsymbol{q}/2) & \Delta \\ \Delta^\dagger & -\mathcal{H}_0(-\boldsymbol{k}-\boldsymbol{q}/2) \end{pmatrix} \hat{\Psi}_{\boldsymbol{k}} \,, \tag{7.6}$$

where the spinor is

$$\hat{\Psi}_{\boldsymbol{k}} = \left( c_{\boldsymbol{k}-\boldsymbol{q}/2\uparrow},\, c_{\boldsymbol{k}-\boldsymbol{q}/2\downarrow},\, c^\dagger_{-\boldsymbol{k}-\boldsymbol{q}/2\uparrow},\, c^\dagger_{-\boldsymbol{k}-\boldsymbol{q}/2\downarrow} \right)^T . \tag{7.7}$$

The Hamiltonian in the summation above can be diagonalized. The eigenvalues give the dispersion and band structure. In fig. 7.2, we show the bands. Again, we predict a horizontal shift in the bands, lifting the spin degeneracy.

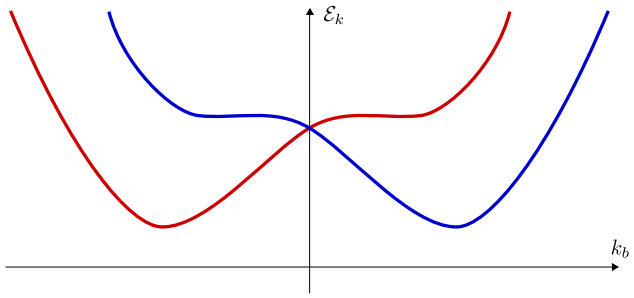


Figure 7.2: Energy dispersion for a two-dimensional curved superconducting sheet at $k_s = 0$. The spin degeneracy is lifted, and the bands are shifted horizontally.

When showing the dispersion obtained from the Bogoliubov-de Gennes method, we again use the momentum variable $k_b$. Since we sum over $k_b$ in eq. (5.34), we essentially are solving one-dimensional systems and changing the momentum for each term. Therefore, we can use the eigenenergies from the diagonalization to extract the dispersion [136]. For a superconducting tunnel with $N_s = 99$ and $N_b = 99$ sites, we obtain the dispersions given in fig. 7.3. We have highlighted the trend of the two spin species to show the similarity to fig. 7.2. Apart from the parabola to cosine approximation in the discretized dispersion, they are similar.

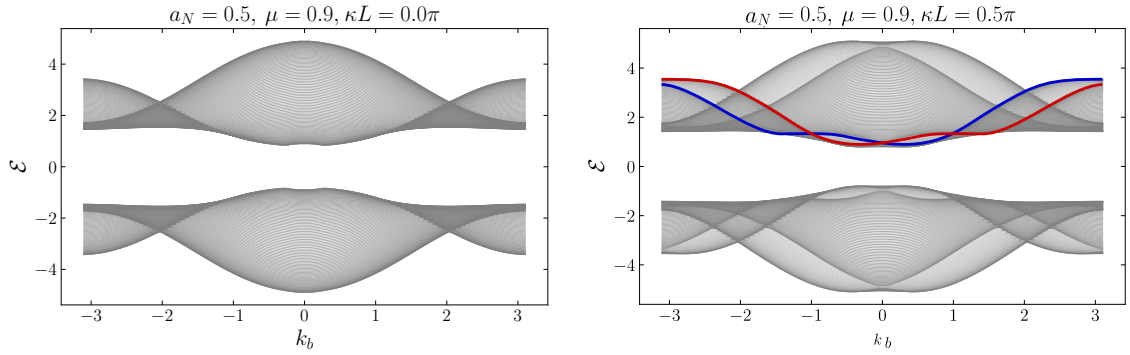


(a) (b)

Figure 7.3: The energy spectrum for a superconducting tunnel with (a) $\kappa L = 0$ and (b) $\kappa L = \pi$, where $L$ is the length in the tangential direction. We have used a $99 \times 99$ lattice, $U = 2$ and $T = 0.1$

If we extract the eigenenergies and the spectrum for a curved S-N-S junction, it is similar. However, there are lines within the gap; they are the Andreev bound states discussed in the previous chapter. The strain-induced spin-orbit coupling also lifts their degeneracy since electrons and holes carry the Andreev bound states. In fig. 7.4, we show the dispersion for the S-N-S tunnel and highlight the bound states. We do note that the energies do not cross zero or touch; they are topologically trivial [137]. There are more bound states in the two-dimensional case than in the one-dimensional if the number of lattice sites in the tangential direction is the same. This is because the electrons with energies below the superconducting gap, bound to the normal metal, may have a binormal component in their velocity. It opens up for more bound states to accumulate the correct phase by not traveling perpendicular to the interfaces. As in the one-dimensional Josephson junction, the bands also shift vertically, so the gap closes for high spin-orbit strengths.

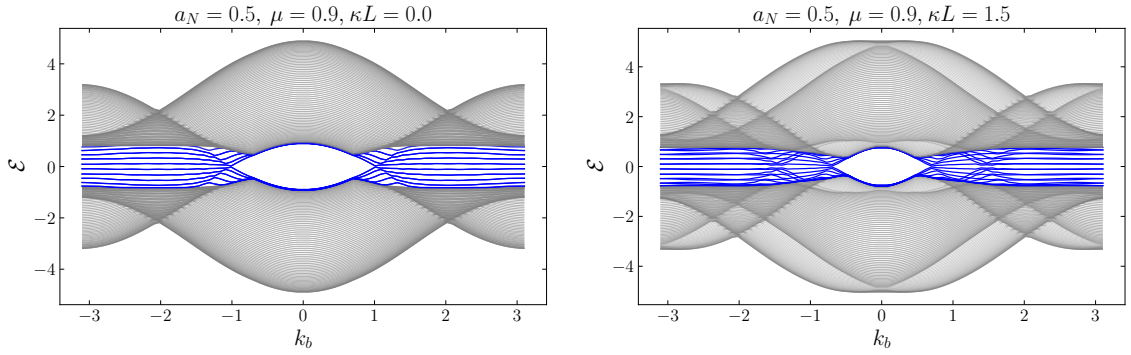


(a) (b)

Figure 7.4: The energy spectrum for a Josephson junction tunnel with (a) $\kappa L = 0$ and (b) $\kappa L = 1.5$, where $L$ is the length of the entire junction in the tangential direction. We have used a lattice with $N_S = 35$, $N_N = 11$, and $N_b = 81$ sites. We set $U = 1.4$ and $T = 0.1$.

## 7.2 Magnetization

Due to the binormal component in the strain-induces spin-orbit field, we get a spin-magnetization in the two-dimensional S-N-S junction. In the binormal component of the spin-orbit field, the momentum is coupled to the tangential curvilinear Pauli matrix $\sigma_T$. Because we assume periodic boundary conditions, this term becomes an onsite, spin- and momentum-dependent potential. This can be seen in eq. (5.24), where we get a factor which translates to $\sin k_b\, \sigma_T$ in this geometry. The derivation details can be found in appendix C.3, which results in the form implemented numerically. This subsection will consider a square junction with $N_S = 20$, $N_N = 21$ lattice sites in the superconductors and normal metal in the tangential direction, respectively. Therefore, it has $N_b = 60$ sites in the binormal direction. We use $U = 1.5$, $a_N = 0.5$ and $T = 0.05$. For reasons that will become apparent, we will vary the remaining variables. We assume the chemical potential is identical in the normal metal and the superconductors, so we write it as $\mu$.

As in the previous chapter, the strain-induced spin-orbit coupling is a source of p-wave correlations. We have determined that in one dimension, the tangential component $A_T$ of the field containing $\sigma_B$ is responsible for generating $\mathcal{P}_0^s$ correlations wherever the structure has curvature and the intrinsic $\mathcal{S}_0$ pairings are present. If we assume that we have two different coefficients $\alpha_{N,1}$ and $\alpha_{N,2}$, we can check which components of the spin-orbit field

$\boldsymbol{A}(s) = \alpha_{N,1}\,\sigma_B\hat{\mathcal{T}}(s) + \alpha_{N,2}\,\sigma_T\hat{\mathcal{B}}(s)$ produces which correlations in the two-dimensional junction. If we set $\alpha_{N,2} = 0$ and $\alpha_{N,1} \neq 0$, we find that we get $\mathcal{P}_0^s$ correlations, exactly like in one dimension. For $\alpha_{N,1} = 0$ and $\alpha_{N,2} \neq 0$, we get spin-polarized triplets $\mathcal{P}_\sigma^b$. In the previous chapter, we argued that $\sigma_T$ and $\sigma_N$ should induce spin-polarized p-wave pairings, so it is consistent that we obtain these in two dimensions. The spin-polarized pairings mentioned are p-wave pairings with the lobes oriented in the binormal direction. We were unable to obtain these before because we were constrained to the tangential direction only. In fig. 7.5, we show the amplitudes for the singlet pairing and the gap $|\Delta|$. We also show the non-zero p-wave pairings for $\kappa = \pi$, $\phi = \pi/2$, and $\mu = 1$. Notice that in fig. 7.5b the pairings $\mathcal{P}_\uparrow^b$ and $\mathcal{P}_\downarrow^b$ are not equal in magnitude. This results in the generation of a finite spin magnetization along the spin axis, which is the binormal direction.

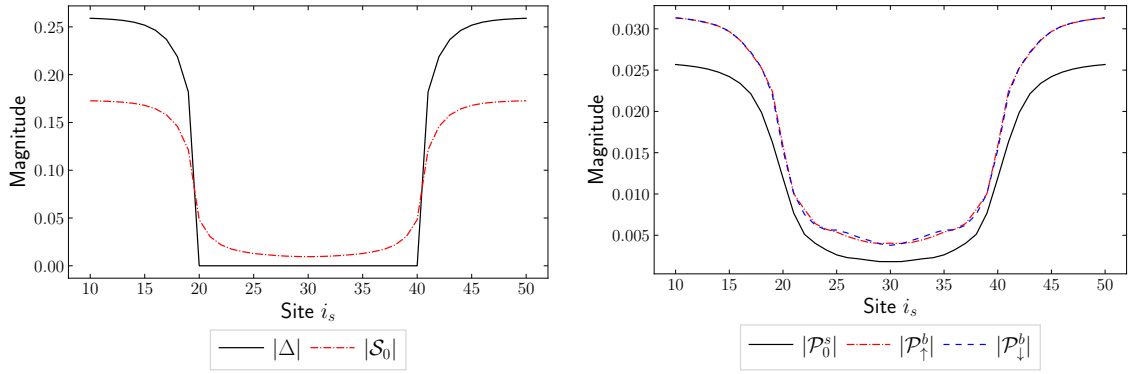


(a) (b)

Figure 7.5: (a) The magnitude of the gap and singlet pair correlations throughout the junction. (b) The p-wave triplet corrections are present due to the strain-induced spin-orbit coupling. (a) and (b) show the same system with $\phi = \pi/2$, $\mu = 1$, $T = 0.05$, and $\kappa L = \pi$, where $L$ is the length of the entire junction in the tangential direction.

The chemical potential plays a crucial role in generating the spin magnetization in the normal metal. The chemical potential can control the amount of p-wave pairings we get in the junction. In section 6.6, we showed that the gap magnitude would vary with $\mu$ when solving the gap equation self-consistently in a superconductor. This also affects the p-wave amplitudes as they are created from the s-wave amplitudes. However, the correspondence is not one-to-one; p-wave pairings vanish for $\mu = 0$. In fig. 7.6, we show real and imaginary parts of the spin-polarized p-wave triplet pairings. The correlations get a $\pi$ phase difference for changing the sign of $\mu$. The spin magnetization in the binormal direction $S^B$ also changes sign with the chemical potential. We show that the other directions have zero spin magnetization $S^{S,N} = 0$ for completeness.

The phase difference across the junction is the final component that is needed to induce spin magnetization in the normal metal. It creates the difference in magnitude between the spin-polarized p-wave correlations $\mathcal{P}_\uparrow^b$ and $\mathcal{P}_\downarrow^b$. In addition to having unequal magnitudes, the overall phases of the correlations also become different. This can be seen from fig. 7.6a because the real and imaginary parts do not vary equally; the $\mathcal{P}_\uparrow^b$ amplitude is not simply a constant factor times $\mathcal{P}_\downarrow^b$. In fig. 7.7a, we show that the difference in magnitude depends on the superconductors' phase difference. For zero phase difference, the magnitudes are equal and have the same phase. For $\phi < \pi$, the magnitudes and phases become unequal, which results in a finite spin magnetization. In fig. 7.7b, we show the dependence of the

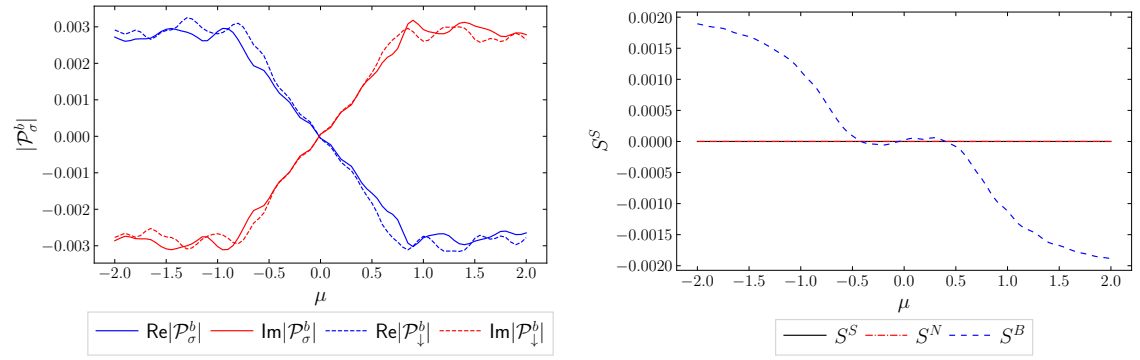


(a) (b)

Figure 7.6: (a) The spin-polarized p-wave triplet pairings and (b) the spin magnetizations as functions of the chemical potential $\mu$. We used $\phi = \pi/2$, $T = 0.05$, and $\kappa L = \pi$, where $L$ is the length of the entire junction in the tangential direction.

magnitude of the spin magnetization as a function of the phase difference. As expected, it vanishes for $\phi = 0$ and $\phi = \pi$. It has a sinusoidal form, similar to the charge current, which we will investigate next.

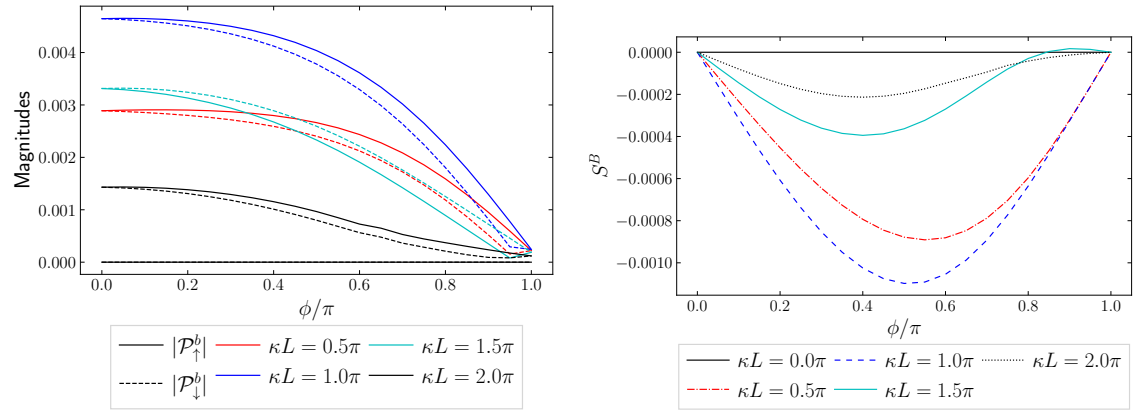


(a) (b)

Figure 7.7: (a) The spin-polarized p-wave triplet pairings and (b) the spin magnetizations as functions of the phase difference $\phi$. We used $\mu = 1$, $T = 0.05$, and denoted the length of the entire junction in the tangential direction $L$.

## 7.3 Currents

In the two-dimensional S-N-S junction, we can also induce a $0-\pi$ transition, similar to the one in section 6.6. As in the previous section, we consider a square junction with $N_S = 20$, $N_N = 21$ lattice sites in the superconductors and normal metal in the tangential direction and $N_b = 60$ sites in the binormal direction. We use $U = 1.5$, $a_N = 0.5$ and $T = 0.05$. In fig. 7.8a, we show the $0-\pi$ transition, which takes place when the spin-orbit contribution $\langle I^s \rangle_\alpha$ surpasses the hopping contribution $\langle I^s \rangle_t$ in magnitude. As with the p-wave pairings, the magnitudes of the current contributions depend on the chemical potential. In fig. 7.8b, we show this dependence and find that the total charge current is the highest for $\mu = 0$.

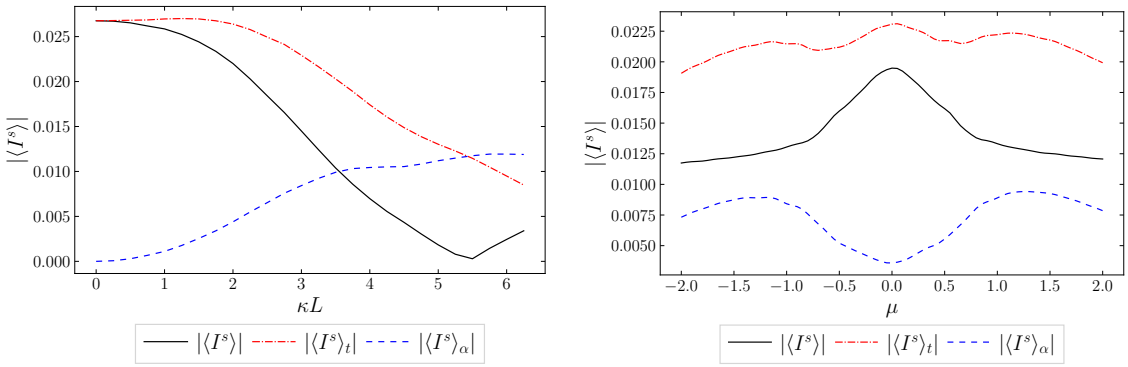


(a) (b)

Figure 7.8: (a) The $0-\pi$ transition for increasing curvature, and (b) the current contributions as a function of the chemical potential $\mu$. We used $\phi = \pi/2$. In (a), $\mu = 1$, and in (b) $\kappa L = \pi$. Here, $L$ denotes the length of the entire junction in the tangential direction.

In a two-dimensional system, there are more Andreev bound states compared to a one-dimensional system. We have previously argued for this statement and depicted them in fig. 7.4. As the gap decreases with increasing curvatures, only a few of the many bound states disappear, which have smaller contributions to the charge current than in the one-dimensional analysis. The direction of the charge current and the change in direction depend only on the magnitudes of $\langle I^s\rangle_t$ and $\langle I^s\rangle_\alpha$. Since the density of Andreev bound states is high, and many survive even when the junction is made into a cylinder, the skewness in the phase-current plots should remain unchanged. In fig. 7.9, we show the charge current contributions as a function of the phase difference $\phi$. As argued, they are skewed towards $\phi = \pi$ for all $\kappa$. For $\kappa L = 2\pi$ in fig. 7.9b, it is less skewed but still in the same direction. We highlight this line because it is past the $0-\pi$ transition, where the skewness direction had changed in the one-dimensional junction.

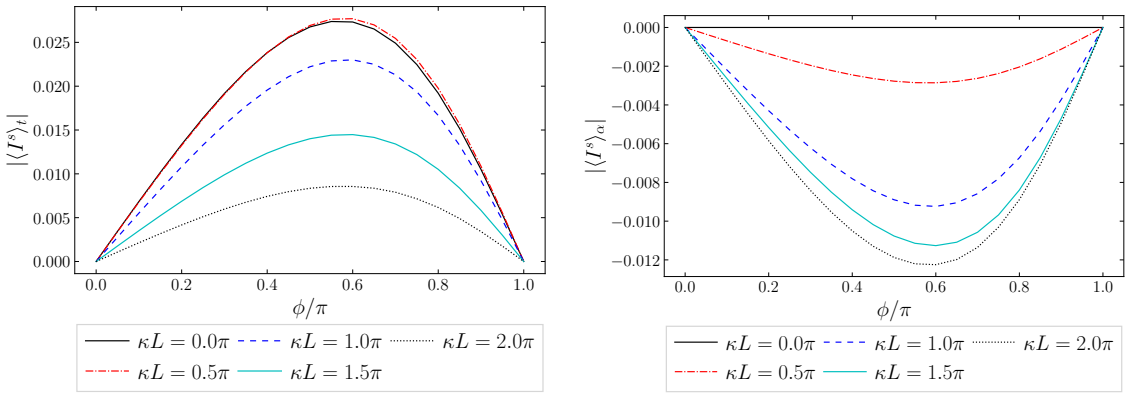


(a) (b)

Figure 7.9: Shows the phase-current relation for the (a) hopping and (b) spin-orbit contribution to the charge current for different curvatures. We used $\mu = 1$, and the total length of the junction in the tangential direction is denoted $L$.

Lastly, we consider the spin current across the junction. The strain-induced spin-orbit coupling in our junction will create a spin-current [138]. We use the expression given in eq. (5.76). There is one crucial point to keep in mind, however: the spin-orbit coupling prevents the spin $\boldsymbol{S}$ from being a good quantum number [139]. Since we show the spin-current in areas with spin-orbit coupling, it is not a conserved quantity. In fig. 7.10, we show the binormal component of the spin current in the tangential direction, $\langle I_S^{s,b} \rangle$. It shows that the spin-current increases with the curvature. It also reaches its maximum for zero chemical potential, as shown in fig. 7.10b. Although we have not shown it, $\langle I_S^{s,b} \rangle$ is independent of the phase difference between the superconductors. Therefore, the spin current will be highest for a junction with high curvature and low chemical potential, regardless of the phase difference between the superconductors.

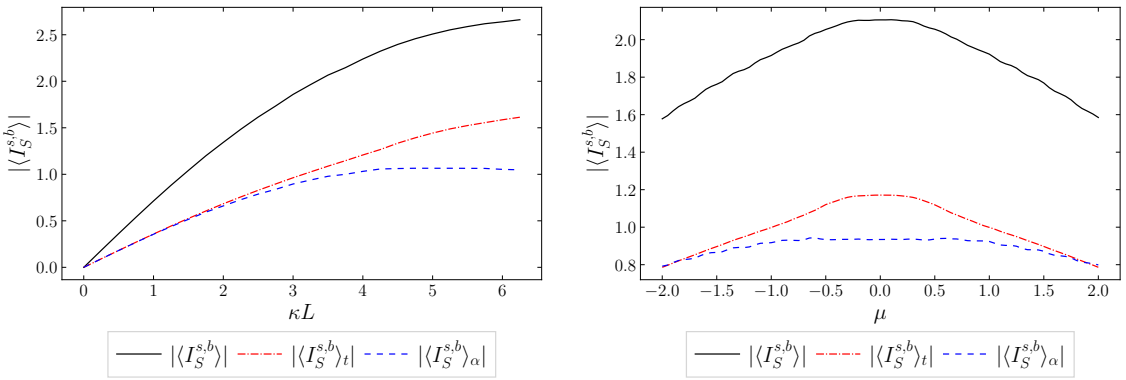


(a) (b)

Figure 7.10: The $b$-component of the total spin current in the $s$-direction as a function of the (a) curvature and (b) chemical potential. We used $\phi = \pi/2$. In (a), $\mu = 1$, and in (b) $\kappa L = \pi$. Here, $L$ denotes the length of the entire junction in the tangential direction.

# Chapter 8

# Conclusion and outlook

We have shown that curvature and strain have the potential to alter superconducting pair correlations in superconductors and Josephson junctions. We derived curvilinear coordinate systems for different geometries and the resulting strain-induced spin-orbit coupling to study these effects. We also derived the curvilinear Pauli matrices for one-dimensional space curves with and without torsion.

To build an intuition for the interplay between the exchange field in a ferromagnet and the intrinsic spin-orbit coupling in the dirty limit, we solved the Usadel equation numerically for straight S-F-S systems. Then, we added curvature, which, for the ferromagnet, created a curvature-induced spin-orbit coupling. A curved ferromagnet alone was sufficient to create spin-triplet correlations, and we showed that the strain-induced spin-orbit coupling was additive to the curvature. The curvature could change the state of the junction and induce a $0 - \pi$ transition. We also derived the Eilenberger equation in curvilinear coordinates to investigate increases in the p-wave contribution but found no contributions to the gap in a curved superconductor.

In the clean limit, we found that curving superconductors with considerable strain-induced spin-orbit coupling will alter the superconducting gap. We showed that the magnitude will vary depending on the curvature. We also showed that the orbital symmetry will be mixed, and we obtain p-wave correlations. As an example, we analyzed superconducting rings and applied strain by squeezing them into ellipses. This created high strain at the vertices, and the p-wave correlations were localized there. We also found that strong strain-induced spin-orbit coupling will kill the superconductivity entirely.

We found that we can induce $0 - \pi$ transitions in the clean limit as well. If the strain-induced spin-orbit coupling is strong, we can induce the transition without a ferromagnet in the weak link. The transition takes place in both one- and two-dimensional curved S-N-S junctions. We also found that in two-dimensional Josephson junctions, the strain-induced spin-orbit coupling creates a finite spin-magnetization in the binormal direction. Lastly, we showed that the non-conserved spin current will be highest for a junction with high curvature and low chemical potential.

Further extensions of this work could include studying stacked thin films. In chapter 7, we neglected the thickness of the junction, so one could consider a geometry like the one depicted in fig. 8.1. This is an interesting geometry since the Christoffel symbols are non-zero. Therefore, one would get an extra partial derivative in the Hamiltonian. The kinetic

and spin-orbit part of the Hamiltonian can be written as

$$\mathcal{H} = -\frac{\hbar^2}{2m}\mathcal{G}^{\mu\nu}\left(\partial_\mu\partial_\nu - \Gamma^\lambda_{\mu\nu}\partial_\lambda\right) - \frac{i\hbar}{m}\frac{\epsilon^{\lambda\mu\nu}}{\sqrt{|\mathcal{G}|}}\alpha_\lambda\sigma_\mu\partial_\nu\,, \tag{8.1}$$

where the greek indecies run over $s, n, b$. Since the Christoffel symbols differ from zero, the curvilinear Pauli matrices are not given by $\sigma_{T,N,B} \neq \sigma_{s,n,b}$. If one assumes that $\tau(s) = 0$, and only considers the cross-section of the junction, $b = 0$, the Hamiltonian reads

$$\mathcal{H} = \frac{-\hbar^2}{2m}\left(\partial_s^2 + \frac{1}{\eta(s,n)^2}\partial_n^2\right) - \frac{\hbar^2}{2m}\frac{\kappa(s)}{\eta(s,n)}\partial_n - \frac{i\hbar}{m}\frac{1}{\eta(s,n)}\alpha_N\sigma_B\partial_s\,, \tag{8.2}$$

which should display different curvature phenomena than those discussed in this thesis.

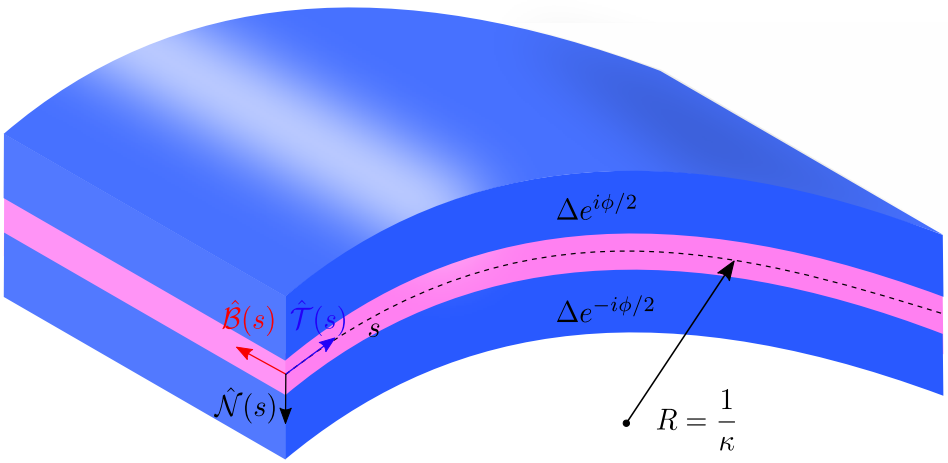


Figure 8.1: Stacked thin-films with curvature, where the $(s, n)$-plane might display novel phenomena.

Another possible extension is to investigate what happens when curving superconducting thin films with an intrinsic p-wave orbital symmetry. In one-dimensional Rashba wires, it has been shown that curvature can generate edge states and topological insulating phases [42]. Therefore, it could be interesting to investigate if one could induce corner modes in a two-dimensional setup. One likely needs curvature in both in-plane axes. Therefore, the Frenet-Serret equations do not suffice, and two principle curvatures are needed. The appropriate framework has been developed in ref. [140], using differential geometry instead of the Frenet-Serret frame.

This thesis has analyzed Josephson junctions in the dirty and clean limit and found interesting phenomena in curved superconductors in the clean limit. However, this work has numerous possibilities for further extensions, and curvature in condensed matter systems remains an active research area.

# Bibliography


[1] D. Saha, M. Holub, P. Bhattacharya, and D. Basu, in *Comprehensive semiconductor science and technology*, edited by P. Bhattacharya, R. Fornari, and H. Kamimura (Elsevier, Amsterdam, 2011), pp. 563–614.

[2] V. Masson-Delmotte, P. Zhai, A. Pirani, S. L. Connors, C. Péan, S. Berger, N. Caud, Y. Chen, L. Goldfarb, M. Gomis, et al., "Climate change 2021: the physical science basis", Contribution of working group I to the sixth assessment report of the intergovernmental panel on climate change **2**, 2391 (2021).

[3] F. Pulizzi, "Spintronics", Nature materials **11**, 367 (2012).

[4] A. Hirohata, K. Yamada, Y. Nakatani, I.-L. Prejbeanu, B. Diény, P. Pirro, and B. Hillebrands, "Review on spintronics: principles and device applications", Journal of Magnetism and Magnetic Materials **509**, 166711 (2020).

[5] K. Heshami, D. G. England, P. C. Humphreys, P. J. Bustard, V. M. Acosta, J. Nunn, and B. J. Sussman, "Quantum memories: emerging applications and recent advances", Journal of modern optics **63**, 2005 (2016).

[6] P. Vernaz-Gris, K. Huang, M. Cao, A. S. Sheremet, and J. Laurat, "Highly-efficient quantum memory for polarization qubits in a spatially-multiplexed cold atomic ensemble", Nature communications **9**, 363 (2018).

[7] I. Žutić, J. Fabian, and S. D. Sarma, "Spintronics: fundamentals and applications", Reviews of modern physics **76**, 323 (2004).

[8] J. Linder and J. W. Robinson, "Superconducting spintronics", Nature Physics **11**, 307 (2015).

[9] M. Eschrig et al., "Spin-polarized supercurrents for spintronics", Phys. Today **64**, 43 (2011).

[10] H. K. Onnes, "The superconductivity of mercury", Comm. Phys. Lab. Univ. Leiden **122**, 124 (1911).

[11] J. Bardeen, L. N. Cooper, and J. R. Schrieffer, "Theory of superconductivity", Physical review **108**, 1175 (1957).

[12] F. S. Bergeret, A. F. Volkov, and K. B. Efetov, "Odd triplet superconductivity and related phenomena in superconductor-ferromagnet structures", Rev. Mod. Phys. **77**, 1321 (2005).

[13] F. London and H. London, "The electromagnetic equations of the supraconductor", Proceedings of the Royal Society of London. Series A-Mathematical and Physical Sciences **149**, 71 (1935).

[14] V. L. Ginzburg, V. L. Ginzburg, and L. Landau, *On the theory of superconductivity* (Springer, 2009).

[15] M. Sigrist, "Introduction to unconventional superconductivity", in Aip conference proceedings, Vol. 789, 1 (American Institute of Physics, 2005), pp. 165–243.

[16] C. Tsuei and J. Kirtley, "Pairing symmetry in cuprate superconductors", Reviews of Modern Physics **72**, 969 (2000).

[17] J.-P. Brison, *P-wave superconductivity and d-vector representation*, 2021.

[18] A. P. Mackenzie and Y. Maeno, "The superconductivity of sr 2 ruo 4 and the physics of spin-triplet pairing", Reviews of Modern Physics **75**, 657 (2003).

[19] J. Hara and K. Nagai, "A polar state in a slab as a soluble model of p-wave fermi superfluid in finite geometry", Progress of theoretical physics **76**, 1237 (1986).

[20] Y. Nagato and K. Nagai, "Surface and size effect of a $d_{xy}$-state superconductor", Physical Review B **51**, 16254 (1995).

[21] M. Sato and S. Fujimoto, "Majorana fermions and topology in superconductors", Journal of the Physical Society of Japan **85**, 072001 (2016).

[22] C. Beenakker, "Search for majorana fermions in superconductors", Annu. Rev. Condens. Matter Phys. **4**, 113 (2013).

[23] N. Gnezdilov, B. van Heck, M. Diez, J. A. Hutasoit, and C. Beenakker, "Topologically protected charge transfer along the edge of a chiral p-wave superconductor", Physical Review B **92**, 121406 (2015).

[24] A. Y. Kitaev, "Unpaired majorana fermions in quantum wires", Physics-uspekhi **44**, 131 (2001).

[25] W. Meissner and R. Ochsenfeld, "Ein neuer effekt bei eintritt der supraleitfähigkeit", Naturwissenschaften **21**, 787 (1933).

[26] S. F. Saipuddin, A. Hashim, and N. E. Suhaimi, in *Superconducting materials: fundamentals, synthesis and applications* (Springer, 2022), pp. 123–146.

[27] M. Tinkham, *Introduction to superconductivity* (2004).

[28] P. Weiss, "L'hypothèse du champ moléculaire et la propriété ferromagnétique", J. Phys. Theor. Appl. **6**, 661 (1907).

[29] W. Heisenberg, "Zur theorie des ferromagnetismus, 1928", Z. Phys **49**, 619.

[30] F. Bergeret, A. F. Volkov, and K. B. Efetov, "Odd triplet superconductivity and related phenomena in superconductor-ferromagnet structures", Reviews of modern physics **77**, 1321 (2005).

[31] A. I. Buzdin, "Proximity effects in superconductor-ferromagnet heterostructures", Reviews of modern physics **77**, 935 (2005).

[32] B. Pannetier and H. Courtois, "Andreev reflection and proximity effect", Journal of low temperature physics **118**, 599 (2000).

[33] B. Josephson, "Possible new effects in superconductive tunnelling", Physics Letters **1**, 251 (1962).

[34] J. Robinson, J. Witt, and M. Blamire, "Controlled injection of spin-triplet supercurrents into a strong ferromagnet", Science **329**, 59 (2010).

[35] C. Ortix, "Quantum mechanics of a spin-orbit coupled electron constrained to a space curve", Physical Review B **91**, 245412 (2015).

[36] P. Gentile, M. Cuoco, and C. Ortix, "Curvature-induced rashba spin–orbit interaction in strain-driven nanostructures", in Spin, Vol. 3, 03 (World Scientific, 2013), p. 1340002.

[37] Z.-J. Ying, P. Gentile, C. Ortix, and M. Cuoco, "Designing electron spin textures and spin interferometers by shape deformations", Physical Review B **94**, 081406 (2016).

[38] K. S. Das, D. Makarov, P. Gentile, M. Cuoco, B. J. Van Wees, C. Ortix, and I. J. Vera-Marun, "Independent geometrical control of spin and charge resistances in curved spintronics", Nano letters **19**, 6839 (2019).

[39] P. Gentile, M. Cuoco, O. M. Volkov, Z.-J. Ying, I. J. Vera-Marun, D. Makarov, and C. Ortix, "Electronic materials with nanoscale curved geometries", Nature Electronics **5**, 551 (2022).

[40] D. Makarov, O. M. Volkov, A. Kákay, O. V. Pylypovskyi, B. Budinská, and O. V. Dobrovolskiy, "New dimension in magnetism and superconductivity: 3d and curvilinear nanoarchitectures", Advanced Materials **34**, 2101758 (2022).

[41] V. M. Fomin and O. V. Dobrovolskiy, "A perspective on superconductivity in curved 3d nanoarchitectures", Applied Physics Letters **120** (2022).

[42] P. Gentile, M. Cuoco, and C. Ortix, "Edge states and topological insulating phases generated by curving a nanowire with rashba spin-orbit coupling", Physical Review Letters **115**, 256801 (2015).

[43] S. Pandey, N. Scopigno, P. Gentile, M. Cuoco, and C. Ortix, "Topological quantum pump in serpentine-shaped semiconducting narrow channels", Physical Review B **97**, 241103 (2018).

[44] G. Francica, M. Cuoco, and P. Gentile, "Topological superconducting phases and josephson effect in curved superconductors with time reversal invariance", Physical Review B **101**, 094504 (2020).

[45] A. M. Turner, V. Vitelli, and D. R. Nelson, "Vortices on curved surfaces", Reviews of Modern Physics **82**, 1301 (2010).

[46] V. M. Fomin, R. O. Rezaev, and O. G. Schmidt, "Tunable generation of correlated vortices in open superconductor tubes", Nano letters **12**, 1282 (2012).

[47] Z.-J. Ying, M. Cuoco, C. Ortix, and P. Gentile, "Tuning pairing amplitude and spin-triplet texture by curving superconducting nanostructures", Physical Review B **96**, 100506 (2017).

[48] M. Martínez-Pérez and D. Koelle, "Nanosquids: basics and recent advances phys. sci. rev", arXiv preprint arXiv:1609.06182 (2016).

[49] D. Vasyukov, Y. Anahory, L. Embon, D. Halbertal, J. Cuppens, L. Neeman, A. Finkler, Y. Segev, Y. Myasoedov, M. L. Rappaport, et al., "A scanning superconducting quantum interference device with single electron spin sensitivity", Nature nanotechnology **8**, 639 (2013).

[50] T. Salamone, M. B. Svendsen, M. Amundsen, and S. Jacobsen, "Curvature-induced long-range supercurrents in diffusive superconductor-ferromagnet-superconductor josephson junctions with a dynamic 0- $\pi$ transition", Physical Review B **104**, L060505 (2021).

[51] T. Salamone, H. G. Hugdal, M. Amundsen, and S. H. Jacobsen, "Curvature control of the superconducting proximity effect in diffusive ferromagnetic nanowires", Physical Review B **105**, 134511 (2022).

[52] T. Salamone, H. G. Hugdal, M. Amundsen, and S. H. Jacobsen, "Electrical control of superconducting spin valves using ferromagnetic helices", arXiv:2404.05798 (2024).

[53] A. J. Skarpeid, H. G. Hugdal, T. Salamone, M. Amundsen, and S. H. Jacobsen, "Non-constant geometric curvature for tailored spin-orbit coupling and chirality in superconductor-magnet heterostructures", Journal of Physics: Condensed Matter (2024).

[54] T. Salamone, M. Skjærpe, H. G. Hugdal, M. Amundsen, and S. H. Jacobsen, "Interface probe for antiferromagnets using geometric curvature", Physical Review B **109**, 094508 (2024).

[55] Z.-J. Ying, M. Cuoco, P. Gentile, and C. Ortix, "Josephson current in rashba-based superconducting nanowires with geometric misalignment: rashba-based superconducting nanowires with geometric misalignment", in 2017 16th international superconductive electronics conference (isec) (IEEE, 2017), pp. 1–3.

[56] A. Kopasov, A. Kutlin, and A. Mel'nikov, "Geometry controlled superconducting diode and anomalous josephson effect triggered by the topological phase transition in curved proximitized nanowires", Physical Review B **103**, 144520 (2021).

[57] K. Dullemond and K. Peeters, "Introduction to tensor calculus", (1991).

[58] D. E. Neuenschwander, *Tensor calculus for physics*, Vol. 422 (John Hopkins University Press, 2014).

[59] M. M. Odashima, B. G. Prado, and E. Vernek, "Pedagogical introduction to equilibrium green's functions: condensed-matter examples with numerical implementations", Revista Brasileira de Ensino de Física **39** (2016).

[60] D. M. Cannell, *George green: mathematician and physicist 1793–1841: the background to his life and work* (SIAM, 2001).

[61] G. Green, *An essay on the application of mathematical analysis to the theories of electricity and magnetism*, Vol. 3 (author, 1889).

[62] M. B. M. Svendsen, "Diffusive spin-orbit coupled superconductor-ferromagnet proximity systems", Master's thesis (NTNU, 2020).

[63] T. Salamone, "Proximity effects in nanostructures with geometric curvature for superconducting spintronics", PhD thesis (NTNU, 2023).

[64] M. B. M. Svendsen, "Curvature in superconductor-ferromagnet structures", Master's thesis (NTNU, 2021).

[65] E. Rashba, "Properties of semiconductors with an extremum loop. i. cyclotron and combinational resonance in a magnetic field perpendicular to the plane of the loop", Sov. Phys.-Solid State **2**, 1109 (1960).

[66] G. Dresselhaus, "Spin-orbit coupling effects in zinc blende structures", Physical Review **100**, 580 (1955).

[67] S. H. Jacobsen, J. A. Ouassou, and J. Linder, "Critical temperature and tunneling spectroscopy of superconductor-ferromagnet hybrids with intrinsic rashba-dresselhaus spin-orbit coupling", Physical Review B **92**, 024510 (2015).

[68] J. Bardeen and W. Shockley, "Deformation potentials and mobilities in non-polar crystals", Physical review **80**, 72 (1950).

[69] C. Herring and E. Vogt, "Transport and deformation-potential theory for many-valley semiconductors with anisotropic scattering", Phys. Rev. **101**, 944 (1956).

[70] C. G. Van de Walle, "Band lineups and deformation potentials in the model-solid theory", Physical review B **39**, 1871 (1989).

[71] F. Bergeret and I. Tokatly, "Spin-orbit coupling as a source of long-range triplet proximity effect in superconductor-ferromagnet hybrid structures", Physical Review B **89**, 134517 (2014).

[72] F. Bergeret and I. Tokatly, "Singlet-triplet conversion and the long-range proximity effect in superconductor-ferromagnet structures with generic spin dependent fields", Physical review letters **110**, 117003 (2013).

[73] R. da Costa, "Quantum mechanics of a constrained particle", Physical Review A **23**, 1982 (1981).

[74] H. Jensen and H. Koppe, "Quantum mechanics with constraints", Annals of Physics **63**, 586 (1971).

[75] V. Chandrasekhar, "Proximity-coupled systems: quasiclassical theory of superconductivity", The Physics of Superconductors: Vol. II. Superconductivity in Nanostructures, High-$T_c$ and Novel Superconductors, Organic Superconductors, 55 (2004).

[76] L. P. Pitaevskii and E. Lifshitz, *Physical kinetics: volume 10*, Vol. 10 (Butterworth-Heinemann, 2012).

[77] L. V. Keldysh, in *Selected papers of leonid v keldysh* (World Scientific, 2024), pp. 47–55.

[78] J. Linder, T. Yokoyama, and A. Sudbø, "Role of interface transparency and spin-dependent scattering in diffusive ferromagnet/superconductor heterostructures", Physical Review B **77**, 174514 (2008).

[79] G. Eilenberger, "Transformation of gorkov's equation for type ii superconductors into transport-like equations", Zeitschrift für Physik A Hadrons and nuclei **214**, 195 (1968).

[80] A. Larkin and Y. N. Ovchinnikov, "Quasi-classical method in the theory of superconductivity", ZH EKSPER TEOR FIZ **55** (1968).

[81] W. Belzig, F. K. Wilhelm, C. Bruder, G. Schön, and A. D. Zaikin, "Quasiclassical green's function approach to mesoscopic superconductivity", Superlattices and microstructures **25**, 1251 (1999).

[82] M. Amundsen and J. Linder, "Quasiclassical theory for interfaces with spin-orbit coupling", Physical Review B **100**, 064502 (2019).

[83] M. Amundsen, "Proximity effects in superconducting hybrid structures with spin-dependent interactions", PhD thesis (NTNU, 2020).

[84] H. Bruus and K. Flensberg, *Many-body quantum theory in condensed matter physics: an introduction* (OUP Oxford, 2004).

[85] J. P. Morten, "Spin and charge transport in dirty superconductors", Master's thesis (NTNU, 2005).

[86] J. Rammer and H. Smith, "Quantum field-theoretical methods in transport theory of metals", Reviews of modern physics **58**, 323 (1986).

[87] S. H. Jacobsen and J. Linder, "Giant triplet proximity effect in $\pi$-biased josephson junctions with spin-orbit coupling", Physical Review B **92**, 024501 (2015).

[88] A. Shelankov, "Two-particle tunneling in a normal metal–semiconductor contact", Sov. Phys. Solid State **26**, 981 (1984).

[89] A. Zaitsev, "Quasiclassical equations of the theory of superconductivity for contiguous metals and the properties of constricted microcontacts", Zh. Eksp. Teor. Fiz **86**, 1742 (1984).

[90] S.-K. Yip, "Josephson current between d-wave superconductors through an interface with finite transmission", Journal of low temperature physics **109**, 547 (1997).

[91] M. Ozana and A. Shelankov, "Superconductivity in multiple interface geometry: applicability of quasiclassical theory", Journal of low temperature physics **124**, 223 (2001).

[92] M. Eschrig, "Distribution functions in nonequilibrium theory of superconductivity and andreev spectroscopy in unconventional superconductors", Physical Review B **61**, 9061 (2000).

[93] M. Fogelström, "Josephson currents through spin-active interfaces", Physical Review B **62**, 11812 (2000).

[94] E. Zhao, T. Löfwander, and J. Sauls, "Nonequilibrium superconductivity near spin-active interfaces", Physical Review B **70**, 134510 (2004).

[95] T. Lück, P. Schwab, U. Eckern, and A. Shelankov, "Disordered josephson junctions of d-wave superconductors", Physical Review B **68**, 174524 (2003).

[96] M. Y. Kuprianov and V. Lukichev, "Influence of boundary transparency on the critical current of "dirty" ss's structures", Zh. Eksp. Teor. Fiz **94**, 139 (1988).

[97] Y. V. Nazarov, "Novel circuit theory of andreev reflection", Superlattices and microstructures **25**, 1221 (1999).

[98] M. Eschrig, A. Cottet, W. Belzig, and J. Linder, "General boundary conditions for quasiclassical theory of superconductivity in the diffusive limit: application to strongly spin-polarized systems", New Journal of Physics **17**, 083037 (2015).

[99] H. G. Hugdal, J. Linder, and S. H. Jacobsen, "Quasiclassical theory for the superconducting proximity effect in dirac materials", Physical Review B **95**, 235403 (2017).

[100] J. Linder, M. Amundsen, and V. Risinggård, "Intrinsic superspin hall current", Physical Review B **96**, 094512 (2017).

[101] P.-G. De Gennes, *Superconductivity of metals and alloys* (CRC press, 1966).

[102] J.-X. Zhu, *Bogoliubov-de gennes method and its applications*, Vol. 924 (Springer, 2016).

[103] T. Hegstad, "Supercurrent 0-$\pi$ oscillations induced by spin-orbit coupling", Master's thesis (NTNU, 2022).

[104] V. Risinggård and J. Linder, "Direct and inverse superspin hall effect in two-dimensional systems: electrical detection of spin supercurrents", Physical Review B **99**, 174505 (2019).

[105] L. G. Johnsen, "Controllable superconducting phase transition and magnetization reorientation due to spin-orbit interactions", Master's thesis (NTNU, 2019).

[106] L. G. Johnsen, "The magnetic field driven superconductor–metal transition in disordered hole-overdoped cuprates", Journal of Physics: Condensed Matter **35**, 115601 (2023).

[107] E. W. Hodt, C. Cirillo, A. Di Bernardo, C. Attanasio, and J. Linder, "Critical temperature of triplet superconductor-ferromagnet bilayers as a probe for pairing symmetry", arXiv:2402.10266 (2024).

[108] C. Sun and J. Linder, "Supercurrent-induced spin switching via indirect exchange interaction", arXiv:2310.09324 (2023).

[109] J. Linder and A. V. Balatsky, "Odd-frequency superconductivity", Reviews of Modern Physics **91**, 045005 (2019).

[110] V. Berezinskii, "Novaya model'anizotropnoy fazy sverkhtekuchego he3 (new model of the anisotropic phase of superfluid he3)", Pis' ma Zh. Eksp. Teor. Fiz. **20**, 628 (1974).

[111] T. Yokoyama, Y. Tanaka, and A. A. Golubov, "Resonant proximity effect in normal metal/diffusive ferromagnet/superconductor junctions", Physical Review B **73**, 094501 (2006).

[112] S. Kawabata, Y. Asano, Y. Tanaka, and A. A. Golubov, "Robustness of spin-triplet pairing and singlet–triplet pairing crossover in superconductor/ferromagnet hybrids", Journal of the Physical Society of Japan **82**, 124702 (2013).

[113] J. A. Ouassou, "Density of states and critical temperature in superconductor/ferromagnet structures with spin-orbit coupling", Master's thesis (NTNU, 2015).

[114] D. D. Sheka, V. P. Kravchuk, and Y. Gaididei, "Curvature effects in statics and dynamics of low dimensional magnets", Journal of Physics A: Mathematical and Theoretical **48**, 125202 (2015).

[115] T. Kontos, M. Aprili, J. Lesueur, and X. Grison, "Inhomogeneous superconductivity induced in a ferromagnet by proximity effect", Physical review letters **86**, 304 (2001).

[116] I. Bobkova and A. Bobkov, "Quasiclassical theory of magnetoelectric effects in superconducting heterostructures in the presence of spin-orbit coupling", Physical Review B **95**, 184518 (2017).

[117] P. Burset, B. Lu, S. Tamura, and Y. Tanaka, "Current fluctuations in unconventional superconductor junctions with impurity scattering", Physical Review B **95**, 224502 (2017).

[118] J. Cayao and A. M. Black-Schaffer, "Odd-frequency superconducting pairing in junctions with rashba spin-orbit coupling", Physical Review B **98**, 075425 (2018).

[119] C. R. Reeg and D. L. Maslov, "Proximity-induced triplet superconductivity in rashba materials", Physical Review B **92**, 134512 (2015).

[120] Y. Tanaka, Y. Tanuma, and A. A. Golubov, "Odd-frequency pairing in normal-metal/superconductor junctions", Physical Review B **76**, 054522 (2007).

[121] A. Buzdin and A. Koshelev, "Periodic alternating 0-and $\pi$-junction structures as realization of $\varphi$-josephson junctions", Physical Review B **67**, 220504 (2003).

[122] T. Kontos, M. Aprili, J. Lesueur, F. Genêt, B. Stephanidis, and R. Boursier, "Josephson junction through a thin ferromagnetic layer: negative coupling", Physical review letters **89**, 137007 (2002).

[123] V. Ryazanov, V. Oboznov, A. Y. Rusanov, A. Veretennikov, A. A. Golubov, and J. Aarts, "Coupling of two superconductors through a ferromagnet: evidence for a $\pi$ junction", Physical review letters **86**, 2427 (2001).

[124] M. Amundsen, J. Linder, J. W. Robinson, I. Žutić, and N. Banerjee, "Colloquium: spin-orbit effects in superconducting hybrid structures", arXiv:2210.03549 (2022).

[125] P. Coleman, *Introduction to many-body physics* (Cambridge University Press, 2015).

[126] A. Droghetti, I. Rungger, A. Rubio, and I. V. Tokatly, "Spin-orbit induced equilibrium spin currents in materials", Physical Review B **105**, 024409 (2022).

[127] E. I. Rashba, "Spin currents in thermodynamic equilibrium: the challenge of discerning transport currents", Physical Review B **68**, 241315 (2003).

[128] V. Stanev and V. Galitski, "Quasiclassical eilenberger theory of the topological proximity effect in a superconducting nanowire", Physical Review B **89**, 174521 (2014).

[129] L. P. Gor'kov and E. I. Rashba, "Superconducting 2d system with lifted spin degeneracy: mixed singlet-triplet state", Physical Review Letters **87**, 037004 (2001).

[130] T. Yu and M. Wu, "Gapped triplet p-wave superconductivity in strong spin-orbit-coupled semiconductor quantum wells in proximity to s-wave superconductor", Physical Review B **93**, 195308 (2016).

[131] A. M. Black-Schaffer and S. Doniach, "Self-consistent solution for proximity effect and josephson current in ballistic graphene sns josephson junctions", Physical Review B **78**, 024504 (2008).

[132] J. Sauls, *Andreev bound states and their signatures*, 2018.

[133] D. Willsch, D. Rieger, P. Winkel, M. Willsch, C. Dickel, J. Krause, Y. Ando, R. Lescanne, Z. Leghtas, N. T. Bronn, et al., "Observation of josephson harmonics in tunnel junctions", Nature Physics, 1 (2024).

[134] M. Amundsen, "Quasiclassical theory beyond 1d: supercurrents and topological excitations", Master's thesis (NTNU, 2016).

[135] E. H. Fyhn, "Green's function approach to quantum phenomena in heterostructures with spin-polarization and coherence", PhD thesis (NTNU, 2023).

[136] J. J. He, T. Liang, Y. Tanaka, and N. Nagaosa, "Platform of chiral majorana edge modes and its quantum transport phenomena", Communications Physics **2**, 149 (2019).

[137] E. Prada, P. San-Jose, M. W. de Moor, A. Geresdi, E. J. Lee, J. Klinovaja, D. Loss, J. Nygård, R. Aguado, and L. P. Kouwenhoven, "From andreev to majorana bound states in hybrid superconductor–semiconductor nanowires", Nature Reviews Physics **2**, 575 (2020).

[138] S. Maekawa, S. O. Valenzuela, E. Saitoh, and T. Kimura, *Spin current*, Vol. 22 (Oxford University Press, 2017).

[139] H. Bulou, L. Joly, J.-M. Mariot, and F. Scheurer, *Magnetism and accelerator-based light sources: proceedings of the 7th international school "synchrotron radiation and magnetism", mittelwihr (france), 2018* (Springer Nature, 2021).

[140] M. A. Tjøtta, "Superconductive transport in curved thin film ferromagnets", Master's thesis (NTNU, 2024).

[141] C. W. Groth, M. Wimmer, A. R. Akhmerov, and X. Waintal, "Kwant: a software package for quantum transport", New Journal of Physics **16**, 063065 (2014).

# Appendix A

# Derivation Christoffel symbol

In this appendix, we give the derivation of the first Christoffel symbol $\Gamma^s_{\mu\nu}$ of the second kind, which is

$$\begin{aligned}\Gamma^s_{\mu\nu} = \quad & \frac{1}{2}\mathcal{G}^{ss}\left[\partial_\nu \mathcal{G}_{\mu s} + \partial_\mu \mathcal{G}_{s\nu} - \partial_s \mathcal{G}_{\mu\nu}\right] \\ & + \frac{1}{2}\mathcal{G}^{sn}\left[\partial_\nu \mathcal{G}_{\mu n} + \partial_\mu \mathcal{G}_{n\nu} - \partial_n \mathcal{G}_{\mu\nu}\right] \\ & + \frac{1}{2}\mathcal{G}^{sb}\left[\partial_\nu \mathcal{G}_{\mu b} + \partial_\mu \mathcal{G}_{b\nu} - \partial_b \mathcal{G}_{\mu\nu}\right]. \end{aligned} \tag{A.1}$$

Note that the expression is not the same as in eq. (3.7) since the metric is not diagonal for a parametrization with torsion. Thus, the inverse metric runs over all indices of $\sigma$ in eq. (2.25). In the following, we separately calculate each line in eq. (A.1). The first line in the equation above for the Christoffel symbol is

$$\begin{aligned}&\frac{1}{2}\mathcal{G}^{ss}\left[\partial_\nu \mathcal{G}_{\mu s} + \partial_\mu \mathcal{G}_{s\nu} - \partial_s \mathcal{G}_{\mu\nu}\right] = \\ &\quad \frac{1}{2}\mathcal{G}^{ss}\begin{pmatrix} \partial_s\left(\eta(s,n)^2 + \zeta(s,n,b)^2\right) & \partial_n\left(\eta(s,n)^2 + \zeta(s,n,b)^2\right) & \partial_b\left(\eta(s,n)^2 + \zeta(s,n,b)^2\right) \\ \partial_s\left(-b\tau(s)\right) & \partial_n\left(-b\tau(s)\right) & \partial_b\left(-b\tau(s)\right) \\ \partial_s\left(n\tau(s)\right) & \partial_n\left(n\tau(s)\right) & \partial_b\left(n\tau(s)\right) \end{pmatrix} \\ &\quad + \frac{1}{2}\mathcal{G}^{ss}\begin{pmatrix} \partial_s\left(\eta(s,n)^2 + \zeta(s,n,b)^2\right) & \partial_s\left(-b\tau(s)\right) & \partial_s\left(n\tau(s)\right) \\ \partial_n\left(\eta(s,n)^2 + \zeta(s,n,b)^2\right) & \partial_n\left(-b\tau(s)\right) & \partial_n\left(n\tau(s)\right) \\ \partial_b\left(\eta(s,n)^2 + \zeta(s,n,b)^2\right) & \partial_b\left(-b\tau(s)\right) & \partial_b\left(n\tau(s)\right) \end{pmatrix} \\ &\quad - \frac{1}{2}\mathcal{G}^{ss}\begin{pmatrix} \partial_s\left(\eta(s,n)^2 + \zeta(s,n,b)^2\right) & \partial_s\left(-b\tau(s)\right) & \partial_s\left(n\tau(s)\right) \\ \partial_s\left(-b\tau(s)\right) & \partial_s\left(1\right) & \partial_s\left(0\right) \\ \partial_s\left(n\tau(s)\right) & \partial_s\left(0\right) & \partial_s\left(1\right) \end{pmatrix} \\ &= \frac{1}{2}\mathcal{G}^{ss}\begin{pmatrix} \partial_s\left(\eta(s,n)^2 + \zeta(s,n,b)^2\right) & \partial_n\left(\eta(s,n)^2 + \zeta(s,n,b)^2\right) & \partial_b\left(\eta(s,n)^2 + \zeta(s,n,b)^2\right) \\ \partial_n\left(\eta(s,n)^2 + \zeta(s,n,b)^2\right) & 0 & 0 \\ \partial_b\left(\eta(s,n)^2 + \zeta(s,n,b)^2\right) & 0 & 0 \end{pmatrix}. \end{aligned} \tag{A.2}$$

Moving on to the second line in eq. (A.1), we get

$$\begin{aligned}&\frac{1}{2}\mathcal{G}^{sn}\left[\partial_\nu \mathcal{G}_{\mu n} + \partial_\mu \mathcal{G}_{n\nu} - \partial_n \mathcal{G}_{\mu\nu}\right] = \\ &\quad \frac{1}{2}\mathcal{G}^{sn}\begin{pmatrix} \partial_s\left(-b\tau(s)\right) & \partial_n\left(-b\tau(s)\right) & \partial_b\left(-b\tau(s)\right) \\ \partial_s\left(1\right) & \partial_n\left(1\right) & \partial_b\left(1\right) \\ \partial_s\left(0\right) & \partial_n\left(0\right) & \partial_b\left(0\right) \end{pmatrix} \end{aligned}$$

$$
\begin{aligned}
&+\frac{1}{2}\mathcal{G}^{sn}\begin{pmatrix}\partial_s\left(-b\tau(s)\right) & \partial_s\left(1\right) & \partial_s\left(0\right)\\ \partial_n\left(-b\tau(s)\right) & \partial_n\left(1\right) & \partial_n\left(0\right)\\ \partial_b\left(-b\tau(s)\right) & \partial_b\left(1\right) & \partial_b\left(0\right)\end{pmatrix}\\
&-\frac{1}{2}\mathcal{G}^{sn}\begin{pmatrix}\partial_n\left(\eta(s,n)^2+\zeta(s,n,b)^2\right) & \partial_n\left(-b\tau(s)\right) & \partial_n\left(n\tau(s)\right)\\ \partial_n\left(-b\tau(s)\right) & \partial_n\left(1\right) & \partial_n\left(0\right)\\ \partial_n\left(n\tau(s)\right) & \partial_n\left(0\right) & \partial_n\left(1\right)\end{pmatrix}\\
&=\frac{1}{2}\mathcal{G}^{sn}\begin{pmatrix}2\partial_s\left(-b\tau(s)\right)-\partial_n\left(\eta(s,n)^2+\zeta(s,n,b)^2\right) & 0 & -2\tau(s)\\ 0 & 0 & 0\\ -2\tau(s) & 0 & 0\end{pmatrix}. \qquad \text{(A.3)}
\end{aligned}
$$

Finally, the third and last line in eq. (A.1) evaluates to

$$
\begin{aligned}
&\frac{1}{2}\mathcal{G}^{sb}\left[\partial_\nu\mathcal{G}_{\mu b}+\partial_\mu\mathcal{G}_{b\nu}-\partial_b\mathcal{G}_{\mu\nu}\right]=\\
&\quad\frac{1}{2}\mathcal{G}^{sb}\begin{pmatrix}\partial_s\left(n\tau(s)\right) & \partial_n\left(n\tau(s)\right) & \partial_b\left(n\tau(s)\right)\\ \partial_s\left(0\right) & \partial_n\left(0\right) & \partial_b\left(0\right)\\ \partial_s\left(1\right) & \partial_n\left(1\right) & \partial_b\left(1\right)\end{pmatrix}\\
&\quad+\frac{1}{2}\mathcal{G}^{sb}\begin{pmatrix}\partial_s\left(n\tau(s)\right) & \partial_s\left(0\right) & \partial_s\left(1\right)\\ \partial_n\left(n\tau(s)\right) & \partial_n\left(0\right) & \partial_n\left(1\right)\\ \partial_b\left(n\tau(s)\right) & \partial_b\left(0\right) & \partial_b\left(1\right)\end{pmatrix}\\
&\quad-\frac{1}{2}\mathcal{G}^{sb}\begin{pmatrix}\partial_b\left(\eta(s,n)^2+\zeta(s,n,b)^2\right) & \partial_b\left(-b\tau(s)\right) & \partial_b\left(n\tau(s)\right)\\ \partial_b\left(-b\tau(s)\right) & \partial_b\left(1\right) & \partial_b\left(0\right)\\ \partial_b\left(n\tau(s)\right) & \partial_b\left(0\right) & \partial_b\left(1\right)\end{pmatrix}\\
&=\frac{1}{2}\mathcal{G}^{sb}\begin{pmatrix}2\partial_s\left(-b\tau(s)\right)-\partial_b\left(\eta(s,n)^2+\zeta(s,n,b)^2\right) & 2\tau(s) & 0\\ 2\tau(s) & 0 & 0\\ 0 & 0 & 0\end{pmatrix}. \qquad \text{(A.4)}
\end{aligned}
$$

Having all three terms, we can sum up the contributions. However, we do it elementwise since we do not need to calculate both $\Gamma^s_{\mu\nu}$ and $\Gamma^s_{\nu\mu}$. It can be seen directly from eqs. (A.2) to (A.4), so no further proof is necessary. We start with the first element, which is

$$
\begin{aligned}
\Gamma^s_{ss} =&\frac{1}{2\eta(s,n)^2}\left[\partial_s\big(\eta(s,n)^2+\zeta(s,n,b)^2\big)-2b\tau(s)\partial_s(b\tau(s))-b\tau(s)\partial_n\big(\eta(s,n)^2+\zeta(s,n,b)^2\big)\right.\\
&\left.+n\tau(s)\partial_b\big(\eta(s,n)^2+\zeta(s,n,b)^2\big)-2n\tau(s)\partial_s(n\tau(s))\right]\\
=&\frac{1}{\eta(s,n)}\left[\partial_s\eta(s,n)+b\tau(s)\kappa(s)\right]. \qquad \text{(A.5)}
\end{aligned}
$$

The rest of the elements are,

$$
\Gamma^s_{sn}=\frac{1}{2\eta(s,n)}\left[\partial_n\big(\eta(s,n)^2+\zeta(s,n,b)^2\big)-2n\tau(s)^2\right]=-\frac{\kappa(s)}{\eta(s,n)}, \qquad \text{(A.6)}
$$

$$
\Gamma^s_{sb}=\frac{1}{2\eta(s,n)}\left[\partial_b\big(\eta(s,n)^2+\zeta(s,n,b)^2\big)-2b\tau(s)^2\right]=0. \qquad \text{(A.7)}
$$

The calculations for the other Christoffel symbols are identical to the one already presented. Thus, we do not present them.

# Appendix B

# Gradient approximation derivation

This appendix will investigate how the change of coordinates affects the bullet product. However, first, we need to define the product. We consider the Dyson equation (4.13) to give the product meaning, where we first introduced the notation. Intuitively, when and where the propagators interact with the external potential should not be fixed. Contributions from interaction anywhere and at any time should contribute as long as the particle arrives at the appropriate time and place. Thus, the product should be both a matrix multiplication and an integral over all possible positions and times. The bullet product is defined as

$$(A \bullet B)\ (\boldsymbol{r}_1, t_1; \boldsymbol{r}_2, t_2) = \int d^3r' \int dt' A(\boldsymbol{r}_1, t_1; \boldsymbol{r}', t') B(\boldsymbol{r}', t'; \boldsymbol{r}_2, t_2). \tag{B.1}$$

Next, we will see how this definition is affected by the mixed representation. Specifically, we will derive a practical approximation for the quasiclassical approximation in the mixed representation. Our starting point is the definition in eq. (B.1). When this is expressed in terms of the relative and center-of-mass coordinates defined in eq. (4.44), we can write the product as

$$(A \bullet B)(\boldsymbol{R}, T; \boldsymbol{r}, t) = \int d^3r \int dt\ A\left(\boldsymbol{R} + \frac{\boldsymbol{r}}{2}, T + \frac{t}{2}; \boldsymbol{r}', t'\right)\ B\left(\boldsymbol{r}', t'; \boldsymbol{R} - \frac{\boldsymbol{r}}{2}, T - \frac{t}{2}\right). \tag{B.2}$$

Next, to lighten the notation, we will write everything in four-vector notation. That is $X = (T,\ \boldsymbol{R})$ for the center-of-mass and $x = (t,\ \boldsymbol{r})$ for the relative coordinate. In addition we Fourier transform $x \to P = (\mathcal{E},\ \boldsymbol{p})$ the product, so we have

$$(A \bullet B)(X, P) = \int d^4x' \int d^4x\, e^{iPx} A\left(X + \frac{x}{2}, x'\right)\ B\left(x', X - \frac{x}{2}\right), \tag{B.3}$$

where the exponent $Px$ should be understood as the Lorentz invariant product $P_\mu x^\mu = P_\mu g^{\mu\nu} x_\nu$. Since we integrate over the whole domain of $x'$, we can shift it by $X$ without changing the result. [85] We get

$$(A \bullet B)(X, P) = \int d^4x' \int d^4x\, e^{iPx} A\left(X + \frac{x}{2}, x' + X\right)\ B\left(x' + X, X - \frac{x}{2}\right). \tag{B.4}$$

Next, we introduce a coordinate transformation, simplifying our expression later. The new coordinates are given by

$$x = u + v, \qquad\qquad x' = \frac{u - v}{2}, \tag{B.5}$$

so that $dxdx' \to |J(u,v)|dudv$, where the Jacobian has a value of $J(u,v) = -1$, which does not change the sign of the expression because of the absolute value. [64] Thus, the coordinate transformation gives us

$$(A \bullet B)(X,P) = \int du \int dv\, e^{iP(u+v)}\, A\left(X + \frac{u+v}{2}, \frac{u-v}{2} + X\right)\, B\left(\frac{u-v}{2} + X, X + \frac{u+v}{2}\right). \tag{B.6}$$

Next, we do a Taylor expansion of $A$ in $u$ and $B$ in $v$, both about zero. The series is

$$A\left(X + \frac{u+v}{2}, \frac{u-v}{2} + X\right) = \sum_n \frac{1}{n!}\left(\frac{1}{2}\right)^n \nabla_X^n\, A\left(X + \frac{v}{2}, X - \frac{v}{2}\right) u^n, \tag{B.7}$$

$$B\left(X + \frac{u-v}{2}, X - \frac{u+v}{2}\right) = \sum_m \frac{1}{m!}\left(\frac{-1}{2}\right)^m \nabla_X^m\, B\left(X + \frac{u}{2}, X - \frac{u}{2}\right) v^m. \tag{B.8}$$

Note that $A$ is independent of $u$, and $B$ is independent of $v$, which means the integrals over $u$ and $v$ can be separated in the bullet product. Inserting the Taylor series of $A$ and $B$, the product now takes the form

$$(A \bullet B)(X,P) = \sum_n \sum_m \frac{1}{n!}\frac{1}{m!}\left(\frac{1}{2}\right)^n \left(\frac{-1}{2}\right)^m \left[\int dv\, \nabla_X^n\, A\left(X + \frac{v}{2}, X - \frac{v}{2}\right) e^{iPv} v^m\right] \times \left[\int du\, \nabla_X^m\, B\left(X + \frac{u}{2}, X - \frac{u}{2}\right) e^{iPu} u^n\right]. \tag{B.9}$$

We rewrite the last part in the square brackets as $e^{iPu}u^n = (-i)^n \nabla_P^n e^{iPu}$. This gives us

$$(A \bullet B)(X,P) = \sum_n \sum_m \frac{1}{n!}\frac{1}{m!}\left(\frac{-i}{2}\right)^n \left(\frac{i}{2}\right)^m \nabla_P^m \nabla_X^n \left[\int dv\, A\left(X + \frac{v}{2}, X - \frac{v}{2}\right) e^{iPv}\right] \times \nabla_P^n \nabla_X^m \left[\int du\, B\left(X + \frac{u}{2}, X - \frac{u}{2}\right) e^{iPu}\right]. \tag{B.10}$$

Next, we notice that the integrals inside the square brackets are simply the Fourier transform to $P$ space of the coordinate $v$ and $u$, respectively. In the following, we use the superscript of the nabla operator to write upon which matrix it acts explicitly. This means, for instance, $\left(\nabla_X^n A\right)\left(\nabla_P^m B\right) = \left(\nabla_X^A\right)^n \left(\nabla_P^B\right)^m AB$. Using the Taylor series of the exponential function, which is

$$\sum_n \frac{1}{n!}\left(\frac{-i}{2}\right)^n \left(\nabla_X^A\right)^n \left(\nabla_P^B\right)^n = e^{\frac{-i}{2}\nabla_X^A \nabla_P^B}, \tag{B.11}$$

the bullet product can be written as

$$(A \bullet B)(X,P) = e^{\frac{i}{2}\left(\nabla_X^B \nabla_P^A - \nabla_X^A \nabla_P^B\right)}\, A(X,P)\, B(X,P). \tag{B.12}$$

Switching back to three-vector notation, this becomes

$$(A \bullet B)(\boldsymbol{R},T,\boldsymbol{p},\mathcal{E}) = e^{\frac{i}{2}\left(\partial_T^B \partial_{\mathcal{E}}^A - \partial_T^A \partial_{\mathcal{E}}^B\right)} e^{\frac{i}{2}\left(\nabla_{\boldsymbol{R}}^A \nabla_{\boldsymbol{p}}^B - \nabla_{\boldsymbol{R}}^B \nabla_{\boldsymbol{p}}^A\right)}\, A(\boldsymbol{R},T,\boldsymbol{p},\mathcal{E})\, B(\boldsymbol{R},T,\boldsymbol{p},\mathcal{E}), \tag{B.13}$$

which expanded to the first order can be approximated as

$$(A \bullet B)(\boldsymbol{R},T,\boldsymbol{p},\mathcal{E}) \approx \left[1 + \frac{i}{2}\left(\partial_T^B \partial_{\mathcal{E}}^A - \partial_T^A \partial_{\mathcal{E}}^B + \nabla_{\boldsymbol{R}}^A \nabla_{\boldsymbol{p}}^B - \nabla_{\boldsymbol{R}}^B \nabla_{\boldsymbol{p}}^A\right)\right]\, A(\boldsymbol{R},T,\boldsymbol{p},\mathcal{E})\, B(\boldsymbol{R},T,\boldsymbol{p},\mathcal{E}). \tag{B.14}$$

In the Gor'kov equation (4.43), for instance, we have used the bullet commutator defined as $[A,B]^\bullet = A \bullet B - B \bullet A$. We can use the first-order approximation to write it as

$$[A,B]^\bullet \approx [A,B] + \frac{i}{2}\big(\{\partial_{\mathcal{E}} A, \partial_T B\} - \{\partial_T A, \partial_{\mathcal{E}} B\} + \{\nabla_{\boldsymbol{R}} A, \nabla_{\boldsymbol{p}} B\} - \{\nabla_{\boldsymbol{p}} A, \nabla_{\boldsymbol{R}} B\}\big), \tag{B.15}$$

where the ordinary anti-commutator was inserted.

# Appendix C

# Continuum Hamiltonian discretization

There are several ways to discretize a continuum Hamiltonian. We have chosen to use localized Wannier orbitals in chapter 5. These are in principle known, and the hopping amplitudes can be calculated directly from the integrals in eqs. (5.5) and (5.6). We will show how to obtain the nearest neighbor vector and spin-orbit hopping amplitudes by a crude approximation equivalent to a finite difference scheme, which is a common discretization technique.

## C.1 Nearest neighbor vector

We will begin from eq. (5.6) and insert the definition of the derivative. We can write

$$\begin{aligned}\alpha_{ij}^{\sigma\sigma'} &= i\alpha\,(\boldsymbol{n}\times\boldsymbol{\sigma})^{\sigma\sigma'}\cdot\int d\boldsymbol{r}\; w^*(\boldsymbol{r}-\boldsymbol{R}_i)\nabla w(\boldsymbol{r}-\boldsymbol{R}_j)\\ &= \lim_{d\to 0} i\alpha\,(\boldsymbol{n}\times\boldsymbol{\sigma})^{\sigma\sigma'}\cdot\int d\boldsymbol{r}\; w^*(\boldsymbol{r}-\boldsymbol{R}_i)\,\frac{\hat{\boldsymbol{d}}}{2d}\left[w(\boldsymbol{r}-\boldsymbol{R}_j-\boldsymbol{d})-w(\boldsymbol{r}-\boldsymbol{R}_j+\boldsymbol{d})\right],\end{aligned} \tag{C.1}$$

where $d$ is the distance between nearest neighbors. However, we cannot let $d\to 0$, so we approximate the derivative. This is equivalent to the central difference scheme. We can therefore write

$$\begin{aligned}\alpha_{ij}^{\sigma\sigma'} &= \frac{i\alpha}{2d}\,(\boldsymbol{n}\times\boldsymbol{\sigma})^{\sigma\sigma'}\cdot\hat{\boldsymbol{d}}\int d\boldsymbol{r}\; w^*(\boldsymbol{r}-\boldsymbol{R}_i)\left[w(\boldsymbol{r}-\boldsymbol{R}_j-\boldsymbol{d})-w(\boldsymbol{r}-\boldsymbol{R}_j+\boldsymbol{d})\right]\\ &= \frac{i\alpha}{2d}\,(\boldsymbol{n}\times\boldsymbol{\sigma})^{\sigma\sigma'}\cdot\hat{\boldsymbol{d}}\Big[\delta(\boldsymbol{R}_i-\boldsymbol{R}_j-\boldsymbol{d})-\delta(\boldsymbol{R}_i-\boldsymbol{R}_j+\boldsymbol{d})\Big]\\ &= \frac{i\alpha}{2d}\,(\boldsymbol{n}\times\boldsymbol{\sigma})^{\sigma\sigma'}\cdot\boldsymbol{d}_{ij}\,.\end{aligned} \tag{C.2}$$

Under an interchange of hopping direction, the nearest neighbor vector changes sign, $\boldsymbol{d}_{ij}=-\boldsymbol{d}_{ji}$. The relations in eq. (5.8) can be derived easily

$$\left(\alpha_{ji}^{\sigma'\sigma}\right)^* = \frac{-i\alpha}{2d}(\boldsymbol{n}\times\boldsymbol{\sigma})^{\sigma\sigma'}\cdot(-\boldsymbol{d}_{ij}) = \alpha_{ij}^{\sigma\sigma'}\,, \tag{C.3}$$

where we used that $(\boldsymbol{n}\times\boldsymbol{\sigma}^*)^{\sigma'\sigma}=(\boldsymbol{n}\times\boldsymbol{\sigma})^{\sigma\sigma'}$. In the next section, we see what happens if the Pauli matrices are position-dependent as well. The spin-orbit term maps to the lattice are somewhat different, but the relations in eq. (5.8) are still valid.

## C.2 Discrete 1D strain-induced spin-orbit Hamiltonian

In this section, we consider the spin-orbit field in eq. (3.44). Since the curvilinear Pauli-matrices have a position dependence, we have to write the intrinsic contribution to the continuum Hamiltonian as

$$\mathcal{H}_{rsoc} = \sum_{\sigma\sigma'} \int d\boldsymbol{r}\, \psi^\dagger_\sigma(\boldsymbol{r})\, \frac{i\alpha_B}{2}\, \hat{\mathcal{T}}(\boldsymbol{r}) \cdot \big[\sigma_N(\boldsymbol{r})\nabla + \nabla\sigma_N(\boldsymbol{r})\big]\psi_{\sigma'}(\boldsymbol{r}), \tag{C.4}$$

where the second term in the brackets assures the Hamiltonian is Hermitian. If we again use the Wannier orbitals, partial integration, and assume the surface term vanishes, we get

$$\begin{aligned}
\mathcal{H}_{rsoc} &= \sum_{\sigma\sigma'}\sum_{ij} c^\dagger_{i\sigma}c_{j\sigma}\, \frac{i\alpha_B}{2}\, \hat{\mathcal{T}} \cdot \Big[\int d\boldsymbol{r}\, \sigma_N(\boldsymbol{r}) w^*(\boldsymbol{r}-\boldsymbol{R}_i)\nabla w(\boldsymbol{r}-\boldsymbol{R}_j) \\
&\qquad\qquad - \int d\boldsymbol{r}\, \sigma_N(\boldsymbol{r})\nabla w^*(\boldsymbol{r}-\boldsymbol{R}_i)\, w(\boldsymbol{r}-\boldsymbol{R}_j)\Big] \\
&= \sum_{\sigma\sigma'}\sum_{ij} c^\dagger_{i\sigma}c_{j\sigma}\, \frac{i\alpha_B}{4d}\, \hat{\mathcal{T}} \cdot \hat{\boldsymbol{d}}\Big[\int d\boldsymbol{r}\, \sigma_N(\boldsymbol{r}) w^*(\boldsymbol{r}-\boldsymbol{R}_i)\big[w(\boldsymbol{r}-\boldsymbol{R}_j-\boldsymbol{d}) - w(\boldsymbol{r}-\boldsymbol{R}_j+\boldsymbol{d})\big] \\
&\qquad\qquad - \int d\boldsymbol{r}\, \sigma_N(\boldsymbol{r})\big[w^*(\boldsymbol{r}-\boldsymbol{R}_i+\boldsymbol{d}) - w^*(\boldsymbol{r}-\boldsymbol{R}_i-\boldsymbol{d})\big]\, w(\boldsymbol{r}-\boldsymbol{R}_j)\Big] \\
&= \sum_{\sigma\sigma'}\sum_{\langle ij\rangle} c^\dagger_{i\sigma}c_{j\sigma}\, \frac{i\alpha_B}{4d}\, \big[\sigma_N(\boldsymbol{R}_i) + \sigma_N(\boldsymbol{R}_j)\big]\hat{\mathcal{T}} \cdot \boldsymbol{d}_{ij}\,.
\end{aligned} \tag{C.5}$$

This is consistent with the discretized expression in [42]. We could also write $\hat{\mathcal{T}} \cdot \boldsymbol{d}_{ij} = d^T_{ij}$. Next, we consider the strain-induced contribution. We don't assume a torsion-free wire, therefore the Hamiltonian becomes

$$\begin{aligned}
\mathcal{H}_\kappa &= -\sum_{\sigma\sigma'} \int d\boldsymbol{r}\, \psi^\dagger_\sigma(\boldsymbol{r})\, \frac{i\alpha_N}{2}\, \hat{\mathcal{T}}(\boldsymbol{r}) \cdot \big[\sigma_B(\boldsymbol{r})\nabla + \nabla\sigma_B(\boldsymbol{r})\big]\psi_{\sigma'}(\boldsymbol{r}) \\
&= -\sum_{\sigma\sigma'}\sum_{\langle ij\rangle} c^\dagger_{i\sigma}c_{j\sigma}\, \frac{i\alpha_N}{4d}\, \big[\sigma_B(\boldsymbol{R}_i) + \sigma_B(\boldsymbol{R}_j)\big] d^T_{ij}\,,
\end{aligned} \tag{C.6}$$

where the derivation is the same as above. In the analysis in the main text, we don't consider a wire with torsion and variable curvature; we only consider variable curvature or a helix. Note that the above expressions assume a one-dimensional wire, as in the main text. However, if we were to consider the thickness of the material as in fig. 3.2, the nearest neighbor vector would have a dependence on the normal coordinate $n$ to account for the variable strain. For a circular geometry, we have

$$\mathcal{H}_\kappa = -\sum_{\sigma\sigma'}\sum_{\langle ij\rangle} c^\dagger_{i\sigma}c_{j\sigma}\, \frac{i\alpha_N}{2d}\, \sigma_B\, d^T_{ij}\,. \tag{C.7}$$

## C.3 Discrete 2D strain-induced spin-orbit Hamiltonian

If we consider the 2D Hamiltonian with strain-induced spin-orbit coupling as in eq. (3.48), the relevant part becomes

$$\begin{aligned}
\mathcal{H}_{soc} &= \sum_{\sigma\sigma'} \int d\boldsymbol{r}\, \psi^\dagger_\sigma(\boldsymbol{r}) \left[ i\alpha_N \sigma_B(\boldsymbol{r})\, \hat{\mathcal{T}}(\boldsymbol{r}) \cdot \nabla - i\alpha_N \sigma_T(\boldsymbol{r})\, \hat{\mathcal{B}}(\boldsymbol{r}) \cdot \nabla \right]^{\sigma\sigma'} \psi_{\sigma'}(\boldsymbol{r}) \\
&= \sum_{\sigma\sigma' ij} c^\dagger_{i\sigma} c_{j\sigma'}\, i\alpha_N \int d\boldsymbol{r}\, w^*(\boldsymbol{r} - \boldsymbol{R}_i) \left[ \sigma_B(\boldsymbol{r}) \hat{\mathcal{T}}(\boldsymbol{r}) - \sigma_T(\boldsymbol{r}) \hat{\mathcal{B}}(\boldsymbol{r}) \right]^{\sigma\sigma'} \cdot \nabla w(\boldsymbol{r} - \boldsymbol{R}_j) \\
&= \sum_{\sigma\sigma'\langle ij\rangle} c^\dagger_{i\sigma} c_{j\sigma'}\, i\alpha_N \left[ \sigma_B\, d^T_{ij} - \sigma_{i,T}\, d^B_{ij} \right]^{\sigma\sigma'} \\
&= \sum_{\sigma\sigma'\langle ij\rangle_s} c^\dagger_{i\sigma} c_{j\sigma'}\, i\alpha_N\, \sigma_B^{\sigma\sigma'}\, d^T_{ij} - \sum_{\sigma\sigma'\langle ij\rangle_b} c^\dagger_{i\sigma} c_{j\sigma'}\, i\alpha_N\, \sigma^{\sigma\sigma'}_{i,T}\, d^B_{ij} \\
&= \sum_{\sigma\sigma'\langle ij\rangle_s} c^\dagger_{i\sigma} c_{j\sigma'}\, \alpha^{\sigma\sigma'}_{ij} + \sum_{\sigma\sigma'\langle ij\rangle_b} c^\dagger_{i\sigma} c_{j\sigma'}\, a^{\sigma\sigma'}_{ii}\, d^B_{ij}\,.
\end{aligned} \tag{C.8}$$

In the above, we used that $\sigma_T$ and $\sigma_B$ is constant in the binormal direction. Thus, in the second term, the curvilinear Pauli matrix only depends on the tangential coordinate: $\sigma_{i,T}$. In the main text, we only investigate 2D systems where this is true. Applying periodic boundary conditions and taking the mean in the binormal direction of the first term, we get

$$\begin{aligned}
\sum_{\sigma\sigma'\langle ij\rangle_s} c^\dagger_{i\sigma} c_{j\sigma'}\, \alpha^{\sigma\sigma'}_{ij} &= \frac{1}{N_b} \sum_{\langle i_s j_s\rangle i_b} \sum_{\sigma\sigma'} \sum_{k_b, k'_b} \alpha^{\sigma\sigma'}_{i_s,j_s} c^\dagger_{i_s,k_b,\sigma} c_{j_s,k'_b,\sigma'} e^{i(k'_b - k_b) i_b} \\
&= \sum_{\langle i_s j_s\rangle} \sum_{\sigma\sigma'} \sum_{k_b} \alpha^{\sigma\sigma'}_{i_s,j_s} c^\dagger_{i_s,k_b,\sigma} c_{j_s,k_b,\sigma'}\,.
\end{aligned} \tag{C.9}$$

Taking the mean in the binormal direction of the hopping in the same direction gives

$$\begin{aligned}
\sum_{\sigma\sigma'\langle ij\rangle_b} c^\dagger_{i\sigma} c_{j\sigma'}\, a^{\sigma\sigma'}_{ii}\, d^B_{ij} &= \frac{1}{N_b} \sum_{i_s, i_b} \sum_{k_b, k'_b} \sum_{\pm} \pm e^{\pm i k_b}\, a^{\sigma\sigma'}_{i_s} e^{i(k'_b - k_b) i_b}\, c^\dagger_{i_s,k_b,\sigma} c_{i_s,k'_b,\sigma'} \\
&= \sum_{i_s,k_b} \sum_{\sigma\sigma'} 2i \sin k_b\, a^{\sigma\sigma'}_{i_s}\, c^\dagger_{i_s,k_b,\sigma} c_{i_s,k_b,\sigma'} \\
&= \sum_{i_s,k_b} \sum_{\sigma\sigma'} \epsilon^{\sigma\sigma'}_{i_s,k_b}\, c^\dagger_{i_s,k_b,\sigma} c_{i_s,k_b,\sigma'}\,.
\end{aligned} \tag{C.10}$$

To express the above terms in Nambu⊗spin space, we find relations similar to eq. (5.8). We can write down the following relations for the spin-orbit hopping amplitudes:

$$\alpha^{\sigma\sigma'}_{i_s,j_s} = i\alpha_N \sigma_B^{\sigma\sigma'} d^T_{i_s,j_s} = \left( \alpha^{\sigma'\sigma}_{j_s,i_s} \right)^*\,, \tag{C.11}$$

$$\epsilon^{\sigma\sigma'}_{i_s,k_b} = 2 \sin k_b\, \alpha_N \sigma^{\sigma\sigma'}_{i_s,T} = -\left( \epsilon^{\sigma'\sigma}_{i_s,-k_b} \right)^*\,. \tag{C.12}$$

The spin-orbit part of the Hamiltonian is therefore

$$\begin{aligned}
\mathcal{H}_{soc} = &\sum_{\langle i_s j_s\rangle} \sum_{\sigma\sigma'} \sum_{k_b} \left[ \alpha^{\sigma\sigma'}_{i_s,j_s} c^\dagger_{i_s,k_b,\sigma} c_{j_s,k_b,\sigma'} - \left( \alpha^{\sigma\sigma'}_{i_s,j_s} \right)^*\, c_{i_s,-k_b,\sigma} c^\dagger_{j_s,-k_b,\sigma'} \right] \\
&+ \sum_{i_s,k_b} \sum_{\sigma\sigma'} \left[ \epsilon^{\sigma\sigma'}_{i_s,k_b}\, c^\dagger_{i_s,k_b,\sigma} c_{i_s,k_b,\sigma'} + \left( \epsilon^{\sigma\sigma'}_{i_s,k_b} \right)^*\, c_{i_s,-k_b,\sigma} c^\dagger_{i_s,-k_b,\sigma'} \right].
\end{aligned} \tag{C.13}$$

# Appendix D

# Derivation expectation values on a lattice

## D.1 Superconducting gap

For the gap, we find the singlet pairing $\uparrow\downarrow - \downarrow\uparrow$ at each point on the lattice. Because of the periodic boundary conditions in the $y$-direction, we take the mean in that direction. We can write this as

$$\begin{aligned}
\Delta_{i_x} &= \frac{1}{N_y}\sum_{i_y}\frac{U_i}{2}\left[\langle c_{i,\uparrow}c_{i,\downarrow}\rangle - \langle c_{i,\downarrow}c_{i,\uparrow}\rangle\right] \\
&= \frac{U_{i_x}}{2N_y}\sum_{k_y,k_y'}\frac{1}{N_y}\sum_{i_y} e^{i(k_y+k_y')i_y}\left[\langle c_{i_x,k_y,\uparrow}c_{i_x,k_y',\downarrow}\rangle - c_{i_x,k_y,\downarrow}c_{i_x,k_y',\uparrow}\right] \\
&= \frac{U_{i_x}}{2N_y}\sum_{k_y}\left[\langle c_{i_x,k_y,\uparrow}c_{i_x,-k_y,\downarrow}\rangle - \langle c_{i_x,-k_y,\downarrow}c_{i_x,k_y,\uparrow}\rangle\right] \\
&= \frac{U_{i_x}}{2N_y}\sum_{k_y}\sum_{n,m}\left[u_{i_x,n,k_y}x^*_{i_x,m,k_y}\langle\gamma_{n,k_y}\gamma^\dagger_{m,k_y}\rangle - x^*_{i_x,n,k_y}u_{i_x,m,k_y}\langle\gamma^\dagger_{n,k_y}\gamma_{m,k_y}\rangle\right]. \qquad \text{(D.1)}
\end{aligned}$$

Next, we split the $k_y$ sum into the positive, negative, and $k_y = 0$ contribution not to keep linearly dependent quasiparticle operators. We find that

$$\begin{aligned}
\Delta_{i_x} = \frac{U_{i_x}}{2N_y}\sum_{n,m}\Bigg\{ &\sum_{k_y>0}\left[u_{i_x,n,k_y}x^*_{i_x,m,k_y}\langle\gamma_{n,k_y}\gamma^\dagger_{m,k_y}\rangle - x^*_{i_x,n,k_y}u_{i_x,m,k_y}\langle\gamma^\dagger_{n,k_y}\gamma_{m,k_y}\rangle\right] \\
&+ \sum_{k_y<0}\left[u_{i_x,n,k_y}x^*_{i_x,m,k_y}\langle\gamma_{n,k_y}\gamma^\dagger_{m,k_y}\rangle - x^*_{i_x,n,k_y}u_{i_x,m,k_y}\langle\gamma^\dagger_{n,k_y}\gamma_{m,k_y}\rangle\right] \\
&+ \sum_{k_y=0}\left[u_{i_x,n,0}x^*_{i_x,m,0}\langle\gamma_{n,0}\gamma^\dagger_{m,0}\rangle - x^*_{i_x,n,0}u_{i_x,m,0}\langle\gamma^\dagger_{n,0}\gamma_{m,0}\rangle\right]\Bigg\} \\
= \frac{U_{i_x}}{2N_y}\Bigg\{ &\sum_{n,m,k_y>0}\left[u_{i_x,n,k_y}x^*_{i_x,m,k_y}\langle\gamma_{n,k_y}\gamma^\dagger_{m,k_y}\rangle - x^*_{i_x,n,k_y}u_{i_x,m,k_y}\langle\gamma^\dagger_{n,k_y}\gamma_{m,k_y}\rangle\right] \\
&+ \sum_{n,m,k_y>0}\left[u_{i_x,n,-k_y}x^*_{i_x,m,-k_y}\langle\gamma_{n,-k_y}\gamma^\dagger_{m,-k_y}\rangle - x^*_{i_x,n,-k_y}u_{i_x,m,-k_y}\langle\gamma^\dagger_{n,-k_y}\gamma_{m,-k_y}\rangle\right] \\
&+ \sum_{n,m=1}^{2N}\left[u_{i_x,n,0}x^*_{i_x,m,0}\langle\gamma_{n,0}\gamma^\dagger_{m,0}\rangle - x^*_{i_x,n,0}u_{i_x,m,0}\langle\gamma^\dagger_{n,0}\gamma_{m,0}\rangle\right]
\end{aligned}$$

$$
\begin{aligned}
&+\sum_{n,m=2N+1}^{4N}\Big[u_{i_x,n,0}x^*_{i_x,m,0}\langle\gamma_{n,0}\gamma^\dagger_{m,0}\rangle - x^*_{i_x,n,0}u_{i_x,m,0}\langle\gamma^\dagger_{n,0}\gamma_{m,0}\rangle\Big]\Big\}\\
&=\frac{U_{i_x}}{2N_y}\Bigg\{\sum_{n,m,k_y>0}\Big[u_{i_x,n,k_y}x^*_{i_x,m,k_y}\langle\gamma_{n,k_y}\gamma^\dagger_{m,k_y}\rangle - x^*_{i_x,n,k_y}u_{i_x,m,k_y}\langle\gamma^\dagger_{n,k_y}\gamma_{m,k_y}\rangle\Big]\\
&\quad+\sum_{n,m,k_y>0}\Big[w^*_{i_x,n,k_y}v_{i_x,m,k_y}\langle\gamma^\dagger_{n,k_y}\gamma_{m,k_y}\rangle - v_{i_x,n,k_y}w^*_{i_x,m,k_y}\langle\gamma_{n,k_y}\gamma^\dagger_{m,k_y}\rangle\Big]\\
&\quad+\sum_{n,m=1}^{2N}\Big[u_{i_x,n,0}x^*_{i_x,m,0}\langle\gamma_{n,0}\gamma^\dagger_{m,0}\rangle - x^*_{i_x,n,0}u_{i_x,m,0}\langle\gamma^\dagger_{n,0}\gamma_{m,0}\rangle\Big]\\
&\quad+\sum_{n,m=1}^{2N}\Big[w^*_{i_x,n,0}v_{i_x,m,0}\langle\gamma^\dagger_{n,0}\gamma_{m,0}\rangle - v_{i_x,n,0}w^*_{i_x,m,0}\langle\gamma_{n,0}\gamma^\dagger_{m,0}\rangle\Big]\Bigg\}\\
&=\frac{U_{i_x}}{2N_y}\Bigg\{\sum_{n,k_y>0}\Big[u_{i_x,n,k_y}x^*_{i_x,n,k_y}f(-2\mathcal{E}_{n,k_y}) - x^*_{i_x,n,k_y}u_{i_x,n,k_y}f(2\mathcal{E}_{n,k_y})\Big]\\
&\quad+\sum_{n,k_y>0}\Big[w^*_{i_x,n,k_y}v_{i_x,n,k_y}f(2\mathcal{E}_{n,k_y}) - v_{i_x,n,k_y}w^*_{i_x,n,k_y}f(-2\mathcal{E}_{n,k_y})\Big]\\
&\quad+\sum_{\mathcal{E}_n\geq 0}\big[u_{i_x,n,0}x^*_{i_x,n,0}f(-2\mathcal{E}_{n,0}) - x^*_{i_x,n,0}u_{i_x,m,0}f(2\mathcal{E}_{n,0})\big]\\
&\quad+\sum_{\mathcal{E}_n\geq 0}\big[w^*_{i_x,n,0}v_{i_x,m,0}f(2\mathcal{E}_{n,0}) - v_{i_x,n,0}w^*_{i_x,m,0}f(-2\mathcal{E}_{n,0})\big]\Bigg\}\\
&=\frac{U_{i_x}}{2N_y}\Bigg\{\sum_{n,k_y>0}\Big[u_{i_x,n,k_y}x^*_{i_x,n,k_y} - v_{i_x,n,k_y}w^*_{i_x,n,k_y}\Big]\tanh\left(\beta\mathcal{E}_{n,k_y}\right)\\
&\quad+\sum_{\mathcal{E}_n\geq 0}\big[u_{i_x,n,0}x^*_{i_x,n,0} - w^*_{i_x,n,0}v_{i_x,m,0}\big]\tanh\left(\beta\mathcal{E}_{n,0}\right)\Bigg\},
\end{aligned}
\tag{D.2}
$$

where we have used that $\langle\gamma^\dagger_{n,k_y}\gamma_{m,k_y}\rangle = f(2\mathcal{E}_{n,k_y})\delta_{n,m}$. We have also inserted the relation $f(-2\mathcal{E}) - f(2\mathcal{E}) = \tanh(\beta\mathcal{E})$. Note that the sum ends up having the same form as the one we defined in eq. (5.58).

## D.2 Singlet and triplet amplitudes

We begin with the s-wave pairing. It is calculated the same way as the gap, not including the pairing potential $U_{i_x}$. Therefore, we can write down the expression without any explicit calculation.

$$
\begin{aligned}
\mathcal{S}_{i_x,0} = \frac{1}{2N_y}\Bigg\{&\sum_{n,k_y>0}\Big[u_{i_x,n,k_y}x^*_{i_x,n,k_y} - v_{i_x,n,k_y}w^*_{i_x,n,k_y}\Big]\tanh\left(\beta\mathcal{E}_{n,k_y}\right)\\
&+\sum_{\mathcal{E}_n\geq 0}\big[u_{i_x,n,0}x^*_{i_x,n,0} - w^*_{i_x,n,0}v_{i_x,m,0}\big]\tanh\left(\beta\mathcal{E}_{n,0}\right)\Bigg\}.
\end{aligned}
\tag{D.3}
$$

Next, we derive the p-wave triplets. We have six different p-wave amplitudes, the threefold degeneracy of the spin in both the $x$- and $y$-direction. We begin with the zero-projection

px-wave amplitude, which is

$$
\begin{aligned}
\mathcal{P}^{x}_{i_x,0} &= \frac{1}{N_y}\sum_{i_y}\sum_{\pm}\pm\frac{1}{2}\left[\langle c_{i,\uparrow}c_{i\pm\hat{x},\downarrow}\rangle + \langle c_{i,\downarrow}c_{i\pm\hat{x},\uparrow}\rangle\right] \\
&= \frac{1}{2N_y}\sum_{k_y,k_y'}\sum_{\pm}\sum_{i_y}\pm\frac{1}{N_y}e^{i(k_y+k_y')i_y}\left[\langle c_{i_x,k_y,\uparrow}c_{i_x\pm1,k_y',\downarrow}\rangle + \langle c_{i_x,k_y,\downarrow}c_{i_x\pm1,k_y',\uparrow}\rangle\right] \\
&= \frac{1}{2N_y}\sum_{n,m,k_y}\sum_{\pm}\pm\left[u_{i_x,n,k_y}x^{*}_{i_x\pm1,m,k_y}\langle\gamma_{n,k_y}\gamma^{\dagger}_{m,k_y}\rangle + x^{*}_{i_x,n,k_y}u_{i_x\pm1,m,k_y}\langle\gamma^{\dagger}_{n,k_y}\gamma_{m,k_y}\rangle\right] \\
&= \frac{1}{2N_y}\sum_{\pm}\pm\Bigg\{\sum_{n,m}\sum_{k_y>0}\left[u_{i_x,n,k_y}x^{*}_{i_x\pm1,m,k_y}\langle\gamma_{n,k_y}\gamma^{\dagger}_{m,k_y}\rangle + x^{*}_{i_x,n,k_y}u_{i_x\pm1,m,k_y}\langle\gamma^{\dagger}_{n,k_y}\gamma_{m,k_y}\rangle\right] \\
&\qquad + \sum_{n,m}\sum_{k_y>0}\left[w^{*}_{i_x,n,k_y}v_{i_x\pm1,m,k_y}\langle\gamma^{\dagger}_{n,k_y}\gamma_{m,k_y}\rangle + v_{i_x,n,k_y}w^{*}_{i_x\pm1,m,k_y}\langle\gamma_{n,k_y}\gamma^{\dagger}_{m,k_y}\rangle\right] \\
&\qquad + \sum_{n,m=1}^{2N_x}\left[u_{i_x,n,0}x^{*}_{i_x\pm1,m,0}\langle\gamma_{n,0}\gamma^{\dagger}_{m,0}\rangle + x^{*}_{i_x,n,0}u_{i_x\pm1,m,0}\langle\gamma^{\dagger}_{n,0}\gamma_{m,0}\rangle\right] \\
&\qquad + \sum_{n,m=1}^{2N_x}\left[w^{*}_{i_x,n,0}v_{i_x\pm1,m,0}\langle\gamma^{\dagger}_{n,0}\gamma_{m,0}\rangle + v_{i_x,n,0}w^{*}_{i_x\pm1,m,0}\langle\gamma_{n,0}\gamma^{\dagger}_{m,0}\rangle\right]\Bigg\} \\
&= \frac{1}{2N_y}{\sum_{n,k_y}}'\sum_{\pm}\pm\Big[\left(x^{*}_{i_x\pm1,n,k_y}u_{i_x,n,k_y} + w^{*}_{i_x\pm1,n,k_y}v_{i_x,n,k_y}\right)f(-2\mathcal{E}_{n,k_y}) \\
&\qquad\qquad + \left(x^{*}_{i_x,n,k_y}u_{i_x\pm1,n,k_y} + w^{*}_{i_x,n,k_y}v_{i_x\pm1,n,k_y}\right)f(2\mathcal{E}_{n,k_y})\Big]\,. \qquad \text{(D.4)}
\end{aligned}
$$

As stated in the main text, the $\pm$ in the expression above was added since the lobes of the p-wave orbital have opposite signs. Thus, without it, they cancel, and we are left with zero. For the remaining amplitudes, we add the $\pm$ as well. The spin-polarized px-wave amplitudes are

$$
\begin{aligned}
\mathcal{P}^{x}_{i_x,\uparrow} &= \frac{1}{N_y}\sum_{i_y}\sum_{\pm}\pm\langle c_{i,\uparrow}c_{i\pm\hat{x},\uparrow}\rangle \\
&= \frac{1}{N_y}\sum_{k_y,k_y'}\sum_{\pm}\sum_{i_y}\pm\frac{1}{N_y}e^{i(k_y+k_y')i_y}\langle c_{i_x,k_y,\uparrow}c_{i_x\pm1,k_y',\uparrow}\rangle \\
&= \frac{1}{N_y}\sum_{n,m,k_y}\sum_{\pm}\pm w^{*}_{i_x,n,k_y}u_{i_x\pm1,m,k_y}\langle\gamma^{\dagger}_{n,k_y}\gamma_{m,k_y}\rangle \\
&= \frac{1}{N_y}\sum_{\pm}\pm\Bigg\{\sum_{n,m}\sum_{k_y>0}\left[w^{*}_{i_x,n,k_y}u_{i_x\pm1,m,k_y}\langle\gamma^{\dagger}_{n,k_y}\gamma_{m,k_y}\rangle + u_{i_x,n,k_y}w^{*}_{i_x\pm1,m,k_y}\langle\gamma_{n,k_y}\gamma^{\dagger}_{m,k_y}\rangle\right] \\
&\qquad + \sum_{n,m=1}^{2N_x}\left[w^{*}_{i_x,n,0}u_{i_x\pm1,m,0}\langle\gamma^{\dagger}_{n,0}\gamma_{m,0}\rangle + u_{i_x,n,0}w^{*}_{i_x\pm1,m,0}\langle\gamma_{n,0}\gamma^{\dagger}_{m,0}\rangle\right]\Bigg\} \\
&= \frac{1}{2N_y}{\sum_{n,k_y}}'\sum_{\pm}\pm\left[w^{*}_{i_x,n,k_y}u_{i_x\pm1,n,k_y}f(2\mathcal{E}_{n,k_y}) + w^{*}_{i_x\pm1,n,k_y}u_{i_x,n,k_y}f(-2\mathcal{E}_{n,k_y})\right], \qquad \text{(D.5)}
\end{aligned}
$$

$$
\begin{aligned}
\mathcal{P}^{x}_{i_x,\downarrow} &= \frac{1}{N_y}\sum_{i_y}\sum_{\pm}\pm\langle c_{i,\downarrow}c_{i\pm\hat{x},\downarrow}\rangle \\
&= \frac{1}{N_y}\sum_{k_y,k_y'}\sum_{\pm}\sum_{i_y}\pm\frac{1}{N_y}e^{i(k_y+k_y')i_y}\langle c_{i_x,k_y,\downarrow}c_{i_x\pm1,k_y',\downarrow}\rangle \\
&= \frac{1}{N_y}\sum_{n,m,k_y}\sum_{\pm}\pm x^{*}_{i_x,n,k_y}v_{i_x\pm1,m,k_y}\langle\gamma^{\dagger}_{n,k_y}\gamma_{m,k_y}\rangle \\
&= \frac{1}{N_y}\sum_{\pm}\pm\Bigg\{\sum_{n,m}\sum_{k_y>0}\Big[x^{*}_{i_x,n,k_y}v_{i_x\pm1,m,k_y}\langle\gamma^{\dagger}_{n,k_y}\gamma_{m,k_y}\rangle + v_{i_x,n,k_y}x^{*}_{i_x\pm1,m,k_y}\langle\gamma_{n,k_y}\gamma^{\dagger}_{m,k_y}\rangle\Big] \\
&\qquad + \sum_{n,m=1}^{2N_x}\Big[x^{*}_{i_x,n,0}v_{i_x\pm1,m,0}\langle\gamma^{\dagger}_{n,0}\gamma_{m,0}\rangle + v_{i_x,n,0}x^{*}_{i_x\pm1,m,0}\langle\gamma_{n,0}\gamma^{\dagger}_{m,0}\rangle\Big]\Bigg\} \\
&= \frac{1}{2N_y}{\sum_{n,k_y}}'\sum_{\pm}\pm\Big[x^{*}_{i_x,n,k_y}v_{i_x\pm1,n,k_y}f(2\mathcal{E}_{n,k_y}) + x^{*}_{i_x\pm1,n,k_y}v_{i_x,n,k_y}f(-2\mathcal{E}_{n,k_y})\Big]\,. \qquad \text{(D.6)}
\end{aligned}
$$

The py-wave amplitudes are found the same way. However, due to the periodic boundary conditions, they only have onsite contributions. We begin with the zero spin-projection amplitude, which is

$$
\begin{aligned}
\mathcal{P}^{y}_{i_x,0} &= \frac{1}{2N_y}\sum_{i_y}\sum_{\pm}\pm\left[\langle c_{i,\uparrow}c_{i\pm\hat{y},\downarrow}\rangle + \langle c_{i,\downarrow}c_{i\pm\hat{y},\uparrow}\rangle\right] \\
&= \frac{1}{2N_y}\sum_{k_y,k_y'}\sum_{\pm}\sum_{i_y}\pm\frac{1}{N_y}e^{ik_yi_y+ik_y'(i_y\pm1)}\Big[\langle c_{i_x,k_y,\uparrow}c_{i_x,k_y',\downarrow}\rangle + \langle c_{i_x,k_y,\downarrow}c_{i_x,k_y',\uparrow}\rangle\Big] \\
&= \frac{1}{2N_y}\sum_{k_y}\sum_{\pm}\pm\Big[\langle c_{i_x,k_y,\uparrow}c_{i_x,-k_y,\downarrow}\rangle e^{\mp ik_y} + \langle c_{i_x,-k_y,\downarrow}c_{i_x,k_y,\uparrow}\rangle e^{\pm ik_y}\Big] \\
&= \frac{1}{2N_y}\sum_{n,m,k_y}\sum_{\pm}\pm\Big[e^{\mp ik_y}u_{i_x,n,k_y}x^{*}_{i_x,m,k_y}\langle\gamma_n\gamma^{\dagger}_m\rangle + e^{\pm ik_y}x^{*}_{i_x,n,k_y}u_{i_x,m,k_y}\langle\gamma^{\dagger}_n\gamma_m\rangle\Big] \\
&= \frac{1}{2N_y}\sum_{\pm}\pm\Bigg\{\sum_{n,m}\sum_{k_y>0}\Big[e^{\mp ik_y}u_{i_x,n,k_y}x^{*}_{i_x,m,k_y}\langle\gamma_{n,k_y}\gamma^{\dagger}_{m,k_y}\rangle + e^{\pm ik_y}x^{*}_{i_x,n,k_y}u_{i_x,m,k_y}\langle\gamma^{\dagger}_{n,k_y}\gamma_{m,k_y}\rangle\Big] \\
&\qquad + \sum_{n,m}\sum_{k_y>0}\Big[e^{\pm ik_y}w^{*}_{i_x,n,k_y}v_{i_x,m,k_y}\langle\gamma^{\dagger}_{n,k_y}\gamma_{m,k_y}\rangle + e^{\mp ik_y}v_{i_x,n,k_y}w^{*}_{i_x,m,k_y}\langle\gamma_{n,k_y}\gamma^{\dagger}_{m,k_y}\rangle\Big] \\
&\qquad + \sum_{n,m=1}^{2N_x}\Big[u_{i_x,n,0}x^{*}_{i_x,m,0}\langle\gamma_{n,0}\gamma^{\dagger}_{m,0}\rangle + x^{*}_{i_x,n,0}u_{i_x,m,0}\langle\gamma^{\dagger}_{n,0}\gamma_{m,0}\rangle\Big] \\
&\qquad + \sum_{n,m=1}^{2N_x}\Big[w^{*}_{i_x,n,0}v_{i_x,m,0}\langle\gamma^{\dagger}_{n,0}\gamma_{m,0}\rangle + v_{i_x,n,0}w^{*}_{i_x,m,0}\langle\gamma_{n,0}\gamma^{\dagger}_{m,0}\rangle\Big]\Bigg\} \\
&= \frac{-i}{N_y}{\sum_{n,k_y}}'\sin(k_y)\Big[x^{*}_{i_x,n,k_y}u_{i_x,n,k_y} + w^{*}_{i_x,n,k_y}v_{i_x,n,k_y}\Big]\tanh\big(\beta\mathcal{E}_{n,k_y}\big)\,. \qquad \text{(D.7)}
\end{aligned}
$$

Here we have used that $e^{ix}-e^{-ix}=2i\sin x$. Note also that we have written the sum with $\sum'_{n,k_y}$ since the $\sin(k_y)$ kills the $k_y=0$ sum which vanishes because of the $\pm$ sum. The same happens for the spin-polarized amplitudes,

$$
\begin{aligned}
\mathcal{P}^{y}_{i_x,\uparrow} &= \frac{1}{N_y}\sum_{i_y}\sum_{\pm} \pm\langle c_{i,\uparrow}c_{i\pm\hat{y},\uparrow}\rangle \\
&= \frac{1}{N_y}\sum_{k_y,k_y'}\sum_{\pm}\sum_{i_y} \pm\frac{1}{N_y}e^{ik_y i_y + ik_y'(i_y\pm 1)}\langle c_{i_x,k_y,\uparrow}c_{i_x,k_y',\uparrow}\rangle \\
&= \frac{1}{N_y}\sum_{k_y}\sum_{\pm} \pm e^{\pm ik_y}\langle c_{i_x,-k_y,\uparrow}c_{i_x,k_y,\uparrow}\rangle \\
&= \frac{2i}{N_y}\sum_{n,m,k_y} \sin(k_y)\, u_{i_x,n,k_y}w^{*}_{i_x,m,k_y}\langle \gamma^{\dagger}_{n,m,k_y}\gamma_{m,k_y}\rangle \\
&= \frac{2i}{N_y}\sum_{n,m,k_y>0}\Big[\sin(k_y)\, u_{i_x,n,k_y}w^{*}_{i_x,m,k_y}\langle \gamma^{\dagger}_{n,k_y}\gamma_{m,k_y}\rangle + \sin(-k_y)\, w^{*}_{i_x,n,k_y}u_{i_x,m,k_y}\langle \gamma_{n,k_y}\gamma^{\dagger}_{m,k_y}\rangle\Big] \\
&= \frac{2i}{N_y}\sum_{n,k_y>0}\sin(k_y)\Big[\, u_{i_x,n,k_y}w^{*}_{i_x,m,k_y}f(2\mathcal{E}_{n,k_y}) - \, w^{*}_{i_x,n,k_y}u_{i_x,m,k_y}f(-2\mathcal{E}_{n,k_y})\Big] \\
&= \frac{-2i}{N_y}{\sum_{n,k_y}}' \sin(k_y)w^{*}_{i_x,n,k_y}u_{i_x,n,k_y}\tanh\big(\beta\mathcal{E}_{n,k_y}\big)\,, \qquad \text{(D.8)}
\end{aligned}
$$

$$
\begin{aligned}
\mathcal{P}^{y}_{i_x,\downarrow} &= \frac{1}{N_y}\sum_{i_y}\sum_{\pm} \pm\langle c_{i,\downarrow}c_{i\pm\hat{y},\downarrow}\rangle \\
&= \frac{1}{N_y}\sum_{k_y,k_y'}\sum_{\pm}\sum_{i_y} \pm\frac{1}{N_y}e^{ik_y i_y + ik_y'(i_y\pm 1)}\langle c_{i_x,k_y,\downarrow}c_{i_x,k_y',\downarrow}\rangle \\
&= \frac{1}{N_y}\sum_{k_y}\sum_{\pm} \pm e^{\pm ik_y}\langle c_{i_x,-k_y,\downarrow}c_{i_x,k_y,\downarrow}\rangle \\
&= \frac{2i}{N_y}\sum_{n,m,k_y} \sin(k_y)\, v_{i_x,n,k_y}x^{*}_{i_x,m,k_y}\langle \gamma^{\dagger}_{n,m,k_y}\gamma_{m,k_y}\rangle \\
&= \frac{2i}{N_y}\sum_{n,m,k_y>0}\Big[\sin(k_y)\, v_{i_x,n,k_y}x^{*}_{i_x,m,k_y}\langle \gamma^{\dagger}_{n,k_y}\gamma_{m,k_y}\rangle + \sin(-k_y)\, x^{*}_{i_x,n,k_y}v_{i_x,m,k_y}\langle \gamma_{n,k_y}\gamma^{\dagger}_{m,k_y}\rangle\Big] \\
&= \frac{2i}{N_y}\sum_{n,k_y>0}\sin(k_y)\Big[\, v_{i_x,n,k_y}x^{*}_{i_x,m,k_y}f(2\mathcal{E}_{n,k_y}) - \, x^{*}_{i_x,n,k_y}v_{i_x,m,k_y}f(-2\mathcal{E}_{n,k_y})\Big] \\
&= \frac{-2i}{N_y}{\sum_{n,k_y}}' \sin(k_y)x^{*}_{i_x,n,k_y}v_{i_x,n,k_y}\tanh\big(\beta\mathcal{E}_{n,k_y}\big)\,. \qquad \text{(D.9)}
\end{aligned}
$$

## D.3 Charge current

In this subsection we will derive a general expression for the charge current. To obtain an expression for the current, we begin with the charge continuity equation [104], which is

$$\partial_t\rho_i = -\nabla\cdot\boldsymbol{j}_i\,, \qquad \text{(D.10)}$$

where $\rho_i$ is the charge density, and $\boldsymbol{j}_i$ is the current density at site $i$. Since we begin from a general expression, the indexes may contain a $x$- and $y$-component, so $i = (i_x, i_y)$. We

will reintroduce periodic boundary conditions at a later point. We find the total current by integrating over one unit-cell volume $\Omega$. Then, we use Green's theorem to integrate over the boundary $\partial\Omega$ of the unit cell. This gives

$$\int_\Omega d\boldsymbol{r}\,(\nabla\cdot\boldsymbol{j}_i) = \int_{\partial\Omega} dS\,(\boldsymbol{j}_i\cdot\hat{\boldsymbol{e}}_m) = \sum_m I_{i,m}\,, \tag{D.11}$$

where $\hat{\boldsymbol{e}}_m$ denotes the normal vector to the boundary. Thus, the current $I_{i,m}$ is the current flowing out of surface $m$, and its sign is determined by $\hat{\boldsymbol{e}}_m$. The integrated time derivative of the charge density can be rewritten using Heisenberg's equation of motion. This relates it to the Hamiltonian of the system by

$$\int_\Omega d\boldsymbol{r}\,\partial_t\rho_i = \partial_t Q_i = i\,[\mathcal{H},\,Q_i]\,. \tag{D.12}$$

Therefore, we can write the continuity equation from before as

$$\sum_m I_{i,m} = -i\,[\mathcal{H},\,Q_i]\,, \tag{D.13}$$

where $\mathcal{H}$ is the Hamiltonian given in eq. (5.12) not assuming periodic boundary conditions yet, and the charge is given by $Q_i = \sum_\sigma c^\dagger_{i,\sigma}c_{i,\sigma}$. Next, we calculate term by term the commutation with the Hamiltonian. In these calculations, we will make use of the commutation following relations

$$\left[n_{i,\sigma},\,c^\dagger_{j,\sigma'}\right] = \delta_{i,j}\delta_{\sigma,\sigma'}c^\dagger_{i,\sigma}\,, \qquad \left[n_{i,\sigma},\,c_{j,\sigma'}\right] = -\delta_{i,j}\delta_{\sigma,\sigma'}c_{i,\sigma}\,. \tag{D.14}$$

The first term in eq. (5.12) is the onsite chemical potential. The commutation with $Q_i$ gives

$$\begin{aligned}
\left[\sum_{i,\sigma}\mu_i c^\dagger_{i,\sigma}c_{i,\sigma},\,\sum_{\sigma'}n_{j,\sigma'}\right] =& \sum_{i,\sigma,\sigma'}\mu_i\left[c^\dagger_{i,\sigma}c_{i,\sigma}n_{j,\sigma'} - n_{j,\sigma'}c^\dagger_{i,\sigma}c_{i,\sigma}\right]\\
=& \sum_{i,\sigma,\sigma'}\mu_i\left[c^\dagger_{i,\sigma}\left(\delta_{i,j}\delta_{\sigma,\sigma'}c_{j,\sigma'} + n_{j,\sigma'}c_{i,\sigma}\right) - \left(\delta_{i,j}\delta_{\sigma,\sigma'}c^\dagger_{j,\sigma'} + c^\dagger_{i,\sigma}n_{j,\sigma'}\right)c_{i,\sigma}\right]\\
=& \sum_{i,\sigma,\sigma'}\mu_i\delta_{i,j}\delta_{\sigma,\sigma'}\left[c^\dagger_{i,\sigma}c_{j,\sigma'} - c^\dagger_{j,\sigma'}c_{i,\sigma}\right]\\
=& \sum_{\sigma}\mu_j\left[c^\dagger_{j,\sigma}c_{j,\sigma} - c^\dagger_{j,\sigma}c_{j,\sigma}\right] = 0\,.
\end{aligned} \tag{D.15}$$

The next is the nearest neighbor hopping. In this commutation, we will introduce a sum over the nearest neighbor difference $\delta$, which is $\pm\hat{x}, \pm\hat{y}$. The commutator becomes

$$\begin{aligned}
\left[\sum_{\langle ij\rangle,\sigma}t_{i,j}c^\dagger_{i,\sigma}c_{j,\sigma},\,\sum_{\sigma'}n_{l,\sigma'}\right] =& \sum_{\langle ij\rangle,\sigma,\sigma'}t_{i,j}\left[c^\dagger_{i,\sigma}c_{j,\sigma}n_{l,\sigma'} - n_{l,\sigma'}c^\dagger_{i,\sigma}c_{j,\sigma}\right]\\
=& \sum_{\langle ij\rangle,\sigma,\sigma'}t_{i,j}\left[c^\dagger_{i,\sigma}\left(\delta_{j,l}\delta_{\sigma,\sigma'}c_{l,\sigma'} + n_{l,\sigma'}c_{j,\sigma}\right) - \left(\delta_{i,l}\delta_{\sigma,\sigma'}c^\dagger_{l,\sigma'} + c^\dagger_{i,\sigma}n_{l,\sigma'}\right)c_{j,\sigma}\right]\\
=& \sum_{\langle ij\rangle,\sigma}t_{i,j}\left[c^\dagger_{i,\sigma}c_{l,\sigma}\delta_{j,l} - c^\dagger_{l,\sigma}c_{j,\sigma}\delta_{i,l}\right]\\
=& \sum_{i,\delta,\sigma}t_{i,i+\delta}\left[c^\dagger_{i,\sigma}c_{l,\sigma}\delta_{i+\delta,l} - c^\dagger_{l,\sigma}c_{i+\delta,\sigma}\delta_{i,l}\right]
\end{aligned}$$

$$
\begin{aligned}
&= \sum_{\delta,\sigma} \left[ t_{l-\delta,l} c^\dagger_{l-\delta,\sigma} c_{l,\sigma} - t_{l,l+\delta} c^\dagger_{l,\sigma} c_{l+\delta,\sigma} \right] \\
&= \sum_{\sigma,\pm} \left[ t_{l,l\pm\hat{x}} c^\dagger_{l\mp\hat{x},\sigma} c_{l,\sigma} - t_{l,l\pm\hat{x}} c^\dagger_{l,\sigma} c_{l\pm\hat{x},\sigma} + t_{l,l\pm\hat{y}} c^\dagger_{l\mp\hat{y},\sigma} c_{l,\sigma} - t_{l,l\pm\hat{y}} c^\dagger_{l,\sigma} c_{l\pm\hat{y},\sigma} \right] .
\end{aligned} \tag{D.16}
$$

The third term is the spin-orbit coupling. It can be thought of as spin-dependent hopping; therefore, we follow the same procedure as above. This yields

$$
\begin{aligned}
\left[ \sum_{\langle ij \rangle,\sigma_1,\sigma_2} \alpha^{\sigma_1,\sigma_2}_{i,j} c^\dagger_{i,\sigma_1} c_{j,\sigma_2}, \sum_{\sigma_3} n_{l,\sigma_3} \right] &= \sum_{\langle ij \rangle} \sum_{\sigma_1,\sigma_2,\sigma_3} \alpha^{\sigma_1,\sigma_2}_{i,j} \left[ c^\dagger_{i,\sigma_1} c_{j,\sigma_2} n_{l,\sigma_3} - n_{l,\sigma_3} c^\dagger_{i,\sigma_1} c_{j,\sigma_2} \right] \\
&= \sum_{\langle ij \rangle} \sum_{\sigma_1,\sigma_2,\sigma_3} \alpha^{\sigma_1,\sigma_2}_{i,j} \Big[ c^\dagger_{i,\sigma_1} \left( \delta_{j,l} \delta_{\sigma_2,\sigma_3} c_{l,\sigma_3} + n_{l,\sigma_3} c_{j,\sigma_2} \right) \\
&\qquad - \left( \delta_{i,l} \delta_{\sigma_1,\sigma_3} c^\dagger_{l,\sigma_3} + c^\dagger_{i,\sigma_1} n_{l,\sigma_3} \right) c_{j,\sigma_2} \Big] \\
&= \sum_{i,\delta,\sigma_1,\sigma_3} \alpha^{\sigma_1,\sigma_3}_{i,i+\delta} \left[ c^\dagger_{i,\sigma_1} c_{l,\sigma_3} \delta_{i+\delta,l} - c^\dagger_{l,\sigma_1} c_{i+\delta,\sigma_3} \delta_{i,l} \right] \\
&= \sum_{\sigma_1,\sigma_3,\pm} \pm \Big[ a^{\sigma_1,\sigma_3}_{l\mp\hat{x},l} c^\dagger_{l\mp\hat{x},\sigma_1} c_{l,\sigma_3} - a^{\sigma_1,\sigma_3}_{l,l\pm\hat{x}} c^\dagger_{l,\sigma_1} c_{l\pm\hat{x},\sigma_3} \\
&\qquad + a^{\sigma_1,\sigma_3}_{l\mp\hat{y},l} c^\dagger_{l\mp\hat{y},\sigma_1} c_{l,\sigma_3} - a^{\sigma_1,\sigma_3}_{l,l\pm\hat{y}} c^\dagger_{l,\sigma_1} c_{l\pm\hat{y},\sigma_3} \Big] ,
\end{aligned} \tag{D.17}
$$

where we inserted to nearest neighbor vector to get the sum $\sum_\pm$. Lastly, we have the superconducting term. We consider the electron and hole parts separately. From this, we get the following contributions

$$
\begin{aligned}
\left[ \sum_i \Delta_i c^\dagger_{i,\uparrow} c^\dagger_{i,\downarrow}, \sum_\sigma n_{j,\sigma} \right] &= \sum_{i,\sigma} \Delta_i \left[ c^\dagger_{i,\uparrow} c^\dagger_{i,\downarrow} n_{j,\sigma} - n_{j,\sigma} c^\dagger_{i,\uparrow} c^\dagger_{i,\downarrow} \right] \\
&= \sum_{i,\sigma} \Delta_i \left[ c^\dagger_{i,\uparrow} \left( n_{j,\sigma} c^\dagger_{i,\downarrow} - \delta_{i,j} \delta_{\downarrow,\sigma} c^\dagger_{j,\sigma} \right) - \left( c^\dagger_{i,\uparrow} n_{j,\sigma} + \delta_{i,j} \delta_{\sigma,\uparrow} c^\dagger_{j,\sigma} \right) c^\dagger_{i,\downarrow} \right] \\
&= -2\Delta_j c^\dagger_{j\uparrow} c^\dagger_{j\downarrow} ,
\end{aligned} \tag{D.18}
$$

$$
\begin{aligned}
\left[ \sum_i \Delta^*_i c_{i,\downarrow} c_{i,\uparrow}, \sum_\sigma n_{j,\sigma} \right] &= \sum_{i,\sigma} \Delta^*_i \left[ c_{i,\downarrow} c_{i,\uparrow} n_{j,\sigma} - n_{j,\sigma} c_{i,\downarrow} c_{i,\uparrow} \right] \\
&= \sum_{i,\sigma} \Delta^*_i \left[ c_{i,\downarrow} \left( n_{j,\sigma} c_{i,\uparrow} + \delta_{i,j} \delta_{\uparrow,\sigma} c_{j,\sigma} \right) - \left( c_{i,\downarrow} n_{j,\sigma} - \delta_{i,j} \delta_{\sigma,\downarrow} c_{j,\sigma} \right) c_{i,\uparrow} \right] \\
&= 2\Delta^*_j c_{j\downarrow} c_{j\uparrow} .
\end{aligned} \tag{D.19}
$$

Since we have chosen conventional superconductivity, we only have an onsite attractive interaction contribution. Thus, it might seem strange that it should contribute to the charge current. However, if we take the thermal and quantum average, we see that does, in fact, not contribute. This is easily seen when inserting the average,

$$
\begin{aligned}
\left\langle -2\Delta_j c^\dagger_{j,\uparrow} c^\dagger_{j,\downarrow} + 2\Delta^*_j c_{j,\downarrow} c_{j,\uparrow} \right\rangle &= 2\Delta^*_j \langle c_{j,\downarrow} c_{j,\uparrow} \rangle - 2\Delta_j \langle c^\dagger_{j,\uparrow} c^\dagger_{j,\downarrow} \rangle \\
&= 2\Delta^*_j \Delta_j - 2\Delta_j \Delta^*_j = 0 .
\end{aligned} \tag{D.20}
$$

Before doing the same with the other commutators, we choose a current direction. We choose the charge current in the $x$-direction to have a positive sign in the positive $x$-direction. We begin with the contribution from the hopping term to the current in the $x$-direction. We define $I^{x,t}_{i,\pm}$ as the contribution from $t$ to the current through the unit cell at $i \pm \hat{x}/2$. The contributions through the right and left unit cell face are respectively

$$I^{x,t}_{i,+} = i \sum_{\sigma} \left[ t_{i,i-\hat{x}} c^{\dagger}_{i+\hat{x},\sigma} c_{i,\sigma} - t_{i,i+\hat{x}} c^{\dagger}_{i,\sigma} c_{i+\hat{x},\sigma} \right] , \tag{D.21}$$

$$I^{x,t}_{i,-} = i \sum_{\sigma} \left[ t_{i,i+\hat{x}} c^{\dagger}_{i-\hat{x},\sigma} c_{i,\sigma} - t_{i,i-\hat{x}} c^{\dagger}_{i,\sigma} c_{i-\hat{x},\sigma} \right] . \tag{D.22}$$

The total current contribution is therefore $I^{x,t}_{i} = I^{x,t}_{i,+} - I^{x,t}_{i,-}$. Taking the thermal and quantum average, as well as the mean in the $y$-direction, we get

$$\begin{aligned}
\langle I^{x}_{i_x} \rangle_t &= \frac{i}{N_y} \sum_{i_y,\sigma} \Big\langle t_{i,i-\hat{x}} \left( c^{\dagger}_{i+\hat{x},\sigma} c_{i,\sigma} + c^{\dagger}_{i,\sigma} c_{i-\hat{x},\sigma} \right) - t_{i,i+\hat{x}} \left( c^{\dagger}_{i,\sigma} c_{i+\hat{x},\sigma} + c^{\dagger}_{i-\hat{x},\sigma} c_{i,\sigma} \right) \Big\rangle \\
&= \frac{i}{N_y} \sum_{k_y,k'_y,\sigma} \sum_{i_y} \frac{1}{N_y} e^{i(k'_y - k_y) i_y} \Big[ t_{i,i-\hat{x}} \left( \langle c^{\dagger}_{i_x+1,k_y,\sigma} c_{i_x,k'_y,\sigma} \rangle + \langle c^{\dagger}_{i_x,k_y,\sigma} c_{i_x-1,k'_y,\sigma} \rangle \right) \\
&\qquad - t_{i,i+\hat{x}} \left( \langle c^{\dagger}_{i_x,k_y,\sigma} c_{i_x+1,k'_y,\sigma} \rangle + \langle c^{\dagger}_{i_x-1,k_y,\sigma} c_{i_x,k'_y,\sigma} \rangle \right) \Big] \\
&= \frac{i}{N_y} \sum_{k_y,\sigma} \Big[ t_{i,i-\hat{x}} \left( \langle c^{\dagger}_{i_x+1,k_y,\sigma} c_{i_x,k_y,\sigma} \rangle + \langle c^{\dagger}_{i_x,k_y,\sigma} c_{i_x-1,k_y,\sigma} \rangle \right) \\
&\quad - t_{i,i+\hat{x}} \left( \langle c^{\dagger}_{i_x,k_y,\sigma} c_{i_x+1,k_y,\sigma} \rangle + \langle c^{\dagger}_{i_x-1,k_y,\sigma} c_{i_x,k_y,\sigma} \rangle \right) \Big] \\
&= \frac{i}{N_y} \sum_{n,m,k_y} \Big[ t_{i_x,i_x-1} \left( u^{*}_{i_x+1,n,k_y} u_{i_x,n,k_y} + u^{*}_{i_x,n,k_y} u_{i_x-1,n,k_y} \right) \\
&\quad + t_{i_x,i_x-1} \left( v^{*}_{i_x+1,n,k_y} v_{i_x,m,k_y} + v^{*}_{i_x,n,k_y} v_{i_x-1,m,k_y} \right) \\
&\quad - t_{i_x,i_x+1} \left( u^{*}_{i_x,n,k_y} u_{i_x+1,m,k_y} + u^{*}_{i_x-1,n,k_y} u_{i_x,m,k_y} \right) \\
&\quad - t_{i_x,i_x+1} \left( v^{*}_{i_x,n,k_y} v_{i_x+1,m,k_y} + v^{*}_{i_x-1,n,k_y} v_{i_x,m,k_y} \right) \Big] \langle \gamma^{\dagger}_{n,k_y} \gamma_{m,k_y} \rangle \\
&= \frac{it}{N_y} \Big\{ \sum_{n,m} \sum_{k_y>0} \Big[ u^{*}_{i_x+1,n,k_y} u_{i,m,k_y} + v^{*}_{i_x+1,n,k_y} v_{i_x,m,k_y} + u^{*}_{i_x,n,k_y} u_{i_x-1,m,k_y} \\
&\quad + v^{*}_{i_x,n,k_y} v_{i_x-1,m,k_y} - u^{*}_{i_x-1,n,k_y} u_{i,m,k_y} - v^{*}_{i_x-1,n,k_y} v_{i,m,k_y} \\
&\quad - u^{*}_{i_x,n,k_y} u_{i+1,m,k_y} - v^{*}_{i_x,n,k_y} v_{i+1,m,k_y} \Big] \langle \gamma^{\dagger}_{n,k_y} \gamma_{m,k_y} \rangle \\
&\quad + \sum_{n,m} \sum_{k_y>0} \Big[ w_{i_x+1,n,k_y} w^{*}_{i,m,k_y} + x_{i_x+1,n,k_y} x^{*}_{i_x,m,k_y} + w_{i_x,n,k_y} w^{*}_{i_x-1,m,k_y} \\
&\quad + x_{i_x,n,k_y} x^{*}_{i_x-1,m,k_y} - w_{i_x-1,n,k_y} w^{*}_{i,m,k_y} - x_{i_x-1,n,k_y} x^{*}_{i,m,k_y} \\
&\quad - w_{i_x,n,k_y} w^{*}_{i+1,m,k_y} - x_{i_x,n,k_y} x^{*}_{i+1,m,k_y} \Big] \langle \gamma_{n,k_y} \gamma^{\dagger}_{m,k_y} \rangle \\
&\quad + \sum_{n,m=1}^{2N_x} \Big[ u^{*}_{i_x+1,n,0} u_{i,m,0} + v^{*}_{i_x+1,n,0} v_{i_x,m,0} + u^{*}_{i_x,n,0} u_{i_x-1,m,0} + v^{*}_{i_x,n,0} v_{i_x-1,m,0}
\end{aligned}$$

$$
\begin{aligned}
&- u^*_{i_x-1,n,0}u_{i,m,0} - v^*_{i_x-1,n,0}v_{i,m,0} - u^*_{i_x,n,0}u_{i+1,m,0} - v^*_{i_x,n,0}v_{i+1,m,0}\Big]\langle\gamma^\dagger_{n,0}\gamma_{m,0}\rangle \\
&+ \sum_{n,m=1}^{2N_x}\Big[w_{i_x+1,n,0}w^*_{i,m,0} + x_{i_x+1,n,0}x^*_{i_x,m,0} + w_{i_x,n,0}w^*_{i_x-1,m,0} + x_{i_x,n,0}x^*_{i_x-1,m,0} \\
&- w_{i_x-1,n,0}w^*_{i,m,0} - x_{i_x-1,n,0}x^*_{i,m,0} - w_{i_x,n,0}w^*_{i+1,m,0} - x_{i_x,n,0}x^*_{i+1,m,0}\Big]\langle\gamma_{n,0}\gamma^\dagger_{m,0}\rangle \\
&= \frac{-2t}{N_y}\sum_{\pm}\sum_{n,k_y}{}' \pm\Big[\mathfrak{Im}\{u^*_{i_x\pm1,n,k_y}u_{i_x,n,k_y} + v^*_{i_x\pm1,n,k_y}v_{i_x,n,k_y}\}f(2\mathcal{E}_{n,k_y}) \\
&- \mathfrak{Im}\{w^*_{i_x\pm1,n,k_y}w_{i_x,n,k_y} + x^*_{i_x\pm1,n,k_y}x_{i_x\,n,k_y}\}f(-2\mathcal{E}_{n,k_y})\Big], \qquad \text{(D.23)}
\end{aligned}
$$

where we have assumed constant hopping amplitude everywhere. Also, we used the relation $z - z^* = 2i\,\mathfrak{Im}\{z\}$ for the complex eigenvector elements. If we have no spin-orbit coupling, this is the total charge current. However, we also calculate the contribution from the spin-orbit coupling. Our starting point is once again the contributions in the two opposite directions,

$$
I^{x,\alpha}_{i,+} = \sum_{\sigma,\sigma'}\left[-a^{\sigma,\sigma'}_{i+\hat{x},i}c^\dagger_{i+\hat{x},\sigma}c_{i,\sigma'} - a^{\sigma,\sigma'}_{i,i+\hat{x}}c^\dagger_{i,\sigma}c_{i+\hat{x},\sigma'}\right], \qquad \text{(D.24)}
$$

$$
I^{x,\alpha}_{i,-} = \sum_{\sigma,\sigma'}\left[a^{\sigma,\sigma'}_{i-\hat{x},i}c^\dagger_{i-\hat{x},\sigma}c_{i,\sigma'} + a^{\sigma,\sigma'}_{i,i-\hat{x}}c^\dagger_{i,\sigma}c_{i-\hat{x},\sigma'}\right]. \qquad \text{(D.25)}
$$

Again, we take the thermal and quantum average as well as the mean in the $y$-direction of $I^{x,\alpha}_i = I^{x,\alpha}_{i,+} - I^{x,\alpha}_{i,-}$. Doing this gives

$$
\begin{aligned}
\langle I^x_{i_x}\rangle_\alpha &= \frac{-i}{N_y^2}\sum_{\sigma,\sigma'}\sum_{k_y,k'_y}\sum_{i_y}\sum_{\pm}e^{i(k'_y-k_y)i_y}\left[a^{\sigma,\sigma'}_{i\pm\hat{x},i}\langle c^\dagger_{i_x\pm1,k_y,\sigma}c_{i_x,k'_y,\sigma'}\rangle + a^{\sigma,\sigma'}_{i,i\pm\hat{x}}\langle c^\dagger_{i_x,k_y,\sigma}c_{i_x\pm1,k'_y,\sigma'}\rangle\right] \\
&= \frac{-i}{N_y}\sum_{k_y,\sigma,\sigma'}\sum_{\pm}\left[a^{\sigma,\sigma'}_{i_x\pm1,i_x}\langle c^\dagger_{i_x\pm1,k_y,\sigma}c_{i_x,k_y,\sigma'}\rangle + a^{\sigma,\sigma'}_{i_x,i_x\pm1}\langle c^\dagger_{i_x,k_y,\sigma}c_{i_x\mp1,k_y,\sigma'}\rangle\right] \\
&= \frac{-i}{N_y}\sum_{n,m,k_y}\sum_{\pm}\Big[a^{\uparrow,\uparrow}_{i_x\pm1,i_x}u^*_{i_x\pm1,n,k_y}u_{i_x,m,k_y} + a^{\uparrow,\uparrow}_{i_x,i_x\pm1}u^*_{i_x,n,k_y}u_{i_x\pm1,m,k_y} \\
&\qquad + a^{\uparrow\downarrow}_{i_x\pm1,i_x}u^*_{i_x\pm1,n,k_y}v_{i_x,m,k_y} + a^{\uparrow\downarrow}_{i_x,i_x\pm1}u^*_{i_x,n,k_y}v_{i_x\pm1,m,k_y} \\
&\qquad + a^{\downarrow\uparrow}_{i_x\pm1,i_x}v^*_{i_x\pm1,n,k_y}u_{i_x,m,k_y} + a^{\downarrow\uparrow}_{i_x,i_x\pm1}v^*_{i_x,n,k_y}u_{i_x\pm1,m,k_y} \\
&\qquad + a^{\downarrow\downarrow}_{i_x\pm1,i_x}v^*_{i_x\pm1,n,k_y}v_{i_x,m,k_y} + a^{\downarrow\downarrow}_{i_x,i_x\pm1}v^*_{i_x,n,k_y}v_{i_x\pm1,m,k_y}\Big]\langle\gamma^\dagger_{n,k_y}\gamma_{m,k_y}\rangle \\
&= \frac{-i}{N_y}\sum_{n,m,k_y}\sum_{\pm}\Big[a^{\uparrow,\uparrow}_{i_x\pm1,i_x}u^*_{i_x\pm1,n,k_y}u_{i_x,m,k_y} - \left(a^{\uparrow,\uparrow}_{i_x\pm1,i_x}\right)^* u^*_{i_x,n,k_y}u_{i_x\pm1,m,k_y} \\
&\qquad + a^{\uparrow\downarrow}_{i_x\pm1,i_x}u^*_{i_x\pm1,n,k_y}v_{i_x,m,k_y} - \left(a^{\downarrow\uparrow}_{i_x\pm1,i_x}\right)^* u^*_{i_x,n,k_y}v_{i_x\pm1,m,k_y} \\
&\qquad + a^{\downarrow\uparrow}_{i_x,i_x\pm1}v^*_{i_x\pm1,n,k_y}u_{i_x,m,k_y} - \left(a^{\uparrow\downarrow}_{i_x\pm1,i_x}\right)^* v^*_{i_x,n,k_y}u_{i_x\pm1,m,k_y} \\
&\qquad + a^{\downarrow\downarrow}_{i_x\pm1,i_x}v^*_{i_x\pm1,n,k_y}v_{i_x,m,k_y} - \left(a^{\downarrow\downarrow}_{i_x\pm1,i_x}\right)^* v^*_{i_x,n,k_y}v_{i_x\pm1,m,k_y}\Big]\langle\gamma^\dagger_{n,k_y}\gamma_{m,k_y}\rangle
\end{aligned}
$$

$$
\begin{aligned}
&= \frac{-i}{N_y}\sum_{\pm}\Bigg[\sum_{n,m,k_y>0}\mathfrak{Im}\big\{a^{\uparrow,\uparrow}_{i_x\pm1,i_x}u^*_{i_x\pm1,n,k_y}u_{i_x,m,k_y}+a^{\uparrow\downarrow}_{i_x\pm1,i_x}u^*_{i_x\pm1,n,k_y}v_{i_x,m,k_y}\\
&\qquad+a^{\downarrow\uparrow}_{i_x,i_x\pm1}v^*_{i_x\pm1,n,k_y}u_{i_x,m,k_y}+a^{\downarrow\downarrow}_{i_x\pm1,i_x}v^*_{i_x\pm1,n,k_y}v_{i_x,m,k_y}\big\}\langle\gamma^\dagger_{n,k_y}\gamma_{m,k_y}\rangle\\
&\quad+\sum_{n,m,k_y>0}\mathfrak{Im}\big\{a^{\uparrow,\uparrow}_{i_x\pm1,i_x}w_{i_x\pm1,n,k_y}w^*_{i_x,m,k_y}+a^{\uparrow\downarrow}_{i_x\pm1,i_x}w_{i_x\pm1,n,k_y}x^*_{i_x,m,k_y}\\
&\qquad+a^{\downarrow\uparrow}_{i_x,i_x\pm1}x_{i_x\pm1,n,k_y}w^*_{i_x,m,k_y}+a^{\downarrow\downarrow}_{i_x\pm1,i_x}x_{i_x\pm1,n,k_y}x^*_{i_x,m,k_y}\big\}\langle\gamma_{n,k_y}\gamma^\dagger_{m,k_y}\rangle\\
&\quad+\sum_{n,m=1}^{2N_x}\mathfrak{Im}\big\{a^{\uparrow,\uparrow}_{i_x\pm1,i_x}u^*_{i_x\pm1,n,0}u_{i_x,m,0}+a^{\uparrow\downarrow}_{i_x\pm1,i_x}u^*_{i_x\pm1,n,0}v_{i_x,m,0}\\
&\qquad+a^{\downarrow\uparrow}_{i_x,i_x\pm1}v^*_{i_x\pm1,n,0}u_{i_x,m,0}+a^{\downarrow\downarrow}_{i_x\pm1,i_x}v^*_{i_x\pm1,n,0}v_{i_x,m,0}\big\}\langle\gamma^\dagger_{n,0}\gamma_{m,0}\rangle\\
&\quad+\sum_{n,m=1}^{2N_x}\mathfrak{Im}\big\{a^{\uparrow,\uparrow}_{i_x\pm1,i_x}w_{i_x\pm1,n,0}w^*_{i_x,m,0}+a^{\uparrow\downarrow}_{i_x\pm1,i_x}w_{i_x\pm1,n,0}x^*_{i_x,m,0}\\
&\qquad+a^{\downarrow\uparrow}_{i_x,i_x\pm1}x_{i_x\pm1,n,0}w^*_{i_x,m,0}+a^{\downarrow\downarrow}_{i_x\pm1,i_x}x_{i_x\pm1,n,0}x^*_{i_x,m,0}\big\}\langle\gamma_{n,0}\gamma^\dagger_{m,0}\rangle\Bigg]\\
&= \frac{2}{N_y}\sum_{\pm}{\sum_{n,k_y}}'\Bigg[\mathfrak{Im}\{a^{\uparrow\uparrow}_{i_x\pm1,i_x}u^*_{i_x\pm1,n,k_y}u_{i_x,n,k_y}+a^{\uparrow\downarrow}_{i_x\pm1,i_x}u^*_{i_x\pm1,n,k_y}v_{i_x,n,k_y}\\
&\qquad+a^{\downarrow\uparrow}_{i_x\pm1,i_x}v^*_{i_x\pm1,n,k_y}u_{i_x,n,k_y}+a^{\downarrow\downarrow}_{i_x\pm1,i_x}v^*_{i_x\pm1,n,k_y}v_{i_x,n,k_y}\}f(2\mathcal{E}_{n,k_y})\\
&\quad+\mathfrak{Im}\{a^{\uparrow\uparrow}_{i_x\pm1,i_x}w^*_{i_x,n,k_y}w_{i_x\pm1,n,k_y}+a^{\uparrow\downarrow}_{i_x\pm1,i_x}x^*_{i_x,n,k_y}w_{i_x\pm1,n,k_y}\\
&\qquad+a^{\downarrow\uparrow}_{i_x\pm1,i_x}w^*_{i_x,n,k_y}x_{i_x\pm1,n,k_y}+a^{\downarrow\downarrow}_{i_x\pm1,i_x}x^*_{i_x,n,k_y}x_{i_x\pm1,n,k_y}\}f(-2\mathcal{E}_{n,k_y})\Bigg].
\end{aligned}
\tag{D.26}
$$

As evident from the equation above, this contribution depends on the form of the spin-orbit coupling. The exact form depends on whether there is intrinsic symmetry breaking, which results in spin-orbit, and if the system is curved. The strain-induced spin-orbit field is dependent on the exact geometry of the system. Generally, we can write

$$
\begin{aligned}
\langle I^x_{i_x}\rangle =&\frac{-2t}{N_y}\sum_{\pm}{\sum_{n,k_y}}'\pm\Bigg[\mathfrak{Im}\{u^*_{i_x\pm1,n,k_y}u_{i_x,n,k_y}+v^*_{i_x\pm1,n,k_y}v_{i_x,n,k_y}\}f(2\mathcal{E}_{n,k_y})\\
&\qquad-\mathfrak{Im}\{w^*_{i_x\pm1,n,k_y}w_{i_x,n,k_y}+x^*_{i_x\pm1,n,k_y}x_{i_x\,n,k_y}\}f(-2\mathcal{E}_{n,k_y})\Bigg]\\
&+\frac{2}{N_y}\sum_{\pm}{\sum_{n,k_y}}'\Bigg[\mathfrak{Im}\{a^{\uparrow\uparrow}_{i_x\pm1,i_x}u^*_{i_x\pm1,n,k_y}u_{i_x,n,k_y}+a^{\uparrow\downarrow}_{i_x\pm1,i_x}u^*_{i_x\pm1,n,k_y}v_{i_x,n,k_y}\\
&\qquad+a^{\downarrow\uparrow}_{i_x\pm1,i_x}v^*_{i_x\pm1,n,k_y}u_{i_x,n,k_y}+a^{\downarrow\downarrow}_{i_x\pm1,i_x}v^*_{i_x\pm1,n,k_y}v_{i_x,n,k_y}\}f(2\mathcal{E}_{n,k_y})\\
&\quad+\mathfrak{Im}\{a^{\uparrow\uparrow}_{i_x\pm1,i_x}w^*_{i_x,n,k_y}w_{i_x\pm1,n,k_y}+a^{\uparrow\downarrow}_{i_x\pm1,i_x}x^*_{i_x,n,k_y}w_{i_x\pm1,n,k_y}\\
&\qquad+a^{\downarrow\uparrow}_{i_x\pm1,i_x}w^*_{i_x,n,k_y}x_{i_x\pm1,n,k_y}+a^{\downarrow\downarrow}_{i_x\pm1,i_x}x^*_{i_x,n,k_y}x_{i_x\pm1,n,k_y}\}f(-2\mathcal{E}_{n,k_y})\Bigg].
\end{aligned}
\tag{D.27}
$$

## D.4 Spin current

The spin current can be found in the exact same way as the charge current. However, instead of taking the commutator with the spin operator $\boldsymbol{S}_i = \sum_{\alpha\beta} c^\dagger_{i,\alpha} \boldsymbol{\sigma}^{\alpha\beta} c_{i,\beta}$. Thus, for the $z$-component of the spin current flowing in the $x$-direction $I^{x,z}_S$ the commutator to be calculated is

$$\sum_m I^{S,z}_{i,m} = -i[\mathcal{H}, S^z_i]\,, \tag{D.28}$$

where $S^z_i = \sum_\sigma \sigma c^\dagger_{i,\sigma} c_{i,\sigma}$. Therefore, there is only a sign-change on the second number operator compared to the charge current derivation. One can immediately write down the commutator between the hopping term and the spin operator,

$$\begin{aligned}\left[\sum_{\langle ij\rangle,\sigma} t_{ij} c^\dagger_{i,\sigma} c_{i,\sigma},\, \sum_{\sigma'} \sigma' n_{l,\sigma'}\right] = \sum_{\sigma,\pm}\Big[&\sigma t_{l,l\pm\hat{x}} (c^\dagger_{l\mp\hat{x},\sigma} c_{l,\sigma} - c^\dagger_{l,\sigma} c_{l\pm\hat{x},\sigma}) \\ &+ \sigma t_{l,l\pm\hat{y}} (c^\dagger_{l\mp\hat{y},\sigma} c_{l,\sigma} - c^\dagger_{l,\sigma} c_{l\pm\hat{y},\sigma})\Big]\,.\end{aligned} \tag{D.29}$$

A similar thing happens to the spin-orbit term. We get that

$$\begin{aligned}\left[\sum_{\langle ij\rangle,\sigma_1,\sigma_2} \alpha^{\sigma_1,\sigma_2}_{ij} c^\dagger_{i,\sigma_1} c_{i,\sigma_2},\, \sum_{\sigma_3} \sigma_3 n_{l,\sigma_3}\right] = \sum_{\sigma_1,\sigma_2,\pm} \pm \Big[&a^{\sigma_1,\sigma_2}_{l\mp\hat{x},l} \sigma_2 c^\dagger_{l\mp\hat{x},\sigma_1} c_{l,\sigma_2} - a^{\sigma_1,\sigma_2}_{l,l\pm\hat{x}} \sigma_1 c^\dagger_{l,\sigma_1} c_{l\pm\sigma_2,\sigma_2} \\ &+ a^{\sigma_1,\sigma_2}_{l\mp\hat{y},l} \sigma_2 c^\dagger_{l\mp\hat{y},\sigma_1} c_{l,\sigma_2} - a^{\sigma_1,\sigma_2}_{l,l\pm\hat{y}} \sigma_1 c^\dagger_{l,\sigma_1} c_{l\pm\sigma_2,\sigma_2}\Big]\,.\end{aligned} \tag{D.30}$$

From this, we can see that in the $z$-component, we only have to change the sign of the spin-down parts. The final expression we obtain is

$$\begin{aligned}\langle I^{x,z}_{S,i_x}\rangle =& \frac{-2t}{N_y} \sum_\pm {\sum_{n,k_y}}' \pm \Big[\mathfrak{Im}\{u^*_{i_x\pm1,n,k_y} u_{i_x,n,k_y} - v^*_{i_x\pm1,n,k_y} v_{i_x,n,k_y}\} f(2\mathcal{E}_{n,k_y}) \\ &- \mathfrak{Im}\{w^*_{i_x\pm1,n,k_y} w_{i_x,n,k_y} - x^*_{i_x\pm1,n,k_y} x_{i_x,n,k_y}\} f(-2\mathcal{E}_{n,k_y})\Big] \\ &+ \frac{2}{N_y} \sum_\pm {\sum_{n,k_y}}' \Big[\mathfrak{Im}\{a^{\uparrow\uparrow}_{i_x\pm1,i_x} u^*_{i_x\pm1,n,k_y} u_{i_x,n,k_y} - a^{\uparrow\downarrow}_{i_x\pm1,i_x} u^*_{i_x\pm1,n,k_y} v_{i_x,n,k_y} \\ &+ a^{\downarrow\uparrow}_{i_x\pm1,i_x} v^*_{i_x\pm1,n,k_y} u_{i_x,n,k_y} - a^{\downarrow\downarrow}_{i_x\pm1,i_x} v^*_{i_x\pm1,n,k_y} v_{i_x,n,k_y}\} f(2\mathcal{E}_{n,k_y}) \\ &+ \mathfrak{Im}\{a^{\uparrow\uparrow}_{i_x\pm1,i_x} w^*_{i_x,n,k_y} w_{i_x\pm1,n,k_y} - a^{\uparrow\downarrow}_{i_x\pm1,i_x} x^*_{i_x,n,k_y} w_{i_x\pm1,n,k_y} \\ &+ a^{\downarrow\uparrow}_{i_x\pm1,i_x} w^*_{i_x,n,k_y} x_{i_x\pm1,n,k_y} - a^{\downarrow\downarrow}_{i_x\pm1,i_x} x^*_{i_x,n,k_y} x_{i_x\pm1,n,k_y}\} f(-2\mathcal{E}_{n,k_y})\Big]\,.\end{aligned} \tag{D.31}$$

## D.5 Spin magnetization

Here, we will derive the expressions for the amplitude of the spin magnetization. We can generally write it as $\boldsymbol{S}_i = \langle c^\dagger_{i,\alpha} \boldsymbol{\sigma}^{\alpha\beta} c_{i,\beta} \rangle$, where we have neglected constant prefactors. In the three different directions in the lab frame, we have

$$S_i^x = \langle c^\dagger_{i,\uparrow} c_{i,\downarrow} \rangle + \langle c^\dagger_{i,\downarrow} c_{i,\uparrow} \rangle \,, \quad S_i^y = i\langle c^\dagger_{i,\downarrow} c_{i,\uparrow} \rangle - i\langle c^\dagger_{i,\uparrow} c_{i,\downarrow} \rangle \,, \quad S_i^z = \langle c^\dagger_{i,\uparrow} c_{i,\uparrow} \rangle - \langle c^\dagger_{i,\downarrow} c_{i,\downarrow} \rangle \,.$$

Taking the mean in the $y$-direction as before, the amplitudes become

$$\begin{aligned}
S^x_{i_x} &= \frac{1}{N} \sum_{i_y} \sum_{k_y, k_y'} \frac{1}{N_y} e^{i(k_y' - k_y) i_y} \left[ \langle c^\dagger_{i_x,k_y,\uparrow} c_{i_x,k_y',\downarrow} \rangle + \langle c^\dagger_{i_x,k_y,\downarrow} c_{i_x,k_y',\uparrow} \rangle \right] \\
&= \frac{1}{N_y} \sum_{k_y} \left[ \langle c^\dagger_{i_x,k_y,\uparrow} c_{i_x,k_y,\downarrow} \rangle + \langle c^\dagger_{i_x,k_y,\downarrow} c_{i_x,k_y,\uparrow} \rangle \right] \\
&= \frac{1}{N_y} \sum_{n,m,k_y} \left[ u^*_{i_x,n,k_y} v_{i_x,m,k_y} + v^*_{i_x,n,k_y} u_{i_x,m,k_y} \right] \langle \gamma^\dagger_{n,k_y} \gamma_{m,k_y} \rangle \\
&= \frac{2}{N_y} \sum_{n,m,k_y} \mathfrak{Re} \left\{ u^*_{i_x,n,k_y} v_{i_x,m,k_y} \right\} \langle \gamma^\dagger_{n,k_y} \gamma_{m,k_y} \rangle \,, \\
&= \frac{2}{N_y} \Bigg\{ \sum_{n,m,k_y>0} \left[ \mathfrak{Re} \left\{ u^*_{i_x,n,k_y} v_{i_x,m,k_y} \right\} \langle \gamma^\dagger_{n,k_y} \gamma_{m,k_y} \rangle + \mathfrak{Re} \left\{ w_{i_x,n,k_y} x^*_{i_x,m,k_y} \right\} \langle \gamma_{n,k_y} \gamma^\dagger_{m,k_y} \rangle \right] \\
&\qquad + \sum_{n,m=1}^{2N_x} \left[ \mathfrak{Re} \left\{ u^*_{i_x,n,0} v_{i_x,m,0} \right\} \langle \gamma^\dagger_{n,0} \gamma_{m,0} \rangle + \mathfrak{Re} \left\{ w_{i_x,n,0} x^*_{i_x,m,0} \right\} \langle \gamma_{n,0} \gamma^\dagger_{m,0} \rangle \right] \Bigg\} \\
&= \frac{2}{N_y} {\sum_{n,k_y}}' \left[ \mathfrak{Re}\{ u^*_{i_x,n,k_y} v_{i_x,n,k_y} \} \, f(2\mathcal{E}_{n,k_y}) + \mathfrak{Re}\{ x^*_{i_x,n,k_y} w_{i_x,n,k_y} \} \, f(-2\mathcal{E}_{n,k_y}) \right] , \quad \text{(D.32)}
\end{aligned}$$

$$\begin{aligned}
S^x_{i_x} &= \frac{1}{N} \sum_{i_y} \sum_{k_y, k_y'} \frac{1}{N_y} e^{i(k_y' - k_y) i_y} \left[ \langle c^\dagger_{i_x,k_y,\uparrow} c_{i_x,k_y',\downarrow} \rangle - \langle c^\dagger_{i_x,k_y,\downarrow} c_{i_x,k_y',\uparrow} \rangle \right] \\
&= \frac{1}{N_y} \sum_{k_y} \left[ \langle c^\dagger_{i_x,k_y,\uparrow} c_{i_x,k_y,\downarrow} \rangle - \langle c^\dagger_{i_x,k_y,\downarrow} c_{i_x,k_y,\uparrow} \rangle \right] \\
&= \frac{1}{N_y} \sum_{n,m,k_y} \left[ u^*_{i_x,n,k_y} v_{i_x,m,k_y} - v^*_{i_x,n,k_y} u_{i_x,m,k_y} \right] \langle \gamma^\dagger_{n,k_y} \gamma_{m,k_y} \rangle \\
&= \frac{2}{N_y} \sum_{n,m,k_y} \mathfrak{Im} \left\{ u^*_{i_x,n,k_y} v_{i_x,m,k_y} \right\} \langle \gamma^\dagger_{n,k_y} \gamma_{m,k_y} \rangle \,, \\
&= \frac{2}{N_y} \Bigg\{ \sum_{n,m,k_y>0} \mathfrak{Im} \left\{ u^*_{i_x,n,k_y} v_{i_x,m,k_y} \right\} \langle \gamma^\dagger_{n,k_y} \gamma_{m,k_y} \rangle + \mathfrak{Im} \left\{ w_{i_x,n,k_y} x^*_{i_x,m,k_y} \right\} \langle \gamma_{n,k_y} \gamma^\dagger_{m,k_y} \rangle \\
&\qquad + \sum_{n,m=1}^{2N_x} \mathfrak{Im} \left\{ u^*_{i_x,n,0} v_{i_x,m,0} \right\} \langle \gamma^\dagger_{n,0} \gamma_{m,0} \rangle + \mathfrak{Im} \left\{ w_{i_x,n,0} x^*_{i_x,m,0} \right\} \langle \gamma_{n,0} \gamma^\dagger_{m,0} \rangle \Bigg\} \\
&= \frac{2}{N_y} {\sum_{n,k_y}}' \left[ \mathfrak{Im}\{ u^*_{i_x,n,k_y} v_{i_x,n,k_y} \} \, f(2\mathcal{E}_{n,k_y}) + \mathfrak{Im}\{ x^*_{i_x,n,k_y} w_{i_x,n,k_y} \} \, f(-2\mathcal{E}_{n,k_y}) \right] , \quad \text{(D.33)}
\end{aligned}$$

$$S^z_{i_x} = \frac{1}{N_y} \sum_{i_y} \sum_{k_y, k_y'} \frac{1}{N_y} e^{i(k_y' - k_y) i_y} \left[ \langle c^\dagger_{i_x,k_y,\uparrow} c_{i_x,k_y',\uparrow} \rangle - \langle c^\dagger_{i_x,k_y,\downarrow} c_{i_x,k_y',\downarrow} \rangle \right]$$

$$
\begin{aligned}
&= \frac{1}{N_y} \sum_{k_y} \left[ \langle c^\dagger_{i_x,k_y,\uparrow} c_{i_x,k_y,\uparrow} \rangle - \langle c^\dagger_{i_x,k_y,\downarrow} c_{i_x,k_y,\downarrow} \rangle \right] \\
&= \frac{1}{N_y} \sum_{n,m,k_y} \left[ u^*_{i_x,n,k_y} u_{i_x,m,k_y} - v^*_{i_x,n,k_y} v_{i_x,m,k_y} \right] \langle \gamma^\dagger_{n,k_y} \gamma_{m,k_y} \rangle \\
&= \frac{1}{N_y} \Bigg\{ \sum_{n,m,k_y>0} \Big[ (u^*_{i_x,n,k_y} u_{i_x,m,k_y} - v^*_{i_x,n,k_y} v_{i_x,m,k_y}) \langle \gamma^\dagger_{n,k_y} \gamma_{m,k_y} \rangle \\
&\qquad\qquad + (w_{i_x,n,k_y} w^*_{i_x,m,k_y} - x_{i_x,n,k_y} x^*_{i_x,m,k_y}) \langle \gamma_{n,k_y} \gamma^\dagger_{m,k_y} \rangle \Big] \\
&\qquad \sum_{n,m=1}^{2N_x} \Big[ (u^*_{i_x,n,0} u_{i_x,m,0} - v^*_{i_x,n,0} v_{i_x,m,0}) \langle \gamma^\dagger_{n,0} \gamma_{m,0} \rangle \\
&\qquad\qquad + (w_{i_x,n,0} w^*_{i_x,m,0} - x_{i_x,n,0} x^*_{i_x,m,0}) \langle \gamma_{n,0} \gamma^\dagger_{m,0} \rangle \Big] \Bigg\} \\
&= \frac{2}{N_y} \sum_{n,k_y}{}' \Big[ \left( |u_{i_x,n,k_y}|^2 - |v_{i_x,n,k_y}|^2 \right) \, f(2\mathcal{E}_{n,k_y}) + \left( |w_{i_x,n,k_y}|^2 - |x_{i_x,n,k_y}|^2 \right) \, f(-2\mathcal{E}_{n,k_y}) \Big] \, .
\end{aligned}
\tag{D.34}
$$

It is also possible to express the spin magnetization in curvilinear coordinates, not the lab frame, since these might be more intuitive. It can be done in two ways: We take the elements of $\boldsymbol{S}_i$ in the lab frame and change the basis using the parametrization. Alternatively, the Pauli-vector can be replaced by the curvilinear one, such that $S_i^{T,N,B} = \langle c^\dagger_{i,\alpha} \sigma^{\alpha\beta}_{T,N,B} c_{i,\beta} \rangle$.

# Appendix E

# Code

## E.1 Numerical implementation

In this appendix, we give an explanation for the numerical code to produce the results in the main text. The code for the quasiclassical theory uses `MATLAB` and `bvp6c`. The latter is a sixth-order boundary value solver. We solve the Riccati parametrized equations for each element of a vector `energies` and use the obtained $\gamma$ matrices as a guess for the next energy. The initial guess is a normal metal. To help with the numerical stability, we add a small imaginary contribution `1e-3i` to the energy. We also distribute the phase difference between the S-F-S systems' superconductors equally between them. The functions `Usadel_curved` and `Eilenberger_curved_SC` return the elements of $\gamma, \tilde{\gamma}$ and their derivatives as a vector. The equations in section 4.9 can be used to obtain physical observational quantities. The functions `Usadel_curved` and `Eilenberger_curved_SC` can be called to get the Green's function and its derivatives.

The lattice code was written in `Python`, and uses the library `kwant` [141] to build the Hamiltonian in eq. (5.33). It is a package for numerical quantum transport calculations in the tight-binding model. However, we only use it for the functions `kwant.lattice` and `kwant.Builder()` which lets us build the Hamiltonian easily. Diagonalization of the Hamiltonian is done with `np.linalg.eigh()` function from `numpy`, which returns the eigenvalues `self.E` and eigenvectors `self.P` in our classes. The classes are built such that they return an object that can call on expectation values directly and is solved self-consistently. The self-consistency iterations are done by diagonalizing the Hamiltonian and calculating the gap given in eq. (5.59). The new gap is compared to the old one, and if the maximum difference is below the convergence criteria, the iterations stop. All other expectation values are calculated as detailed in the main text, using the eigenvector `self.P` with the eigenvalues `self.E`. Since we effectively only solve one-dimensional systems, labeling the sites is trivial. If we have a junction with phase difference $\phi$, we apply the phase $-\phi/2$ to the first superconductor and $\phi/2$ to the second. Then, we solve for the gap magnitude self-consistently, as described above. It is common practice to only lock the phase in a few lattice points at the ends of the superconductors [100, 104, 131], but this increases the iterations needed to fulfill the convergence criteria drastically.

The code is not included in the thesis but is available upon a reasonable request.

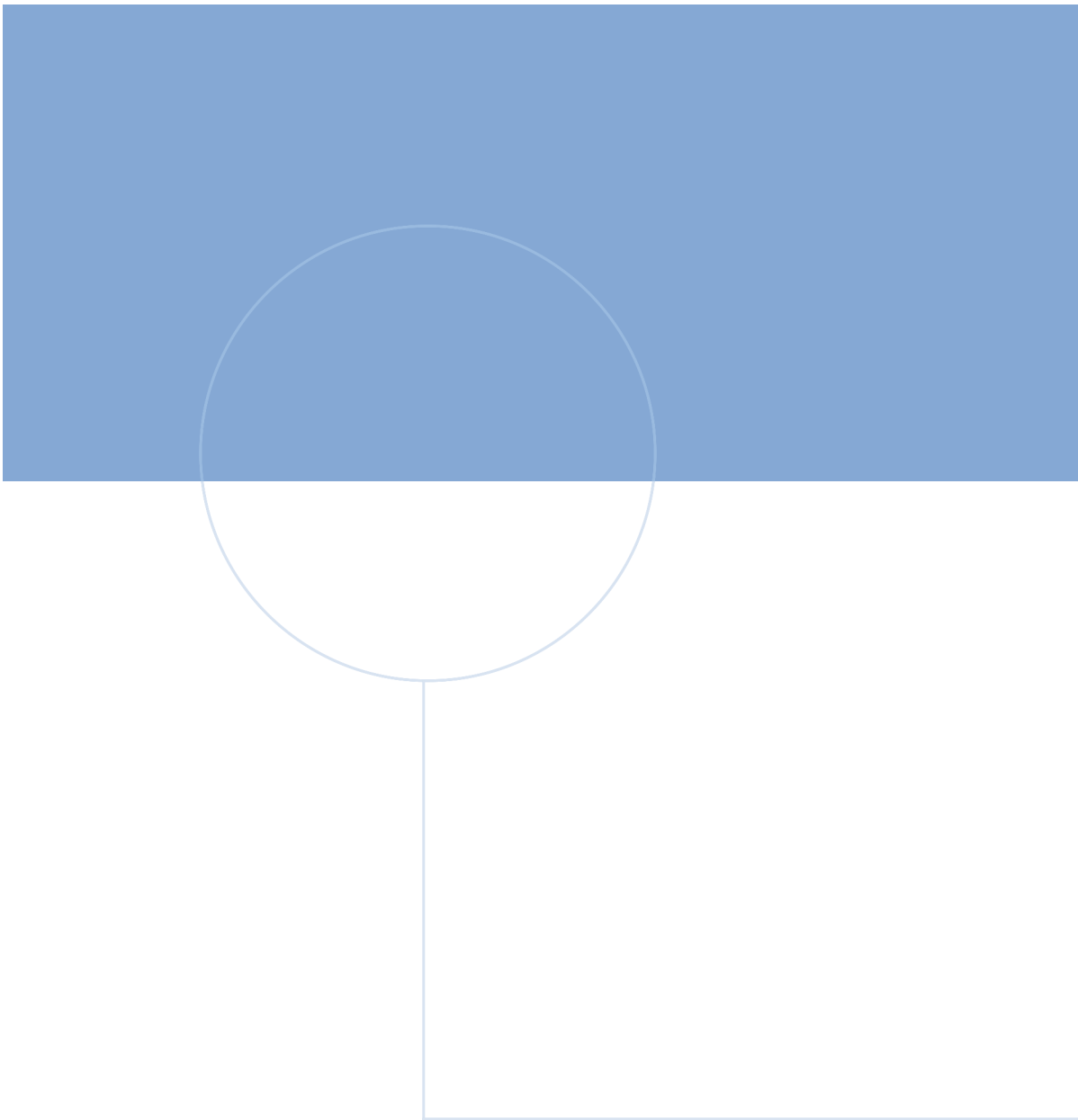

NTNU

Norwegian University of
Science and Technology